



Insights into the Human Oral Microbiome and Alzheimer's Disease

By

Anna Barlach Pritchard

A thesis submitted in partial fulfilment of the requirements for the degree
of Doctor of Philosophy at the University of Central Lancashire

March 2022

STUDENT DECLARATION FORM

Type of Award __PhD_____

School __Pharmacy and Biomedical Sciences _____

1. Concurrent registration for two or more academic awards

I declare that while registered as a candidate for the research degree, I have not been a registered candidate or enrolled student for another award of the University or other academic or professional institution

2. Material submitted for another award

I declare that no material contained in the thesis has been used in any other submission for an academic award and is solely my own work

3. Collaboration

Where a candidate's research programme is part of a collaborative project, the thesis must indicate in addition clearly the candidate's individual contribution and the extent of the collaboration. Please state below:

I declare that the next generation sequencing (NGS) data was obtained from work carried out at Oslo University as specified in the methods of chapter 3.

4. Use of a Proof-reader

No proof-reading service was used in the compilation of this thesis.

Signature of Candidate _____*ABRPritchard*_____

Print name: Anna Barlach Pritchard_____

Abstract

INTRODUCTION: The reason why some individuals develop sporadic Alzheimer's disease (AD) and others are unaffected remains unresolved. One theory still to be elucidated is the role of the oral microbiome in neurodegeneration. The effects of key pathogens and virulence factors associated with gum disease such as *Porphyromonas gingivalis* (*P. gingivalis*) on neuropathology is of interest and discoveries in this field could lead to development of novel therapeutics and preventative strategies. Chronic infections and inflammation are known to weaken the first line of defence for the brain; the blood brain barrier (BBB).

AIM: The aim of this study was to investigate the potential contribution from pathogens of the periodontal microbiome to the development of AD and whether the mediators produced during periodontal disease (PD), such as *P. gingivalis* outer membrane vesicles (OMV) and Lipopolysaccharides (LPS), were capable of inducing changes associated with inflammatory BBB damage.

RESULTS: The association between a microbial presence in the brain and AD pathology was confirmed by high throughput genomic analysis and PCR analysis of human post-mortem tissues from AD patients and age matched controls. Brain microbiome analysis was carried out by next generation sequencing (NGS) to genus level. Bacterial reads in AD patients (n=9) were 9-fold higher compared to controls (n=6), with a dominance of Proteobacteria, Bacteroidetes, Actinobacteria and Firmicutes. PCR amplification at UCLan was applied to the post-mortem brain samples using bacterial and fungal primers. These investigations provided limited data and limitations of the utilised methods were acknowledged.

An *in vitro* BBB model, composed of primary-derived human astrocytes (HA), pericytes (HBPC) and brain microvascular endothelial cells (HBMEC), cultured in a transwell system representing the neurovascular unit of the BBB, was utilised to evaluate the effects of *P. gingivalis* virulence factors (LPS and OMVs). The integrity of the BBB after application of *P. gingivalis* LPS (unconjugated and fluorescein isothiocyanate (FITC) - conjugated) and OMVs were investigated and correlated with transport of LPS across the barrier. A significant decrease ($p \leq 0.05$) in transendothelial electrical resistance (TEER) was observed when unconjugated *P. gingivalis* LPS (0.3, 10, 100 $\mu\text{g/ml}$) and *P. gingivalis* OMVs (0.1, 0.3, 50 and 100 $\mu\text{g/ml}$) were applied to the BBB relative to the control (FITC-alone), but the response was not concentration dependent (no significant difference between groups).

The TEER values did not recover to pre-treatment baseline as measured by a significant deficit in TEER ($p \leq 0.05$) after application of unconjugated *P. gingivalis* LPS and OMVs. The application of *P. gingivalis* LPS-FITC conjugate in conjunction with 10 $\mu\text{g/ml}$ *P. gingivalis* OMVs showed a similar pattern in terms of TEER response. Application of *P. gingivalis* OMVs to a monoculture of HBMEC was evaluated using immunofluorescence microscopy and showed disruption of the tight junction zona occludens protein (ZO-1) after addition of 0.3 $\mu\text{g/mL}$ *P. gingivalis* OMVs compared to controls (media only).

CONCLUSION: These findings show that the integrity of tight junctions of the human BBB could be weakened by association with *P. gingivalis* virulence factors LPS and OMVs containing proteolytic enzymes (gingipains). *P. gingivalis* LPS act through toll-like receptor 4 (TLR4) and it has been shown that rodent cells are less sensitive to this than human cells. This highlights the importance of developing models as close to human

anatomy and physiology as possible. The BBB and monolayer models utilised in this study were found to be valuable tools for further cell-bacteria interaction studies.

FUTURE WORK: The recognition that no PD bacterial cell has been found in the brain emphasises the need to learn more about the virulence factors produced in PD, such as LPS and gingipains and to gain information about how a chronic oral infection affects the BBB. The findings in this study provide additional information of the processes involved in virulence factor-CNS interactions, potentially suggesting how chronic periodontal disease in middle to later life could increase the risk of late onset dementia such as AD.

Table of contents

Abstract	3
Table of contents	5
Acknowledgements	10
Table of Figures.....	11
List of tables	19
List of abbreviations	20
Chapter 1	26
Introduction	26
1. Background	27
1.1 Alzheimer’s disease incidence/ prevalence.....	29
1.1.1 Alzheimer’s disease pathogenesis.....	31
1.1.2 The hypotheses driving research into Alzheimer’s disease.....	34
1.1.2.1 The amyloid cascade hypothesis	35
1.1.2.2 The vascular dysregulation hypothesis	36
1.1.2.3 The calcium homeostasis hypothesis.....	36
1.1.2.4 The cholinergic hypothesis	37
1.1.2.5 The mitochondrial cascade hypothesis	37
1.1.2.6 The metal ion hypothesis	37
1.1.2.7 The lymphatic system hypothesis	38
1.1.2.8 The Tau-hypothesis	38
1.1.2.9 The inflammatory hypothesis	39
1.1.3 Prognosis/ Treatment/Prevention of AD.....	42
1.2 Periodontal disease	44
1.2.1 <i>Porphyromonas gingivalis</i>	49
1.3 The link between Alzheimer’s disease and periodontal disease.....	54
1.4 The blood-brain-barrier (BBB).....	60
1.4.1 BBB anatomy.....	60
1.4.2 BBB functions	63
1.4.3 Transport across the BBB.....	65
1.4.4 BBB change in function	67
1.4.4.1 Non-disruptive BBB changes:	68
1.4.4.2 Disruptive changes:	70
1.4.5 Route from blood to brain and potential for neuroinflammation induction	71
1.5 Originality, Hypothesis and Overall Aims and Objectives.....	77

1.6 Justification of choice of methodology	78
Chapter 2	79
Genomic analysis	79
2.1 Introduction, aims and objectives.....	80
2.2 Materials and methods for NGS.....	81
2.2.1 Human brain tissue, sample selection	81
2.2.2. DNA extraction of human brain samples for NGS and PCR screening at.....	86
UCLan.....	86
2.2.3 PCR amplification and purification of amplicons for the purpose of NGS.	87
2.2.4 Data analysis by MiSeq SOP MOTRUR	91
2.2.5 Materials and methods for PCR analysis carried out at UCLan.....	92
2.2.5.1 Sample selection	92
2.2.5.2 PCR amplification of human brain samples AP1-40 at UCLan	92
2.3 Results	98
2.3.1 Results NGS.....	98
2.3.1.1 Bacterial community profiling	99
2.3.2 Results PCR carried out at UCLan	108
2.3.2.1 Annealing temperature	109
2.3.2.2 MgCl ₂	114
2.3.2.3 DMSO.....	115
2.3.2.4 Template concentrations.....	117
2.3.2.5 Human samples.....	120
2.4 Discussion – NGS and PCR	133
2.5 Conclusion.....	148
Chapter 3	150
BBB-model techniques, characterisation and optimisation of <i>in vitro</i> model	150
3.1. Introduction, aim and objectives	151
3.2 Materials.....	152
3.3 Methods for <i>in vitro</i> BBB model	152
3.3.1 Coating of tissue culture flasks and cell thawing	152
3.3.2 Sub culturing of cells.....	153
3.3.3 Freezing of cells	154
3.3.4 Cell counting.....	155
3.3.5 Methods for characterization and optimisation of the <i>in vitro</i> BBB model cell lines	155
3.4 Results	157
3.4.1 Cell line growth kinetics	157
3.4.2 Cell morphology.....	160

3.5 Discussion.....	161
3.6 Conclusion.....	164
Chapter 4.....	165
The <i>in vitro</i> Blood Brain Barrier model and <i>P. gingivalis</i> Lipopolysaccharide application	165
4.1 Introduction, aims and objectives of BBB model with <i>P. gingivalis</i> LPS study	166
4.2 Materials.....	169
4.3 <i>In vitro</i> BBB model methods	169
4.3.1 Coating of inserts for triculture BBB model	169
4.3.2 Seeding primary cells triculture on the transwell inserts.....	170
4.3.3 Testing the integrity of the <i>in vitro</i> BBB model and standard curves.....	171
4.3.4 Human IL-6 ELISA.....	173
4.3.5 <i>In vitro</i> BBB Methods testing barrier integrity after virulence factor application	175
4.3.5.1 Application of <i>P. gingivalis</i> LPS to the <i>in vitro</i> BBB model at various	176
concentrations, permeability tested with Evans Blue permeability assay	176
4.3.5.2 Application of <i>P. gingivalis</i> LPS to the <i>in vitro</i> BBB model at various	177
concentrations, permeability tested with FITC-dextran permeability assay	177
4.3.5.3 <i>P. gingivalis</i> LPS-FITC conjugates application to the <i>in vitro</i> BBB model in	178
various concentrations and checked with FITC- dextran permeability assay	178
4.3.5.3.1 <i>P. gingivalis</i> LPS conjugate from Dojindo.....	178
4.3.5.3.2 <i>P. gingivalis</i> LPS conjugate from Nanocs.....	180
4.3.5.3.3 Application of LPS-FITC conjugates (Dojindo and Nanocs) to the <i>in vitro</i>	180
BBB model	180
4.3.5.4 Human IL-6 ELISA of HBPC assay after application of unconjugated and	182
FITC- conjugated <i>P. gingivalis</i> LPS	182
4.4 Results	182
4.4.1 Results from <i>P. gingivalis</i> LPS application to <i>in vitro</i> BBB model and Evans Blue	182
Dye permeability assay.	182
4.4.2 Results from <i>P. gingivalis</i> LPS application to <i>in vitro</i> BBB model and FITC-	186
dextran permeability assay	186
4.4.3 Results from application of <i>P. gingivalis</i> LPS-FITC conjugates on the <i>in vitro</i>	193
BBB model	193
4.4.3.1 Results Dojindo conjugate	193
4.4.3.2 Results Nanocs <i>P. gingivalis</i> LPS conjugate.....	195
4.4.4 Results IL-6 ELISA	203
4.5 Discussion.....	205
4.6 Conclusion.....	215

Chapter 5	217
<i>In vitro</i> BBB model with <i>P. gingivalis</i> Outer membrane vesicles and lipopolysaccharide application	217
5.1 Introduction, Aims and Objectives of <i>in vitro</i> BBB model with <i>P. gingivalis</i> OMV and LPS application study	218
5.2 Materials and methods	219
5.2.1 Cultivation of <i>P. gingivalis</i>	220
5.2.2 Gram stain of <i>P. gingivalis</i>	221
5.2.3 Isolation of <i>P. gingivalis</i> outer membrane vesicles	222
5.2.4 Measurement of size of outer membrane vesicles	222
5.2.5 Human IL-6 ELISA testing OMV on HBPC	223
5.2.6 Application of <i>P. gingivalis</i> OMVs to the <i>in vitro</i> BBB model	223
5.2.6.1 <i>In vitro</i> BBB model test protocol with <i>P. gingivalis</i> OMVs application	223
5.2.6.2 Application of FITC conjugated <i>P. gingivalis</i> LPS with OMVs to the <i>in vitro</i> BBB model	224
5.3 Results	225
5.3.1 Results cultivation of <i>P. gingivalis</i> FDC 381	225
5.3.2 Extraction of OMVs from <i>P. gingivalis</i> FDC 381 and measurement in Zetasizer ...	228
5.3.3 IL-6 ELISA after application of OMVs to HBPC	229
5.3.4 Effect of <i>P. gingivalis</i> OMVs to the <i>in vitro</i> BBB model	230
5.3.5 Application of conjugated FITC <i>P. gingivalis</i> LPS combined with 10 µg/ml	233
<i>P. gingivalis</i> OMV to the <i>in vitro</i> BBB model	233
5.4 Discussion	236
5.5 Conclusion	240
Chapter 6	241
Assessment of <i>P. gingivalis</i> virulence factors interaction with HBMEC in monolayer, measured by immunofluorescence microscopy	241
6.1 Introduction, aims and objectives of <i>P. gingivalis</i> OMVs and LPS application to	242
HBMEC in monolayer study	242
6.2. Materials	243
6.3 Methods	243
6.3.1 Method HBMEC monolayer model	243
6.3.2 Immunofluorescent protocol for detection of tight junction proteins	244
6.4 Results	245
6.5 Discussion	249
6.6 Conclusion	255
Chapter 7	256
Thesis conclusion and future work	256

Thesis conclusion.....	257
Future work	263
References.....	266
Appendix 1: Additional information	329
Appendix 2 Additional information from BBB model study	332

Acknowledgements

I would like to thank a number of people who has supported me during my studies and have made this journey a great experience. First of all, StJohn, thank you for inspiring me to keep learning for the past 10 years and for always being ready to answer my many questions! You are incredible and continue to amaze me.

A huge thank you to Jane Alder my DOS for your continuous support in the past 4 years, you truly are a great woman and scientist!

Thank you to Clare Lawrence for all your help, I think you are brilliant and an excellent teacher!

I would like to thank Glyn Morton for his support and inspiration throughout the project, you are a legend, thank you!

Also, I would like to thank my two sons Thomas and Alex for putting up with my long hours in the laboratory and ready meals late at night, at least one of you learned to cook as a consequence. I am so proud of both of you. I would also like to say “tak” to my mum Tove, for telling me at a very young age that I could do anything if I set my mind to it, you were right mum, your unconditional support has shaped who I am today.

I am also so very grateful to my dad, Jørgen for always being there for me and having my back. I love you all.

I would also like to thank the Faculty of Dental Surgery, Royal College of Surgeons England for the pump priming grant and the kind donation from The Norah and Fred Roberts Memorial Trust which helped fund my materials for the project.

Table of Figures

Figure number		Page number
1.1	Cleavage of the amyloid precursor protein (APP).....	32
1.2	Schematic illustrating the macroscopic features relating to shrinkage (wider sulci, compared with non-Alzheimer's disease (AD) brain), unique to the AD brain, which equates to inflammatory condition.....	41
1.3	Establishment of microbial dysbiosis in periodontal disease.....	45
1.4	<i>Porphyromonas gingivalis</i> is linked to the development of multiple chronic inflammatory conditions.....	47
1.5	Tight junctions of the blood brain barrier.....	61
1.6	Transportation across the BBB.....	67
2.1	Conserved, variable, hypervariable regions within the 16S rRNA gene.....	88
2.2	Bacterial reads at phylum level in AD and control cases.....	104
2.3	Spread of identified reads at genus level in AD cases.....	105
2.4	Spread of identified reads at genus level in control cases analysed	106
2.5	Number of bacterial reads by high throughput analysis in relation to post mortem delay.....	107
2.6	Optimisation reactions with mammalian and fungal primer sets.....	111
2.7	Mammalian primers 167musGapdhf and 167musGapdhr with un-spiked mouse brain DNA template at incremental annealing temperature.....	112
2.8	<i>Escherichia coli</i> template with mammalian primer at incremental temperature increases.....	112

2.9	Un-spiked mouse gDNA template with bacterial primers F342 and F18R at increments in annealing temperature.....	113
2.10	<i>Escherichia coli</i> template with mammalian primer at incremental temperature increases.....	113
2.11	<i>Escherichia coli</i> or mouse template with primer set F342 and F18R at various concentrations of MgCl ₂	115
2.12	DMSO optimisation gel, <i>Escherichia coli</i> template at 0.08 ng/μl with primer set F342 and F18R and the same primers applied to distilled water controls.....	116
2.13	Quantification test for sensitivity of fungal primer set.....	117
2.14	Quantification test for sensitivity of fungal primer set applied to mouse brain gDNA spiked with <i>Candida albicans</i> gDNA template.....	118
2.15	Quantification test for sensitivity of bacterial primer set.....	119
2.16	Quantification test of mouse brain gDNA spiked with <i>Escherichia coli</i> template.....	119
2.17	The mammalian primers (167musF/R) and the bacterial primer set F342/F18R applied to the human gDNA samples AP7 and AP12-17.....	122
2.18	The mammalian primers (167musGapdhF/R) applied to the human gDNA sample AP7 and the bacterial primer set F342/F18R applied to the human gDNA (AP7).....	123
2.19	Fungal primer set ITSF1/2 applied to the human gDNA (AP7 and AP1).....	123

2.20	Visualisation of PCR product by electrophoresis from reactions with gDNA from human samples AP3-7 and the primer set F342/F18R.....	124
2.21	Visualisation of PCR product by electrophoresis from reactions with gDNA from human samples AP12,AP16,AP20,AP21,AP22,AP23 and AP24, with the primer set F342/F18R.....	125
2.22	Visualisation of PCR product by electrophoresis from reactions with gDNA from human samples AP26, AP28, AP29, AP30, AP31, AP37 and AP40.....	126
3.1	Cell count over time of primary cell lines.....	159
3.2	Three primary cell lines (HBPC, HBMEC and HA).....	160
4.1	Transwell cell culture system and primary cell location in BBB model.	171
4.2	Standard curve for permeability assay with Evans Blue Dye.....	184
4.3	TEER readings and permeability of EBD in a <i>P. gingivalis</i> LPS 1 µg/ml, b no LPS (Evans Blue 1µg/ml), c <i>P. gingivalis</i> LPS + EB (1:1 µg/mL), d TEER only.....	185
4.4	Modelling the magnitude and rate of change in TEER after application of test sample to the <i>in vitro</i> BBB model.....	187
4.5	Changes in BBB integrity measured by calculating the magnitude of decrease in TEER in response to application of unconjugated <i>P. gingivalis</i> LPS (A) and the magnitude of deficit in recovery of TEER 72 hours post application of unconjugated <i>P. gingivalis</i> LPS relative to initial	

	baseline TEER (B).....	188
4.6	FITC-dextran 3-5 kD standard curve for permeability assay in in vitro BBB model.....	190
4.7	Shows the percentage of FITC-dextran (3-5 kDa) permeating through the <i>in vitro</i> BBB after incubation with increasing concentrations of unconjugated <i>P. gingivalis</i> LPS (0-100 µg/ mL) for 1 h (A); 4 h (B); 24 h (C); 48 h (D); 72 h (E) and all exposure times compared together (F)...	191
4.8	TEER (Ohms/cm ²) compared to % Appearance at different test protocols: a – FITC only, b- 0.1 µg/ml <i>P. gingivalis</i> LPS, c- 0.3 µg/ml <i>P. gingivalis</i> LPS, d – 1 µg/ml <i>P. gingivalis</i> LPS, e – 10 µg/ml <i>P. gingivalis</i> LPS, f – 100 µg/ml <i>P. gingivalis</i> LPS.....	192
4.9	TEER control well, Data presented as Mean +/- SD.....	193
4.10	Standard curve produced from the Dojindo FITC- <i>P. gingivalis</i> LPS conjugate in media.....	194
4.11	Standard curve produced from the Dojindo FITC- <i>P. gingivalis</i> LPS conjugate in HBSS.....	195
4.12	Standard curve a. Nanocs conjugate with media only b. media and with citrate buffer c. FITC dextran 3-5 kD.....	196
4.13	Changes in BBB integrity measured by calculating the magnitude of decrease in TEER in response to application of conjugated FITC- <i>P. gingivalis</i> LPS (Nanocs in media) (A) and the magnitude of deficit in	

	recovery of TEER 72 hours post application of conjugated FITC- <i>P. gingivalis</i> LPS (Nanocs in media) relative to initial baseline TEER (B).....	197
4.14	Percentage appearance of FITC <i>P. gingivalis</i> LPS conjugate on the apical side of the <i>in vitro</i> BBB model relative to the stock FITC <i>P. gingivalis</i> LPS administered to the basolateral side after 1 h (A); 4 h (B); 24 h (C); 48 h (D); 72 (E) and a comparison of all time points (E).....	199
4.15	TEER and % appearance of Nanocs LPS conjugate diluted in citrate buffer and media. a. 100 µg/ml Nanocs with CB and media, b. 50 µg/ml Nanocs with CB and media c. 1 µg/ml Nanocs with CB and media, d. TEER only control.....	201
4.16	A Difference in the magnitude of change (Y1-Y2) between the TEER response in the wells with application of Nanocs conjugate in citrate buffer and media solution compared to the controls (TEER or FITC-dextran only), B Difference between highest TEER and recovery value after application of Nanocs LPS conjugate suspended in citrate buffer with media.....	202
4.17	Example of standard curve of human IL-6 concentration (pg/ml) applied in ELISA test of biological activity of reagents applied to BBB model.....	203
4.18	ELISA of Human IL-6 response to applications of reagents to HBPC in monolayer and incubation for 4 hours. A <i>P. gingivalis</i> LPS and Dojindo	

	<i>P. gingivalis</i> conjugate B Nanocs <i>P. gingivalis</i> conjugate Data shown as Mean +/-SD (N= 9).....	204
5.1	A, <i>P. gingivalis</i> FDC 381 Gram stain, scale bar represents 80 µm and B, <i>P. gingivalis</i> FDC 381 on FAA Neomycin (E&O, UK) shows coccobacillus at x100 and Black stain colonies of the strain with haemolytic halos.....	227
5.2	Zetasizer reading of particle size in <i>P. gingivalis</i> OMV isolated from broth culture.....	228
5.3	Standard curve for measurement of Human IL-6 levels by ELISA after application of <i>P. gingivalis</i> OMVs to HBPC in monolayer.....	229
5.4	Levels of IL-6 secreted by HBPC after incubation with <i>P. gingivalis</i> OMV and PM only.....	230
5.5	Changes in BBB integrity measured by calculating the magnitude of decrease in TEER in response to application of <i>P. gingivalis</i> OMVs (A) and the magnitude of deficit in recovery of TEER 72 h post application of conjugated <i>P. gingivalis</i> OMVs relative to initial baseline TEER (B).....	231
5.6	Percentage appearance of FITC-dextran (3-5 kDa) on the apical side of the <i>in vitro</i> BBB model after application of <i>P. gingivalis</i> OMVs, percentage appearance relative to the stock FITC-dextran administered to the basolateral side after 1 h (A); 4 h (B); 24 h (C); 48 h (D); 72 (E) and a comparison of all time points (E).....	232
5.7	Changes in BBB integrity measured by calculating the magnitude of	

	decrease in TEER in response to application of FITC <i>P. gingivalis</i> LPS conjugate and 10 µg/ml <i>P. gingivalis</i> OMVs (A) and the magnitude of deficit in recovery of TEER 72 hours post application of FITC <i>P. gingivalis</i> LPS conjugate and 10 µg/ml <i>P. gingivalis</i> OMVs relative to initial baseline TEER (B).....	234
5.8	Percentage appearance of FITC <i>P. gingivalis</i> LPS conjugate on the basolateral side of the <i>in vitro</i> BBB model relative to the stock administered to the apical side	235
6.1	A. HBMEC fluorescent protocol Claudin5 Mab 1:100 + Cy5 anti rabbit IgG 1:800, with 5 washes. B. HBMEC fluorescent protocol Jam1 Mab 1:100 and Cy5 anti mouse IgG 1:400 10 washes.....	245
6.2	Immunofluorescent study of application of <i>P. gingivalis</i> virulence factors to HBMEC cells. HBMEC cells in monolayer were treated with EBM (A-C), unconjugated 0.3 µg/ml <i>P. gingivalis</i> LPS (D-F), 0.1 µg/ml <i>P. gingivalis</i> OMVs (G-I) or 0.3 µg/ml <i>P. gingivalis</i> OMVs (J-L) for 24 hours. Panels A, D, G and J show the nuclei stained with DAPI and detected at 358 nm (blue). Panels B, E, H and K show Cy5 signal detected at 646 nm (red) detecting the primary ZO-1 (D6L1E).....	248
6.3	Systemic <i>P. gingivalis</i> disrupting endothelial tight junctions by degrading PECAM1 and VE cadherin by gingipain proteolysis increasing the	

endothelial permeability (Hajishengallis, 2021).....250

6.4 The cerebral endothelial cells junction structure. The main transmembrane tight junction proteins are Claudin 5 and Occludin. ZO-1 connects the actin skeleton to the tight junctions and VE cadherin forms the majority of adherens junctions interacting with the cytoplasmic anchor proteins: β -catenin, plakoglobin (γ -catenin), and p120 linking to the cytoskeleton (Li *et al.*, 2018).....251

List of tables

Table number	Page number
1.1 <i>P. gingivalis</i> has been linked to organ pathologies remote from the oral cavity.....	48
1.2 Known virulence factors associated with <i>P. gingivalis</i> and their known effects on the tissues and components in the oral cavity.....	50
2.1 Samples selected for gDNA analysis, age, sex, post-mortem delay, Braak stage, pH and COD.....	83
2.2 Materials used for DNA extraction for sequencing amplification.....	87
2.3 Reagents used in amplification for NGS.....	89
2.4 Primers used in the NGS.....	90
2.5 Primer combinations applied in amplification before NGS of samples AP1-40.....	91
2.6 PCR program used for amplification before NGS.....	91
2.7 Mastermix content for PCR amplification at UCLan.....	95
2.8 Primer sequences and properties (IDT, UK).....	96
2.9 PCR amplification protocols at UCLan.....	97
2.10 Overview of total bacterial reads in AD and non-AD cases by NGS.....	101
2.11 Summary of results from PCR at UCLan and NGS.....	127
3.1 Comparison of growth kinetics of HBMEC, HPC and HA in media with either single donor serum or multiple donor serum.....	158
5.1 Materials for cultivation of <i>P. gingivalis</i>	221

List of abbreviations

2D	two dimensional
3D	three dimensional
A α	amyloid alpha
A β	amyloid- β
ABC	ATP binding cassette
ABM	astrocyte basal media
AD	Alzheimer's Disease
AF-6	affadin 6
AGT-II	alkylguanine DNA alkyltransferases II
AJs	adherens junctions
AMT	Adsorptive mediated transcytosis
ANP	Atrial natriuretic peptide
ApoE	apolipoprotein E
APP	Amyloid precursor protein
ATP	Adenosine triphosphate
AWERB	Animal Welfare Ethical Review Board
BBB	blood brain barrier
BCSFB	blood cerebrospinal fluid barrier
BLC	basolateral compartment

CAMs	cell adhesion molecules
CB	citrate buffer
CCL2	chemokine ligand 2
CCR7	chemokine receptor type 7
CD	cardiovascular disease
sCD14	soluble cluster of differentiation 14 receptor
CFU	colony-forming unit
ChAT	choline acetyltransferase
Cl5	Claudin 5
CNS	central nervous system
COD	cause of death
CRISPR-cas	clustered regularly interspaced palindromic repeats associated protein
CSF	cerebrospinal fluid
DLS	dynamic light scattering analysis
DMSO	Dimethyl sulfoxide
EBD	Evans blue dye
EDTA	Ethylenediaminetetraacetic acid
EBM	endothelial basal media
ELISA	enzyme-linked immunosorbent assay
ESAM	endothelial cell selective adhesion molecule
EVOM	epithelial volt/ohm meter

FimA	fibrillin
FISH	fluorescence in situ hybridisation
FITC	Fluorescein isothiocyanate
GCPII	glutamate carboxypeptidase II
gDNA	genomic Deoxyribonucleic acid
GI	gastrointestinal
GLUT-1	Glucose transporter 1
HA	human astrocytes
HBMEC	human brain microvascular endothelial cell
HBPC	human brain pericytes
HBSS	Hank's Balanced Salt Solution
HOMD	human oral microbiome database
HRP	horseradish peroxidase
ICAM-1	intercellular adhesion molecule 1
IDE	insulin-degrading enzyme
IGF-1 and IGF-2	Insulin-like growth factors 1 and 2
IL-2	Interleukin 2
IL-6	Interleukin 6
ISF	interstitial fluids
ITS	internal transcribed spacer
Jam-1	junctional adhesion molecule-1

Kgp	lysine specific gingipains
LAMP	Loop-mediated isothermal amplification
LFA	lymphocyte function associated antigen
LPS	lipopolysaccharide
LRP1	lipoprotein receptor related protein 1
MCI	mild cognitive impairment
MMP-9	matrix metalloproteinase 9
MMPs	matrix metalloproteinases
NBTR	Newcastle brain tissue resource
NEP	neprilysin
NFTs	neurofibrillary tangles
NGS	next generation sequencing
NMDA	N-methyl-D-aspartate
NMWL	nominal molecular weight limit
NO	Nitric Oxide
NVU	neurovascular unit
OD	optical density
OMVs	outer membrane vesicles
P38 MAPK	p38 mitogen-activated protein kinase
PAMP	pathogen associated molecular pattern
Papp	apparent permeability

PBM	pericyte basal media
PBS	phosphate buffer solution
PCR	polymerase chain reaction
PD	periodontal disease
PECAM	platelet endothelial cell adhesion molecule
<i>P. gingivalis</i>	<i>Porphyromonas gingivalis</i>
PGs	prostaglandins
PGE2	prostaglandin E 2
P-gp	P-glycoprotein
PHFs	paired helical filaments
PNS	peripheral nervous system
PPAD	peptidylarginine deaminase
PPE	personal protective equipment
p-Tau	hyperphosphorylated Tau protein
RCT	randomised controlled trials
RgpA/B	arginine specific gingipains
Rpm	revolutions per minute
TEER	transendothelial electrical resistance
TGF- β	transformation growth factor-beta
Th17	T helper 17
TJs	Tight junctions

TLR4	Toll Like Receptor 4
TNF- α	Tumor necrosis factor alpha
TLR4	toll like receptor 4
TMB	tetramethylbenzidine
Treg	T-regulatory cell
TSB	tryptic soy broth
VE-cadherin	vascular endothelial cadherin
VLA-4	very adherent antigen 4
VLDLR	very low-density lipoprotein receptor
ZO-1	zona occludens 1

Chapter 1

Introduction

1. Background

The reason why some individuals develop sporadic Alzheimer's Disease (AD) while others are unaffected remains unresolved. AD is the most common cause of cognitive impairment in individuals over 65 years of age (Atri, 2019) presenting with symptoms such as amnesia, functional impairment and behavioural changes (Atri, 2019). The development, progression and clinical decline seen in AD can present in a heterogenous manner, but mild cognitive impairment (MCI) is typically the only early symptom, potentially leaving the disease to go undetected for long periods (Atri, 2019). There is currently no effective treatment for AD or a way of slowing or stopping the rate of neurodegeneration, only symptomatic treatments are available. A body of evidence has emerged over the past decade which supports a possible role of microorganisms in the development of neurodegeneration, which includes epidemiological data (Chen *et al.*, 2017), post-mortem (Alonso *et al.*, 2017; Emery *et al.*, 2017) and experimental studies (Dominy *et al.*, 2019; Illievski *et al.*, 2018). The evidence suggests that microorganisms potentially linked to AD may be viral, bacterial or fungal in origin (Alonso *et al.*, 2017; Miklossy, 2016; Itzhaki *et al.*, 2016, Pritchard *et al.*, 2017).

It is known that there are multiple risk factors for developing sporadic AD, the most significant being advanced age (Pritchard *et al.*, 2017). However, the possibility of microorganisms playing a role as a causative factor for AD, opens new possibilities for the discovery of novel preventative measures and therapeutic targets. Pivotal to the discovery of such novel drug targets is the need to create research models that are representative of human physiology and disease state.

AD is a chronic neurodegenerative condition which is known to develop over decades, displaying histological hallmarks of extracellular amyloid- β (A β) plaques and hyperphosphorylated intracellular tau tangles within the brain parenchyma (Braak and Braak, 1995). AD can also be considered as a chronic inflammatory disease and has been linked to inflammatory events (Fulop *et al.*, 2021) such as traumatic brain injury or

vascular disease. The subsequent activation of the immune system and release of appropriate inflammatory mediators is a protective response following a brain injury. Predisposing factors such as age, genetics, illness, or lifestyle habits (smoking, diet, exercise) (Guo *et al.*, 2020), may leave the individual susceptible to developing a persistent inflammatory trigger, leading to a chronic tissue reaction with devastating toxic effects at a cellular level (Sevenich, 2018) and even initiating a path to recognised AD pathology (Fulop *et al.*, 2021). Sporadic AD presents late in life in individuals who may not have an overt history of an acute inflammatory event, but the pathological end point is the same (Sevenich, 2018). The search for a trigger of raised levels of pro-inflammatory mediators and oxidative stress, identified in AD patients goes on.

The detection of remnants of multiple microorganisms in post-mortem brains from AD individuals and the notion that A β can behave as an anti-microbial peptide (Soscia *et al.*, 2010; Kumar *et al.*, 2016), means that an external (chronic) assault on brain tissues, for example infection by an oral periodontal disease bacterium such as *Porphyromonas gingivalis* (*P. gingivalis*), could cumulatively damage brain tissue and even lead to low level neurodegenerative changes decades before a clinical diagnosis of AD presents (Sevenich, 2018).

Periodontal disease (PD) is a chronic infection caused by bacteria in the gums around teeth represented by microbial dysbiosis and tissue destruction (Hajishengallis *et al.*, 2012; Hajishengallis and Lamont, 2012). PD has been linked to other organ specific disease such as Alzheimer's disease, arthritis, Parkinson's disease, atherosclerosis, and diabetes mellitus (Olsen *et al.*, 2020; Holmstrup *et al.*, 2017). The progression of PD in humans is determined by microbiological, environmental and genetic factors (multiple polymorphisms) (Kozak *et al.*, 2020). PD can go undiagnosed for years and even if oral hygiene measures are improved, there is a potential of bacteraemia(s) of periodontal pathogens when chewing foods or cleaning teeth (both daily brushing and dental scaling) (Forner *et al.*, 2006). Forner *et al.* (2006) measured bacteraemia in individuals with PD

after such tasks and found they induced bacterial loads in the range of 0.11 - 2.67 CFU/ml for up to 30 minutes after the event. It is this repetitive bacterial load in the circulation which is proposed to contribute to a systemic chronic inflammatory state.

The evidence of links between remote organ disease and the keystone PD pathogen *P. gingivalis* has increased in the past decade, including pathologies such as atherosclerotic plaques in arteries (Taylor-Robinson *et al.*, 2002). This makes *P. gingivalis* a prime candidate for potential involvement with remote pathology at the BBB. The increased focus on *P. gingivalis* has led to numerous investigations of how this bacterium is able to play such a central part in the development and persistence of PD (Hajishengallis and Lamont, 2014; Olsen *et al.*, 2018; Olsen *et al.*, 2016) and this evidence base supported the rationale for focusing on *P. gingivalis* and its virulence factors in this thesis.

This thesis thus poses the questions, could the influx of *P. gingivalis* virulence factors into the circulation, renewed daily by chewing or tooth brushing (Forner *et al.*, 2006) be sufficient to cause damage to the blood brain barrier (BBB)? Is there evidence of PD bacterial gDNA in the brains of deceased AD patients compared to age matched controls?

1.1 Alzheimer's disease incidence/ prevalence

There are currently 50 million people in the world with dementia and this is estimated to increase to 152 million people by 2050 (Patterson, 2018; Kaur *et al.*, 2021); the increasing age of the population contributing significantly to this development. Dementia is a clinical condition which presents with changes in behaviour or functional decline and most commonly accompanied by cognitive problems such as forgetfulness (Atri, 2019). Dementia can present at any age but is mainly associated with progressed age.

The evidence of dementia incidence and prevalence trends worldwide is mixed (Prince *et al.*, 2016). This is mainly due to heterogeneity between studies making it difficult to draw robust conclusions, but there have been reports of recent decline in incidence in some western countries (USA, UK and Sweden) (Stephan *et al.*, 2018). The consensus is that this decline is in response to public health campaigns and improvements in population vascular health (Prince *et al.*, 2016; Stephan *et al.*, 2018).

In 2019, there were an estimated 850 000 people living with dementia in the UK (Wittenberg *et al.*, 2020) and though Matthews *et al.*, (2016) suggested that the incidence of dementia in the UK has fallen by as much as 20% in the past two decades, this condition will still affect a large population group with devastating consequences.

Alzheimer's disease (AD) is the most common type of dementia causing around 60–80% of all cases (Gaugler *et al.*, 2016). AD is characterized by cognitive deficit, such as confusion and memory deficit. The person may also struggle to problem solve or follow a plan. In the early stages this is most often mild (MCI), however as the disease progresses, the person may completely forget familiar places, people and tasks such as writing and speaking (Atri, 2019).

AD has a complex, multifactorial aetiology with no definitive known causal mechanism. The limited treatment options make it a challenging condition in which neuropsychiatrists/ neurologists can do little to help their patients (Pritchard *et al.*, 2017). The relentless progression of the disease and downward spiral of patient's cognitive function impacts both the patient and their carers. Furthermore, the rising aging population and the predicted increase in the prevalence of the disease has immediate and long-term socioeconomic implications (Prince *et al.*, 2014). Classically there are two forms of this neurodegenerative condition. The familial/ early-onset form displaying an earlier manifestation (<65 years of age), albeit in fewer (<5%) AD cases and the sporadic/ late onset form which accounts for the majority (95%) of AD cases, where susceptibility

genes (described below) and their co-expressing environmental factors appear to exert influence (Bekris *et al.*, 2010).

1.1.1 Alzheimer's disease pathogenesis

AD has a bi-phasic criterion of diagnosis, which involves correlation of the clinical presentation and neuropathological examination at post-mortem (Braak and Braak, 1995). Despite the difference between familial and sporadic AD, the underlying neuropathology remains common to both forms. The two diagnostic neuropathological hallmarks are numerous extracellular deposits of amyloid-beta ($A\beta$ plaques) and hyperphosphorylation of neurofibrillary tangles (NFTs) in the frontal cortex and the hippocampal areas of the brain (Braak and Braak, 1995). Amyloid precursor protein (APP) is a protein situated in the neuronal cell membrane; part of APP is inside the membrane and part is outside (O'Brien and Wong, 2011) (Figure 1.1). APP helps cell repair and growth and is recycled continuously. APP can be cleaved by the enzymes alpha and gamma secretase to soluble peptides, however if the enzyme beta secretase cleaves APP with gamma secretase sequentially, the result is the amyloid beta peptide which can clump to form the senile $A\beta$ plaques (Figure 1.1).

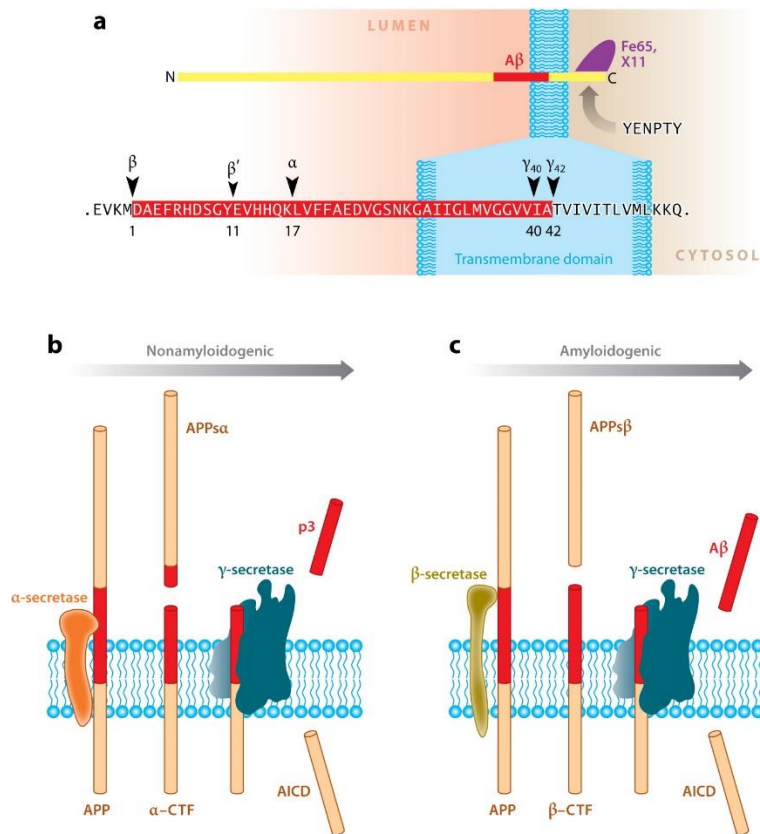


Figure 1.1 Cleavage of the amyloid precursor protein (APP) occurs by the two pathways. a. amyloid precursor protein (APP) is situated in the cell membrane of the neurone, partly inside and outside. The APP is recycled continuously and can be cleaved by different enzymes. b. if APP is cleaved by α -secretase followed by γ -secretase the product is a soluble peptide (p3) (non-amyloidogenic). c. If APP is cleaved by the enzyme β -secretase followed by γ -secretase, this produces the A β peptide which can misfold and aggregate to form A β plaques (amyloidogenic). Taken from O'Brien and Wong, 2011.

In the brain, the A β has many isoforms of different length, the most significant being the 40 residue A β 1-40 (most abundant in the brain) and the 42 residue peptide A β 1-42 (significantly increased in senile plaques observed in AD patient brains) (McGeer *et al.*, 2017). The A β peptides can exist as a soluble oligomers (monomers, dimers etc) in native conformation or as insoluble aggregates known as amyloid fibrils. The senile plaques are composed of densely packed A β 1-42, which morphologically can appear as stable β helical sheets or a tangle of A β oligomers and are known to be cytotoxic, causing demise of surrounding neurons (McGeer *et al.*, 2017).

The NFTs, located within cortical neurons, are composed of paired helical filaments (PHFs) and tau protein, the latter of which undergoes posttranslational modification in the form of hyperphosphorylation (p-tau). These classic diagnostic hallmark proteins establish in the brain of the AD individual while the asymptomatic developing neuropathology progress, sometimes over decades (Pritchard *et al.*, 2017).

Diagnosing AD early has benefits to the prognosis of the patient, as though no cure exists today, therapeutics slowing the progression of the disease are available (described in 1.1.3). Changes in the brain can be detected years before any dementia symptoms occur. These include measurable biochemical and neurophysiological changes and even anatomical alterations in the brain (Atri, 2019). Clinical criteria for diagnosing AD include history taking from the person or someone close to them and an objective cognitive assessment, of which there are various models (McKhann *et al.*, 2011). Neuroimaging and laboratory tests are also applied as part of the clinical diagnostic process. These include MRI scans of the brain, as atrophy of the hippocampus and the cortex of the temporal and parietal lobes are seen in AD (Atri, 2019). Amyloid or tau brain PET scans can also be useful in combination with blood or spinal fluid testing for elevated biomarkers such as A β 42, tau and phosphorylated tau (Teunissen *et al.*, 2022).

At post-mortem the brain tissues can be examined and staged according to the histological progression of AD, this staging system of AD related brain changes was developed by Braak and Braak (1991). Braak staging sets out a characteristic distribution pattern of AD induced neurofibrillary tangles and neuropil threads which allows the examiner to allocate the tissues to one of six stages of neurodegeneration (Braak and Braak, 1991). The lower two stages indicate only mild changes in sections of the brain, whereas the higher stages (five and six) are represented by much wider destruction. The Braak staging is used both clinically and in AD research. Therriault *et al.*, (2022) used PET scans to compare clinical symptoms and biomarkers to the Braak stage and found

that Braak stage one and two displayed no or only mild impairment, whereas stages five and six were incompatible with a normal level of cognition and function.

It is evident that the development of AD is related to the presence of both NFT and A β 1–42 plaques, but it is not fully understood how the two hallmarks are associated or interact. The defence and homeostasis of the neural tissues are mainly provided by astroglia and microglial cells and astroglia pathology has been linked to AD (Verkhatsky *et al.*, 2019a). In AD patients, a range of astrocyte pathologies have been identified in different stages of the disease and the main states are astrocytopathy with i) astroglial atrophy and functional loss and ii) reactive atrogliosis signified by hypertrophy of the cells. These changes (beyond the homeostatic protective steady state) to the function of the astrocytes causes an imbalance of ions and neurotransmitters presenting clinically as a reduction in synaptic function and neuronal hyper excitability (Verkhatsky *et al.*, 2019b), ultimately affecting cognitive function.

1.1.2 The hypotheses driving research into Alzheimer's disease

The research into AD over the past 20 years has been driven by a number of causative hypotheses. Though the main hallmarks seen in patients with AD are still A β plaques and NFTs, it is now evident that most AD patients have multiple pathologies present simultaneously and that certain clinical findings in AD patients overlap with patients diagnosed with other neurodegenerative conditions (Molinuevo *et al.*, 2018). This is why there has not been a single hypothesis that can explain the development of AD pathology. Even completely cognitively normal patients can display the same amount of A β plaques as someone with AD dementia, which has cast doubt on some of the main disease hypothesis (Pritchard *et al.*, 2017). Plaque formation is therefore seen as a natural part of ageing in some individuals and this emphasises that there are still a

significant number of unknown factors related to AD which require investigation.

The immunology of the brain is increasingly becoming a central part of the research in AD, predominantly the role of microglia (Spangenberg and Green, 2017) and the neurovascular unit (NVU). Much further knowledge of how the cells of the brain communicate and work together is required in order to understand AD pathology development. An outline of current AD hypotheses is detailed below.

1.1.2.1 The amyloid cascade hypothesis

The dominant hypothesis of progression of AD remains the “amyloid cascade”. This hypothesis suggests that a gradual deposition of A β triggers an inflammatory response, changing the homeostasis in the brain of kinase and phosphatase activity. This in turn induces oxidative stress and unbalances ion levels, leading to the formation of NFT's, followed by neuronal loss and synaptic dysfunction (Selkoe and Hardy, 2016).

Drug discovery programmes have focussed on reducing A β accumulation in the brain by targeting synthesis or clearance pathways. Clearance can be achieved by: i) drainage of interstitial fluid into the cerebrospinal fluid (CSF) via perivascular basement membranes; ii) phagocytosis by microglia or astrocytes; iii) receptor mediated P-glycoprotein (P-gp) efflux, such as lipoprotein receptor related protein 1 (LRP1) transport or very low-density lipoprotein receptor (VLDLR) or iii) enzymatic degradation by proteases including neprilysin (NEP), insulin-degrading enzyme (IDE), matrix metalloproteinase (MMP-9) and glutamate carboxypeptidase II (GCPII) (Yoon and Jo, 2012).

There is some evidence of genetic predisposition, however more recent studies and clinical drug trials have suggested that the soluble type of A β may be more toxic to the brain than the plaques themselves (Sengupta *et al.*, 2016) and therefore the original amyloid cascade hypothesis has recently faced some criticism. Doubt surrounding this hypothesis has also arisen due to numerous failures of clinical trials targeting the main

components of the theory and the presence of A β plaques in normal aged brains as mentioned previously (Pritchard *et al.*, 2017).

1.1.2.2 The vascular dysregulation hypothesis

Vascular pathology in the brain will reduce oxygen and nutrient supply and cause cell damage and dysfunction of the BBB (Di Marco *et al.*, 2015). These events lead to oxidative stress and inflammation, which has a toxic effect on the neurons (Di Marco *et al.*, 2015). The reduction in oxygen is thought to increase the activities of enzymes involved with cleaving APP to A β peptides and the induced disruption of the BBB means the clearance of these peptides is reduced, resulting in an accumulation (Salminen *et al.*, 2017). The link between vascular disease and AD does support this theory, but AD is not seen exclusively in this group of individuals and not every individual with vascular disease develops AD (Attems and Jellinger, 2014).

1.1.2.3 The calcium homeostasis hypothesis

An early manifestation of AD is a dysregulation showing elevated levels of calcium in the brain cells (Wang *et al.*, 2020). The intracellular levels of calcium near A β plaques are significantly increased, thus it has been hypothesised, that the early amyloid plaque forming pathways can remodel the calcium signalling pathways in the brain and cause the learning problems and memory deficits, seen in the early stages of dementia (described previously). This could also contribute to the neurodegeneration seen in the later stages of the disease (Berridge, 2010).

1.1.2.4 The cholinergic hypothesis

The cholinergic hypothesis of AD was developed in the 1970s based on the findings that individuals with AD have reduced levels of acetylcholine in the hippocampus and neocortex of the brain (Drachman and Leavitt, 1974). Impaired acetylcholine signalling is associated with dysfunction of muscle activity, short term memory and learning, which are also features of early AD presentation (Drachman and Leavitt, 1974). Acetylcholine dysfunction in the brains of individuals with AD has been attributed to reduced activity in the converting enzyme choline acetyltransferase (ChAT). Cognitive loss was observed in these patients, however there is no evidence of a direct aetiopathological relation between these findings (Kaur *et al.*, 2021).

1.1.2.5 The mitochondrial cascade hypothesis

Mitochondrial structural and functional differences have been observed in brain cells of AD patients (Swerdlow, 2018) and theories of either a primary or secondary mitochondrial cascade of AD have emerged. The primary cascade theory attributes impaired mitochondrial function to cause the accumulation of A β in the brain and the secondary cascade theory is centred on the A β causing the mitochondrial dysfunction (Area-Gomez *et al.*, 2018). It is currently not known whether the mitochondrial dysfunction observed in AD patients is an end-stage artifact or a disease associated finding or a contributing factor to the pathological development of AD (Swerdlow, 2018).

1.1.2.6 The metal ion hypothesis

The finding that the homeostasis of some metal ions was altered in the brains of AD patients and that this related to the level of A β plaques development and tau

accumulation, has fuelled the theory that metal ions of zinc, copper and iron could play a role in the pathological development of AD (Wang *et al.*, 2020). An elevated level of iron in the brains of AD patients has been attributed to neuronal death seen in the neurodegeneration (Levi and Finazzi, 2014). Both increased and reduced levels of copper and zinc have been implicated in AD, highlighting the sensitivity of the physiological functions of the brain to an imbalance of metal ions (Wang *et al.*, 2020). The subsequent oxidative stress brought on by ion imbalance could be a potential factor contributing to AD (Wang *et al.*, 2020).

1.1.2.7 The lymphatic system hypothesis

The glial-lymphatic system of the brain and the clearance of metabolic waste such as A β protein has recently been hypothesised to play a central role in AD development (Ding *et al.*, 2021). The activity of this clearance system is highly elevated during sleep and therefore sleep deprivation has been linked to reduced clearance of A β , suggesting a potential contribution to an imbalance and this protein aggregating in the brain (Xie *et al.*, 2013). This theory has also sought to explain how certain conditions where dysfunction or impairment of the glial-lymphatic system is seen (such as chronic traumatic encephalopathy, normal pressure hydrocephalus and diabetes mellitus) can be linked to development of AD (Ding *et al.*, 2021).

1.1.2.8 The Tau-hypothesis

One of the hallmarks of AD neural pathology is the presence of intraneuronal neurofibrillary tangles (NFT) of hyperphosphorylated tau protein (Do Carmo *et al.*, 2021) which has also been associated with other neurodegenerative disease (tauopathies) (Do Carmo *et al.*, 2021). Tau, the microtubule associated protein is found both intra and extra

cellularly in normal brain parenchyma and has an important physiological role in neurons regulating the assembly and maintenance of structure and stability of microtubules (Tapia-Rojas *et al.*, 2019). Abnormally hyperphosphorylated tau (p-tau) proteins misfold and become detached from microtubules and form aggregates with other tau proteins causing accumulation of insoluble filament tangles (NFTs) in neurons. Extensive investigations have researched the intracellular seeding and spread between cells of abnormal tau to reveal how the hyperphosphorylated proteins can become established and contribute to neurodegeneration (Frost *et al.*, 2009).

1.1.2.9 The inflammatory hypothesis

Neuroinflammation is part of the disease state of AD and it is thought that A β plaques and phosphorylated tau (p-tau) induce inflammation, characterised by activated astrocytes and microglial cells (Bronzuoli *et al.*, 2016). A prolonged activation can induce a pro-inflammatory phenotype in the astrocytes-microglial unit. This can cause the astrocytes and microglial cells to lose their protective and homeostatic abilities and as they often work in synchrony to maintain synaptic development and remodelling, these functions can be affected (Bronzuoli *et al.*, 2016). The subsequent pro-inflammatory molecules released can lead to neuronal death and induce further A β and p-tau formation (Bronzuoli *et al.*, 2016).

An infective cause of the inflammatory hypothesis of AD has been revisited in recent years, where it is proposed that the innate protection of the brain against infections deals with acute events, however, if a chronic microorganism assault on the BBB and cells involved with the homeostasis of the brain occurs, pathways are induced to initiate AD pathology (Pritchard *et al.*, 2017) (Figure 1.2). The finding that A β is an antimicrobial peptide (Soscia *et al.*, 2010; Kumar *et al.*, 2016) has fuelled the hypothesis that AD is

initiated by microbials, inducing a response in the brain leading to the formation of senile plaques and p-tau.

Hundreds of synergistic species of bacteria reside within the organ specific microbiomes (nose, mouth, skin, blood and gastrointestinal (GI) tract) and these outnumber the entire cells making up the human body. The importance of the benefits of the host microbiome and the balance for maintenance of health is beginning to be realised (Valdes *et al.*, 2018). It is thought that both microorganisms from the resident microbiome (oral and GI) and external pathogens can be potential participants in the induction of AD (Nara *et al.*, 2021). The findings of numerous microorganism components in AD post-mortem brains from bacteria, virus and fungi (Hill *et al.*, 2014; Itzhaki, 2016; Lukiw, 2016; Pistollato *et al.*, 2016; Alonso *et al.*, 2017; Harris and Harris, 2017; Jiang *et al.*, 2017; Maheshwari and Eslick, 2017; Zhao *et al.*, 2017) suggest that it is likely that a community of microorganisms may be involved in triggering AD.

Since it is established that A β can act as an antimicrobial peptide (Soscia *et al.*, 2010), an expected consequence to microorganisms entering the brain would be that of death, specifically in the context of AD. This together with the already highly inflamed environment of the AD brain, ongoing glial cell activity is likely to kill bacteria and prevent brain abscesses forming, whilst only retaining bacterial virulence factors such as LPS and microbial gDNA signatures in the brain tissues. The induction of A β formation would then act as an enforcement of the inflammatory state, especially if chronic activation of immune cells in the brain could lead to “senescence” of the immune cells, reducing the clearance of A β . The seed is sown to a circle of events which could lead to the pathological hallmarks seen in AD. From an infection hypothesis point of view, the heterogeneity of susceptibility and risk factors for developing late onset AD could be explained by different triggers interacting with genetic and immunologic factors in the host (Costa *et al.*, 2017; Carter *et al.*, 2017).

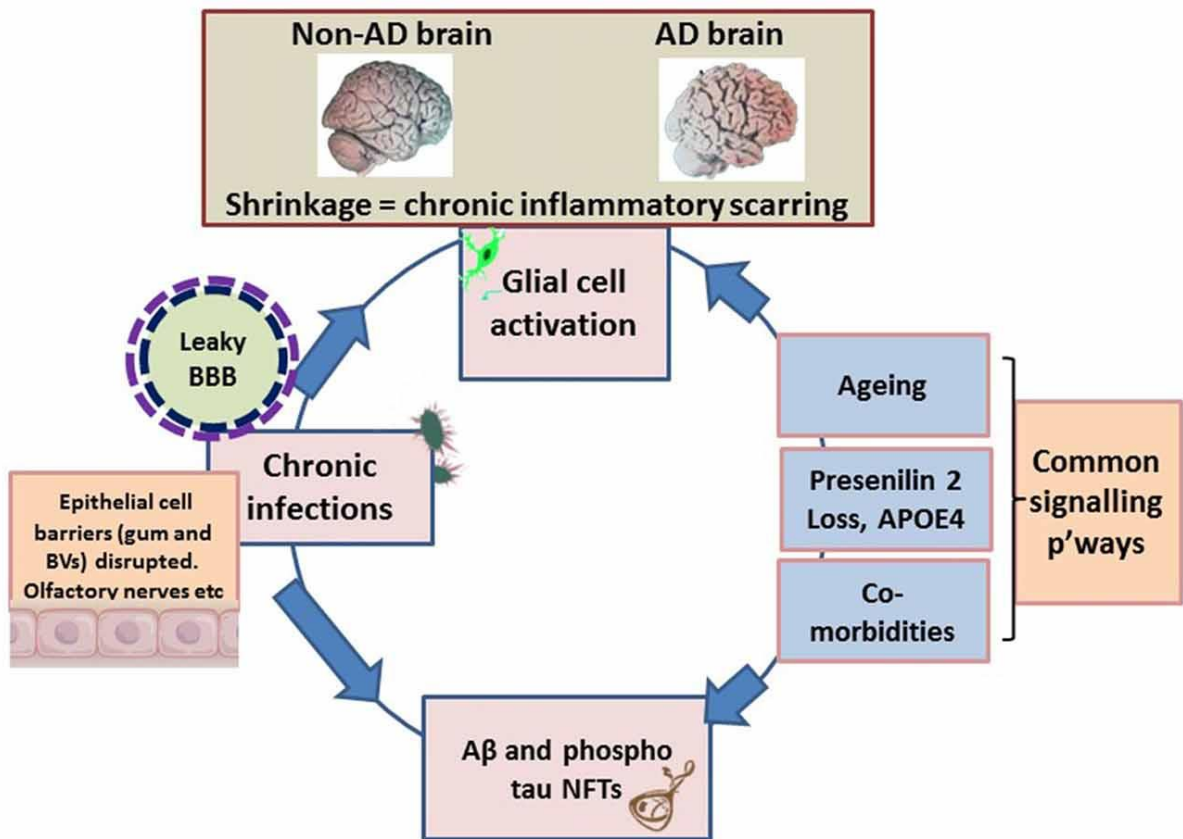


Figure 1.2 Schematic illustrating the macroscopic features relating to shrinkage (wider sulci, compared with non-Alzheimer's disease (AD) brain), unique to the AD brain, which equates to inflammatory condition. The pathogens disrupt the epithelial cell-to-cell proteins of the gingivae through their proteases. The epithelial/endothelial barriers of capillaries disrupted for effective bacteremia to take place. Environmental factors are the inflammophilic microorganisms with potential to subvert hosts immune defenses that also contribute to common inflammatory activities/pathways as well as contributing to proteostasis. At this stage the brain's resilience is markedly compromised and the blood-brain barrier (BBB) is becoming defective. The endotoxin intolerance/further inflammation tip the brain into disease (taken from Pritchard et al., 2017).

The suggested sequence of AD pathophysiology likely to follow infections would be A β deposition and glial cell activation. These events may also provide an explanation for age-related glial cell priming resulting in an exaggerated immune reactivity to secondary insult (Jayadev et al., 2013; Fan et al., 2017; Wu et al., 2017).

1.1.3 Prognosis/ Treatment/Prevention of AD

There is currently no cure for AD, but an increased awareness of the disease and improvements in diagnostic techniques and community response to the disease has improved the outlook for the AD patients. There is a small selection of drugs available which can reduce some of the symptoms of AD, however the ultimate path of the disease is steady decline in cognitive and motor functional abilities, accelerating a state of ageing, often resulting in death following a course of infections.

Diagnosis of AD is often late in the development of the disease when the brain is at organ failure stage (previously described). Conducting clinical trials with drugs which can prevent the accumulation of senile plaques poses ethical problems, such as leaving control individuals without active treatment. The lack of a cure for AD has guided substantial research efforts to identifying risk factors for AD with an aim to increase the knowledge of prevention of onset of the disease (Rosenberg *et al.*, 2018).

Recognised modifiable risk factors for developing dementia late in life include midlife hypertension, high cholesterol, obesity, diabetes mellitus, smoking, physical inactivity, depression and low levels of education (Rosenberg *et al.*, 2018). In the absence of any therapeutic advances, the prevention of AD is increasingly being recognised and supported as an important area of research to inform community health strategies.

There is currently no drug which can prevent AD, though one drug has recently obtained FDA licence in the USA (aducanumab) on the premise of reducing A β plaques in the brains of AD patients (Walsh *et al.*, 2021), though there has been controversy surrounding this treatment and trials are still ongoing and some have been inconclusive (Walsh *et al.*, 2021).

There are currently multiple clinical trials testing anti-A β monoclonal antibodies, targeting different sites on the A β peptide (such as aducanumab) (Jin *et al.*, 2018). The lack of

highly efficacious novel therapeutic discoveries has been attributed to a relative lack of target selectivity and the late stage of the disease where intervention has been directed. This has meant designing clinical trials is difficult, due to AD having a complex aetiology and considerable heterogeneity in the late-stage pathophysiology (Jin *et al.*, 2018).

The use of blood and cerebrospinal fluid biomarkers (mainly the latter) can potentially indicate early AD pathology presence, before any clinical symptoms are displayed (as previously described) (Molinuevo *et al.*, 2018) and markers for cerebrospinal fluid (CSF) A β 42, total tau and p-tau are mainly being used in drug development programmes and clinical trials but are also used in some countries as part of the AD diagnostic pathway. The importance of early diagnosis is paramount in AD management and essential for the improvement of the efficacy of pharmacological interventions available for AD. Before aducanumab was approved for human use, the treatment of AD encompassed two types of drugs, which reduced some of the symptoms of AD: i) cholinesterase inhibitors and ii) n-methyl-d-aspartate (NMDA) receptor antagonists (Szeto and Lewis, 2016). Donepezil, rivastigmine and galantamine binds and reversibly inactivates the cholinesterase resulting in inhibition of the hydrolysis of acetylcholine (Szeto and Lewis, 2016). This increases acetylcholine concentrations at cholinergic synapses, thereby increasing neurotransmission (Szeto and Lewis, 2016). Clinical trials have shown that donepezil can ameliorate the cognitive ability of AD patients (Ma *et al.*, 2018; Jia *et al.*, 2017), and decrease the A β level in peripheral blood. This is beneficial as aggregation of serum A β can elevate oxygen-free radicals and pro-inflammatory cytokines, leading to apoptosis and neurodegenerative changes (Ma *et al.*, 2018).

An NMDA receptor antagonist (such as memantine) blocks the effects of glutamate (the dominant fast-acting neurotransmitter in the brain), which is released in excessive amounts in the brains of people with AD (Khan and Bloom, 2016). Free-floating glutamate in the brain is highly toxic and causes damage to brain cells and disrupts neuronal activity (Ma *et al.*, 2018). p- tau is thought to become displaced to somato-

dendritic compartments, where it will interact with A β and cause excessive activation of the NMDA receptors (Khan and Bloom, 2016).

A meta- analysis of 41 randomised controlled trials (RCT) (Dou *et al.*, 2018) indicated that galantamine and donepezil could give the best efficacy in cognition in individuals with mild to moderate AD. For the moderate to severe patients, it has been found that combination therapy (memantine with donepezil) and donepezil (a once-daily high dose tablet) provided the best outcome (Sabbagh *et al.*, 2016). It has also been highlighted how the combination drug and once daily administration, is beneficial to AD patients cared for in the home by relatives, to ease the carer burden (Kishi *et al.*, 2017).

The influx of microorganisms into the CNS earlier in life could be another modifiable risk factor for developing AD, i.e., the prevention of chronic inflammatory states could potentially be a major factor in the future prevention of AD. A chronic supply of bacteria to the CNS could be generated by the dysbiotic infection in periodontal pocket seen in chronic PD.

1.2 Periodontal disease

The oral cavity is a home to over 770 different taxa and undoubtedly, this specific microbiome will keep growing as changing bacterial species are included (Deo and Deshmukh, 2019).

Periodontal disease (PD) is one of the most common chronic polymicrobial infections in humans, characterized by loss of tooth supporting tissues due to the host's immuno-inflammatory responses. PD is prevalent in individuals with poor oral hygiene and a high dental plaque index (Paganini-Hill *et al.*, 2012) and is associated with ulceration of the periodontal pocket lining. This breach in the epithelial integument allows access to the

systemic circulation of those bacteria present in the region of the disease process (Genco and Van Dyke, 2010).

At present, much smaller numbers (1×10^9 /pocket) of mixed bacterial phyla (Loesche and Lopatin, 1998) are associated with periodontitis within this subgingival niche compared to the oral cavity where 1×10^{11} bacteria/mg of dental plaque are recorded (Li *et al.*, 2000). Dental plaque is a biofilm of a synergistic microbial community and both genetic and environmental factors can cause it to become dysbiotic, leading to clinical manifestations of periodontitis (Figure 1.3).

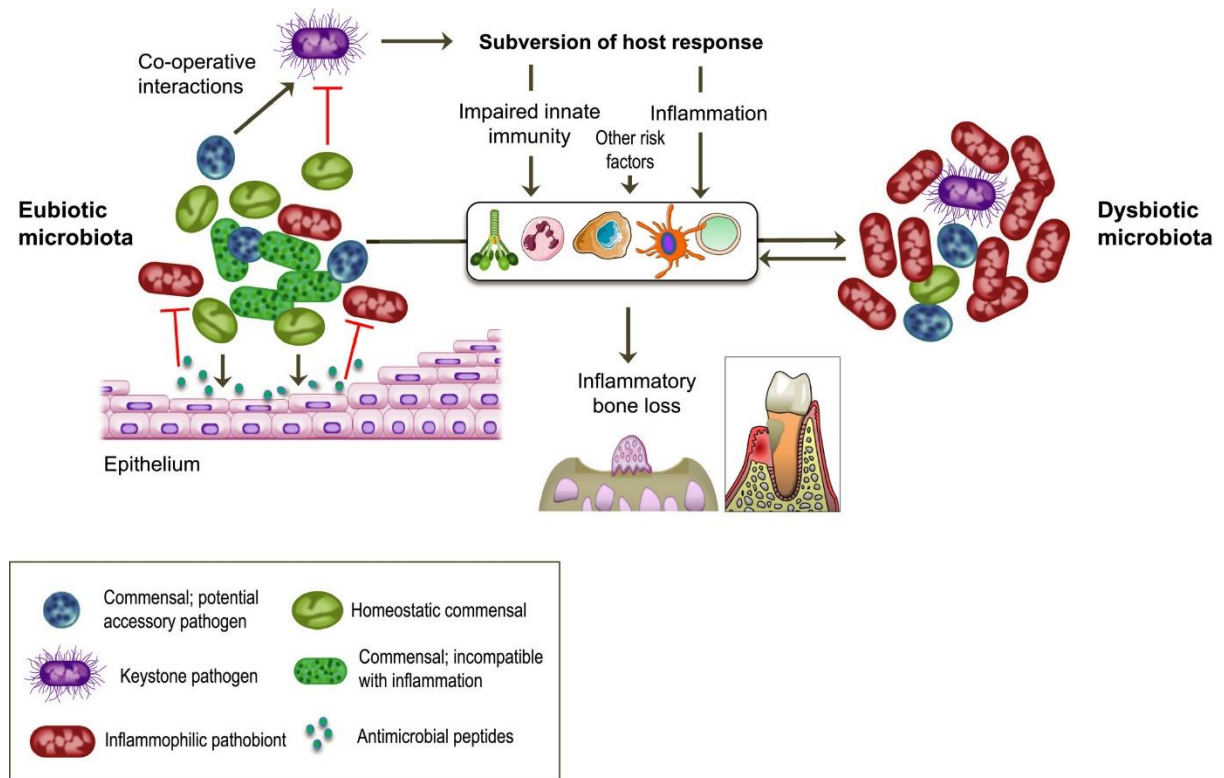


Figure 1.3 The development of plaque biofilm around the gingival margins of the teeth and the presence of keystone pathogens such as *P. gingivalis* can lead to dysbiosis in the microbial community. The development of dysbiosis is governed by factors such as host response and environmental factors and if the state becomes chronic it will lead to inflammatory attachment and bone loss. (Hajishengallis and Lamont, 2000).

It has been established for a while that the progress of periodontal disease is driven by dysbiotic periodontal microbial communities, where certain microbes stand out as potentially modulating the environment towards a diseased state. These alpha bugs or keystone pathogens can disrupt the homeostasis in tissues even in low numbers.

One such example of an opportunistic keystone periodontal pathogen is *Porphyromonas gingivalis* (*P. gingivalis*), which to date, 19 strains have been identified with varying pathogenicity and ability to invade cells and tissues, such as gingival epithelial and mucosa (Chen *et al.*, 2017b). This Gram-negative anaerobic rod can change both the composition and synergy of a biofilm community, influence how the host responds to the insult and is a master immune evader (Hajishengallis and Lamont, 2016).

P. gingivalis rely on early colonizers such as Gram+ streptococci to get a foothold (Nara *et al.*, 2021), then bridging cultures such as *Fusobacterium nucleatum* (Sbordone and Bortolaia, 2003) allows *P. gingivalis* to colonize later and in smaller numbers.

Regarding PD, we can no longer look at a microorganism and say it belongs to a certain group, either commensal or pathogenic. It simply depends on how the microbe interacts with other members of the biofilm and the state of the host. The concept of nososymbiocity reflects how microorganisms in the indigenous community can have the potential to cause disease. Some common examples of bacteria in the periodontal microbiome include *P. gingivalis*, as mentioned previously, as well as *Tannerella forsythia*, *Prevotella intermedia*, *Eikenella corrodens*, *Fusobacterium nucleatum*, *Aggregatibacter actinomycetemcomitans* and *Treponema denticola* (Hajishengallis and Lamont, 2014).

It is recognised that *P. gingivalis* plays a role in remote organ pathology, in particular chronic inflammatory conditions, as well as PD (Mulhall *et al.*, 2020). The increased evidence base in recent years has added to our growing understanding of how important oral health is to systemic health (Bregaint *et al.*, 2022). A summary of some of the links

between *P. gingivalis* and remote organ pathology are shown in Figure 1.4 and Table 1.1. Though it is not yet fully clear whether it is the *P. gingivalis* bacterial cells or their virulence factors that are the inducers of the conditions seen in organs remote to the oral cavity (Bregaint *et al.*, 2022).

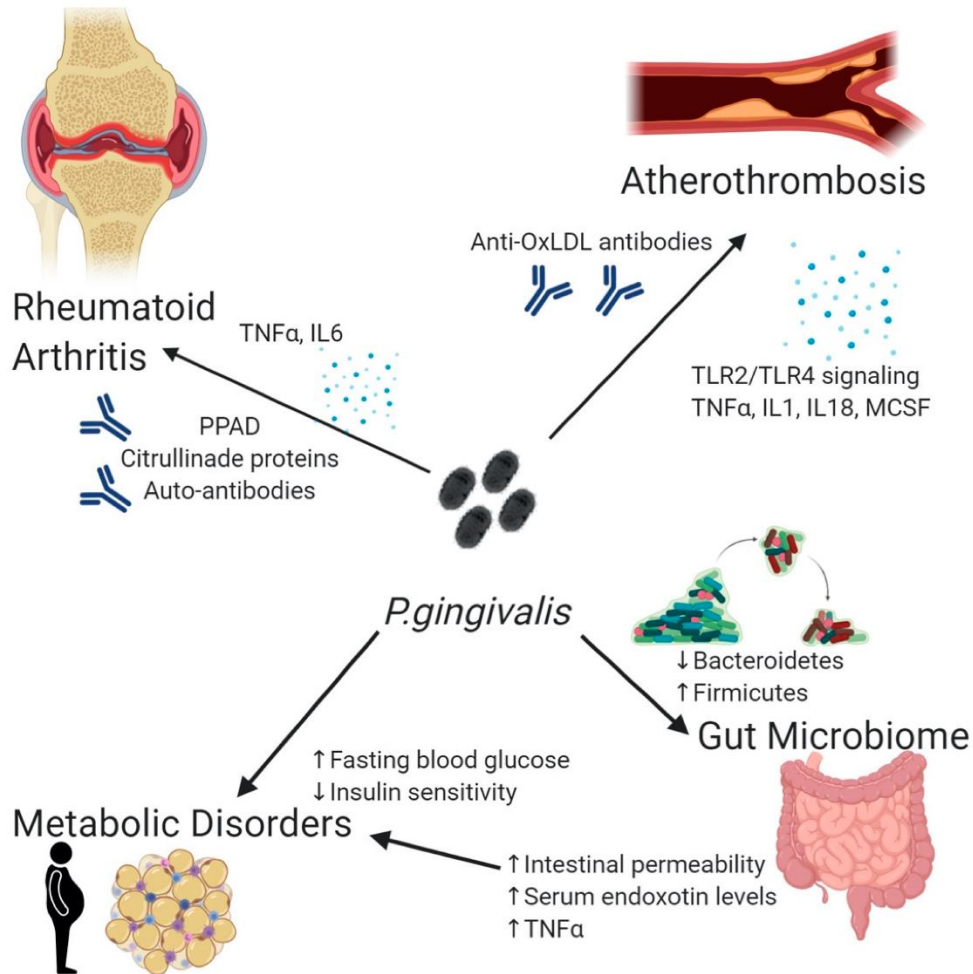


Figure 1.4 *Porphyromonas gingivalis* is linked to the development of multiple chronic inflammatory conditions. Through the cross-reactive antibodies (atherothrombosis, rheumatoid arthritis), increased levels of systemic inflammation (atherothrombosis, rheumatoid arthritis, gut microbiome dysbiosis, metabolic disorders), as well as overall microbiome dysbiosis. (\uparrow = increase \downarrow = decrease) (taken from Mulhall *et al.*, 2020).

Table 1.1 *P. gingivalis* has been linked to organ pathologies remote from the oral cavity such as AD, rheumatoid arthritis, adverse pregnancy outcomes (mainly in the first trimester), cardiovascular, liver and respiratory disease.

<i>P. gingivalis</i> links to pathology outside the oral cavity	
organ	pathology
Brain	Neurodegeneration (Langisch <i>et al.</i> , 2018; Illievski <i>et al.</i> , 2018)
Joints	Rheumatoid arthritis (de Molon <i>et al.</i> , 2019; Moen <i>et al.</i> , 2006)
Placenta	Averse pregnancy outcomes (Reyes <i>et al.</i> , 2017)
Heart/ Coronary arteries	Cardiovascular disease, atherosclerotic plaques formation (Herzberg and Meyer, 1996; Bohnstedt <i>et al.</i> , 2010)
Lungs	Exacerbation of chronic obstructive pulmonary disease (COPD) (Takahashi <i>et al.</i> , 2012; Nagaoka <i>et al.</i> , 2017)
Liver	Non-fatty liver disease, pancreatic cancer (Yoneda <i>et al.</i> , 2012; Michaud 2012)
GI system	GI microbiome dysbiosis, metabolic disorders (Mulhall <i>et al.</i> , 2020)

The chronicity of periodontal disease, resulting in a potentially prolonged assault by a group of pathogens on the host's system, opens the opportunity of specific microorganisms inducing a state where the host's threshold for disease exceeds that of health allowing local and remote organ pathology to develop and *P. gingivalis* is recognised as a key player in this process.

1.2.1 *Porphyromonas gingivalis*

P. gingivalis, an anaerobic black pigmented Gram-negative coccobacillus, is a key pathogen of PD, though it only constitutes 0.8 % of the biofilm in PD (Kumar *et al.*, 2006).

P. gingivalis has numerous mechanisms by which it can affect the surrounding tissues including: i) endotoxin or lipopolysaccharide (LPS) mainly located on the outer membrane and ii) via release of outer membrane vesicles (OMVs) by the Type IX secretion system (Nara *et al.*, 2021). These OMVs are packed full of proteolytic enzymes, gingipains, more accurately lysine specific gingipains (Kgp) and arginine specific gingipains (RgpA/B) (Vermilyea *et al.*, 2021).

A unique virulence factor to *P. gingivalis* is peptidylarginine deaminase (PPAD) which citrullinates peptides (Nara *et al.*, 2021). *P. gingivalis* is non spore forming and normally classed as immotile, however Vermilyea *et al.*, (2021) recently showed that *P. gingivalis* strain 381 is capable of migration, allowing cells to translocate along a surface. This study also found that the PPAD transcription was increased during this process and that PPAD positively impacted on the cells production of OMVs, which would then result in increased proteolysis (Vermilyea *et al.*, 2021). The authors stated that PPAD are regulators of arginine levels (substrate for PPAD), digestion of proteins, the wetting zone required for cell translocation and citrullination of adhesion domains on the bacteria itself (Vermilyea *et al.*, 2021) which highlights the importance of this enzyme to the virulence of the bacteria. See Table 1.2 for a full list of known virulence factors associated with *P. gingivalis* and the direct effect they have on the cells in the oral cavity.

Table 1.2 Known virulence factors associated with *P. gingivalis* and their known effects on the tissues and components in the oral cavity (Bregaint et al., 2022, Xu et al., 2020; Nara et al., 2021; Tribble et al., 2007)

Virulence factor associated with <i>P. gingivalis</i>	Direct effect on tissues and components of the oral cavity
Lipopolysaccharide (LPS)	Pathogen associated molecular pattern (PAMP) endotoxin inducing host immune response via Toll like receptors (TLR)
Fimbriae	Attach to epithelial cells, fibroblasts and a variety of host molecules and substrates, enhance biofilm formation
Gingipains	Cysteine proteinases, proteolysis of immune components and host tissues, enhancement of interactions with other bacteria in the oral microbione (biofilm), inhibition of coagulation
Capsule	Protective mechanism for <i>P. gingivalis</i> against phagocytosis and cellular killing, co-aggregation in biofilm
Peptidylarginine deaminase (PPAD)	Citrullination of peptides
Outer membrane vesicles (OMV)	Incorporate fimbriae, LPS and gingipains along with other proteins, host immune response (inflammation), internalising in host cells, proteolysis as described above, PAMP
Hemagglutinins	Adherence molecule adherence to gingival tissue cells and erythrocytes prior to lysis
Hemolysins	Heme acquisition from hemoproteins present in saliva, gingival crevicular fluid, and erythrocytes
DNA	Transfer chromosomal DNA between strains to adapt to the environment

P. gingivalis is adapted to tolerate a range of environments such as temperatures from 35 – 39 °C, pH between 5.5 – 8.5 (is both acidophilic and alkaliphilic) and though it is obligatory anaerobic, it tolerates both high and low oxygen tensions (Nara *et al.*, 2021). *P. gingivalis* is asaccharolytic and tolerates nutritionally deficient conditions being oligotrophic, though it does require hemin and Vitamin K for growth (Nara *et al.*, 2021). When *P. gingivalis* causes dysbiosis, an increase in short chain fatty acids is observed. Vermilyea *et al.* (2021) suggested that the citrullination of peptides by PPAD could exacerbate inflammation, if antibodies against these peptide products increases, explaining the association between PD and inflammatory arthritic disease (Vermilyea *et al.*, 2021). *P. gingivalis* is capable of migration between host cells by intercellular translocation (Takeuchi *et al.*, 2011) and it leaves the cells by an endocytotic recycling pathway.

The virulence or invasive ability of a *P. gingivalis* strain can be classified according to the expression of fimbriae, capsule, LPS and gingipains release (Dorn *et al.*, 2000). These virulence factors originate from the mother cell but are disseminated wider by release of OMVs. As an example, the non-capsulated laboratory strain FDC 381 has been shown to invade carcinoma cells 10^3 times more than other *P. gingivalis* strains (Dorn *et al.*, 2000), though FDC 381 is classed as a less virulent type causing only mild localised abscesses (Yoshino *et al.*, 2007). These findings highlight two key aspects of *P. gingivalis* behaviour which have significance for pathological development, the ability of the bacterium to i) invade tissues and ii) modulate the subsequent immune response of the host. Furthermore, a variance between different invasive abilities of OMVs from *P. gingivalis* strains has been attributed to the expression of long fimbriae (not FimA) and the gingipain adhesive domains in the outer membrane (Ha *et al.*, 2020). Fimbriae are surface appendages, which influence the bacterium's ability to adhere to other cells both host and microorganisms in the biofilm and they also affect the motility of the bacterium (Xu *et al.*, 2020). Long or short fimbria are expressed on *P. gingivalis* strains and where

the long fimbriae have been linked to an increased ability of adherence, the short fimbriae are thought to act as a more specific ligand to cell receptors of the host and other microorganisms (Xu *et al.*, 2020). The fimbriae incorporated into OMVs have been found to be more virulent if containing FimA genotypes II and IV (Han *et al.*, 2019), potentially because of an increased activation of the hosts immune response (Xu *et al.*, 2020).

OMVs of *P. gingivalis* are highly enriched in the proteolytic gingipains (RgpA/B and Kgp) located on the surface and the nano sized spheres and they also incorporate high concentrations of LPS and fimbriae (Veith *et al.*, 2014). The OMVs are sustainable in human tissues such as the brain (Abe *et al.*, 1998) and once internalised, OMVs are associated with cell degradation (Furuta *et al.*, 2009) and induction of an innate immune response with a greater intensity than initiated by the bacteria itself.

P. gingivalis OMVs, containing a high concentration of enzymes, are considered to have both harmful and beneficial roles, enabling *P. gingivalis* to regulate its microenvironment (Olsen and Amano, 2015). They have been found to contain 151 identified concentrated molecular components where of 51% are peptidases (Veith *et al.*, 2014). Gingipains are also believed to help *P. gingivalis* evade the immune system, making *P. gingivalis* so successful in establishing a chronic diseased state (Hajishengallis, 2011).

Bacterial adaptive immune systems, such as the clustered regularly interspaced short palindromic repeats associated protein (CRISPR-cas) system has evolved as a way for bacteria to defend themselves (Solbiati *et al.*, 2020) and a component of these are bacteriophages, which are viruses that internalise and kill other bacteria. So far, no bacteriophages have been shown to invade *P. gingivalis* (Nara *et al.*, 2021), which could be a unique defensive trait of this pathogen. The key to how periodontal disease is established and progresses is related to the polymorphism of the microbe and how the host responds (Chen *et al.*, 2017b). *P. gingivalis* can gene transfer, resulting in allele

combinations expressed by higher virulent strains (Olsen *et al.*, 2018) and in combination with its immune evasion abilities (Hajishengallis, 2015), this bacterium can manipulate its environment and other species to become increasingly established.

P. gingivalis has also been shown to dysregulate dendritic cells by disturbing their ability toward autophagy and apoptosis (Meghil *et al.*, 2019) endowing this pathogen with an exceptional ability for self-preservation. Labelled *P. gingivalis* OMVs have also been shown to be taken up by cortical microglial cells in mice, 24 -48 hours after peripheral injection, highlighting the potential reach of this virulence factor (Singhrao and Olsen, 2018). It has even been suggested that OMVs may act as a decoy to the host immune system, diverting attention and thus protecting the mother cell from elimination (Deatherage and Cookson, 2012), forming another element of *P. gingivalis*' immune evasive strategy. The size and proteolytic capacity of the OMVs makes the spread into tissues easier than for the intact bacteria and OMVs are more likely to survive transport to remote organs.

LPS from the outer membrane of Gram-negative bacteria is a powerful pro-inflammatory pathogen associated molecular pattern (PAMP) and previous studies support the capabilities of oral bacterial LPS as an inducer of peripheral inflammatory responses and as an initiating factor in intracerebral inflammatory activity (Dominy *et al.*, 2019; Ilievski *et al.*, 2018). The LPS of *P. gingivalis* has been extensively studied in relation to its pathogenicity. LPS of *P. gingivalis* is found in both a soluble and membrane bound form and binds to toll like receptor 4 (TLR4) enhanced by soluble cluster of differentiation 14 receptor (sCD14) (Nativel *et al.*, 2017) activating pro-inflammatory pathways.

P. gingivalis gingipains also affect cellular functions related to immune signalling.

The role of *P. gingivalis* negating the adaptive immune system relates to suppression of interleukin (IL-2) cytokine secretion (Olsen *et al.*, 2016). The lack of IL-2 enhances innate and humoral immune responses resulting in a different cytokine profile. This changes the

T helper 17 (Th17) cell lineage, in the modulation of the Th17/T-regulatory cell (Treg) clone formation. The result is an imbalance in Th17 and Treg populations (Olsen and Singhrao, 2016). *P. gingivalis* has been shown to secrete OMVs internally in cells but the OMVs affinity to internalise surpasses that of the bacterial cell (Furuta *et al.*, 2009). In summary *P. gingivalis* is a bacterium with a vast arsenal of ways to manipulate its surroundings to cause pathology. OMVs are highly virulent particles which can invade tissues, modulate cellular functions, avoid the immune response and supply the bacterial cells with nutritional components such as proteins and heme (by breaking down hemoglobin) (Veith *et al.*, 2014). The attributes of OMVs makes it plausible that the virulence factors of *P. gingivalis* could manipulate organs remote to the primary niche of *P. gingivalis*.

1.3 The link between Alzheimer's disease and periodontal disease

It is clear from longitudinal monitoring of patients, that chronic periodontitis is associated with declining cognition and animal studies have shown a correlation between the chronic application of *P. gingivalis* orally and the build-up of amyloid-beta (A β) plaques in the brain (Illievski *et al.*, 2018). In periodontitis, the localised bacterial accumulation results in stimulations that elicit inflammation and activation of the innate immune system. Influx of systemic inflammatory cells follows a short time afterwards by an adaptive immune cell response leading to tissue loss (Di Benedetto *et al.*, 2013; Olsen and Singhrao, 2015; Olsen *et al.*, 2016). A recent systematic review in which meta-analysis of periodontitis with AD was conducted, demonstrated a significant association between these two diseases (Odds Ratio (OR) 1.69, 95% CI 1.21–2.35) and an even more significant association was observed in severe form of PD with AD (OR 2.98, 95%

CI 1.58–5.62) (Leira *et al.*, 2017). A population based retrospective study by Chen *et al.* (2017a) demonstrated a 10-year, exposure of chronic periodontitis led to a higher risk (1.707-fold increase) of developing AD. Previous reports have alluded to the existence of an unexplored microbiome in the elderly and AD brains (Riviere *et al.*, 2002), but the age at which infection takes hold in the brain is unknown.

Biomarker studies using positron emission tomography for levels of A β , and magnetic resonance imaging for brain volume, indicate that AD onset begins decades before the clinical picture emerges (McGeer *et al.*, 2017). This implies that age-related priming of glia due to bacterial entry from the host's dysbiotic microbiomes elsewhere in the body (such as oral or GI tract) could provide slow inflammatory damage.

In support, oral pathogens, especially *P. gingivalis*, thrive under toxic inflammatory conditions and if present, may dampen the early pathogenic effects of glial cell activation (Singh Rao *et al.*, 2015). This makes the findings from the study by Chen *et al.*, (2017a), suggesting a 10-year exposure to chronic periodontitis may lead to manifesting AD very plausible (Chen *et al.*, 2017a).

Undoubtedly, a complex aetiology underlies the clinical manifestations seen in AD. Candidate microbes conforming to the AD microbiome would be those that induce immunosuppression, are pathogenic, are able to evade the innate and adaptive immune recognition, incite local inflammation and are incapable of allowing entry of activated peripheral blood myeloid cells in the brain. The periodontal microbiome does concur with the type of expected bacteria in AD brains. As an analogy to the dysbiotic periodontal microbial communities driving periodontal disease, the AD microbiome may reflect similar traits.

P. gingivalis, is a master immune evader and an immunosuppressor of the host through interleukin 2 (IL-2) suppression (Olsen *et al.*, 2016). Although *P. gingivalis* lacks the curli gene (which has been associated with AD pathology), it has alternative inflammatory

mechanisms to indirectly activate β secretases and contribute to host derived A β as well as correlate with loss of mental function (Olsen *et al.*, 2016). *P. gingivalis* and selective spirochetes, have developed immune avoidance strategies threatening the host-microbe homeostasis (Olsen *et al.*, 2016).

Recent studies have managed to identify parts of the microbiome associated with AD post-mortem tissues (Emery *et al.*, 2017; Pisa *et al.*, 2017; and Alonso *et al.*, 2018). Emery *et al.* (2017) found 5–10-fold more bacterial reads in AD post-mortem brain tissues by next generation sequencing and Actinobacteria was the largest component in the AD cases compared to non-AD controls. However, Emery *et al.* (2017) did not find any of the species commonly associated with periodontal disease. Pisa *et al.* (2017) analysed AD brains by polymerase chain reaction (PCR) of the V3–V4 region of the prokaryotic 16S rRNA gene and found that bacterial infection can coexist with fungi in the brain. They found several bacterial species in all the ten AD brains examined and the most prominent presence were of the genus *Burkholderia* (Pisa *et al.*, 2017). This group also found bacteria in the control cases which correlate with other studies of healthy individuals (Branton *et al.*, 2013; Païssé *et al.*, 2016). The same research group went further (Alonso *et al.*, 2018) and examined post-mortem AD brain tissue and non-diseased controls by immunohistochemistry and next-generation sequencing and they examined the difference in younger and older individuals and different sites of the brain. Alonso *et al.* (2018) found presence of both bacteria and fungi in both the AD and control cases. The bacterial phylum Proteobacteria was the most prominent in both AD patients and controls, followed by Firmicutes, Actinobacteria, and Bacteroides. At the family level, *Burkholderiaceae* and *Staphylococcaceae* were present at higher percentages in AD brains than in the control brains and this variation could potentially represent a difference in the pathogenicity of the bacterial population in the brain of diseased individuals (Alonso *et al.*, 2018). Further to this, it was recently shown that repeated oral application of *P. gingivalis* in wild type mice resulted in neurodegeneration

and formation of extracellular A β 1-42 plaques (Illievski *et al.*, 2018).

Since age is the major risk factor for developing AD, then evolving microbiomes may provide dynamics of the microbial communities over time. To this end, Brandscheid *et al.* (2017) examined changes in microbial communities in the GI tract of the 5XFAD AD transgenic mouse model and confirmed changes to microbial communities occurred over time. The changing microbes correlated with changes in trypsin secretions (Brandscheid *et al.*, 2017), implying meat rich diets are indigestible in old age and excess protein may upset the existing microbial community dynamics. If two main phyla of GI tract bacteria are Firmicutes (approximately 80%) and Bacteroidetes (approximately 20%) (Lukiw, 2016); it appears that during aging humans also undergo shifts in favour of Bacteroidetes in their GI tract microbiome (Pistollato *et al.*, 2016). *P. gingivalis* is a species within the genus *Porphyromonas* (within the phylum Bacteroidetes) and with periodontitis becoming more chronic and prevalent in old age, this would imply that the periodontal microbiome offers a relatively early indication of changing microbial dynamics. An AD-specific microbiome might be composed of bacteria from associated dysbiotic microbiomes because microbial infections explain the common inflammatory pathways (Olsen and Singhrao, 2015; Lukiw, 2016; Olsen *et al.*, 2016) and their effects in the elderly brain via the host's peripheral immune responses and related signalling pathways. The predominant signalling cascades participating in the innate immune system in AD pathogenesis include the Toll-like receptor (TLR) pathways. LPS application in rodents demonstrate participation of TLRs, CD14 and NF- κ B signalling cascades (Olsen and Singhrao, 2015; Lukiw, 2016) and indicates that acute phase inflammation is beneficial, whilst chronic organ specific inflammation is detrimental (Dicarlo *et al.*, 2001; Sheng *et al.*, 2003; Lee *et al.*, 2010; Herber-Jonat *et al.*, 2011). *Salmonella abortus equi* LPS inoculations in the hippocampus of rTg4510 mice carrying the parental tau mutations and non-transgenic littermates (Lee *et al.*, 2010), exhibited an initial neuroinflammatory activity, followed by increased Ser199/202 and tau phosphorylation (p-tau Ser396) in the

mutated group (Lee *et al.*, 2010). These results demonstrate the role of several bacteria (host microbiome derived and extrinsic) and host's genetic susceptibility contributing to inflammatory stimuli subsequent to which tau phosphorylation (Lee *et al.*, 2010) takes place. In other words, the signalling pathways participating in innate immune mediator release have the potential to modify the phosphorylation bound tau protein by post-translational means, in the vulnerable host, at any time. Thus, NFT formation could be both dependent and independent of A β deposits.

With relevance to AD pathology, a defective blood brain barrier (BBB) is documented (Montagne *et al.*, 2015; Halliday *et al.*, 2016) and a plausible explanation for the increased permeability is loss of cell-cell tight junctional proteins. Some bacteria such as *P. gingivalis* also contains proteolytic enzymes (gingipains) that cleave and fragment proteins into smaller peptides. The proteolytic activity of gingipains has been shown to target cell-cell adhesion molecules in *in vitro* studies (Katz *et al.*, 2000; Hintermann *et al.*, 2002; Sheets *et al.*, 2005). It is, therefore, likely that gingipains also contribute to the degradation of endothelial cell tight junction proteins and contribute to loss of BBB functional integrity. In support of this hypothesis, *P. gingivalis* infected animal models demonstrated hippocampal damage via inflammation-mediated injury and IgG and gingipains in the cerebral microvasculature (Singh Rao *et al.*, 2017). In addition, the phagocytic oxidative burst of the host's neutrophils and macrophages at a much earlier time point of *P. gingivalis* infection and the oxidative stress response initiated by bacteria can equally damage the hippocampal microvasculature (Rokad *et al.*, 2017).

A permeable BBB also has implications for entry of extra-cerebral amyloid/amyloid-like proteins to the brain and could add to the existing amyloid burden. Furthermore, under appropriate conditions, arginine residues on the end of fragmented proteins can undergo citrullination, a form of post-translational modification, initiated by *P. gingivalis* peptidyl arginine deiminase (Bielecka *et al.*, 2014). This is particularly relevant for retaining C5a activity and attracting immune cells to the brain (Farkas *et al.*, 2003; Bielecka *et al.*,

2014). This may be why AD pathology lacks presence of systemic phagocytes and T/B cells in AD brains.

The working hypothesis proposed here, is that a chronic assault on the BBB from circulating periodontal pathogens and/or their associated virulence factors could lead to disruption of the integrity of the barrier (either by increased permeability or reduction in clearance). Whilst there is some evidence to support the concept, it remains incompletely evidenced in humans and *P. gingivalis* cells have not yet been found in the brain of AD patients or test animals (Olsen *et al.*, 2020). However, human post-mortem studies have found evidence of *P. gingivalis* DNA and virulence factors, LPS and proteases secreted by *P. gingivalis* (gingipains), in the brains of AD individuals (Dominy *et al.*, 2019; Poole *et al.*, 2013). *In vivo* animal studies, investigating the administration of *P. gingivalis* associated virulence factors have shown that these substances travel to and settle in the animal's brain (Poole *et al.*, 2013; Ilievski *et al.*, 2018). Ilievski *et al.* (2018) showed that infection of mice with *P. gingivalis*, induced neuroinflammation and appeared to induce the deposition of intracerebral A β protein, drawing similarities to the human AD pathology. It remains unclear however, whether the reason for the A β protein seen in the brain of the test animals was due to a direct cerebral invasion of intact *P. gingivalis*, its virulence factors such as gingipains or an indirect effect from the inflammatory mediators of systemic infection (Ilievski *et al.*, 2018). The author suggests two pathways for *P. gingivalis* inducing neurodegenerative changes. Either i) *P. gingivalis* can access the brain directly or ii) the bacteria can orchestrate the neurological changes from a distant site of infection, i.e., the periodontal pockets in the oral cavity. The key question remains if or how *P. gingivalis* and its virulence factors access brain tissue, how do they cross the BBB?

1.4 The blood-brain-barrier (BBB)

1.4.1 BBB anatomy

The blood brain barrier provides the brain privileged site status, acting as a semi permeable membrane between it and the systemic circulation. The key elements contributing to this separated existence, are primarily focused on the specialised endothelial structure, which acts to keep harmful substances away from the sensitive neural tissues (Daneman and Prat, 2015). In total the major functional components of the barrier alongside the capillary endothelial cells include tight junctions and adherens junctions, surrounded by a basement membrane, overlaid by foot processes of astrocytes (Daneman and Prat, 2015). Three elements should be considered when reflecting on the physical barrier status of the BBB:

i) The endothelial cells are extremely tightly packed together due to the presence of tight junctions (TJs). So tight that, in contrast to capillaries elsewhere in the body, they prevent the passage of nearly all molecules. Lipid solubility does however enable molecules such as oxygen, carbon dioxide, alcohol and steroids (hormones) to cross the membrane (Daneman and Prat, 2015).

ii) The TJs, represent a collection of specialised transmembrane proteins as shown in Figure 1.5. These include junctional adhesion molecule-1 (JAM-1), occludin and claudin. Additional proteins include zona occludens 1 and 2 (ZO-1 and ZO-2), cingulin, AF-6 and 7H6. They are connected intracellularly to the actin cytoskeleton. Adjacent pericytes and astrocytes contribute to the overall barrier integrity. The organisation of the TJs is further subdivided at the basal end of the cells by a zone called the adherens junction (AJs), composed of additional elements platelet endothelial cell adhesion molecule (PECAM), e-cadherin and nectin (Abbott *et al.*, 2010).

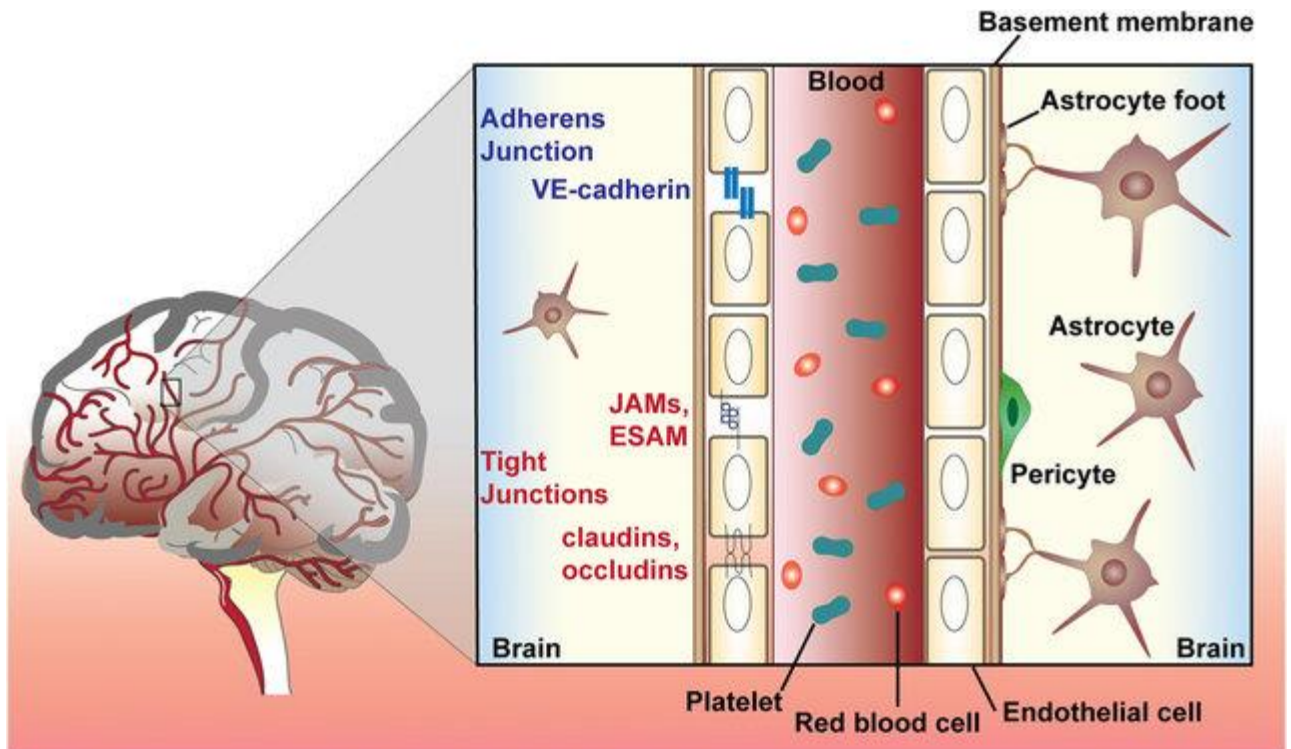


Figure 1.5 The tight junctions (TJs) of the BBB represent a collection of specialised transmembrane proteins. These include junctional adhesion molecule-1 (JAM-1), endothelial cell selective adhesion molecule (ESAM), occludins and claudins. Additional proteins include vascular endothelial (VE)-cadherin. Adjacent pericytes and astrocytes contribute to the overall barrier integrity. The organisation of the TJs is further subdivided at the basal end of the cells by a zone called the adherens junction (AJs) (Abbott *et al.*, 2010). Figure taken from Shergalis *et al.*, 2018.

iii) Specific transport systems enable passage of substances such as glucose and amino acids. In general, anything <400 Daltons and containing <8 hydrogen bonds will be able to cross safely (Daneman and Prat, 2015). It is also noted that the endothelial cells possess low level intracellular mechanisms to facilitate pinocytosis and general vesicular based transport. For example, the insulin receptor is a type of active receptor mediated endocytosis and transcytosis (Daneman and Prat, 2015). Additional histological features include a high number of mitochondria and a prominent basement membrane reaching up to 50nm. There is also evidence of mesenchymal elements such as heparin sulphate, laminin, enactin and type IV collagen (Daneman and Prat, 2015).

When modelling the BBB model in vitro, studies typically utilise three major cell types of the neurovascular unit (NVU): pericytes, astrocytes and endothelial cells seeded on a transwell membrane which mimics the basement membrane.

i) Pericytes: Adjacent to the capillary, but buried within the prominent basement membrane, pericyte cells are found, which possess muscle like properties. They can cover approximately a third of the abluminal surface of micro-vessels (Sims, 2000). They have been associated with regulation of endothelial proliferation, angiogenesis as well as inflammatory responses (Sims, 2000). They can also regulate specific genes integral to the function of the BBB, such as expression patterns in endothelial cells, and they can induce a polarization in the astrocyte end-feet (Armulik *et al.*, 2010). In addition, they help polarise the positioning of astrocyte feet. Without pericytes the endothelial layer demonstrates several dysfunctional features which result in an increased permeability and thus loss of function. Pericytes are abundant on venules and common on capillaries (Sims, 2000) and a high variance is seen between tissues demonstrating functional heterogeneity. In the brain, vascular pericytes are highly involved with the development and maintenance of the BBB and are regulators of angiogenesis and survival of neighbouring endothelial cells and participate in clearance of cellular by-products (Rucker *et al.*, 2000). Interruption to the activity of pericytes has been linked to various diseases such as hypertension, AD, diabetic retinopathy, multiple sclerosis and CNS tumour formation (Allt and Lawrenson, 2001). This is thought to be because of the pericytes close relation to micro vascular endothelial cells, thereby affecting the blood flow.

ii) Astrocytes: The parenchymal contribution to the barrier status is provided by foot processes of nearby astrocytes, which can provide cover of up to 95% of the capillary non luminal surface (Daneman and Prat, 2015). Astrocytes are one of the major cell types in the mammalian brain, providing several supportive functions to neurons in the central nervous system (CNS) (Rudge, 1993). As described previously, when the

homeostatic function of astrocytes fails, either signified by atrophy or reactive hypertrophy as seen in AD, this can lead to neurodegeneration (Nara *et al.*, 2021) and studies have shown that astrocytes are a highly functionally diverse cell group (Shao and McCarthy, 1994).

iii) Endothelial cells: Human brain microvascular endothelial cells (HBMEC) are a significant component of the BBB. These cells have unique properties which sets them apart from peripheral endothelial cells such as the absence of fenestrae and a high intercellular tight junction resistance which results in slower paracellular flux and reduced pinocytotic activity (Daneman and Prat, 2015), limiting the passage of substances from the blood to the brain. The HBMEC express cell adhesion molecules on their surface regulating extravasation of leukocytes into the brain (Daneman and Prat, 2015) making them an important subject for investigation in relation to this project.

1.4.2 BBB functions

The BBB possesses mainly a physical barrier function, originating from the endothelial junction integrity, and a metabolic barrier to restricted transport of endogenous and xenobiotics across the endothelial membrane via the presence of a large number of selective transporters and enzymes such as alkaline phosphatase, gamma glutamyl transpeptidase, monoamine oxidase and cytochrome P450 monooxygenases (Bakhsheshian *et al.* 2016). The barrier can actively export substances from the brain into the capillary, via efflux transporters such as ATP binding cassette transporter (ABCB1) that encodes for p-glycoprotein. This capability will ensure removal of brain metabolites and xenobiotics (Daneman and Prat, 2015; Bakhsheshian *et al.*, 2016). In contrast there are specific transport systems which move substances like glucose and amino acids from the systemic circulation into the brain.

The sub-Classification of BBB functions can be outlined as:

i) **Ion regulation**; maintaining a stable brain parenchymal environment is key for neuronal functioning. Hence specific ion channels and transporters work to maintain parenchymal ion composition. Potassium is kept at a concentration of 2.5 to 2.9 mmol/L in the interstitial fluids (ISF) and the cerebral spinal fluid (CSF), irrespective of the plasma levels which can vary but will usually be around the 4.5 mmol level. In addition, calcium and magnesium levels are closely maintained (Blanchette and Daneman, 2015).

ii) **Neurotransmitter regulation**; glutamate concentration can vary in the circulation. If during periods of high concentration, it can access the brain tissue it will result in unwanted excitatory effects and possible tissue damage. In addition, the transmitters associated with central nervous system (CNS) and peripheral nervous system (PNS) need to be kept separate, to avoid “cross talk” resulting in problems in the numerous bodily functions controlled by the two systems (Blanchette and Daneman, 2015; Helms *et al.*, 2017).

iii) **Macromolecule control**; the BBB must keep macromolecules out of the brain space e.g. albumin, pro-thrombin and plasminogen. If in contact with brain tissue, they can lead to tissue scarring, destruction and even seizures. BBB integrity is thus an imperative (Daneman and Prat, 2015; Barar *et al.*, 2016).

iiii) **Neurotoxin protection**; the BBB ensures neurotoxic substances fail to access the neural tissues. Metabolites or proteins which attempt to penetrate the BBB will be expelled by ATP binding cassette (ABC) transporters, which use energy to actively remove the neurotoxins (efflux pumps) and metabolised by enzymes that work in tandem with transporters, for example CYP and P-gp (Fu, 2018).

iiiii) **Brain nutrition**; Despite the requirements for water soluble nutrients, the BBB prevents access. The only way to facilitate movement is with the aid of specific transport systems to enable their passage across the BBB (Daneman and Prat, 2015).

iiiiii) **Immune regulation**; The endothelial integral structures along with adjacent microglia, contribute to the immune integrity of cerebral tissues to minimise inflammatory brain cell changes in the face of damaging or chronic assaults (Schenk and de Vries, 2016).

1.4.3 Transport across the BBB

The blood brain barrier possesses a number of routes for material to pass in both directions across the barrier summarised in Figure 1.6.

i) **Paracellular (aqueous) diffusion of water**. Substances can pass between the cells of the barrier. The TJs make this difficult, limiting this movement to very small water-soluble molecules (Serlin *et al.*, 2015).

ii) **Lipophilic transcellular diffusion**: This pathway is recognised for the passage of polar and non-polar molecules across the cells of the barrier. Molecules of high lipid solubility, hydrogen bond number less than 5 (between nitrogen and oxygen) and the molecular weight under 450 D are favoured, for example. O₂, CO₂, NO, and H₂O (Serlin *et al.*, 2015).

iii) **Carrier mediated transport proteins**: Binding of substances such as glucose or amino acids to a membrane bound protein transporter, can induce a conformational change on the transporter resulting in movement of the substances from one side of the cell to the other, from high to low concentration, but with energy this direction can be reversed (Serlin *et al.*, 2015). Pumps can be dedicated to promoting purely efflux of substances, particularly drugs. This clearly poses a challenge when attempting to access the brain with therapeutic pharmaceutical agents. Principle amongst these efflux pumps are the ATP Binding Cassette (ABC) transporters such as P-gp and multidrug resistant protein (MRP). P-gp inhibition has been shown to increase the access of anticancer

medication to the brain showing the therapeutic benefits of targeting these sites (Serlin *et al.*, 2015).

iii) **Adsorptive mediated transcytosis (AMT)**: This is an ATP demanding process which will transport substances from the blood vessel luminal surface, across endothelial cytoplasm to release into the cerebral tissues. It begins with the binding of the substances into vacuoles/pits lined with clatherin, attracted not by receptors but possibly by opposing surface charges. The ATP is generated by the relatively high density of mitochondria found in BBB endothelia (Abbott *et al.*, 2010).

iiii) **Receptor mediated endocytosis**: Proteins such as insulin, insulin like growth factors (IGF1, IGF2), angiotensin II, Atrial natriuretic peptide (ANP) and IL-1 have been shown to benefit by this transport system. The role of alkylguanine DNA alkyltransferases II (AGT-II) and IL-1 may be to bind to receptors and increase the transport of other peptides such as insulin and transferrin (Abbott *et al.*, 2010)

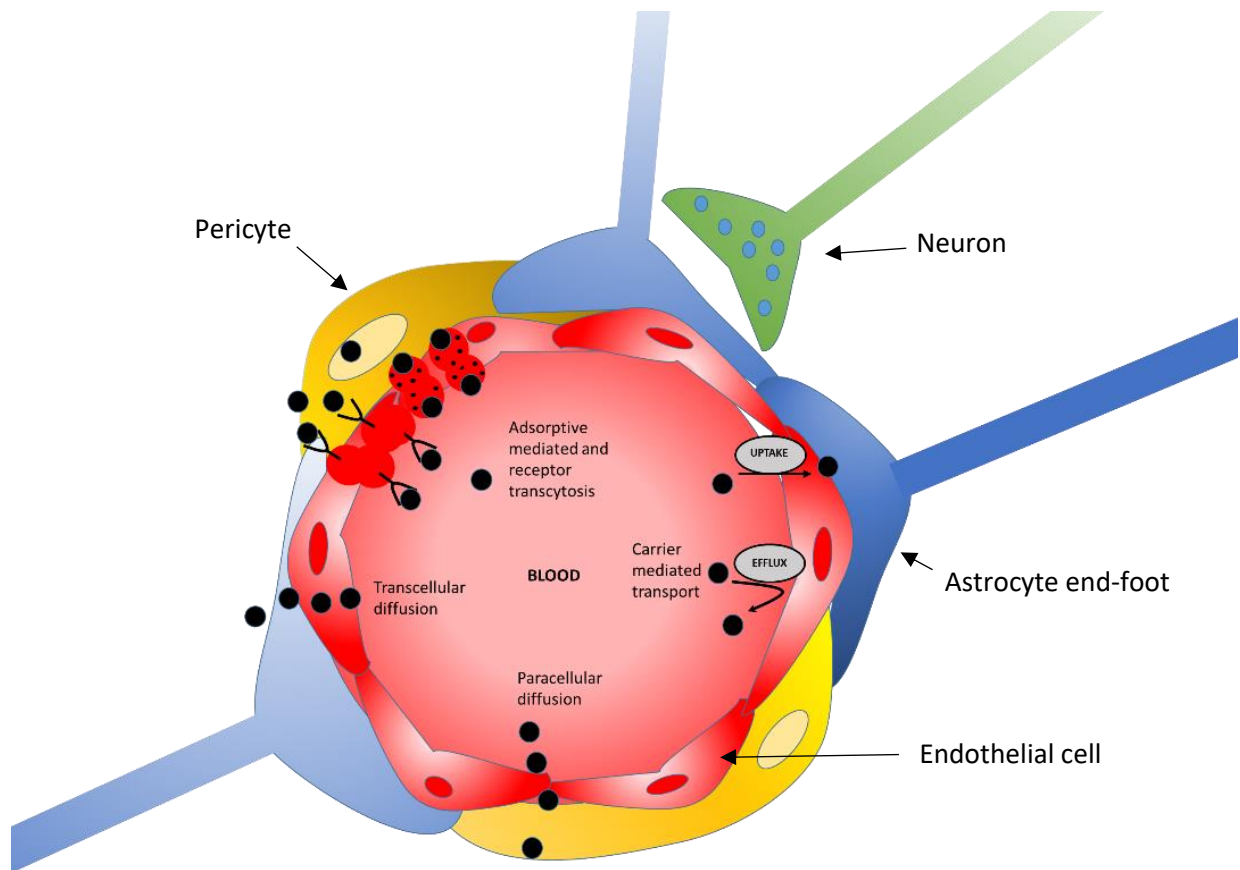


Figure 1.6 Summary of routes for material to pass in both directions across the BBB (Kouki et al., 2022)

1.4.4 BBB change in function

The BBB is influenced by its surrounding environment and variable conditions. These elements exact an influence which can result in a change to the BBB phenotype and even create breaks in its integrity. Those events which can threaten the BBB integument include: starvation, hypoxia (up regulating Glut-1), circulating inflammatory mediators such as histamine and bradykinin resulting in endothelial permeability (Erdő et al., 2017). Additionally, the BBB TJs can succumb to chronically raised blood pressure, hyperosmolality, microwaves, radiation, trauma and ischaemia (Erdő et al., 2017). What is also clear is that sustained exposure to inflammation also results in increased leakage of the

BBB and access to brain tissues of plasma suspended substances normally prevented from gaining entry (Erdő *et al.*, 2017).

Systemic inflammation can exist in acute or chronic forms. The effects can be to initiate changes in brain structure such as the BBB or exacerbate existing conditions (Holmes *et al.*, 2009). The changes which may occur have been described as disruptive and non-disruptive (Varatharaj and Galea, 2017). These are taken to refer to changes at histological and molecular levels respectively, both however will have significant consequences.

1.4.4.1 Non-disruptive BBB changes:

These changes will arise even in the presence of intact TJs. This implies that the degree of inflammatory changes could occur after a long-term exposure to less clinically severe events. The changes associated with non-disruptive, i.e. intact morphologically BBB include:

i) Downregulation of transporters such as the efflux pumps p-glycoprotein, anion pumps for amino acids, leptins and β -amyloid. In contrast evidence suggests some of the influx transport pathways are upregulated for TNF- α and lysosomal enzymes (Varatharaj and Galea, 2017).

ii) Many of the effects are as a result of the presence in the blood of inflammatory mediators such as cytokines. It has been shown that BBB endothelium intracellular pathways are activated by plasma TNF- α and IL-1 β affecting the barrier cells homeostasis (Skelly *et al.*, 2013).

iii) Similarly, IL-1 β and TNF- α will also increase the activity of endothelial cyclooxygenase to release increased amounts of prostaglandin E 2 (PGE2) from the basal surface into the brain parenchyma, whilst at the same time reducing efflux into the vascular lumen (Vasilache *et al.*, 2015; Akanuma *et al.*, 2011). These effects could

explain some of the brain changes noted during the cytokine driven development of fever. Interestingly LPS has been shown to prevent the removal of prostaglandins (PGs) from the brain (Akanuma *et al.*, 2011).

iii) There is evidence to suggest that cells traverse the BBB in a non-disruptive manner. The cells shown to benefit from this pathway are mainly white blood cells namely, lymphocytes, monocytes and neutrophils. The effect appears to be in response to systemic inflammation and the two routes taken are via the endothelium and/or the glia limitans (Wang *et al.*, 2008).

a. The BBB endothelium does not usually express any constitutive selectins, but the presence of pro-inflammatory cytokines $IL-1\beta$, $TNF-\alpha$ as well as LPS, can promote their expression or reveal the presence of P-selectin glycoprotein as well as E-selectin. which creates conditions for neutrophil endothelial surface rolling (Barkalow *et al.*, 1996, Carvalho-Tavares *et al.*, 2000).

b. Once white cells are adherent, the endothelial cell lining releases chemokines such as chemokine ligand 2 (CCL2). This is followed by the expression of leukocyte adherent integrins, such as lymphocyte function associated antigen (LFA) and very adherent antigen (VLA-4) (Chui and Dorovini-Zis, 2010). The chemokines have been shown to come not only from cytokine and LPS activated endothelium but also from parenchymal based microglia. The role of astrocytes is however yet unclear (Zhou *et al.*, 2009).

c. The final arrest step before diapedesis across the endothelial cells, involves the expression of cell adhesion molecules (CAMs), such as ICAM-1 (intercellular adhesion molecule) again, secondary to inflammatory stimulants (Blom *et al.*, 2015).

iiii) Once the leucocyte is through the endothelial cell layer, the final obstacle before reaching the brain parenchyma is the glia limitans of the basement membrane. To that end matrix metallo-proteinases (MMPs) are released by endothelial cells, perivascular

macrophages (microglia) and pericytes. These include MMP-2 and MMP-9 (Agrawal *et al.*, 2006; Pieper *et al.*, 2013).

1.4.4.2 Disruptive changes:

The changes described as non-disruptive can be likened to the changes brought on by exposure to chronic inflammatory changes associated with chronic disorders. However, there are events which present as acute inflammatory conditions, challenging the BBB with higher concentrations of inflammatory mediators. The subsequent changes to the BBB are such that they can be visualised at a microscopic level leading to significant and more acute loss of function.

These changes have been well summarised by Varatharaj and Galea (2017), reviewing the role that LPS plays in the assessment of the BBB and inflammatory interface.

Although critical of the quality of overall evidence the authors summarise the changes as:

- i) BBB endothelium synthesise both nitric oxide (NO) and prostanoids, understood to be central to the changes manifested to the damaged BBB integument (Banks *et al.*, 2015).
- ii) Disruption of tight junctions due to the effects of not only NO and prostanoids but other BBB released factors such as MMPs, oxygen free radical production and disruption of vital intracellular signalling pathways. This creates visible pathways between endothelial cells for cells, toxins and fluids to access the brain parenchyma
- iii) Damage to the endothelial cell membrane, mitochondrial function and promotion of cell death.
- iii) Dysfunction of the apical glycocalyx removing a key barrier layer and increasing paracellular permeability.
- iiii) Degradation of the basal positioned glia limitans.

iiiiii) Damage and disruption to the astrocyte layer.

The summary of changes above highlights the disruption of integrity, which the BBB could potentially sustain from the presence of Gram-negative bacteria.

1.4.5 Route from blood to brain and potential for neuroinflammation induction

The cells of the blood brain barrier, also described as the NVU, comprise of endothelial cells, pericytes, astrocytes and neurons (Muio *et al.*, 2014). The 400 miles of capillaries in the human brain (Cipolla, 2009) makes this the largest potential entry point for pathogens to the CNS, but its intimate integrity affords a significant barrier. This integrity arises from; endothelial cell i) intercellular tight junctions displaying high electrical resistance, limiting any transcytosis compared to peripheral endothelial cells (Sweeney *et al.*, 2018), ii) lack of fenestrae (transcellular pores) and iii) shared basement membrane with pericytes with reduced pinocytotic activity.

The integrity of the BBB is reduced naturally as we age (Verheggen *et al.*, 2020) and multiple neurological conditions have been associated with a “leaky” BBB (Sweeney *et al.*, 2018), including AD and Parkinson’s disease, implying the importance its role in brain homeostasis and risk of age-related neurodegeneration (Olsen *et al.*, 2020). Many of these neurological conditions also present with a raised level of systemic pro-inflammatory cytokines which are also thought capable of contributing to weakening in the barrier’s integument (Lochhead *et al.*, 2020; Brown, 2019).

Studies in mouse apolipoprotein E (ApoE) knock-out models (Methia *et al.*, 2001) and humans who express the E4 isoform of (APOE4), the most prevalent predisposed genetic risk factor for sporadic AD, also show accelerated breakdown of the BBB structure and degeneration of brain capillary pericytes required for barrier integrity (Montagne *et al.*, 2020).

The journey for *P. gingivalis* and associated virulence factors, from the periodontal pocket to the central nervous system (CNS) has been suggested to follow a number of possible routes, such as i) tracking along the trigeminal or olfactory nerves (Dando *et al.*, 2014); ii) by being internalised by peripheral immune cells and subsequently transferring to the CNS or iii) finally arriving in the systemic circulation at the BBB or the blood cerebrospinal fluid barrier (BCSFB) (Coureuil *et al.*, 2017).

Both Gram negative and positive bacteria can cross at the BBB and blood cerebrospinal fluid barrier (BCSFB) interfaces to the CNS by transcytosis. Bacteria such as *Neisseria meningitidis* are able to open endothelial intercellular junctions to cross the CNS barriers in acute infection (Coureuil *et al.*, 2017) and *P. gingivalis* gingipains have been shown to degrade the epithelial Jam-1 protein (Takeuchi *et al.*, 2019) and induce cell adhesion molecule cleavage and apoptosis in human peripheral microvascular endothelial cells (Sheets *et al.*, 2005). *P. gingivalis* has also been demonstrated to induce apoptosis and tight junction disruption in cultured human lung epithelial cells (He *et al.*, 2020). It is not clear however, whether these findings were caused by the bacteria or its virulence factors.

Animal studies have demonstrated that LPS can incite oxidative stress, activation of glial cells and tight junction degradation in the NVU and surrounding cells (Banks *et al.*, 2015; Wang *et al.*, 2017). Though much research has been undertaken to understand the events at the BBB in diseased individuals (Banks *et al.*, 2015; Wang *et al.*, 2017; Pflanzner *et al.*, 2010) and the effects of *P. gingivalis* and its virulence factors on tissues, very little is known about what effect this bacterium and its virulence factors exert on the cells of the blood-brain interface especially in the pre-clinical stages.

Recent evidence suggests that the adaptive immune system may have an important role in suppressing AD neuropathology (Marsh *et al.*, 2016; Olsen *et al.*, 2016). It may therefore be that, with aging and a waning adaptive immune system, AD neuropathology

may be more likely to be evident. Additional to this, both periodontal pathogens (*P. gingivalis* and *Treponema denticola*) show weak responses for attracting systemic inflammatory cells (neutrophils, T/B cells) into the brain (Olsen *et al.*, 2016). The concept of inflammation and macroscopic atrophic appearance (enlarged sulci and ventricles) unique to AD brains may offer similar clues for a pivotal and primary role of inflammation at the organ level. The atrophic appearance of AD brains corroborates inflammation and is a compelling indication of numerous bacteria/bacterial endo/exo/toxins and fungi/viruses observed in association with A β plaques (Hill *et al.*, 2014; Itzhaki, 2016; Lukiw, 2016; Pistollato *et al.*, 2016; Alonso *et al.*, 2017; Harris and Harris, 2017; Jiang *et al.*, 2017; Maheshwari and Eslick, 2017; Zhao *et al.*, 2017). The large microbial biodiversity identified from post-mortem AD brain specimens could be because of the differences in age, diet, lifestyle, geographical environment and disease status, a limitation also recognized by the human microbiome project (Lloyd-Price *et al.*, 2017). This places a greater onus on microbial virulence factor(s)/pathogen associated molecular patterns (PAMPs) than live microbes exerting a pathological effect with the common endpoint of AD. An example of this is the detection of LPS in AD brains with the resulting opsonization of LPS-producing bacteria by glial cells (Poole *et al.*, 2013), and their direct binding with A β plaques (Zhan *et al.*, 2016; Zhao *et al.*, 2017). Undoubtedly, LPS from the outer membrane of Gram-negative bacteria is a powerful pro-inflammatory PAMP. This may carry with it proteolytic enzymes (gingipains, peptidyl deiminases and carbonic anhydrases) and appendages such as fimbriae and curli fibers (curli are functional amyloids housed on the outer membrane of several prokaryotes) and other amyloid-like proteins (Pritchard *et al.*, 2017).

In vivo experimental models have suggested LPS from oral, Gram-negative bacteria have a role in chronic local inflammation (Dicarlo *et al.*, 2001); A β release (Sheng *et al.*, 2003; Wu *et al.*, 2017); worsened cognition (Wu *et al.*, 2017); and tau protein phosphorylation (Lee *et al.*, 2010). *Escherichia coli* (*E. coli*) LPS has been found to co-

localise with AD senile plaques (Zhan *et al.*, 2016; Zhao *et al.*, 2017). In addition, experiments with peripheral inoculations of LPS from *E. coli* in APP transgenic mice (Sheng *et al.*, 2003) have demonstrated increased expression of APP with A β release (Sheng *et al.*, 2003). This result supported the concept of peripheral inflammation as an initiating factor in intracerebral inflammatory activity as well as supporting the release of at least one hallmark (A β) protein (Sheng *et al.*, 2003). Wu *et al.* (2017) demonstrated that repeat injections of LPS from *P. gingivalis* activated cathepsin B (a form of β secretase) indirectly to cleave APP intracellular fragmentation in an age-dependent manner. Functional testing revealed that chronic and systemic administration of *P. gingivalis* LPS in middle-aged mice caused learning and memory deficits (Wu *et al.*, 2017), supporting an AD-like phenotype and giving this PAMP, from an oral keystone pathogen, a more prominent role in AD causality. The predominant signalling cascades participating in the innate immune system in AD pathogenesis as mentioned earlier include CD14, TLRs and the NF- κ B pathways (Lukiw, 2016), the cAMP-signaling pathway, the transformation growth factor-beta signaling pathway (TGF- β) and the p38 mitogen-activated protein kinase signalling (p38 MAPK) pathway. The latter signalling cascade mediates inflammatory and stress responses and is critical in regulating levels of multiple pro-inflammatory cytokines, such as TNF- α , IL-1, IL-6 and IL-8, as well as enzymes involved in inflammatory cascades e.g., cyclooxygenase and inducible nitric oxide synthase (Chen *et al.*, 1999; Underwood *et al.*, 2000; Huang *et al.*, 2004). TNF α cytokine is significantly upregulated in AD (Tarkowski *et al.*, 1999), which could be the result of host's intrinsic genetic factors such as presenilin 2 and ApoE4 allele inheritance (Jayadev *et al.*, 2013; Fan *et al.*, 2017). Co-morbidities such as periodontitis and its aetiological polymicrobial pathogens are also responsible for contributing to this cytokine pool (Kamer *et al.*, 2009). A consequence of high levels of TNF- α is that, together with its converting enzyme, this cytokine can provide positive feedback between the γ -secretase site fragmentations of the APP into amyloid-alpha (A α) (Allen, 2017). Infections also

induce oxidative stress, and this too can have an impact on A α and A β levels through the γ - and β -secretase cleavage of APP (Tamagno *et al.*, 2008).

The evidence thus presented previously suggested that periodontal disease resulted in the introduction of inflammatory mediators and bacteria into the systemic circulation via the pocket epithelial. Local inflammatory mediators, such as TNF- α , IL-1 β and IL-6 generated as a result of periodontal inflammation also access the circulation via the same route. These mediators have been shown to induce acute phase type responses from the liver, with the release of C-reactive protein, fibrinogen and serum amyloid A (Tonetti, 2009; Offenbacher *et al.*, 2009). An alternative mechanism of inducing the same systemic inflammatory state, has been proposed by oral bacteria being swallowed and disturbing the microbiome within the gastrointestinal tract resulting in weakness of the endodermal epithelial integrity, permitting the aforementioned inflammatory mediators access to the circulation (Arimatsu *et al.*, 2014). These products may result in damage to the BBB in pathways highlighted above. In AD, the brain tissue has several features of inflammatory changes (Heneka *et al.*, 2015) which could be a result of a chronic inflammatory assault to the BBB over time, secondary to chronic nature of periodontal disease. Evidence from animal models has also shown that LPS induced systemic inflammation, results in production of systemic TNF- α , IL-1 β and IL-6, which as previously described may have effects upon the BBB, most notably the reduction in A β protein efflux out of the brain, leading to raised parenchymal levels the hallmark of the histology associated with AD tissue markers (Jaeger *et al.*, 2009). In humans this situation is mimicked when raised peripheral levels of pro-inflammatory mediators are proportional to decreased cognitive levels (Holmes *et al.*, 2009). The subsequent changes to the BBB integrity, described above as disruptive or non-disruptive, permit access of systemic inflammatory markers and even bacteria into the brain tissue (VanItallie, 2017). The result is the activation of microglia to a pro-inflammatory state contributing to neurodegeneration.

More recently oral periodontal bacteria have been shown to utilise additional systemic transport mechanisms. *P. gingivalis* has, as a result of pocket debridement, been shown to access the circulation within dendritic cells, subverting the chemokine surface profile, reducing the lymphoid attracting chemokine receptor type 7 (CCR7) and increasing expression of neo-vascular attracted CXCR4 (Miles *et al.*, 2014). Erythrocytes have also been suggested as a bacterial transport pathway, binding complement opsonised *P. gingivalis* onto its surface. This allows *P. gingivalis* access to numerous endothelial surface sites such as the BBB (Belstrøm *et al.*, 2011). Indeed, vascular invasion is facilitated by the *P. gingivalis* fimbriae, FimA and once intracellular, is capable of subverting the usual destructive mechanisms (Xu *et al.*, 2020).

Human *in vitro* BBB models are used to investigate both disease and drug interactions of this interface, providing a very valuable tool to assess permeability, transport and transendothelial electrical resistance (TEER), as well as expression of proteins (Wolff *et al.*, 2015). The benefits of using a human primary-derived cell-based model are numerous and combinations of cells of the NVU have been validated and standardised, for a comprehensive review see (Wolff *et al.*, 2015).

If *P. gingivalis* was shown to induce damage to the BBB of an individual, some time before any neuroinflammation becomes clinically detectable, then the author propose that bacteria or associated virulence factors must be capable of damaging the BBB enough to trigger a change either to its integrity allowing an influx of inflammagens and/or weakening the barrier's normal clearance strategies. If the initial causal factor for the pro-inflammatory state is not resolved, then any subsequent effects of chronic oxidative stress on the NVU cells can lead to loss of redox balance, alterations in numbers and differentiation of T-cells subpopulations and subsequent loss of regulation of the neuroinflammatory response (Solleiro-Villavicencio and Rivas-Arancibia, 2018).

1.5 Originality, Hypothesis and Overall Aims and Objectives

To date, there is still no study which has proven a causative link between PD and AD in humans. No periodontal pathogen cell has been found in any AD brain tissues (man or animal), only PD bacterial gDNA or virulence factors such as LPS or proteolytic enzymes (gingipains). Very little is known about how periodontal bacteria and/or their virulence factors enter the brain tissues.

The working hypothesis was that a microbial cause related to periodontal disease is associated with the loss of BBB integrity and neuroinflammation observed in Alzheimer's disease.

The overall aim of this thesis was to investigate potential links between late onset AD and pathogens associated with PD.

The first main objective was to examine post-mortem AD brain samples and age matched controls for the presence of a microbial remnants (25 AD and 15 age matched controls) by NGS. This was followed up with further screening by PCR, where amplification with fungal and bacterial primers took place.

The second objective was to investigate the effects of a PD keystone pathogen (*P. gingivalis*) virulence factors on the barrier integrity of cells in an *in vitro* human primary cell BBB model and later on in a human brain microvascular endothelial cell (HBMEC) monolayer model. The protocols which were developed to examine the effects of the *P. gingivalis* LPS and OMVs on the human BBB cells, were not previously published so could provide a novel contribution to the scientific evidence pool.

1.6 Justification of choice of methodology

The methods used in this project were selected based on testing the inflammatory hypothesis of AD. If periodontal disease is present, pathogens arising in the oral cavity have the potential to travel to the blood, reaching the BBB interface. Neuroinflammation at the BBB could compromise integrity, exposing brain tissues to putative Alzheimer's aetiological factors.

To provide the most relevant data applicable to humans, post-mortem brain tissue from AD patients and age matched controls were examined for a genetic presence of microorganisms. An all human *in vitro* BBB model, using primary derived short-term cell cultures of the NVU, with human serum and extracellular matrix components was used to predict neuroinflammatory changes at the BBB, as animal models are inherently poor at predicting human disease states. All the primary cell lines utilised in this study were isolated from human brains (cerebral cortex).

It was decided to focus on *P. gingivalis* as a keystone pathogen of the chronic inflammatory disease of the periodontium, as this bacterium has multiple methods of inducing change to human cells and has been linked to AD (Pritchard *et al.*, 2017).

All supplier information for equipment, and reagents/ chemicals are individually listed in Appendix 1, Table 1 and Table 2 respectively.

Chapter 2

Genomic analysis

2.1 Introduction, aims and objectives

The investigations to determine whether there was a microbial presence in AD post-mortem brain samples were emerging in the literature at the start of this project in 2016, but there were no publications at this point with a focus on the oral microbiome. To test the hypothesis whether oral bacteria could contribute to the development of Alzheimer's disease (AD), genomic analysis was applied to post-mortem brain samples from AD patients and non-AD individuals. The intention was to investigate whether circulating periodontal pathogens could have gained access to the brain parenchyma. If evidence of bacterial gDNA was found, the next step was to determine whether there was a difference between the two cohorts (AD verses non-AD individuals). Whilst there is some evidence in the literature to support the hypothesis with respect to the infection hypothesis of AD, it remains incompletely evidenced in humans and *P. gingivalis* cells have not yet been found in the brain of AD patients or test animals (Olsen *et al.*, 2020). If a microbiome of AD was found in post-mortem brains this could lead to further strategies of prevention

Aim

The aim of this study was to determine whether there was a presence of microorganisms or their remnants (bacterial or fungal) in the brains of AD patients compared to controls.

Objectives

1. To carry out high throughput bacterial sequence analysis of 15 post-mortem brain samples from 9 AD patients and 6 sex and age matched controls, potentially to phylum or genus level.

2. To extract gDNA from 40 post-mortem brain samples from 25 AD patients and 15 sex and age matched controls and use the polymerase chain reaction (PCR) amplification to detect gDNA of bacterial and fungal species, to supplement the data from the high throughput analysis

2.2 Materials and methods for NGS

The high throughput methodology in our study was developed in collaboration with Professor Ingar Olsen at Oslo University, who used a commercial laboratory for the main NGS. The sequencing data was analysed following published protocols of similar studies (Sundquist *et al.*, 2007). Only a number of the 40 available post-mortem tissue samples were analysed by high throughput analysis n= 15 (9 AD and 6 controls).

2.2.1 Human brain tissue, sample selection

Following informed consent and local ethical approval (Ref:STEMH 540), human post mortem brain tissues were obtained from Newcastle Brain Tissue Resource (NBTR). All human tissues were used and stored in accordance with the UK Human Tissue Act (2004) (legislation.gov.uk). The selection of the specimens was based on a confirmed diagnosis of late onset Alzheimer's Disease (AD) patients n=25 (≥ 65 years of age, Braak stage 3-6) and patients classed as non- AD n=15 (≥ 65 years of age, Braak stage 0-2) (Table 2.1). Braak staging is a histological staging method used at post-mortem by NBTR to diagnose how advanced the AD was in the patient (Braak and Braak, 1995). The samples were age matched and the gender spread was equal (Table 2.1). The brain sections obtained were from the parietal lobe and arrived as snap frozen tissue blocks in sterile polystyrene tubes in dry ice. Further to the anonymised personal data, post-mortem delay, tissue pH and the cause of death were available to the main researcher

(AP). There was no information available relating to the individuals PD status. All human samples were given individual codes and stored at -80 °C, and all recorded data after this date used this as the sample ID. The persons carrying out the gDNA extraction, amplification and analysis for the high throughput protocol were blinded to the original diagnosis of the patient.

Table 2.1 Samples selected for gDNA analysis, age, sex, post-mortem delay, Braak stage, pH and cause of death (COD).

Case No	Disease Category	PM Delay (hours)	Age and sex	Braak Staging	Bacterial numbers detected by high throughput sequencing	Tissue pH	Bacterial DNA detected by lab PCR	Cause of death as described on certificate
AP1	AD	22	93/M	6	n/a	6.57	No	1a. Pneumonia, 1b. Biliary sepsis; 2. Mixed dementia
AP2	AD	11	89/F	6	n/a	6.42	No	1a Frailty of Old Age 1b diverticular disease, dementia
AP3	AD	17	59/F	6	n/a	5.76	Yes	1a Myocardial Infarction
AP4	AD	12	82/M	6	n/a	6.48	Yes	1a Frailty of old age 2 Alzheimer's Disease
AP5	AD	5	86/F	6	n/a	6.50	Yes	1a. Pneumonia
AP6	AD	22	87/M	6	n/a	6.40	No	1a Frailty of old age
AP7	AD	8	77/F	6	0		Yes	Lt ventricle failure, calcific aortic stenosis
AP8	AD	77	95/F	6	1969	6.77	No	1 Pneumonia 2 Frailty of old age
AP9	AD	57	88/F	6	7	6.54	Yes	1a Senile dementia
AP10	AD	64	82/M	6	173	6.12	Yes	1a Metastatic cancer of the penis; 2 Alzheimer's disease
AP11	AD	30	91/F	6	n/a	5.94	No	Bronchopneumonia, Alzheimer's disease
AP12	AD	26	74/M	5	n/a	6.82	Yes	1.Pulmonary oedema 2nd to cardio myopathy 2. Alzheimer's disease
AP13	AD	52	71/M	6	n/a	6.02	Yes	Posterior Cortical Atrophy (aspiration pneumonia)

AP14	AD	49	90/F	6	n/a	6.42	No	Not known
AP15	AD	83	81/F	6	1	6.40	No	Cerebro Vascular Disease
AP16	AD	23	76/M	6	14	6.50	Yes	Aspiration Pneumonia
AP17	AD	39	80/M	6	19	6.10	Yes	Prostate Cancer with metastases
AP18	AD	48	91/M	3	3088	6.20	Yes	1. Myocardial Ischaemia 2. Old Age, vascular dementia, peripheral vascular disease
AP19	AD	24	80/M	6	n/a	5.95	Yes	? stroke,
AP20	AD	33	75/F	6	n/a	6.20	Yes	Metastatic Bronchogenic Carcinoma
AP21	AD	62	70/M	6	n/a	6.10	Yes	1a Alzheimer's Disease dementia
AP22	AD	29	83/F	5	n/a	6.36	Yes	1a End stage Diffuse Large B Cell Lymphoma
AP23	AD	16	80/M	6	n/a		Yes	Myocardial Infarction
AP24	AD	75	85/M	6	n/a		Yes	Chest infection
AP25	AD	31	80/F	6	13		Yes	Bronchopneumonia
AP26	Non-AD	21	97/F	2	18	6.40	Yes	Pneumonia
AP27	Non-AD	47	65/F	1	n/a	6.07	Yes	Metastatic ovarian cancer; non-Hodgkin's lymphoma
AP28	Non-AD	5	99/F	2	13	6.14	Yes	Congestive heart failure/ Ischemic heart disease
AP29	Non-AD	93	64/M	1	n/a	5.90	Yes	Sudden death - cardiac arrest
AP30	Non-AD	45	85/M	1	n/a	6.14	Yes	1a Prostate Cancer with Base Mets 2a Hypertension Ischemic heart disease and chronic Kidney
AP31	Non-AD	45	84/M	2	n/a	6.54	Yes	n/a

AP32	Non-AD	25	71/M	1	106	6.47	No	Sigmoid adenocarcinoma
AP33	Non-AD	22	73/M	2	n/a	6.24	Yes	Metastatic prostate cancer
AP34	Non-AD	33	87/F	1	n/a	6.42	No	1a Intracerebral haemorrhage 2 hypertension, atrial fibrillation
AP35	Non-AD	39	79/M	2	n/a	6.94	No	Lung Cancer
AP36	Non-AD	7	102/M	2	n/a	6.48	Yes	1a Frailty of old age 1b Ischaemic heart disease
AP37	Non-AD	64	78/M	2	220	6.43	Yes	Ruptured abdominal aortic aneurysm
AP38	Non-AD	47	66/M	2	n/a	6.57	No	Metastatic rectal cancer (mets in liver and lung)
AP39	Non-AD	54	68/M	0	6		No	Bowel Cancer
AP40	Non-AD	45	74/F	2	7		Yes	Acute pulmonary demyelinating polyneuropathy

2.2.2. DNA extraction of human brain samples for NGS and PCR screening at UCLan.

Isolation of gDNA from the snap frozen brain tissue was optimised using molecular grade reagents in Table 2.2 and was carried out using aseptic techniques and sterile equipment in a class 2-safety laminar flow cabinet. 100 mg of the thawed brain sample tissues were resuspended in 0.5 ml lithium acetate (200mM) and 1% SDS and incubated at 70°C for 5 minutes. 1 ml of TE buffer (Table 2.2) was added and vortexed. gDNA was extracted by the addition of equal volume of phenol/ chloroform/ isoamyl alcohol (25:24:1) (pH 8), which were then vortexed for a minute, before being centrifuged at room temperature for 5 minutes at 16,000 x g. The upper aqueous phase was removed and placed in a clean tube. The gDNA was isolated via ethanol precipitation by addition of 0.1 x volume of sodium acetate and 2.5 x volume of 100% ethanol. This was incubated overnight at -20°C. Following precipitation, the samples were centrifuged for 30 minutes at 4 °C and 16,000 x g. The pellet was washed in 70% ice cool ethanol and after centrifugation at 4 °C and 16,000 x g for 2 minutes, the pellet was retained in 50µl of DNA grade water. The gDNA was quantified using the Nanodrop 1000 spectrophotometer (Thermo Scientific) and stored at -20°C. Nanodrop results of 260nm/280nm ratios ≥ 1.7 were included for PCR testing.

The techniques for gDNA extraction and PCR amplification were optimised on mouse brain spiked with *Escherichia coli* and *Candida albicans* as positive controls (culture collection strains), prior to being applied to the human brain samples.

The gDNA samples for the NGS analysis were shipped with courier service to University of Oslo, where the amplification for the NGS took place.

Table 2.2 materials used for DNA extraction of human brain samples AP1-40.

Lithium acetate (LiOAc) sodium dodecyl sulphate (SDS) (Sigma Aldrich, UK) Product code: 517992
Tris EDTA (T.E.) buffer (10 mM Tris pH 8.0, 1 mM EDTA) (Sigma-Aldrich, UK) Product code: 93283
Phenol/chloroform/isoamyl alcohol (Sigma- Aldrich, UK) Product code: 77618
70% and 100% ethanol Product codes: 470198 and 031
3 M sodium acetate (Sigma- Aldrich, UK) Product code: 127-09-3
DNA grade water (Sigma-Aldrich, UK) Product code: W4502

2.2.3 PCR amplification and purification of amplicons for the purpose of NGS.

The PCR amplification and purification of amplicons for the NGS were carried out by Dr Eminike Eribe under the guidance of Professor Ingar Olsen (University of Oslo). Prior to PCR, all the reagents and pipettes were subjected to UV irradiation for 30 min. PCR amplifications were performed on a GeneAmp PCR System 2700 instrument (Applied Biosystem, USA). PCR reactions (Table 2.3) were amplified through standard PCR programs (Table 2.6) using 15 different primer sets (Eurofins Genomics, Ebersberg, Germany, Tables 2.4 and 2.5). *P. gingivalis* gDNA was used as a positive control.

The primers used for the gDNA amplification target the 16S rRNA gene region which is essential for translation of mRNA therefore highly conserved and most bacteria have it. A mix of degenerate primers were used to increase the likeliness of picking up as much bacterial DNA as possible (Table 2.4), as no single region in the 16S rRNA gene or conserved region is universal, i.e., shared by all bacteria (Sunquist *et al.*, 2007). The selected primers were chosen because it was predicted that the V3/V4 and V4/V5 regions provided the highest classification accuracies of 16S rRNA gene variable regions (Sunquist *et al.*, 2007). V4 is a semi-conserved hypervariable region and can provide

resolution at the phylum level as accurately as the full 16S gene while the V3 region is best at identifying the genus (Figure 2.1) (Sunquist *et al.*, 2007).

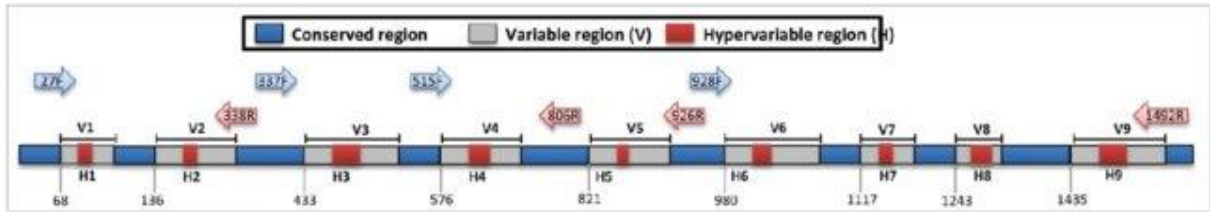


Figure 2.1. Shows conserved, variable, hypervariable regions within the 16S rRNA gene. The conserved regions are blue, variable regions are grey and hypervariable regions are shown in red. Primers are designed in a conserved region to get a PCR product spanning one (V4) or more hypervariable regions including V3, such as F342 for profiling of microbiota. (Shahi *et al.*, 2017).

Combinations of forward and reverse primers were used for targeting the V4 region (Tables 2.4 and 2.5). Index sequences of 8-bp barcodes were incorporated into the primers for multiplex sequencing (labeled in red, Table 2.4) and a flow-cell binding sequence in the forward primers (P5) of: AATGATACGGCGACCACCGAGATCTACAC.

In the forward primers the index sequence was followed by a pad-sequence of TATGGTAATT (labeled in Green Table 2.4), this was linked by GT to the V4f target sequence GTGCCAGCMGCCGCGGTAA (V4 forward end at 519 *E. coli* region) (Sunquist *et al.*, 2007). The reverse primers had a flow-cell binding sequence (P7): CAAGCAGAAGACGGCATACGAGAT and a pad-sequence of AGTCAGTCAG (labelled in green, Table 2.4). The pad sequence was linked to the V4 (CC) reverse primer GGACTACHVGGGTWTCTAAT (the V4 reverse end at 806 *E. coli* region) (Sunquist *et al.*, 2007). Triplicate PCR reactions were performed for each sample and these were separated and visualised by electrophoresis on 1.0 % Seakem agarose gels (Lonza, Switzerland) prepared in 1 x TBE with 1 x GelRed® Nucleic acid stain (Biotium Inc., USA)) and visualized in an UV light box with an EtBr filter. This was carried out to ensure the desired amplification had taken place and the expected size bands with these primer

sets were in the range of 300 – 350 bp (Parada *et al.*, 2016). Amplicons were cleaned using a SequalPrep™ Normalization Plate (96) kit (Invitrogen, Carlsbad) according to the manufacturer’s instructions. The amplified DNA was quantified by Nanodrop (3300 Fluorospectrometer) (Thermo Fisher, USA) and uniform sample concentrations by dilution were secured.

Molecular identifier (MID) tags, 10-mer, were used as sample identifiers (Table 2.4) and the triplicate amplicons were pooled and visualized as described above on 1 % Seakem gels. Equi-microliter of 24 amplicons were pooled together into a single tube and purified using the Agencourt AMPure PCR purification system (Beckman Coulter, CA).

Subsequently this was sent for the NGS platform following the vendor’s instructions (DNA Sequencing Facility, Department of Biochemistry, University of Cambridge, 80 Tennis Court Road, Cambridge, CB2 1GA, UK) where the sequencing was performed using the Illumina MiSeq 500-cycle v2 (2 x 250 bp) kit (Illumina, San Diego, CA).

Table 2.3 Reagents used in PCR amplification for high throughput analysis

Reagent	Final Concentration
Forward primer	0.5 pmol/μl
Reverse primer	0.5 pmol/μl
DNA template	1 ng/μl
AccuPrime™ Pfx SuperMix mixture consisting of (22 U/ml Thermococcus species KOD thermostable polymerase complexed with anti-KOD antibodies, 66 mM Tris-SO ₄ (pH 8.4), 30.8 mM (NH ₄) ₂ SO ₄ , 11 mM KCl, 1.1 mM MgSO ₄ , 330 μM dNTPs, AccuPrime™ proteins and stabilizers) (Invitrogen, Carlsbad, CA, USA).	1x

Table 2.4 Primers (IDT, UK) used in the high throughput amplification. When more than one nucleotide is possible at a particular position in the recognition site, these are described by standard abbreviations to represent ambiguity (W = A or T, M = A or C, H = A or C or T, V = A or C or G, N= any base).

Oligo name	Sequence
V4.SA501	5'- AATGATACGGCGACCACCGAGATCTACACATCGTACGTATGGTAATTGTGTGCCAGCMGCCGCGGTAA -3'
V4.SA502	5'- AATGATACGGCGACCACCGAGATCTACACACTATCTGTATGGTAATTGTGTGCCAGCMGCCGCGGTAA -3'
V4.SA503	5'- AATGATACGGCGACCACCGAGATCTACACTAGCGAGTTATGGTAATTGTGTGCCAGCMGCCGCGGTAA- 3'
V4.SA504	5'- AATGATACGGCGACCACCGAGATCTACACCTGCGTGTTATGGTAATTGTGTGCCAGCMGCCGCGGTAA- 3'
V4.SA507	5'- AATGATACGGCGACCACCGAGATCTACACGGATATCTTATGGTAATTGTGTGCCAGCMGCCGCGGTAA -3'
V4.SA508	5'- AATGATACGGCGACCACCGAGATCTACACGACACCGTTATGGTAATTGTGTGCCAGCMGCCGCGGTAA -3'
V4.SA701	5'-CAAGCAGAAGACGGCATAACGAGATAACTCTCGAGTCAGTCAGCCGGACTACHVGGGTWTCTAAT -3'
V4.SA702	5'-CAAGCAGAAGACGGCATAACGAGATACTATGTCTAGTCAGTCAGCCGGACTACHVGGGTWTCTAAT-3'
V4.SA703	5'-CAAGCAGAAGACGGCATAACGAGATAGTAGCGTAGTCAGTCAGCCGGACTACHVGGGTWTCTAAT-3'
V4.SA704	5'-CAAGCAGAAGACGGCATAACGAGATCAGTGAGTAGTCAGTCAGCCGGACTACHVGGGTWTCTAAT-3'
V4.SA705	5'-CAAGCAGAAGACGGCATAACGAGATCGTACTCAAGTCAGTCAGCCGGACTACHVGGGTW TCTAAT-3'
V4.SA706	5'-CAAGCAGAAGACGGCATAACGAGATCTACGCAGAGTCAGTCAGCCGGACTACHVGGGTWTCTAAT-3'
V4.SA707	5'-CAAGCAGAAGACGGCATAACGAGATGGAGACTAAGTCAGTCAGCCGGACTACHVGGGTWTCTAAT-3'
V4.SA708	5'-CAAGCAGAAGACGGCATAACGAGATGTCGCTCGAGTCAGTCAGCCGG ACTACHVGGGTWTCTAAT-3'
341F (V3F.forsyth)	5'-AATGATACGGCGACCACCGAGATCTACACTATGGTAATTGTCCTACGGGAGGCAGCAG-3'
806R	5'-CAAGCAGAAGACGGCATAACGAGATNNNNNNNNNNNAGTCAGTCAGCC GGACTACHVGGGTWTCTAAT-3'

Table 2.5 Primer combinations applied in PCR reactions of DNA from samples AP1-40 prior to NGS.

341F/701R	341F/705R	507F/806R	503F/806R	503F/701R
502F/701R	504F/806R	341F/806R	341F/703R	503F/702R
501F/702R	341F/707R	503F/703R	508F/702R	507F/702F
341F/702R	504F/702R	507F/703R	504R/703R	

Table 2.6 PCR program used for amplification before NGS.

Action	Time	Temperature
Initial denaturation	5 min	95°C
Denaturation	30cycles of 20s	95°C
Annealing	30s	55°C
Extension	60s	72°C
Final extension	10 min	72°C

2.2.4 Data analysis by MiSeq SOP MOTHUR

The sequence data derived from the sequencing process were trimmed by deleting primers and barcodes, followed by removal of sequences with ambiguous base calls and base pairs as described by Schloss *et al.* (2009).

The number of reads in the data denominates the times an identified sequence was detected in the NGS platform. The microbial diversity in individual samples was estimated with the MOTHUR package (www.mothur.org). 16S rRNA–based sequences were classified from phylum down to the genus level using the RDP Classifier (version 2.2) and a 90% confidence cut-off and the human oral microbiome database (HOMD) database (Chen *et al.*, 2010).

2.2.5 Materials and methods for PCR analysis carried out at UCLan

The oral microbiome includes both bacterial and fungal organisms, therefore human brain samples from AD and control patients were analysed with primers for bacterial and fungal gDNA, by PCR amplification. These studies were conducted at UCLan.

2.2.5.1 Sample selection

Human brain samples were selected as described in 2.2.1.

2.2.5.2 PCR amplification of human brain samples AP1-40 at UCLan

The protocols for isolation of gDNA and primers used in PCR amplification (bacterial, fungal and mammalian) were optimised using gDNA from mouse brains spiked with *Escherichia coli* and *Candida albicans*, prior to using human snap frozen brain tissues. The gDNA extraction method is described in Section 2.2.2 using reagents in Table 2.2. Human brain samples AP1-40 (Table 2.1) were all subjected to testing and were tested with both bacterial (F342 and F18R) and fungal primers (ITS1F and ITS2) (Table 2.8) using a master mix in Table 2.7 and the protocols in Table 2.9. Each PCR reaction was processed with a mammalian primer set (167mus GAPDH forward and 167musGAPDH reverse) (Table 2.8) as a positive control to confirm a successful reaction.

The fungal primers (ITS1F and ITS2) were selected as these pan-fungal universal primers target the internal transcribed spacer (ITS) unit in the 18S rRNA and 28S rRNA gene, enabling a broad range of detection of sequences present in fungal organisms including yeasts, moulds and dermatophytes (Ghannoum *et al.*, 2010). The expected product from this primer pair is in the region of 200 – 250 bp. The 18S rRNA and 28S

rRNA genes are present in all eukaryotes, and humans also have the ITS1 unit, but the sequence is much longer in humans (1074 nucleotides) (Coleman, 2013) than in fungal organisms (150-500 nucleotides). The use of a specific fungal primer pair should therefore allow for distinction between human and fungal sequences.

A primer for detection of mouse gDNA (167mus GAPDH forward and reverse) was included in every reaction as a reference gene or positive control of the PCR reaction. This primer pair targeting mouse glyceraldehyde-3-phosphate dehydrogenase (GAPDH) gDNA which is a constantly expressed gene, also describes as a housekeeping gene, would also amplify GAPDH in human tissue due to genetic overlap between the species (Salingcarnboriboon *et al.*, 2006). The expected product size from this primer pair is a band of 452 bp. All the preliminary optimisation was conducted on mouse brains tissue obtained from mice euthanised as part of a separate study approved by the University of Central Lancashire Animal Welfare Ethical Review Board (AWERB) under Home Office licence (no P42B8A022). This was to ensure the DNA extraction and PCR protocols were working before being applied to the precious human tissue samples.

One of the AD cases (AP7) which had not produced any bacterial reads by NGS was run alongside the other samples in each PCR process as a control.

gDNA extracted directly from *Escherichia coli* and *Candida albicans* (section 2.2.2, using reagents in Table 2.2) were also used as a positive control in the PCR process. Negative controls included DNA grade water or no Taq polymerase (Table 2.7). Aseptic technique was applied to minimise contamination. Reactions were performed in triplicate. Reagents used in the amplifications are outlined in Table 2.7 and 2.8. PCR amplifications were performed on a benchtop Techne Prime thermal cyclers PCR machine (UK).

The PCR products, containing 1x DNA Loading Dye (Thermo-scientific, UK), were run on either a 2.5% (*Escherichia coli*) or 2% (*Candida albicans*) agarose gel (Thermofisher, UK) with 1X TBE buffer, and 1 x GelRed® Nucleic-acid-gel-stain) (Biotium, USA) using an electrophoresis system (RunOne Electrophoresis Cell, Embi Tec, USA) at 100 V. The expected PCR product band sizes visualised on the agarose gel were in the range 150 – 250 bp, which is why the 2-2.5 % agarose gels were selected. Gels were visualised on a Biorad camera using imagelab software (USA).

Table 2.7 Mastermix content for PCR amplification at UCLan

Reagent	Final concentration (bacteria)	Final concentration (mammalian and fungi)
<i>DNA grade water (Sigma-Aldrich,UK)</i>	To final volume	To final volume
<i>Taqbuffer (Sigma-Aldrich,UK)</i>	1x	1x
<i>MgCl₂, 25 mM stock solution (Sigma-Aldrich,UK)</i>	4 mM	2 mM
<i>dNTP stock solution, 10 mM dATP, dCTP, dGTP, dTTP (Sigma-Aldrich,UK)</i>	0.2 mM	0.2 mM
<i>Taq polymerase Taq DNA Polymerase, 5 U/μl in storage buffer: 20 mM Tris- HCl, 100 mM dithiothreitol, 0.1 mM EDTA, 0.5% Nonidet P40 (v/v), 0.5% Tween 20 (v/v), 50% glycerol (v/v), pH 8.0 (+4°C) (Sigma-Aldrich,UK)</i>	1.25 U	1.25 U
<i>Dimethyl Sulfoxide (DMSO) (Sigma-Aldrich,UK)</i>	2%	-
<i>Forward primer IDT(UK)</i>	0.5 μM	0.5 μM
<i>Reverse primer IDT(UK)</i>	0.5 μM	0.5 μM
<i>DNA template</i>	40 ng	40 ng

Table 2.8 Primer sequences and properties used in PCR amplification at UCLan (IDT, UK)

Primer	Sequence (5' to 3')	Study	Gene target	Melting temperature
F342	5'-CCTACGGGAGGCAGCAG 3'	Emery <i>et al.</i> , (2017)	Universal bacterial 16S rRNA primers, 100 nmole DNA Oligo. first band (200 bp) equivalent to the variable region 3 on the majority of bacterial species. The smaller band 2 is consistent with the product size predicted for both the human 18S product (174 bp) and Propionobacteria and Corynebacteria (168bp).	64.8°C
F18R	5'-ATTACCGCGGCTGCTGG 3'	Emery <i>et al.</i> , (2017)		67.4°C
ITS1F	5'-CTTGGTCATTTAGAGGAAGTAA	Ghannoum <i>et al.</i> , 2010	Universal primers able to detect consensus sequences present in a broad range of fungal organisms including yeasts, moulds and dermatophytes (200-250bp reads).	56.6°C
ITS2	5'-GCTGCGTTCTTCATCGATGC	Ghannoum <i>et al.</i> , 2010		68.2°C
167mus Gapdh forward	5'- ACC ACA GTC CAT GCC ATC AC	Salingcamboriboon <i>et al.</i> , 2006 Nauta <i>et al.</i> , 2005	Glyceraldehyde-3-Phosphate Dehydrogenase gene target expected main product size 452bp	66.1°C
167musGapdh reverse	5'- TCC ACC ACC CTG TTG CTG TA			66.6°C

Table 2.9 PCR amplification protocols, the mammalian primers were used as a control to check if the reaction had taken place and therefore the amplification protocol for these were the same as used either for the bacterial or fungal primers.

Action	Time	Temperature bacterial primers	Temperature fungal primers	Cycles
Initial denaturation	5 min	95°C	95°C	1
Denaturation	1 min	95°C	95°C	30
Annealing	1 min	67.8°C	60°C	
Extension	30s	72°C	72°C	
Final extension	7 mins	21°C	21°C	1

2.3 Results

2.3.1 Results NGS

For the high throughput analysis, gDNA extraction of all the 40 human brain samples was carried out at UCLan and samples with a 260nm/280nm ratio above 1.7 were selected for amplification, as a lower ratio may indicate the presence of contaminants (Emery *et al.*, 2017). The minimum concentration of DNA utilized was 10 ng/ μ l. The gDNA was suspended in 70% ethanol and stored at -80°C, before transfer to the University of Oslo for amplification prior to NGS. In Oslo, one sample failed PCR after several trials with different sets of primer combinations. Although the primers 341F and 806R gave amplicons to sufficient levels during the PCR stage, presenting a clear, intense band when viewed by agarose gel electrophoresis, their amplification during high throughput sequencing was poor. This meant that there were not sufficient amounts of amplicon from some of the samples (for samples analysed see Figure 2.2) and it was not possible to analyze those on the sequencing platform. The final number of cases available for high throughput analysis were AD cases n=9 and non-AD cases n= 6 (Table 2.1).

The data from the referenced sequences represented 5284 bacterial reads in the 9 AD cases and 370 bacterial reads in the 6 control cases (Table 2.10) (AD mean per patient - 587 bacterial reads; control mean per patient – 61.6 bacterial reads). The average number of bacterial reads per patient is presented in conjunction to the genus/phylum data in Table 2.10. All the patients examined by high throughput (AD and controls) showed bacterial reads apart from the AD case AP7, where no bacterial gDNA was detected.

2.3.1.1 Bacterial community profiling

Based on the averages of reads per case there was a 9-fold higher number of bacterial reads in the AD cases, with an average number of bacterial reads in the AD cases of 587 and in the control cases of 62 (Table 2.10).

The bacterial reads, based on the 16S rRNA sequences, identified to phylum level in the AD cases consisted of Proteobacteria in abundance (3661 reads, mean per patient – 406.8 reads) followed by Firmicutes (761 reads, mean per patient – 84.6 reads), Bacteroidetes (466 reads, mean per patient - 51.7 reads) and Actinobacteria (393 reads, mean per – 43.6 patient) (Table 2.10 and Figure 2.3).

These phyla were also generally represented in the control cases, but at much lower numbers (Proteobacteria 306 reads, mean per patient – 51), (Firmicutes 31 reads, mean per patient – 5.2), (Bacteroidetes 25 reads, mean per patient – 4.2) and (Actinobacteria 4 reads, mean per patient – 0.7). A small number of Deinococcus-Thermus (Mean – 0.3 in the AD cases) and Fusobacteria (Mean 0.7 in the controls) were also detected (Table 2.10 and Figure 2.4).

Some of the bacterial reads were registered as unclassified. This indicated that there was enough of a sequence to say that this was from a bacterium or in some cases which phylum the organism came from, but not enough information to name it in a specific genus. The bacteria detected in the two groups were of similar origin (phylum) apart from the small number of Fusobacterium which only appeared in the controls.

The data obtained by high throughput sequencing identified bacterial gDNA to genus level and an important discovery was that two samples in the AD group had higher bacterial reads (AP8 – 1969 and AP18 -3088) than the rest of the cases tested.

Where the reads in these two samples represented 95.7% of all the reads detected in the 9 AD cases (Figure 2.2).

The most abundant genera across the AD- samples were *Halomonas* followed by *Pelomonas*, *Brevundimonas*, *Sediminibacterium*, *Staphylococcus*, *Escherichia_Shigella*, *Rhodanobacter*, *Enhydrobacter*, *Streptococcus*, *Veillonella*, *Pseudomonas*, *Brucella*, *Bradyrhizobium*, *Micrococcus*, *Rhizobium*, *Porphyromonas*, *Actinomyces unclassified*, *Methylobacterium*, *Acinetobacter*, *Novosphingobium*, *Chryseobacterium*, *Leifsonia*, *Burkholderia* and *Sphingomonas* (Figure 2.3).

In the control cases the most abundant genera were *Escherichia_Shigella*, *Pseudomonas*, *Pelomonas*, *Bradyrhizobium*, *Sediminibacterium* and *Streptophyta* (Figure 2.4).

Table 2.10 Overview of total bacterial reads in AD and non-AD cases by NGS (Genera in red have been identified in the oral microbiome).

Genus	Reads AD	Mean/patient	Reads non-AD	Mean/patient	Phylum/Family
<i>Actinomyces</i>	0	0	1	0.2	Actinobacteria
<i>Actinomyces_unclassified</i>	119	13.2	0	0	Actinobacteria _unclassified
<i>Brevibacterium</i>	37	4.1	0	0	Actinobacteria
<i>Corynebacterium</i>	1	0.1	2	0.3	Actinobacteria
<i>Brachybacterium</i>	1	0.1	0	0	Actinobacteria
<i>Dietzia</i>	1	0.1	0	0	Actinobacteria
<i>Leifsonia</i>	59	6.6	0	0	Actinobacteria
<i>Leifsonia_unclassified</i>	1	0.1	0	0	
<i>Micrococcus</i>	143	15.9	0	0	Actinobacteria
<i>Micrococcus_unclassified</i>	9	1	0	0	
<i>Rhodococcus</i>	0	0	1	0.2	Actinobacteria
<i>Rhodococcus_unclassified</i>	22	2.4	0	0	
Total Actinobacteria/ of these unclassified	393/151	43.6	4/0	0.67	
<i>Porphyromonas</i>	124	13.8	2	0.3	Bacteroidetes
<i>Prevotella</i>	3	0.3	3	0.5	Bacteroidetes
<i>Sediminibacterium</i>	241	26.8	17	2.8	Bacteroidetes
<i>Spirosoma</i>	2	0.2	0	0	Bacteroidetes
<i>Chryseobacterium</i>	92	10.2	3	0.5	Bacteroidetes
<i>Cloacibacterium</i>	1	0.1	0	0	Bacteroidetes
<i>Flavobacterium</i>	3	0.3	0	0	Bacteroidetes
Total Bacteroidetes/ of these unclassified	466/0	51.7	25/0	4.2	
<i>Meiothermus</i>	2	0.2	0	0	Deinococcus- Thermus
<i>Thermus</i>	1	0.1	0	0	Deinococcus- Thermus
Total Deinococcus-Thermus/ Of these unclassified	3/0	0.3	0/0	0	
<i>Leptotrichia</i>	0	0	2	0.3	Fusobacteria
<i>Leptotrichia_unclassified</i>	0	0	2	0.3	Fusobacteria
Total Fusobacteria, of these unclassified	0/0	0	4/2	0.7	

Genus	Reads AD	Mean/patient	Reads non-AD	Mean/patient	Phylum/Family
<i>Brevundimonas</i>	266	29.5	5	0.8	Proteobacteria
<i>Bradyrhizobium</i>	159	17.6	22	3.7	Proteobacteria
<i>Bradyrhizobium_unclassified</i>	3	0.3	1	0.2	
<i>Brucella</i>	161	17.8	0	0	Proteobacteria
<i>Brucella_unclassified</i>	1	0.1	0	0	
<i>Hyphomicrobium</i>	21	2.3	0	0	Proteobacteria
<i>Pedomicrobium</i>	0	0	1	0.2	Proteobacteria
<i>Methylobacterium</i>	112	12.4	7	1.2	Proteobacteria
<i>Rhizobium</i>	142	15.7	0	0	Proteobacteria
<i>Amaricoccus</i>	1	0.1	0	0	Proteobacteria
<i>Amaricoccus_unclassified</i>	125	13.9	0	0	
<i>Defluviicoccus</i>	2	0.2	0	0	Proteobacteria
<i>Novosphingobium</i>	101	11.2	0	0	Proteobacteria
<i>Sphingomonas</i>	53	5.9	3	0.5	Proteobacteria
<i>Burkholderia</i>	58	6.4	0	0	Proteobacteria
<i>Cupriavidus</i>	2	0.2	0	0	Proteobacteria
<i>Ralstonia</i>	19	2.1	0	0	Proteobacteria
<i>Ralstonia_unclassified</i>	4	0.4	0	0	
<i>Pelomonas</i>	576	64	45	7.5	Proteobacteria
<i>Pelomonas_unclassified</i>	21	2.3	0	0	
<i>Escherichia_Shigella</i>	201	22.3	118	19.7	Proteobacteria
<i>Escherichia_Shigella_unclassified</i>	1	0.1	2	0.3	
<i>Marinobacter</i>	19	2.1	0	0	Proteobacteria
<i>Marinobacter_unclassified</i>	115	12.8	4	0.7	Proteobacteria
<i>Halomonas</i>	624	69.3	2	0.3	Proteobacteria
<i>Halomonas_unclassified</i>	47	5.2	0	0	Proteobacteria
<i>Acinetobacter</i>	106	11.8	0	0	Proteobacteria
<i>Enhydrobacter</i>	185	20.5	10	1.7	Proteobacteria
<i>Pseudomonas</i>	171	19	79	13.2	Proteobacteria
<i>Pseudomonas_unclassified</i>	7	0.8	0	0	
<i>Luteibacter</i>	15	1.7	0	0	Proteobacteria
<i>Rhodanobacter</i>	196	21.8	0	0	Proteobacteria
<i>Stenotrophomonas</i>	27	3	3	0.5	Proteobacteria
<i>Stenotrophomonas_unclassified</i>	120	13.3	4	0.7	
Total Proteobacteria/of these unclassified	3661/443	406.8	306/11	51	

<i>Streptophyta</i>	23	2.6	15	2.5	
<i>Streptophyta</i> _unclassified	89	9.9	0	0	
<i>Paenibacillus</i>	0	0	1	0.2	Firmicutes
<i>Staphylococcus</i>	224	24.9	3	0.5	Firmicutes, Bacilli
<i>Abiotrophia</i>	0	0	4	0.7	Firmicutes, Bacilli
<i>Streptococcus</i>	185	20.6	4	0.7	Firmicutes, Bacilli
<i>Clostridium_sensu_stricto</i>	23	2.6	0	0	Firmicutes
<i>Clostridium_sensu_stricto_unclassified</i>	2	0.2	0	0	Firmicutes
<i>Faecalibacterium</i>	31	3.4	0	0	Firmicutes
<i>Veillonella</i>	180	20	4	0.7	Firmicutes
<i>Veillonella</i> _unclassified	4	0.4	0	0	
Total Firmicutes/ of these unclassified	761/95	84.6	31/0	5.2	
Total reads	5284	587.1	370	61.7	

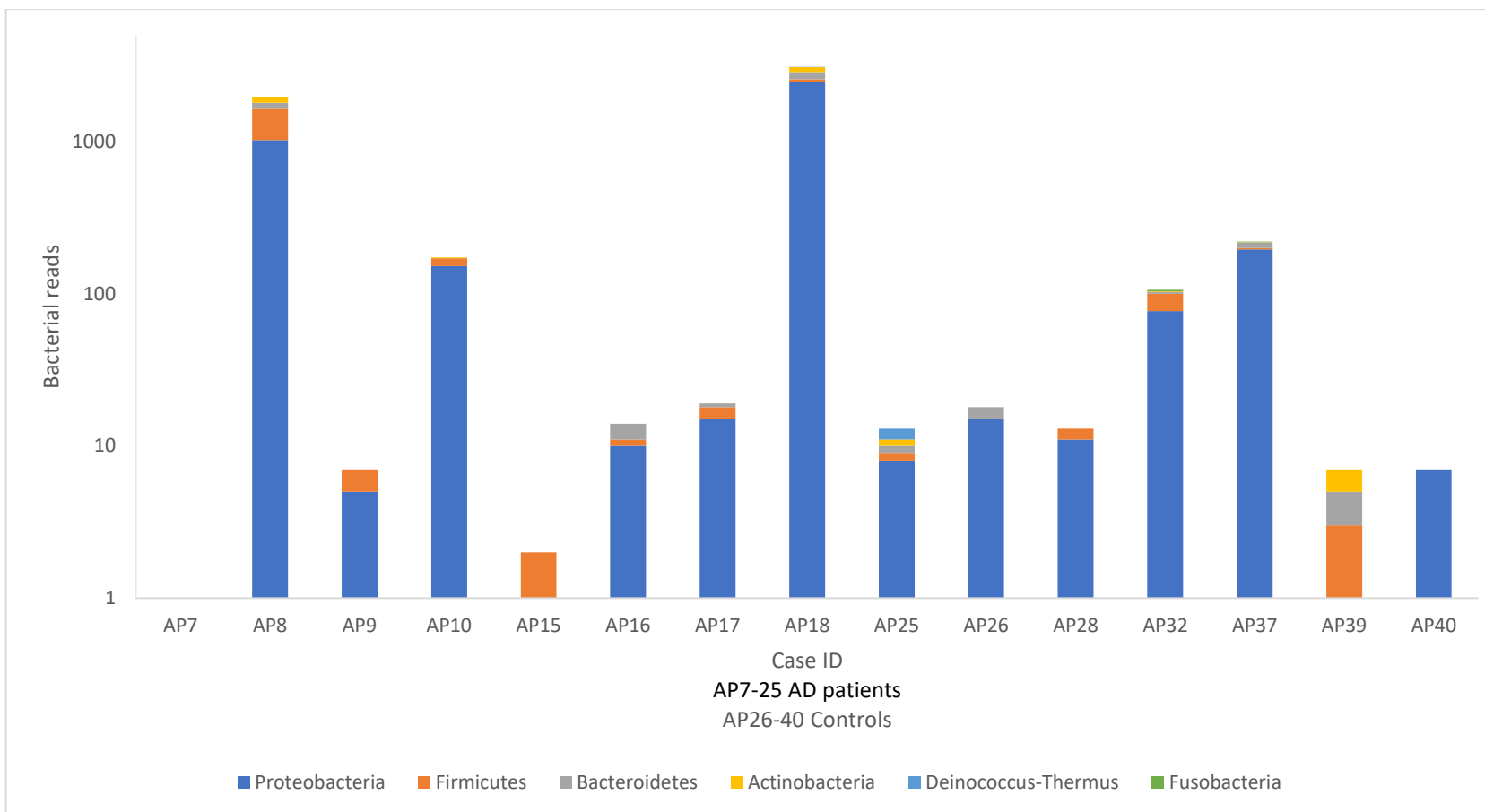


Figure 2.2 Results per case of bacterial reads by NGS at phylum level in AD (AP7-25) and control cases (AP26-40). The results show the bacterial reads, based on the 16S rRNA sequences, identified to phylum level in the AD cases consisted of Proteobacteria in abundance (3661 reads, mean per patient – 406.7 reads) followed by Firmicutes (761 reads, mean per patient – 84.6 reads), Bacteroidetes (466 reads, mean per patient 51.7 reads) and Actinobacteria (393 reads, mean per patient 43.6 reads). These phyla were also generally represented in the control cases, but at much lower numbers (Proteobacteria 306 reads, mean per patient – 51), (Firmicutes 31 reads, mean per patient – 5.2), (Bacteroidetes 25 reads, mean per patient – 4.2) and (Actinobacteria 4 reads, mean per patient – 0.7). A small number of Deinococcus-Thermus (Mean – 0.3 in the AD cases) and Fusobacteria (Mean 0.7 in the controls) were also detected.

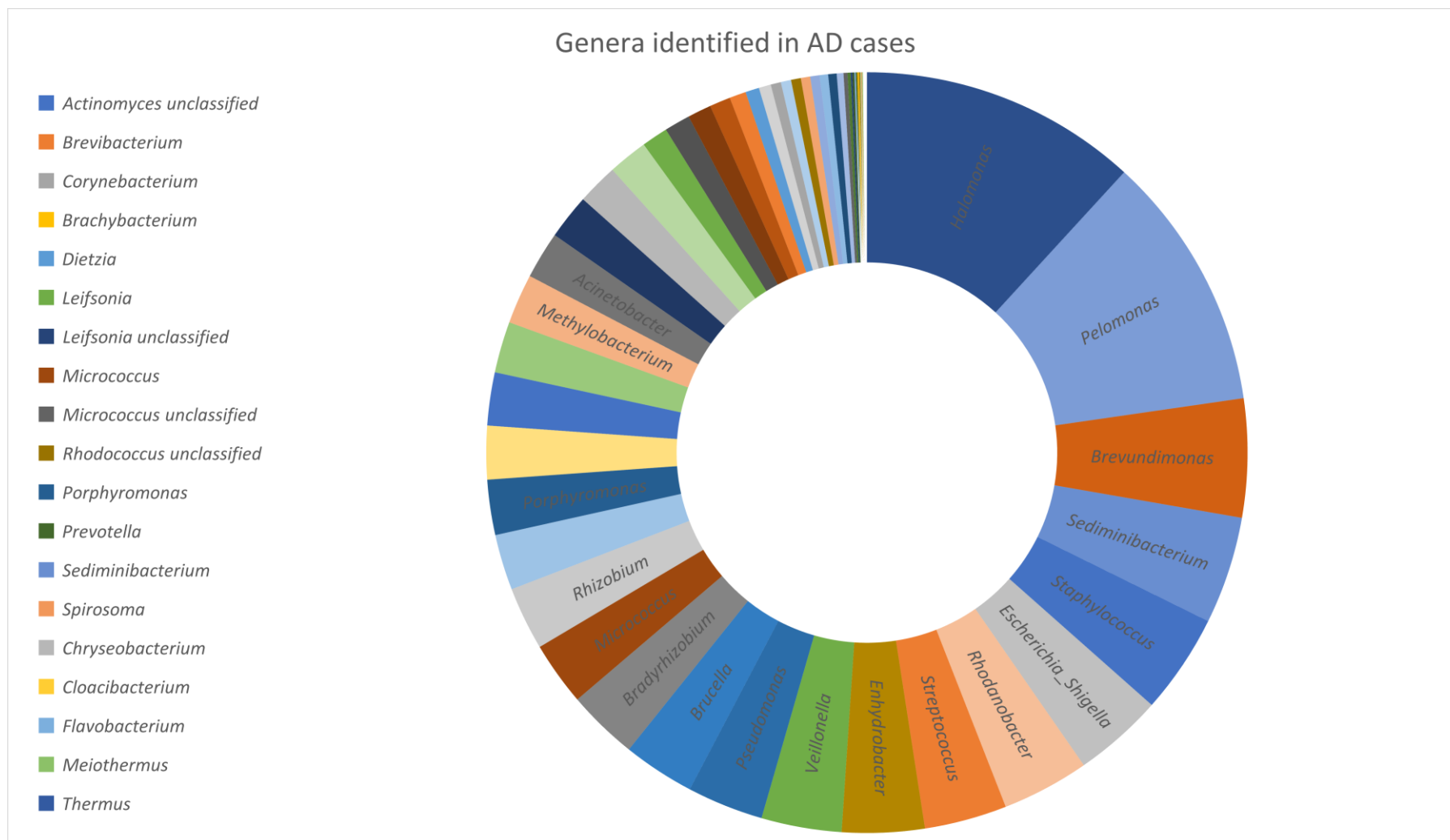


Figure 2.3 Spread of identified reads at genus level in AD cases analysed by NGS. The most abundant genera across the AD- samples were Halomonas followed by Pelomonas, Brevundimonas, Sediminibacterium, Staphylococcus, Escherichia_Shigella, Rhodanobacter, Enhydrobacter, Streptococcus, Veillonella, Pseudomonas, Brucella, Bradyrhizobium, Micrococcus, Rhizobium, Porphyromonas, Actinomyces unclassified, Methylobacterium, Acinetobacter, Novosphingobium, Chryseobacterium, Leifsonia, Burkholderia and Sphingomonas.

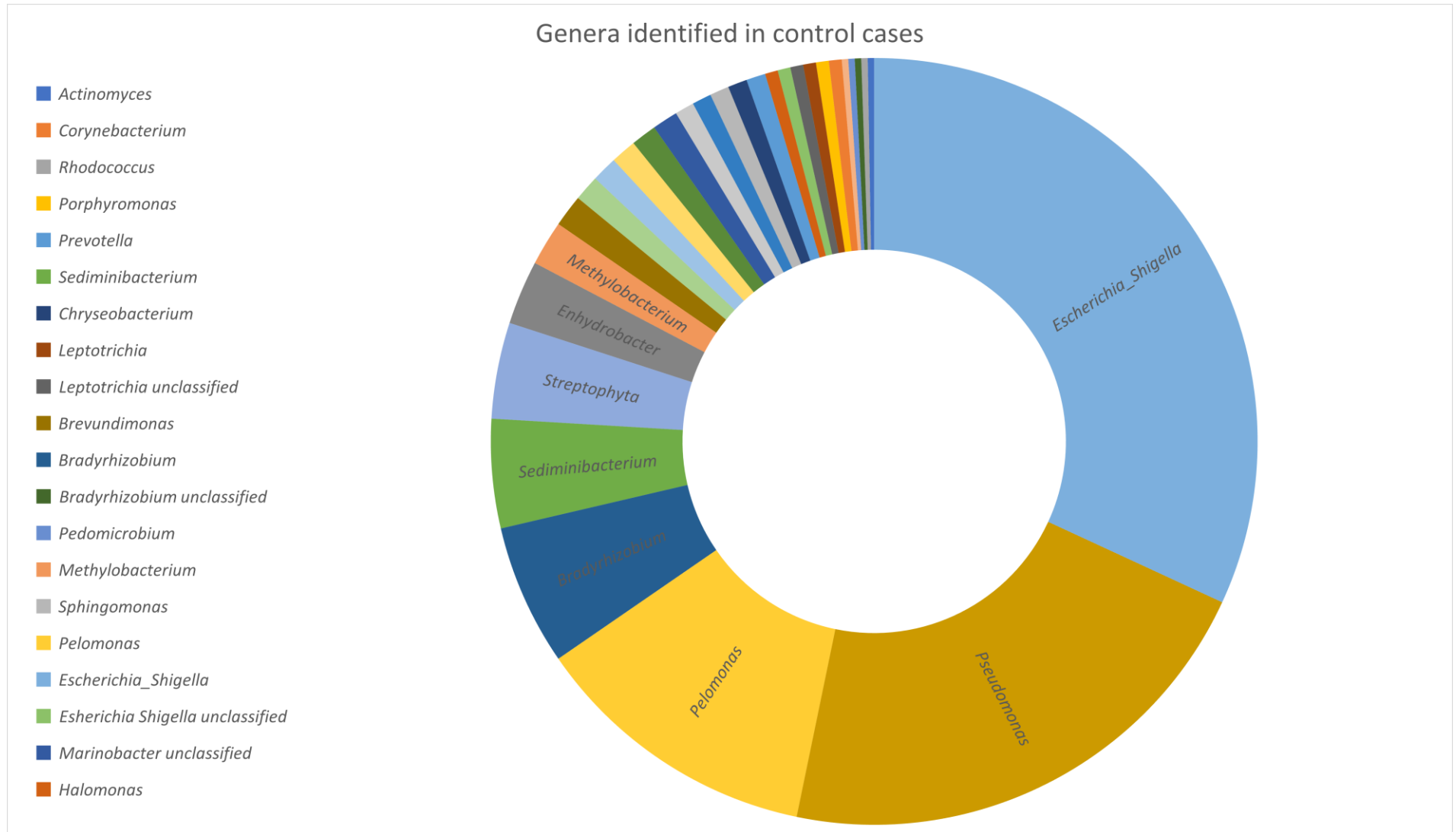


Figure 2.4 Spread of identified reads at genus level in control cases analysed by NGS. In the control cases the most abundant genera were *Escherichia_Shigella*, *Pseudomonas*, *Pelomonas*, *Bradyrhizobium*, *Sediminibacterium* and *Streptophyta*.

One of the weaknesses of bacterial studies of postmortem tissues is the risk of cross contamination at sample collection and delay in collection of the tissues which could potentially give rise to false positives. To determine whether there was a correlation, the delay in obtaining the biopsy was compared to how many bacterial reads were found in the tissue samples. The average post-mortem delay in the AD samples tested by high throughput sequencing were 46 hours and the controls were 44 hours. The average post-mortem delay in all the AD samples tested by PCR at UCLan were 37 hours and 39 hours for the non-AD controls. This shows that both cohorts had a similar delay from the time the person deceased and the point at which the samples were collected. There was no correlation seen between the number of bacterial reads from the NGS and the post-mortem delay (Figure 2.5).

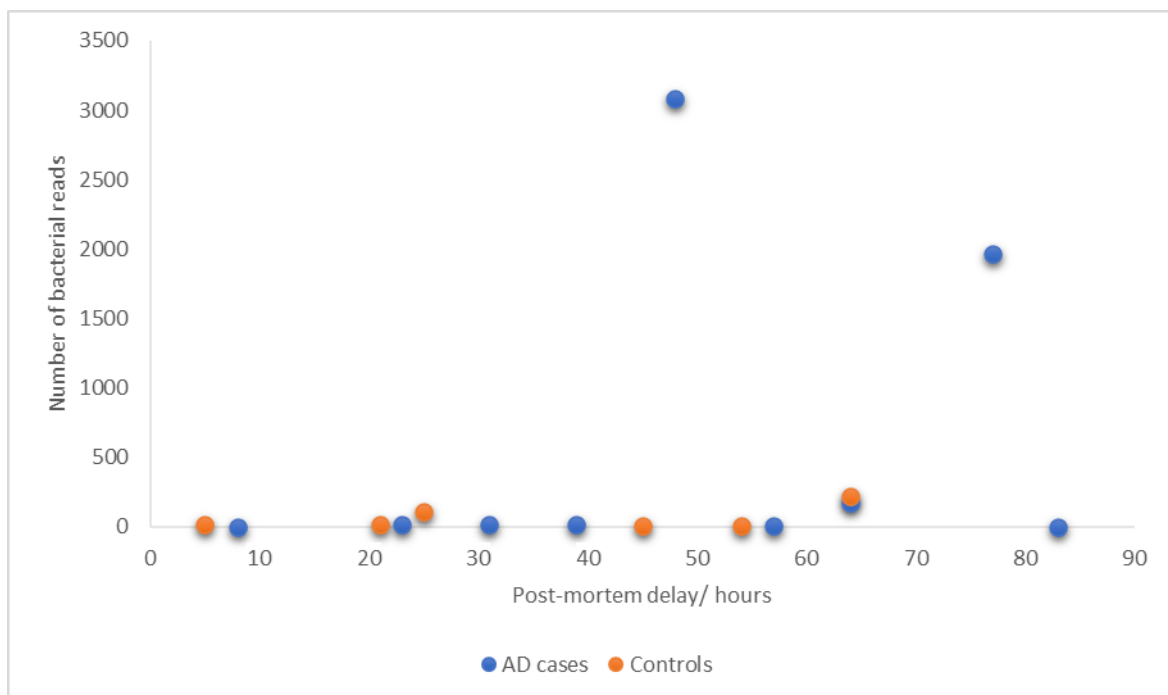


Figure 2.5 Number of bacterial reads by high throughput analysis in relation to post-mortem delay, the AD cases shown in blue and the non-AD controls shown in orange. There was no correlation between bacterial reads by high throughput analysis and postmortem delay.

2.3.2 Results PCR carried out at UCLan

The high throughput sequence analysis had only screened for bacteria and the unsuccessful amplification of some of the post-mortem samples, had reduced the cohort tested by NGS to n=9 AD and n=6 control. Therefore, PCR analysis was performed on all 40 brain samples at UCLan. The bacterial PCR primers (F342 and F18R) were selected as used in the methodology of the study by Emery *et al.*, (2017). These 16S rRNA PCR primers have been shown to have a wide taxonomical coverage of gene sequences from phyla commonly found in the human microbiome including the mouth (Emery *et al.*, 2017), where F342 represents the universal variable region-3 and F18R is the reverse primer (Figure 2.1).

As mentioned previously, the 16S region is essential for translation of mRNA as part of the ribosome, is highly conserved across bacterial species and unique to bacteria without overlap with eukaryotes. This primer pair were suitable for our samples because of the low probability of amplification of human (eukaryotic) RNA sequences (Mori *et al.*, 2014). The expected size product with this primer pair is first a 200 bp band potentially followed by a smaller 174 bp band (Emery *et al.*, 2017).

The PCR assays were optimised to the protocols outlined in Table 2.9 with the PCR master mix in Table 2.7.

The main challenges encountered during the optimising of the PCR method was the visualisation of non-specific products caused by non-specific binding of the primers and the formation of primer dimers when applied to mouse and *Escherichia coli* gDNA. This was mainly occurring with the bacterial primers (Table 2.8). These issues were resolved by altering the annealing temperature, changing the concentration of the DNA template, altering the MgCl₂ concentration, adding DMSO to the reaction and adjusting the agarose gel concentration. The optimisation resolution to these issues is described in further details below.

2.3.2.1 Annealing temperature

The first challenge was to find an annealing temperature where both the mammalian and bacterial or fungal primers produced a band at the same time, without showing non-specific binding. It was important to include the mammalian primers in each reaction as a positive control to ensure a reaction had taken place and there was sufficient gDNA in the reaction. If the annealing temperature is too high the primers may be unable to bind to the template and if too low could bind non-specifically. The annealing time also must be considered, as if too short there may not be enough time in the process for the primers to bind to the template. Initially, the PCR programmes selected were as described in the studies outlined above (Emery *et al.*, 2017; Ghannoum *et al.*, 2010; Salingcarnboriboon *et al.*, 2006 and Nauta *et al.*, 2005).

First the fungal primers were optimised, then the mammalian primers followed by the two primers together. This was carried out by using template from *Candida albicans* culture and mouse brain spiked with *Candida albicans*. Initially the protocols from Ghannoum *et al.*, (2010), Salingcarnboriboon *et al.*, (2006) and Nauta *et al.*, (2005) were applied (annealing temperatures of 50-55 °C), but these did not produce any bands. Therefore, the PCR reactions were commenced at an annealing temperature of 48 °C to allow for a gradual increase as outlined above. Further temperature gradients were tested on a PCR machine allowing for gradients of temperatures in the same process. At these initial protocols the mouse control showed the expected product at 450 bp, but the positive control (*Candida albicans*) and the spiked mouse brain showed a much larger band at 1000 bp and multiple smaller bands larger than 200bp, which would suggest these were non-specific products caused by the primers non-specifically binding to other parts of the *Candida albicans* gDNA. At this stage the negative controls (molecular grade water) showed no band. The negative controls used were mouse brain template with fungal primer, *Candida albicans* template with mammalian primer, molecular grade water instead of template or no Taq polymerase in the

reaction. The fungal primers (ITS1F and ITS2) persisted to show a wide and multiple bands, larger than the expected size the with *Candida albicans* template in the annealing temperature range of 48-52°C (Figure 2.6B, Lane 4) and multiple bands were still seen in the temperature range 60-62.8°C (Figure 2.6A, Lane 4 and 2.6C, Lanes 1,2,3). However, the 1000bp band became less intense with increase in temperature and the smaller bands disappeared at 64.3°C (Figure 2.6C, Lane 4). When incorporating the mammalian primers with the fungal, the best results regarding a reduction in the appearance of the multiple non-specific bands, was seen at the annealing temperature of 60°C (Figure 2.6D), where two bands were seen with the fungal primer set at 500 and 200 bp. When temperatures above 60°C were used in consecutive reactions with *Candida albicans* spiked mouse brain template, all bands disappeared completely above 60°C. The expected size product for the fungal primer set was 200-250bp, but the repeated appearance of the large 500bp band was accepted at this stage in the temperature optimisation as a true amplicon result for both templates of *Candida albicans* and mouse spiked with *Candida albicans*, as it was anticipated that the wide 500bp band could become narrower when applied to the human samples as the concentration of any potential fungal gDNA would likely be much smaller than in the optimisation reactions.

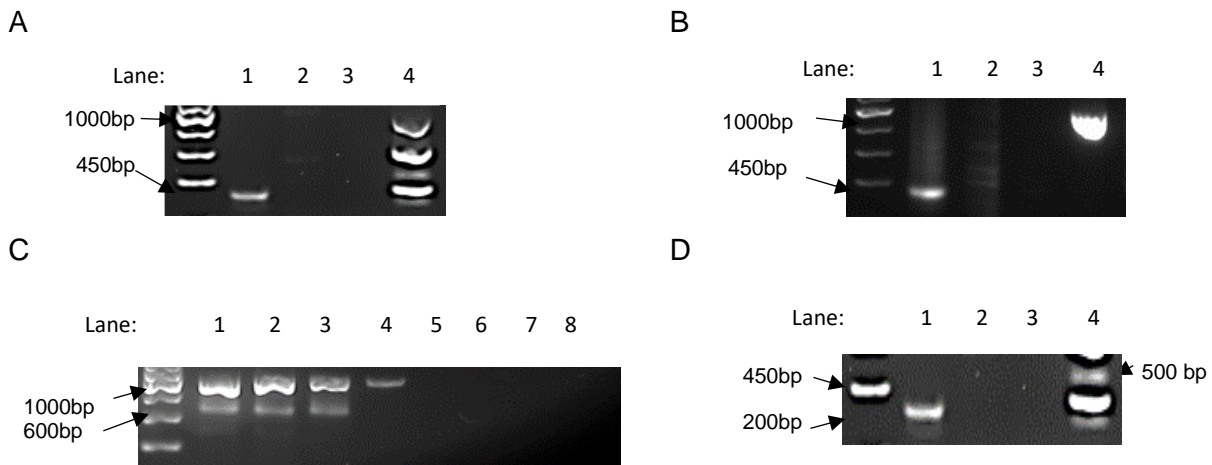


Figure 2.6 Optimisation reactions with mammalian and fungal primer sets. All reactions followed initial 5 min denaturation step at 95°C was followed by 30 cycles of 95°C, 60 s; annealing temperature indicated in each reaction, 30 cycles of 60 s; 30 cycles of 72°C, 30 s with a final 7 min extension at 72°C **A** Mouse brain and *Candida albicans* template with mammalian (167musGapdhf/r) and fungal (ITS1F/2) primers at annealing temperature 60°C. Multiple bands were seen for the fungal primers with *Candida albicans* template at this temperature in lane 4. Lane 1: Mouse + 167musGapdhf/r Lane 2: Mouse + ITS1F,ITS2 Lane 3: *Candida albicans* + 167musGapdhf/r Lane 4: *Candida albicans* + ITS1F,ITS2. **B** Mouse and *Candida albicans* template with mammalian (167musGapdhf/r) and fungal (ITS1F/2) primers at annealing temperature 52°C. A large 1000bp band was seen from the *Candida albicans* template with the fungal primers in lane 4. Lane 1: Mouse + 167musGapdhf/r Lane 2: Mouse + ITS1F, ITS2 Lane 3: *C. albicans* + 167musGapdhf/r Lane 4: *C. albicans* + ITS1F,ITS2. **C** *Candida albicans* template with fungal primers (ITS1F and ITS2) at incremental annealing temperatures. 1000bp band decreases in size with rise in temperature and disappears above 64.3°C. Lane 1: 60 ° C Lane 2: 61.4 ° C Lane 3: 62.8 ° C Lane 4: 64.3 ° C Lane 5: 65.7 ° C Lane 6: 67.2 ° C Lane 7: 68.6 ° C Lane 8: 70 ° C. **D** Combination of mammalian (167musGapdhf/r) and fungal primers (ITS1F/2) applied to mouse brain and *Candida albicans* template at 60°C. The mammalian primer is clear of non-specific bands on the *Candida albicans* template at 60°C, lane 2 and there is an intense 500bp band with *Candida albicans* and the fungal primers (ITS1F,ITS2). Lane 1: Mouse + 167musGapdhf/r Lane 2: Mouse + ITS1F,ITS2 Lane 3: *Candida albicans* + 167musGapdhf/r Lane 4: *Candida albicans* + ITS1F,ITS2.

The mammalian primers (167mus Gapdh forward and 167musGapdh reverse) were found to consistently show a band at 450bp with mouse brain gDNA template in the annealing temperature range of 60-68.6 °C (faint band at 67.2°C) (Figure 2.7).

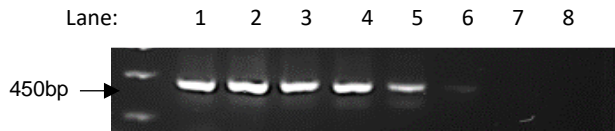


Figure 2.7 Mammalian primers 167musGapdhf and 167musGapdhr with un-spiked mouse brain DNA template at incremental annealing temperature show a band at 450bp in the annealing temperature range of 60-68.6 °C. Lane 1: 60° C Lane 2: 61.4 ° C Lane 3: 62.8 ° C Lane 4: 64.3 ° C Lane 5: 65.7 ° C Lane 6: 67.2 ° C Lane 7: 68.6 ° C Lane 8: 70 ° C. The PCR program was initial 5 min denaturation step at 95°C was followed by 30 cycles of 95°C, 60 s; annealing temperature indicated in each reaction, 30 cycles of 60 s; 30 cycles of 72°C, 30 s with a final 7 min extension at 72°C

The bacterial primers (F342 and F18R) were found to show the expected 200bp band with *Escherichia coli* template in the annealing temperature range 55-67.8°C (Figure 2.8, Lanes 1,2,4) and there were no non-specific bands when the bacterial primers were applied to mouse template in the annealing temperature range 68.6- 70°C (Figure 2.9, Lanes 7,8). After further incremental testing the annealing temperature of 67.8°C was chosen for the reactions with bacterial primers and mammalian primers in conjunction.

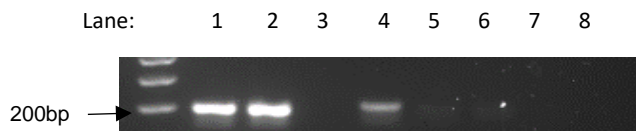


Figure 2.8 *Escherichia coli* with bacterial primers F342 and F18R at increments in annealing temperature. A 200bp band is visualised up to 67.87°C. Lane 1: 67.00° C Lane 2: 67.29° C Lane 3: 67.58° C Lane 4: 67.87° C Lane 5: 68.16° C Lane 6: 68.45° C Lane 7: 68.74° C Lane 8: 69.00° C. The PCR program for the reaction was initial 5 min denaturation step at 95°C was followed by 30 cycles of 95°C, 60 s; annealing temperature indicated in each reaction, 30 cycles of 60 s; 30 cycles of 72°C, 30 s with a final 7 min extension at 72°C.

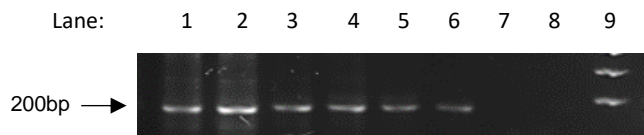


Figure 2.9 Un-spiked mouse gDNA template with bacterial primers F342 and F18R, the non-specific band gone above 68.6°C .
 Lane 1: 60.0° C Lane 2: 61.4° C Lane 3: 62.8° C Lane 4: 64.3° C Lane 5: 65.7 C Lane 6: 67.2° C Lane 7: 68.6° C Lane 8: 70.0° C.
 Lane 9: DNA ladder.

The PCR program for the reaction was initial 5 min denaturation step at 95°C was followed by 30 cycles of 95°C, 60 s; annealing temperature indicated in each reaction, 30 cycles of 60 s; 30 cycles of 72°C, 30 s with a final 7 min extension at 72°C.

The referenced protocol for the bacterial primers (F342 and F18R) (annealing temperature of 65°C) (Emery *et al.*, 2017) was initially applied to template of *Escherichia coli* and mouse spiked with *Escherichia coli* and this showed bands of non-specific binding in some of the negative controls (described above) when the products were visualised. Therefore, a range of temperatures were tested on these templates with the bacterial primer pair and subsequently the mammalian primers were applied also. An example of this optimisation is the *Escherichia coli* template with the mammalian primers (as a control) in the annealing temperature range 55 - 59.3 which showed an undesirable band, but these were not present between 60.7 - 70°C (Figure 2.10, Lanes 5,6,7,8).

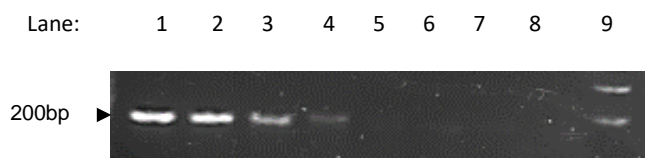


Figure 2.10 *Escherichia coli* template with mammalian primer at incremental temperature increases.

The PCR program for the reaction was initial 5 min denaturation step at 95°C was followed by 30 cycles of 95°C, 60 s; annealing temperature indicated in each reaction, 30 cycles of 60 s; 30 cycles of 72°C, 30 s with a final 7 min extension at 72°C.

The non-specific band is gone at 60.7°C. Lane 1: 55° C Lane 2: 56.4° C Lane 3: 57.9° C Lane 4: 59.3° C Lane 5: 60.7° C
 Lane 6: 62.2° C Lane 7: 63.6° C Lane 8: 65 ° C Lane 9: DNA ladder.

2.3.2.2 MgCl₂

Following optimisation of the annealing temp, the aim was to ensure that the reaction parameters were optimised in order to detect low levels of bacterial/fungal DNA.

This involved investigating MgCl₂ concentration at annealing temperature of 67.8 °C and the potential use of DMSO, which can reduce primer dimers which could relate to the presence of the non-specific bands seen in some of the reactions with the bacterial primer set (F342 and F18R).

Magnesium is a co-factor for Taq polymerase and optimisation of the concentration is important as too little can reduce efficiency of the enzyme. Too much can decrease specificity, as excess Mg²⁺ can stabilise incorrect primer bonding to the template (Markoulatos *et al.*, 2002). The optimal MgCl₂ concentration was found to be 4mM for the bacterial primers applied to *Escherichia coli* or mouse template (Figure 2.11, Lane 3 and 4), as a band with bacterial template was present at the expected size (200bp) at this concentration (Figure 2.11, Lane 4) and there was no band visualised in the mouse control at this concentration (Figure 2.11, Lane 3). Non-specific bands were seen for the other MgCl₂ reactions with mouse template, unless of course these bands were cross contamination.

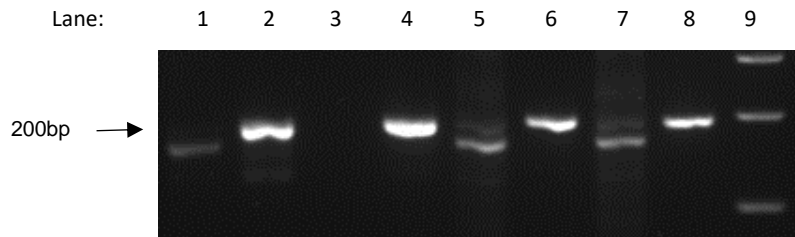


Figure 2.11 *Escherichia coli* or mouse template with primer set F342 and F18R at various concentrations of MgCl₂ at annealing temperature of 67.8 °C . The PCR program for the reaction was initial 5 min denaturation step at 95°C was followed by 30 cycles of 95°C, 60 s; annealing temperature 67.8 °C, 30 cycles of 60 s; 30 cycles of 72°C, 30 s with a final 7 min extension at 72°C. The undesirable non-specific band has gone in the 4 mM MgCl reaction with mouse template (Lane 3). Lane 1: Mouse template with 2mM MgCl₂, Lane 2: *E. coli* template with 2mM MgCl₂, Lane 3: Mouse template with 4mM MgCl₂, Lane 4: *E. coli* template with 4mM MgCl₂, Lane 5: Mouse template with 6mM MgCl₂, Lane 6: *E. coli* template with 6mM MgCl₂, Lane 7: Mouse template with 8mM MgCl₂, Lane 8: *E. coli* template with 8mM MgCl₂, Lane 9: DNA ladder

The MgCl₂ concentration in the reactions with the mammalian and fungal primers were the standard concentration of 2mM for both the mammalian and fungal primers as the appearance of additional bands were not as frequent in these reactions.

2.3.2.3 DMSO

The addition of Dimethyl sulfoxide (DMSO) to the reactions with the bacterial primer set was carried out as outlined above, at this stage non-specific binding appeared to be mainly a feature of the bacterial PCR reactions, rather than the mammalian or fungal.

If a gDNA template is high in G-C (guanine and cytosine), the triple hydrogen bond between G and C makes them more stable during PCR (Kramer and Coen, 2001). This means higher temperatures are required during amplification and the bonds stability can induce secondary structure formation (primer dimers). The bacterial primers utilised (F342 and F18R, Table 2.8) were designed with a high G/C content, which could explain the more frequent

appearance of non-specific binding in these reactions compared to the fungal primer set (ITS 1F and ITS2, Table 2.8).

By adding DMSO to the PCR reaction the denaturing temperature is lowered because the hydrogen bonds are weakened as it changes the conformation of cytosine (Kramer and Coen, 2001). The DMSO also binds to the gDNA and therefore prevent re-annealing of the single strands of gDNA and it increases the annealing of primer to template (Kramer and Coen, 2001). DMSO can thus increase the specificity of a PCR reaction, but too much DMSO can increase the mispairing of bases during PCR and therefore introduce mutations in the process. The optimal quantity of DMSO in the bacterial primer set PCR reaction was found to be 2%. This was concluded as non-specific bands were seen in the reactions with *E. coli* template and no DMSO and in the control with water and 1 % DMSO (Figure 2.12, Lanes 1 and 6).

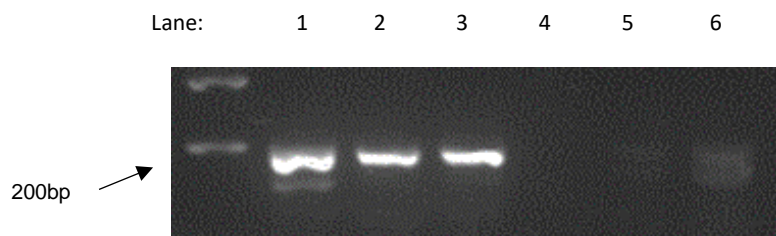


Figure 2.12 DMSO optimisation gel, . The PCR program for the reaction was initial 5 min denaturation step at 95°C was followed by 30 cycles of 95°C, 60 s; annealing temperature 67.8 °C, 30 cycles of 60 s; 30 cycles of 72°C, 30 s with a final 7 min extension at 72°C, 4mM MgCl₂. *Escherichia coli* template at 0.08 ng/μl with primer set F342 and F18R and the same primers applied to distilled water controls, Variations in DMSO concentrations affected the appearance of the bands. In lane 1, a non specific band is seen in the *Escherichia coli* template with no DMSO. In lanes 2 and 3, the expected 200bp band appears with *Escherichia coli* template with 2 % and 1 % DMSO, but in the controls there is an appearance of a non specific band in the negative control with water and 1 % DMSO. Lane 1: *Escherichia coli* template and no DMSO, Lane 2: *Escherichia coli* template and 2% DMSO, Lane 3: *Escherichia coli* template and 1% DMSO, Lane 4: H₂O and no DMSO, Lane 5: H₂O and 2% DMSO, Lane 6: H₂O and 1% DMSO.

2.3.2.4 Template concentrations

At this point in the PCR optimisation, it was important to determine the minimal concentration of bacterial/fungal DNA that can be detected by this method.

The limit of detection has implications for when the primers are applied to the human samples as the level of microbial DNA in the human brain are likely to be very small.

The sensitivity of the bacterial and fungal primers (F342/F18R and ITS1F/ITS2) for detection of the control templates (*Escherichia coli* and *Candida albicans*, quantified by nanodrop) was established by quantification experiments (Figure 2.13 and 2.15). The fungal primer set detected the *Candida albicans* template down to a concentration of 0.02 ng/ul, showing a 200bp and 500bp band at this concentration (Figure 2.13, Lane 5).

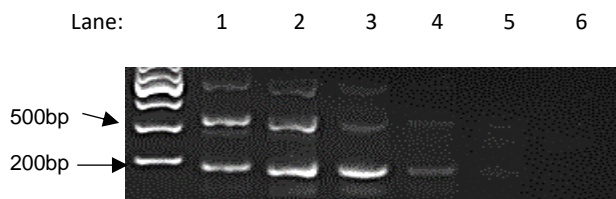


Figure 2.13 Quantification test for sensitivity of fungal primer set. The PCR program for the reaction was initial 5 min denaturation step at 95°C was followed by 30 cycles of 95°C, 60 s; annealing temperature 60 °C, 30 cycles of 60 s; 30 cycles of 72°C, 30 s with a final 7 min extension at 72°C, 2mM MgCl₂. Visualised on 2% agarose gel. The detection limit seen at 0.02 ng/ul of gDNA template from *Candida albicans* producing a 200bp and 500bp band (Lane 5) with the fungal primers ITS1F and ITS2. Lane 1: *C. albicans* 200 ng/ul, Lane 2: *C. albicans* 20 ng/ul, Lane 3: *C. albicans* 2 ng/ul, Lane 4: *C. albicans* 0.2 ng/ul, Lane 5: *C. albicans* 0.02 ng/ul, Lane 6: *C. albicans* 0.002 ng/ul.

These experiments were repeated in the presence of mouse gDNA, as the presence of mice template could potentially change the detection range of the fungal or bacterial template.

gDNA from *Candida albicans* was spiked into a consistent concentration of mouse gDNA to find the lowest concentration that the fungal template could be detected (Figure 2.14). It was found that the fungal primer set applied to mouse brain spiked with *Candida albicans* gDNA

had a detection range down to 0.07 ng/μl (Figure 2.14, Lane 5) which was similar to the detection level of the pure fungal template at 0.02 ng/μl (Figure 2.13, Lane 5), based on the 500bp band.

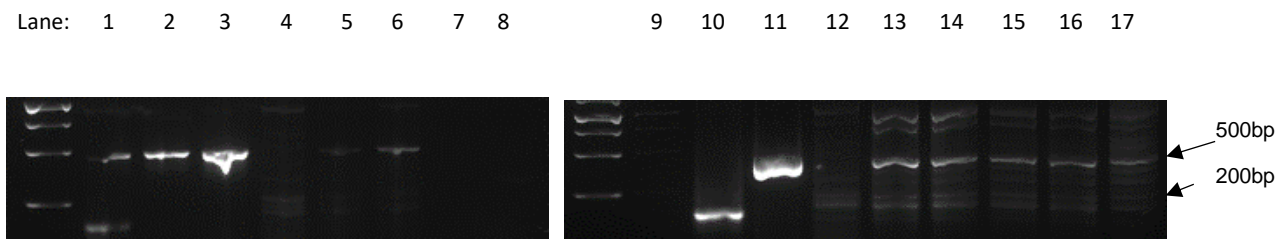


Figure 2.14 Quantification test for sensitivity of fungal primer set applied to mouse brain gDNA spiked with *Candida albicans* gDNA template. The PCR program for the reaction was initial 5 min denaturation step at 95°C was followed by 30 cycles of 95°C, 60 s; annealing temperature 60 °C, 30 cycles of 60 s; 30 cycles of 72°C, 30 s with a final 7 min extension at 72°C, 2mM MgCl₂. Visualised on 2% agarose gel. The detection limit seen at mouse brain gDNA spiked with 0.07 ng/μl of *Candida albicans* gDNA template producing a 500bp band and a less intense band at 200bp with fungal primers ITS1F and ITS2. Lane 1: Mouse and *C. albicans* 0.07 ng/μl with primers 167musGAPDHf/r, Lane 2: *C. albicans* 4 ng/μl with primers ITS1F,ITS2, Lane 3: *C. albicans* 4 ng/μl with primers ITS1F,ITS2, Lane 4: Mouse with ITS1F,ITS2 primers, Lane 5: Mouse and *C. albicans* 0.07 ng/μl with primers ITS1F,ITS2, Lane 6: Mouse and *C. albicans* 0.7 ng/μl with ITS1F,ITS2, Lane 7: Mouse and *C. albicans* 0.007ng/μl with primers ITS1F,ITS2, Lane 8: Mouse and *C. albicans* 0.0007 ng/μl with primers ITS1F,ITS2, Lane 9: molecular water and primers ITS1F,ITS2, Lane 10: Mouse template with primers 167musGAPDHf/r, Lane 11: *C. albicans* 4 ng/μl with primers ITS1F,ITS2, Lane 12: Mouse with primers ITS1F,ITS2, Lane 13: Mouse and *C. albicans* 6.9 ng/μl with primers ITS1F,ITS2, Lane 14: Mouse and *C. albicans* 3.5 ng/μl with primers ITS1F,ITS2, Lane 15: Mouse and *C. albicans* 1.4 ng/μl with primers ITS1F,ITS2, Lane 16: Mouse and *C. albicans* 0,7 ng/μl + ITS1F,ITS2, Lane 17: Mouse and *C. albicans* 0.07 ng/μl with primers ITS1F,ITS2.

The bacterial primer set detected the *Escherichia coli* template down to a concentration of 0.08 ng/μl, visualised by a 200bp band with primers F342 and F18R (Figure 2.15, Lane 3).

The detection level of the *Escherichia coli* template spiked into mouse brain gDNA was seen to be higher (0.16 ng/μl) than when the pure bacterial template was tested with the bacterial primer pair F342 and F18R producing a 200bp band (Figure 2.16, Lane 3).

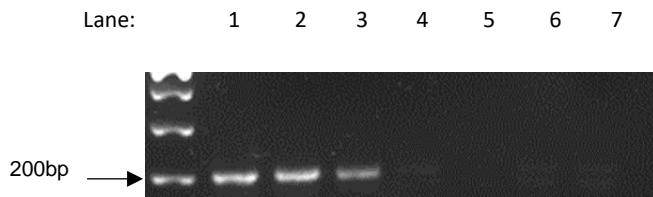


Figure 2.15 Quantification test for sensitivity of bacterial primer set. The PCR program for the reaction was initial 5 min denaturation step at 95°C was followed by 30 cycles of 95°C, 60 s; annealing temperature 67.8 °C, 30 cycles of 60 s; 30 cycles of 72°C, 30 s with a final 7 min extension at 72°C, 4 mM MgCl₂. Visualised on 2.5 % agarose gel. The detection limit seen at 0.08 ng/μl of *Escherichia coli* template producing a 200bp band with primers F342 and F18R (Lane 3). Lane 1: *Escherichia coli* template at 8 ng/μl, Lane 2: *Escherichia coli* template at 0.8 ng/μl, Lane 3: *Escherichia coli* template at 0.08 ng/μl, Lane 4: *Escherichia coli* template at 0,008 ng/μl, Lane 5: *Escherichia coli* template at 0.0008 ng/μl, Lane 6: *Escherichia coli* template with 0.00008 ng/μl, Lane 7: negative control with H₂O instead of template.

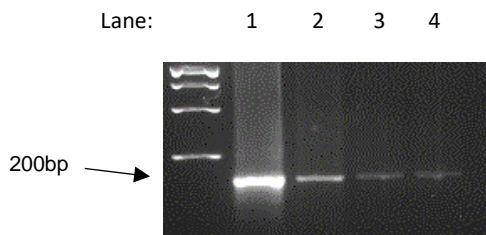


Figure 2.16 Quantification test of mouse brain gDNA spiked with *Escherichia coli* template. The PCR program for the reaction was initial 5 min denaturation step at 95°C was followed by 30 cycles of 95°C, 60 s; annealing temperature 67.8 °C, 30 cycles of 60 s; 30 cycles of 72°C, 30 s with a final 7 min extension at 72°C, 4 mM MgCl₂. Visualised on 2.5 % agarose gel. The detection limit seen in mouse template spiked with 0.16 ng/μl of *Escherichia coli* template producing a 200bp band with primers F342 and F18R. Controls: mouse template with bacterial primer set F342 and F18R, *Escherichia coli* template with primers F342 and F18R (not shown). Lane 1: Mouse template with primers 167musGAPDHf/r, Lane 2: Mouse template and *Escherichia coli* 0.8 ng/μl with F342,F18R, Lane 3: mouse template and *Escherichia coli* 0.4 ng/μl with F342,F18R, Lane 4: Mouse template and *Escherichia coli* 0.16 ng/μl with F342,F18R.

2.3.2.5 Human samples

The gDNA concentration in the extracted template from the human brain samples AP1-40 were measured by nanodrop (Section 2.2.2) and samples with a ratio 260nm/280nm > 1.7 were selected for testing. The ratio of gDNA absorbance maximum to the absorbance at 280 nm is a measure of purity in the gDNA extraction (Wilhelm *et al.*, 2011), the 260nm/280nm ratio above 1.7 was utilised in Emery *et al.* (2017) and readings below this level could indicate contamination with extraction reagents or RNA fragments which could introduce bias in the PCR process (Wilhelm *et al.*, 2011).

The human gDNA sample PCR reactions were tested in the range 0.8 – 6.4 ng/μl gDNA template. It was found that the concentration of 1.6 ng/μl (40 ng template in 25 μl reaction) gave consistent clear bands in the positive control, indicating that this was an optimal PCR template concentration, also the mammalian primer set displayed the expected size bands of 450bp at this concentration (Figure 2.17, Lanes 1,3,5,7,9,11 and 13) (Salingcarnboriboon *et al.*, 2006 and Nauta *et al.*, 2005). Whereas higher template concentrations showed no bands (not shown). Therefore, this concentration was used for the human templates for the PCR amplification of all samples AP1-40. The appearance of an additional band at 170bp with the mammalian primer set in the human samples could be explained by the difference in human and mouse gDNA sequences i.e., introns or exons, or variation in isoforms of GAPDH could account for the additional 170bp band (Margaryan *et al.*, 2015) (Figure 2.17, Lanes 1,3,5,7,9,11,13).

The bacterial (F342F/R) and fungal (ITS1/2) primer sets applied to the human gDNA samples showed no non-specific bands (Bacterial: Figure 2.17, Lanes 2,4,6,8,10,12,14 and Figure 2.18, Lane 2. Fungal: 2.19, Lanes 2,4) and therefore all human samples were tested with the optimised protocols.

The bacterial and mammalian primers applied to the gDNA extracted from the human brain samples AP1-40, showed amplification products at the expected sizes (170bp and 200bp for F342/318R) and 450bp for (167musGapdhF/R) (Emery *et al.*, 2017; Salingcarnboriboon *et al.*, 2006; Nauta *et al.*, 2005). As the optimisation of the bacterial primer set F342/381R had indicated that the presence of a 200bp band represented a positive bacterial sample, this was applied to the evaluation of the human gDNA samples after F342/381R primer set amplification. All the PCR protocols were repeated 3 -4 times for each human sample and the results of all the gels and how results correlate to the findings in the NGS study is summarised in Table 2.11. A sample was determined as positive if all or the majority of the experiments showed a 200bp band (three out of four) or in two out of four if there was a clear intense 200bp band present (Table 2.11). Visualisation of 200bp bands representing the presence of bacterial gDNA were detected in 10 AD samples (40%) (Figure 2.20 and 2.21) and 7 non-AD samples (46%) (Figure 2.22). All samples gave a positive result with the mammalian primers, indicating all reagents were working. The other controls which were applied to the reactions were water instead of template with the bacterial primer set (negative control) and *Escherichia coli* template with the bacterial primer set (positive control) all showed the expected appearance when visualised by electrophoresis. A summary of gels AP1-40 is found below in Table 2.11.

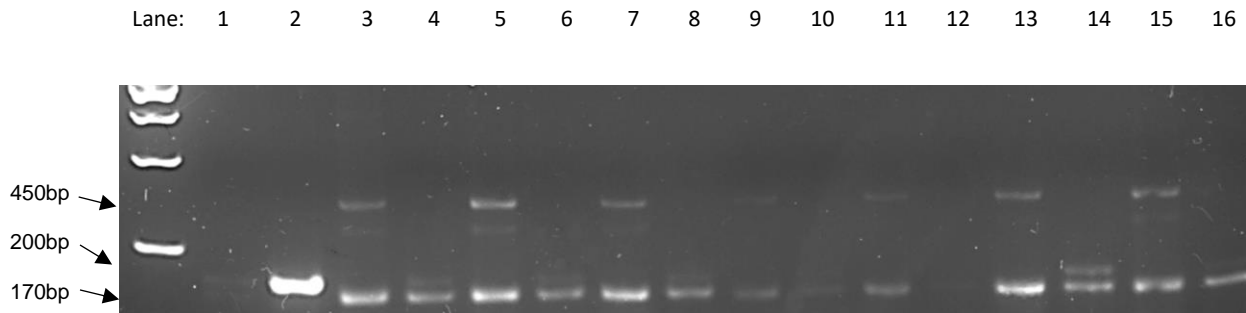


Figure 2.17 The mammalian primers (167musF/R) applied to the human gDNA samples AP7 and AP12-17, showing a 450 bp band as expected and also an additional non-specific 170 bp band, which was accepted as proof of a positive PCR process having taken place. The PCR program for the reaction was initial 5 min denaturation step at 95°C was followed by 30 cycles of 95°C, 60 s; annealing temperature 67.8 °C, 30 cycles of 60 s; 30 cycles of 72°C, 30 s with a final 7 min extension at 72°C, 4 mM MgCl₂. Visualised on 2.5 % agarose gel. Some of the human gDNA samples tested with the bacterial primer set F342/F18R showed a 170bp band only or both a 170 bp and a 200bp band in this reaction (Emery et al., 2017), Sample AP15 showed a very small 170bp band in this reaction. Lane 1: molecular water with primers F342/F18R, Lane 2: E. coli template with primers F342/F18R, Lane 3: AP7 template with primers 167musGapdhF/R, Lane 4: AP7 template with primers F342/F18R, Lane 5: AP12 template with primers 167musGapdhF/R, Lane 6: AP12 template with primers F342/F18R, Lane 7: AP13 template with primers 167musGapdhF/R, Lane 8: AP13 template with primers F342/F18R, Lane 9: AP14 template with primers 167musGapdhF/R, Lane 10: AP14 template with primers F342/F18R, Lane 11: AP15 template with primers 167musGapdhF/R, Lane 12: AP15 template with primers F342/F18R, Lane 13: AP16 template with primers 167musGapdhF/R, Lane 14: AP16 template with primers F342/F18R, Lane 15: AP17 template with primers 167musGapdhF/R, Lane 16: AP17 template with primers F342/F18R.

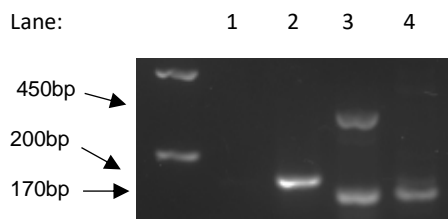


Figure 2.18 Lane 1: molecular water and primers F342/F18R, Lane 2: *E. coli* template and primers F342/F18R, Lane 3: The mammalian primers (167musGapdhF/R) show 450bp and 170bp bands applied to the human gDNA sample AP7 Lane 4: The bacterial primer set F342/F18R applied to the human gDNA AP7 shows no non-specific bands but a 170bp band in this reaction. The PCR program for the reaction was initial 5 min denaturation step at 95°C was followed by 30 cycles of 95°C, 60 s; annealing temperature 67.8 °C, 30 cycles of 60 s; 30 cycles of 72°C, 30 s with a final 7 min extension at 72°C, 4 mM MgCl₂. Visualised on 2.5 % agarose gel.

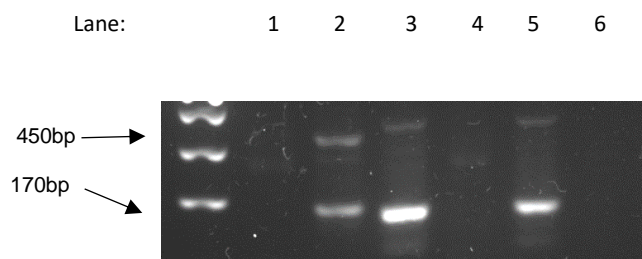


Figure 2.19 Lane 1: molecular water and primers ITSF1/2 Lane 2: *C. albicans* template with primers ITS1/2, Lane 3: AP7 template with primers 167musGapdhF/R, Lane 4: AP7 template with primers ITSF1/2, Lane 5: AP1 template with primers 167musGapdhF/R, Lane 6: AP1 template with primers ITSF1/2. The PCR program for the reaction was initial 5 min denaturation step at 95°C was followed by 30 cycles of 95°C, 60 s; annealing temperature 60 °C, 30 cycles of 60 s; 30 cycles of 72°C, 30 s with a final 7 min extension at 72°C, 2 mM MgCl₂. Visualised on 2.0 % agarose gel. The fungal primer set ITSF1/2 applied to the human gDNA (AP7 and AP1) (Lanes 4 and 6) shows no bands and in the same reaction the mammalian primers (167musGapdhF/R) show 450bp and 170bp bands (Lanes 3 and 5) indicating a PCR reaction has taken place. There were no non-specific bands detected in these reactions with the human samples.

The gDNA extracted from AP1-40 were amplified following the optimised protocols with bacterial, fungal and mammalian primer sets (F342, F18R, ITS1F, ITS2, 167musGapdhf and 167musGapdhr). The earlier PCR results with the fungal primers showed no detection of fungal gDNA in the human samples as no obvious bands were visualised after amplification

with the ITS1F/ITS2 primer set (data not shown). During the repetition of these PCR reactions, problems arose with the amplification process of the fungal primers and it was decided to focus on the bacterial presence in the tissues, thus prioritising these experiments to use the results to support the findings of the high throughput work.

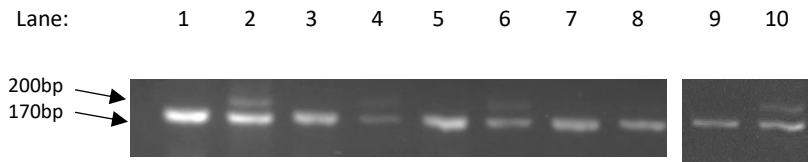


Figure 2.20 Visualisation of PCR product by electrophoresis from reactions with gDNA from human samples AP3-7 and the primer set F342/F18R. The PCR program for the reaction was initial 5 min denaturation step at 95°C was followed by 30 cycles of 95°C, 60 s; annealing temperature 67.8 °C, 30 cycles of 60 s; 30 cycles of 72°C, 30 s with a final 7 min extension at 72°C, 4 mM MgCl₂. Visualised on 2.5 % agarose gel. Lane 1: AP3 template with primers 167musGapdhf/r, Lane 2: AP3 template with primers F342,F18R, Lane 3: AP4 template with primers 167musGapdhf/r, Lane 4: AP4 template with primers F342,F18R, Lane 5: AP5 template with primers 167musGapdhf/r, Lane 6: AP5 template with primers F342,F18R, Lane 7: AP6 template with primers 167musGapdhf/r, Lane 8: AP6 template with primers F342,F18R, Lane 9: AP7 template with primers 167musGapdhf/r, Lane 10: AP7 template with primers F342,F18R. A 200bp band indicating presence of bacterial gDNA in AP3 (Lane 2), AP4 (Lane4), AP5 (Lane 6) and AP7 (Lane 10). The positive controls (human gDNA sample with primer set 167musGapdhf/r) all showed a 170bp and 450bp band (not shown) indicating a PCR reaction had taken place (Lanes 1,3,5,7,9).

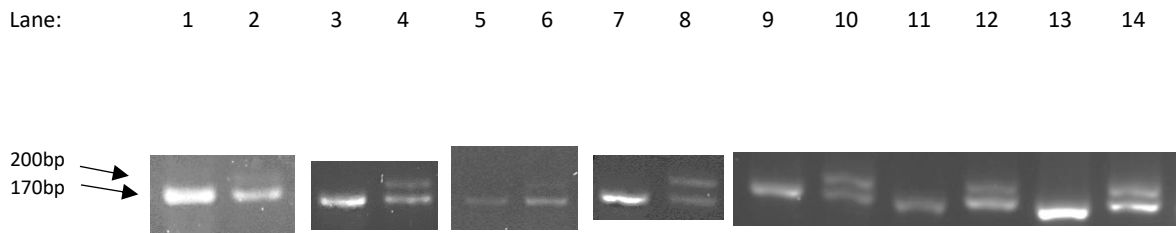


Figure 2.21 Visualisation of PCR product by electrophoresis from reactions with gDNA from human samples

AP12,16,20,21,22,23 and 24, with the primer set F342/F18R, The PCR program for the reaction was initial 5 min denaturation step at 95°C was followed by 30 cycles of 95°C, 60 s; annealing temperature 67.8 °C, 30 cycles of 60 s; 30 cycles of 72°C, 30 s with a final 7 min extension at 72°C, 4 mM MgCl₂. Visualised on 2.5 % agarose gel. showing a 200bp band indicating presence of bacterial gDNA in AP12 (Lane 2), AP16 (Lane 4), AP20 (Lane 6), AP21 (Lane 8), AP22 (Lane 10), AP23 (Lane 12) and AP24 (Lane 14). The positive controls (human gDNA sample with primer set 167musGapdhf/r) all showed a 170bp and 450bp band (not shown) indicating a PCR reaction had taken place (Lanes 1,3,5,7,9,11,13). Lane 1: AP12 template with primers 167musGapdhf/r, Lane 2: AP12 template with primers F342,F18R, Lane 3: AP16 template with primers 167musGapdhf/r, Lane 4: AP16 template with primers F342,F18R, Lane 5: AP20 template with primers 167musGapdhf/r, Lane 6: AP20 template with primers F342,F18R, Lane7: AP21 template with primers 167musGapdhf/r, Lane 8: AP21 template with primers F342,F18R, Lane 9: AP22 template with primers 167musGapdhf/r, Lane 10:AP22 template with primers F342,F18R, Lane 11: AP23 template with primers 167musGapdhf/r, Lane 12: AP23 template with primers F342,F18R, Lane 13: AP24 template with primers 167musGapdhf/r, Lane 14: AP24 template with primers F342,F18R.

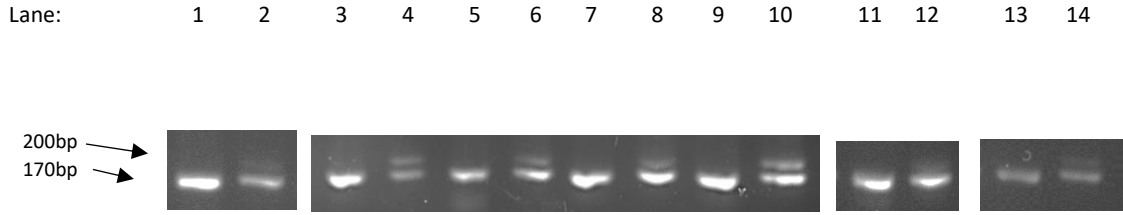


Figure 2.22 Visualisation of PCR product by electrophoresis from reactions with gDNA from human samples AP26, AP28, AP29, AP30, AP31, AP37 and AP40, with the primer set F342/F18R, The PCR program for the reaction was initial 5 min denaturation step at 95°C was followed by 30 cycles of 95°C, 60 s; annealing temperature 67.8 °C, 30 cycles of 60 s; 30 cycles of 72°C, 30 s with a final 7 min extension at 72°C, 4 mM MgCl₂. Visualised on 2.5 % agarose gel. showing a 200bp band indicating presence of bacterial gDNA in AP26 (Lane 2), AP28 (Lane 4), AP29 (Lane 6), AP30 (Lane 8), AP31 (Lane 10), AP37 (Lane 12) and AP40 (Lane 14). The positive controls (human gDNA sample with primer set 167musGapdhf/r) all showed a 170bp and 450bp band (not shown) indicating a PCR reaction had taken place (Lanes 1,3,5,7,9,11,13). Lane 1: AP26 template with primers 167musGapdhf/r, Lane 2: AP26 template with primers F342,F18R, Lane 3: AP28 template with primers 167musGapdhf/r, Lane 4: AP28 template with primers F342,F18R, Lane 5: AP29 template with primers 167musGapdhf/r, Lane 6: AP29 template with primers F342,F18R, Lane 7: AP30 template with primers 167musGapdhf/r, Lane 8: AP30 template with primers F342,F18R, Lane 9: AP31 template with primers 167musGapdhf/r, Lane 10: AP31 template with primers F342,F18R, Lane 11: AP37 template with primers 167musGapdhf/r, Lane 12: AP37 template with primers F342,F18R, Lane 13: AP40 template with primers 167musGapdhf/r, Lane 14: AP40 template with primers F342,F18R.

Table 2.11 Summary of results from PCR at UCLan and High throughput analysis, cases highlighted in green were confirmed to have bacterial gDNA present by the presence of a 200bp band with the bacterial primer set F342/F18R. Samples were tested 3-4 times independently at UCLan.

Sample	Result 1	Result 2	Result 3	Result 4	High throughput data	Results PCR at UCLan
AP1	Band 200bp	negative	negative	negative	Not applied	Negative
AP2	negative	Negative			Not applied	Negative
AP3	Band 200bp -clear	Negative	Negative	Band 200bp -clear	Not applied	Positive
AP4	Band 200bp	Band 200bp	Band 200bp	Negative	Not applied	Positive
AP5	Band 200bp	Band 200bp	Band 200bp	Band 200bp	Not applied	Positive
AP6	Negative	Negative	Negative	Negative	Not applied	Negative
AP7	Band 200bp	Band 200bp	Negative	Band 200bp	0 Reads	Positive
AP8	Negative	Negative	Negative		2282 Reads in total. Actinobacteria 113 Bacteroidetes 165 Deinococcus- Thermus 0 Fusobacteria 0 Proteobacteria 931 Cyanobacteria 176 Firmicutes 897	Negative

AP9	Negative	Band 200bp - faint and 168bp			11 Reads in total Actinobacteria Bacteroidetes Deinococcus- Thermus Fusobacteria Proteobacteria 7 Cyanobacteria Firmicutes 4	Negative, low quality sample.
AP10	Band 200bp	Negative	Negative		185 Reads in total Actinobacteria 2 Bacteroidetes 0 Deinococcus- Thermus 0 Fusobacteria 0 Proteobacteria 149 Cyanobacteria 0 Firmicutes 34	Negative
AP11	Negative	Negative			Not applied	Negative. Sample gDNA low quality, no clear results.
AP12	Band 200bp – faint	Band 200bp - faint	Negative		Not applied	Negative
AP13	Band 200bp – faint	Band 200bp - faint	Negative	Negative	Not applied	Negative
AP14	Negative	Negative	Negative		Not applied	Negative
AP15	Negative	Negative	Negative		1 total Read Firmicute 1	Negative. Sample gDNA low quality, no clear results

AP16	Band 200bp	Band 200bp	Band 200bp		Total Reads 13 Actinobacteria 0 Bacteroidetes 3 Deinococcus- Thermus 0 Fusobacteria 0 Proteobacteria 9 Cyanobacteria 0 Firmicutes 1	Positive
AP17	Band 200bp - faint	Band 200bp – faint	Band 200bp – faint		Total Reads 10 Actinobacteria 0 Bacteroidetes 2 Deinococcus- Thermus 0 Fusobacteria 0 Proteobacteria 5 Cyanobacteria 0 Firmicutes 3	Negative
AP18	Negative	Band 200bp – faint	Negative		Total Reads 3071 Actinobacteria 136 Bacteroidetes 538 Deinococcus- Thermus 1 Fusobacteria 0 Proteobacteria 2255 Cyanobacteria 23 Firmicutes 118	Negative
AP19	Band 200bp – faint	Band 200bp	Band 200bp – faint		Not applied	Negative
AP20	Band 200bp – faint	Negative	Band 200bp		Not applied	Positive

AP21	Band 200bp	Band 200bp	Band 200bp - faint		Not applied	Positive
AP22	Band 200bp	Band 200bp	Band 200bp - faint		Not applied	Positive
AP23	Band 200bp	Band 200bp	Negative		Not applied	Positive
AP24	Band 200bp	Band 200bp	Band 200bp - faint		Not applied	Positive
AP25	Negative	Negative	Band 200bp faint		Total Reads 11 Actinobacteria 1 Bacteroidetes 1 Deinococcus- Thermus 2 Fusobacteria 0 Proteobacteria 6 Cyanobacteria 0 Firmicutes 1	Negative
AP26	Band 200bp – faint	Band 200bp – faint	Band 200bp – faint		Total Reads 19 Actinobacteria 0 Bacteroidetes 4 Deinococcus- Thermus 0 Fusobacteria 0 Proteobacteria 15 Cyanobacteria 0 Firmicutes 0	positive
AP27	Band 200bp – faint	Band 200bp faint	Negative		Not applied	Negative

AP28	Band 200bp and 168bp	Band 200bp and 168bp	Band 200bp and 168bp		Total Reads 12 Actinobacteria 0 Bacteroidetes 0 Deinococcus-Thermus 0 Fusobacteria 0 Proteobacteria 10 Cyanobacteria 0 Firmicutes 2	Positive
AP29	Band 200bp Faint	Band 200bp	Band 200bp – faint		Not applied	Positive
AP30	Band 200bp	Band 200bp – faint	Band 200bp		Not applied	Positive
AP31	Band 200bp	Band 200bp	Band 200bp		Not applied	Positive
AP32	Negative	Negative	Negative		Total Reads 116 Actinobacteria 1 Bacteroidetes 5 Deinococcus-Thermus 0 Fusobacteria 2 Proteobacteria 93 Cyanobacteria 0 Firmicutes 15	Negative
AP33	Faint/unclear	Negative	Band 200bp		Not applied	Negative
AP34	Faint/unclear	Negative			Not applied	Negative. Sample gDNA low quality, no clear results
AP35	Band 200bp - faint	Negative	Negative		Not applied	Negative

AP36	Band 200bp - faint	Band 200bp - faint	Negative		Not applied	Negative
AP37	Band 200bp - faint	Band 200bp - faint	Band 200bp - faint		Total Reads 234 Actinobacteria 1 Bacteroidetes 31 Deinococcus-Thermus 0 Fusobacteria 0 Proteobacteria 193 Cyanobacteria 0 Firmicutes 9	Positive
AP38	Negative	Negative	Negative		Not applied	Negative
AP39	Negative	Negative	Inconclusive		Total Reads 6 Actinobacteria 2 Bacteroidetes 2 Deinococcus-Thermus 0 Fusobacteria 0 Proteobacteria 0 Cyanobacteria 0 Firmicutes 2	Negative
AP40	Band 200bp	Band 200bp	Band 200bp		Total Reads 3 Actinobacteria 0 Bacteroidetes 0 Deinococcus-Thermus 0 Fusobacteria 0 Proteobacteria 3 Cyanobacteria 0 Firmicutes 0	Positive

2.4 Discussion – NGS and PCR

If hypothetically microorganisms from the oral microbiome play a part in the induction of sporadic AD, they would either need to be able to travel to the brain to induce pathological change or be able to do this remotely from the oral niche. To investigate and seek evidence whether circulating periodontal pathogens could have gained access to the brain parenchyma and if there was a potential difference between the two cohorts (AD and controls), genomic analysis was applied to the 40 post-mortem brain samples. As the NGS progressed, the number of samples producing results were n=9 AD cases and n=6 control cases (Table 2.1 and 2.10). From the average read numbers per case there was a 9-fold higher number of bacterial reads in the AD cases. The average number of bacterial reads in the AD cases were 587 and, in the control cases the average was 62 (Table 2.10). The bacterial reads identified in the AD cases at phylum level were Proteobacteria (3661 reads, mean per patient – 406.8 reads), Firmicutes (761 reads, mean per patient – 84.6 reads), Bacteroidetes (466 reads, mean per patient 51.7 reads) and Actinobacteria (393 reads, mean per patient 43.6 reads) (Table 2.10 and Figure 2.3). The same phyla were also found in the control cases but in much lower numbers (Proteobacteria 306 reads (mean per patient – 51), Firmicutes 31 reads (mean per patient – 5.2), Bacteroidetes 25 reads (mean per patient – 4.2) and Actinobacteria 4 reads (mean per patient – 0.7). A small number of Deinococcus-Thermus (Mean – 0.3 in the AD cases) and Fusobacteria (Mean 0.7 in the controls) were also detected (Table 2.10 and Figure 2.4). In NGS analysis, a read indicates that a sequence of 40 – 60 bases has been identified as belonging to a bacterial sequence either at phylum or genus level. Our data correlated to similar genomic studies of AD brains in terms of read numbers and the quantitative difference between the two cohorts (Emery *et al.*, 2017; Alonso *et al.*, 2018). The findings in our study supports the infection hypothesis of AD.

Emery *et al.* (2017) found 5-10-fold higher bacterial reads in AD cases compared to non-AD, the most prolific phylum seen in this study was Actinobacteria. Alonso *et al.* (2018) found

significantly more bacterial reads in AD cases as well and the phyla listed as most prolific were Proteobacteria followed by Firmicutes, Actinobacteria and Bacteroidetes which is very similar to our findings. In these studies, bacteria were found in the control cases as well, however at lower levels, which is also very similar to our findings. The discovery in our study that two of the AD cases had high levels of bacterial reads (AP8- 2282 reads and AP18- 3071 reads) and that one of our AD cases (AP7) had none could indicate that the influx of bacteria to the brain tissues could be due to individual susceptibility. As AD has a number of different risk factors, it is possible that bacterial influx to the brain is one of them. This is supported by the finding that none of our control cases had high levels of bacterial reads, thus the bacteria could be acting as a direct inducer of AD pathology.

More than 1000 different species of bacteria have been found in the human GI tract (Khanna and Tosh, 2014; Zhao *et al.*, 2017) and the most prolific phyla have been identified as: Firmicutes, Bacteroidetes, Actinobacteria and Proteobacteria. Though the ratio in the GI tract of phyla varies between studies, it is recognized that the homeostasis of this microbiome has an important physiological function in maintaining health (Zhao *et al.*, 2017). In a healthy adult the GI tract will contain a relatively low proportion of Proteobacteria (1-4.5%) (Zhao *et al.*, 2017; Shin *et al.*, 2015), but it has been discovered that this can change in certain metabolic and inflammatory disease states and also in patients with AD (Liu *et al.*, 2019). Liu *et al.* (2019) found that AD patients had a GI enrichment in Proteobacteria, in particularly Enterobacteriaceae and this was supported by Biagi *et al.* (2010) who also found that the presence of GI Proteobacteria increases as the individual ages. This correlates with our results, where the whole cohort were aged individuals and the phyla detected in both the AD and control cases were dominated by Proteobacteria. Liu *et al.* (2019) also found a reduction in the ratio of Firmicutes. Some Firmicutes are known to produce beneficial short chain fatty acids known to have a protective effect on the BBB and the gut epithelium (Liu *et al.*, 2019) and support the morphology and function of microglial cells (Fung *et al.*, 2017). These are both factors which are important in the development of pathology of AD, so a

reduction in this protective contribution could potentially leave the individual more vulnerable to AD. This theory has been supported by Mariat *et al.* (2009) who showed that the ratio of Firmicutes does naturally decrease with age (Mariat *et al.*, 2009) and this could play a role in how the BBB becomes less effective as we age.

The enrichment in Proteobacteria seen in our brain samples where the AD cases had an average of 406.8 reads per patient, compared to the controls (51 reads per patient), corresponds with the findings of Liu *et al.* (2019), but we did not find a significant number of Enterobacteriaceae in our samples. The only genus representing this group of Gram-negative bacteria were a relatively small number of *Escherichia Shigella* in both AD patients (M=22.3) and controls (M=19.7). In our study we found an average of 84.6 Firmicutes reads in the AD patients and 5.2 in the controls. If considering the studies described above the reduction in ratio of Firmicutes could be expected, but the much lower number in the non-AD subjects (5.2 reads) does not correlate with the results by Liu *et al.* (2019) as the controls could be expected to have equal or more than the AD patients. Vogt *et al.* (2017) and Larsen *et al.* (2010) have shown that the balance of the GI microbiome changes in patients with AD and that comorbidities such as diabetes type 2 and obesity can affect the ratio of certain phyla. We do not have medical history details about our cohort apart from cause of death, so cannot draw any further conclusions related to the systemic health of our patients, but this highlights the multi factorial and complex interaction between the GI microbiome and remote organs in systemic pathology. Where the interaction between the GI microbiome and the CNS is increasingly a subject of interest in relation to the GI tract-brain axis hypothesis of AD (Larsen *et al.*, 2010).

The most dominant phylum in our samples were Proteobacteria, there after Firmicutes were the second most abundant phylum detected. Two of our samples (AP8 and AP18) showed a high number of Proteobacteria reads (931 and 2255) and though the first samples had a high Firmicute read number (897) the second had far less at 118 reads, suggesting a reduced ratio could be due to progressed age of this individual (Mariat *et al.*, 2009), or be

linked to the progressed disease and immunocompromised state of the individual at the time of death.

In summary, our high throughput analysis data do correlate with studies investigating the GI-CNS axis of AD (Zhao *et al.*, 2017), though the evidence of a natural shift in the GI microbiome due to advanced age also needs to be considered and this complicates the conclusions we can draw from our NGS data. As the highest risk factor for AD is age, it poses the question; is the GI microbiome changing due to age or other comorbidities which are also associated with AD, rather than being the direct cause of AD pathology?

Nevertheless, the knowledge of the GI microbiome and how it changes with age and disease is important in context to our hypothesis as the oral microbiome is closely linked to the GI tract microbiome (Zhao *et al.*, 2017; Pritchard *et al.*, 2017) and the GI tract microbiome could influence the integrity of the BBB, potentially affecting progression of neurodegeneration (Liu *et al.*, 2019). LPS from the GI tract microbiome is considered an important source of inflammatory CNS degeneration (Zhao *et al.*, 2017; Liu *et al.*, 2019) and LPS from *Escherichia coli* has been found in the hippocampus and temporal lobes of AD patients highlighting this Proteobacterial endotoxin as a potential contributor to inflammatory degeneration (Zhao *et al.*, 2017). This is also one of the families of bacteria that Liu *et al.*, (2019) found to have an increased presence in AD patient's faecal matter. As mentioned above, the reads in our samples that link specifically to the GI microbiome were the reads for *Escherichia shigella* in both AD patients (M=22.3) and controls (M=19.7). *Shigella spp.* and *Escherichia coli* are both from the family Enterobacteriaceae. *Shigella spp.* and *Escherichia coli* have 80 – 90% similarity in nucleotide, and distinction between the two is difficult both by 16S rRNA gene sequencing and clinically (Devanga *et al.*, 2017; Khot and Fisher, 2013). The suggestion by Devanga *et al.* (2017) that the technique we have utilized to identify *Escherichia Shigella* in our samples is unsuitable to differentiate between the two genera could have implications for our results. Potentially our reads could have represented *Escherichia coli* which has previously been associated with AD pathology and the oral

microbiome (Pritchard *et al.*, 2017). *Escherichia shigella* and *Escherichia coli* are associated with diarrhoea disease and play a significant epidemiological role in particularly in the elderly and immunocompromised individuals (Zawadzki *et al.*, 2017). It is important to bear in mind the limitations of conclusions drawn from identifying the bacteria even to genus level in our study, as there can be significant pathological differences between species in the same genus. Finding *Escherichia Shigella* in the brain tissues of both AD and control patients could be associated with the advanced age and frailty of the patient group included in our study but an association with AD pathology cannot be excluded.

Escherichia coli has been linked to the oral microbiome. Zawadzki *et al.* (2017) examined the oral microbiome of healthy individuals without PD in the age range 40 – 70 years and found *Escherichia coli* present in all individuals. This genus represented as much as 24% of the bacteria identified in the age group 51 -60 years of age highlighting that the oral cavity can act as a reservoir for microbials with a serious pathological potential (Zawadzki *et al.*, 2017).

Nearly all the genera identified in the NGS analysis have been detected in the oral microbiome (apart from 37 *Brevibacterium* reads in AD cases) (Chen *et al.*, 2010) and out of the total of 5871 reads, 567 could potentially be linked to genera previously associated with periodontal disease, peri-implantitis and gingivitis (478 in AD and 89 in controls) (*Porphyromonas*, *Prevotella*, *Actinomyces*, *Veillonella* and *Pseudomonas*) (Zenobia and Hajishengallis, 2015). One of the samples (AP8) which contained a high number of reads (1969), contained 124 reads which were identified as the genus *Porphyromonas*, and 129 reads were identified as *Veillonella*. There were 3 reads of *Prevotella* in both the AD and controls and 1 read of *Actinomyces* was recorded from a control case. One of the AD cases contained 169 *Pseudomonas* reads (Souto *et al.*, 2014) and 45 *Veillonella* (AP18) and 79 *Pseudomonas* reads were also recorded in the control cases.

The genus *Leptotrichia* has been associated with multiple pathologies in humans and also associated with gingival plaque in both healthy and diseased oral states (chronic periodontitis and peri-implantitis) (Eribe and Olsen, 2017). 4 reads for *Leptotrichia* were found in the controls but none in the AD cases. These findings would not support an association between periodontal pathogens and AD.

92 reads for *Chryseobacterium* were found in the AD cases. *Chryseobacterium* has been identified in subgingival plaque and found to be resistant to chlorhexidine mouthwash (Saleem *et al.*, 2016), however this genus has not yet been linked to periodontal pathology.

The microbiome of periodontal pocket plaque has been investigated repeatedly, but a recent study by Ko *et al.* (2020) investigated the difference in the microbiome of the saliva of periodontally diseased patients before and after successful treatment. They found that the dominant phylum in both healthy and diseased individuals were Firmicutes followed by Bacteroidetes, Proteobacteria, Actinobacteria and Fusobacteria (Ko *et al.*, 2020). They found that there was a shift in the phyla post treatment, which showed the largest difference was in the bacterial reads of Spirochaetes, Synergistetes and Tenericutes (Ko *et al.*, 2020). They also found that Actinobacteria were dominant in healthy individuals' saliva. Though the NGS data did not find a dominance of the genera previously associated with periodontal disease (Zenobia and Hajishengallis, 2015) such as *Porphyromonas*, this genus would not necessarily be high in numbers to have caused periodontal disease. It is an ability of the keystone pathogen *P. gingivalis* to influence the community of microbials and induce dysbiosis causing disease even if relatively low in numbers (Hajishengallis and Lamont, 2016).

Some of the genera identified in our study could be linked to periodontal disease, but we cannot say which species these were and can therefore not draw absolute conclusions of a link between the AD pathology to periodontal disease from the sequencing data.

Other phyla identified with significant pathology in the elderly population were *Staphylococcus* and *Streptococcus* reads in the samples (AD group M= 24.9 and 20.6; control M= 0.5 and 0.7) (Farley, 1995 and McClelland *et al.*, 1999) could be attributed to the progressed frailty and infectious susceptibility of the individuals with AD or an expression of a less efficient BBB barrier and clearance function of waste products in the AD patients compared to the controls (Erdő and Krajcsi, 2019; Montagne *et al.*, 2015).

Other Proteobacteria which were seen in abundance in the AD samples were *Halomonas* and *Pelomonas*. *Halomonas* require NaCl for growth and is usually associated with the environment (Stevens *et al.*, 2013), though it has also been found to cause bacteremia in humans in association with dialysis (Stevens *et al.*, 2013). Park *et al.* (2015) examined the bacterial species in subgingival plaque from healthy and PD individuals by NGS and found that the dominant genus in healthy individuals was *Halomonas* representing 43.7%, whereas *Pelomonas* has been associated with the saliva of HIV patients compared to uninfected individuals (Mukherjee *et al.*, 2018). Gyarmati *et al.* (2015) detected an unusual level of both *Halomonas* and *Pelomonas* by high throughput sequencing in blood samples from immunocompromised patients with febrile neutropenia and though we only have the cause of death information for our cohort, there is no doubt that their immune system would have been weakened either due to Alzheimer's disease or other significant pathology or immunotherapy (Sutherland *et al.*, 2015). This could explain the abundant presence of these Proteobacteria in our samples. The *Halomonas* and *Pelomonas* were mainly detected in two of the AD cases AP8 and AP18 who both had advanced AD at the time of death.

As mentioned in the results (2.3.1) the application of the high throughput analysis protocol to the 40 human brain samples experienced some problems which reduced the analysed cases to n=15 (9 AD cases and 6 controls). One brain gDNA sample failed to amplify by the initial PCR process, other samples did amplify as shown by a band by electrophoresis, but when these were put through the sequencing platform, they failed to produce a result. The NGS company did not provide any details of why some samples failed to produce data.

Factors that could have caused this are multiple (Fakruddin *et al.*, 2012; Yamamoto, 2002). Key stages are the DNA extraction, PCR amplification, visualization of the product and designing the primers (defining the target genes) (Yamamoto, 2002). The quality and quantity of the bacterial gDNA in our samples could have been reduced in the extraction or during storage conditions and handling before PCR was applied, or some samples could have been of poor a quality from the biopsy stage, depending on handling. A high amount of amplicon is required for the NGS analysis as only the original amount of template is copied in every cycle (Tipu and Shabbir, 2015) and potentially the amplification pre sequencing was insufficient for the method. It can be difficult to extract and amplify the microbial gDNA when only present in small amounts in the human brain samples which mostly represents a tissue with a low microbial presence on a high mammalian gDNA background (Yamamoto, 2002). The design and optimisation of the primers for the pre sequencing amplification requires great care as the specificity (target genes) and annealing temperatures can produce nonspecific amplicons, bringing bias to the sequencing results (Yamamoto, 2002).

Primer target selection in the NGS can also affect the amplification of certain organisms over others (Kuczynski *et al.*, 2011; Brooks, 2016) and amplification bias can be introduced due to variations in the 16S rDNA in diverse bacterial genomes, which can also lead to an under or over representation of some organisms (Sundquist *et al.*, 2007). Though the sequencing only uses one primer at the time which reduces the demand for specificity compared to PCR amplification.

In our data there were some bacteria represented in abundance which were unexpected such as *Helomonas*, but a direct link to amplification bias cannot be made here.

The Illumina MiSeq platform utilized in our study, has high quantitative power and accuracy, but in sequencing terms this platform has a relatively short read length in the sequences it can generate (Whon *et al.*, 2018). This can affect the accuracy and sensitivity of the taxonomic detection both by quantity and identity. The short read length(200bp) can lead to

problems allocating the read to an organism which results in the sequence being named as unclassified, this means that in the analysis stage, the unclassified reads which cannot be placed in the phylogenetic tree, carry weight to the total number of bacterial reads (Gloor *et al.*, 2016; Sundquist *et al.*, 2007). This unclassified allocation was seen for multiple reads in our data, which allowed some reads to be classified according to phylum, but not genus and this meant that genus level analysis of interest to the study was lost.

The database for analysing the read data can also be a limiting factor, as some sequences may not have been registered (Sundquist *et al.*, 2007). Differences in primer specificity and genomic target region could introduce bias to the read output for our utilized platform (Whon *et al.*, 2018). As no single region in the 16S rRNA gene or conserved region is shared amongst all bacteria, a mix of primers must be used to increase the amount of bacterial gDNA being amplified before NGS (Whon *et al.*, 2018; Sundquist *et al.*, 2007). The primers utilised in the amplification and sequencing in our investigation, were targeting the single variable region V4 on the 16S rRNA gene as Sundquist *et al.* (2007) described this as a suitable target for our type of samples. However, since 2016 when our NGS took place research has emerged with the advancement in full 16S gene sequencing. One study by Johnson *et al.* (2019) suggest that the V4 region is indeed a poor target area, performing the worst when V1-9 were examined by a series of sequencing methods and this region was particularly poor at identifying genera from the phylum Actinobacteria (Johnson *et al.*, 2019). They also highlighted that targeting the variable regions rather than the full 1500bp gene would lose some of the richness of the microbial pool and limit the detection to genus level. This knowledge could potentially have improved the design of our study in selection of primer combinations and choice of target region and may have increased the number of cases that could have been analyzed by NGS.

When the NGS data had been analysed and it became clear that only part of the cohort had produced a sequencing result (15 out of 40), the investigation was expanded to identify simply whether the samples contained microbial gDNA or not. Therefore, PCR was carried

out again at UCLan on the whole cohort (n= 25 AD cases and n=15 controls).

The aim was to test the 40 samples for the presence of bacterial gDNA, but also for fungal gDNA as both these microorganisms have relevance to oral health and have been linked to AD (Poole *et al.*, 2013 and Carrasco *et al.*, 2017).

The fungal primer pair (ITS1F and ITS2) were designed to amplify ITS units specifically to fungal organisms and were expected to detect a broad range of fungal organisms including *Candida albicans*, and this was used as a positive control in the optimisation of the primers. There were multiple issues with these primers in the optimisation period applied to mouse brain spiked with *Candida albicans*. They were mainly related to the recurrent appearance of bands which were larger than expected (500 – 1000 bp) though these were seen to get smaller with increase in annealing temperatures, the best amplification results (closest to the expected size products visualized by electrophoresis, were found to be at 60 °C. At this annealing temperature the fungal primer pair consistently produced two bands at 500 bp and 200 bp and this was accepted as a true result before progressing to the human samples, as the expected product from the referenced study was 200 bp (Ghannoum *et al.*, 2010). These findings could be related to the design of the primers targeting the repetitive internal transcribed spacer region (ITS) gDNA (Lorenz, 2012) resulting in the larger non-specific products visualised by electrophoresis. Though utilising the ITS region, which is recognised as the bar-coding unit for fungal identification, this region also has limitations (Raja *et al.*, 2017). Schoch *et al.* (2012) found that the ITS region has highest probability of correctly identifying a broad group of fungi but has limitations identifying some which do not have the ITS region, or which ITS region is not very wide such as *Aspergillus* and *Penicillium* (Raja *et al.*, 2017). These findings could also be related to the homologous sequence alignment between the fungal and mouse genome (Thomas and Touchman, 2002), combined with the high mouse gDNA background in the sample and that the ITS lacks specificity genes (Ghannoum *et al.*, 2010). After optimisation of the fungal primers in

conjunction with the mammalian primer set and initial screening of the human brain samples, no fungal gDNA were detected. Also, it was found that this primer set was not consistently working with the human samples. To improve the method the options considered were to redesign the primer pair for further PCR analysis or utilise alternative methods such as fluorescence in situ hybridisation (FISH) or Loop-mediated isothermal amplification (LAMP) as these methods could potentially have provided more specificity (Tsui *et al.*, 2011). Another option could have been to send the samples for NGS with fungal primers. After review of the projects time frame, it was decided to focus on the presence of bacterial gDNA in the human brain samples as this would be of most value to the project combined with the results of the high throughput analysis. The initial screening of the human samples with the fungal primer set did not reveal any fungal gDNA in the samples.

The bacterial primer pair (F342 and F18R) (Emery *et al.*, 2017) were targeting the highly conserved 16S rRNA region of the bacterial genome. This primer set were selected as they have been shown to have a wide taxonomic spectrum of oral bacteria with a low probability of amplifying eukaryotic sequences (Emery *et al.*, 2017). These primers were expected to produce one or two bands; a bacterial 16S rRNA gene amplification (200bp) and potentially a band of 168bps for *Propionobacteria* and *Corynebacteria*, but they could also potentially amplify the mammalian 18S rRNA genes (174bp) (Emery *et al.*, 2017). When the bacterial primers were applied to *Escherichia coli* and spiked mouse brain, visualisation of the amplicon showed bands at 200 bp (Figures 2.10, 2.16 and 2.18) which was expected. When F342 and F18R were applied to the human brain samples two bands were seen at 170 bp and 200 bp (Figure 2.22, 2.23 and 2.24). Therefore, when all 40 human samples were tested, if there was an appearance of a 200bp band, visualised by electrophoresis, this was recorded as the sample being positive to a bacterial gDNA presence. The mammalian primers showed a band at 450 bp and was used as a control of a PCR process having taken place (Figure 2.20, 2.21 and 2.22).

PCR and NGS are different techniques, PCR produces a template product by exponential amplification in every cycle, whereas NGS examines the template amplicon and identifies the sequence of this product (Yamamoto, 2002). Amplification with the bacterial and mammalian primers (F342, F18R and 167musGAPDHf/r) detected bacterial gDNA in 10 AD samples (25%) and 7 controls (47%) (Table 2.11). 8 AD cases and 3 control cases from the group that did not produce a high throughput result, tested positive for bacterial gDNA with the primer set F342 and F18R (AP3, AP4, AP5, AP20, AP21, AP22, AP23, AP24 and AP29, AP30, AP31). These samples produced a 200bp band with F342 and F18R but bacterial DNA were not amplified in the pre- NGS PCR primer combinations, in order to be tested by sequencing. This could be due to the quality of the DNA samples or other factors could have failed in the PCR reaction, the potential causes are multiple (Fakruddin *et al.*, 2012). Also, differences in the design of the primers used in the two PCR processes could cause this difference, the differences in genes targeted in the two amplifications could have caused the different detection of bacterial gDNA by the two methods (Table 2.11). As previously discussed, the primers were designed to target different variable regions of the bacterial gDNA which could result in targets being missed or over amplified over others (Emery *et al.*, 2017; Sundquist *et al.*, 2007). One of the samples (AP7) tested positive for bacterial gDNA using the primers F342 and F18R (Figure 2.20), the sample repeatedly showed a band of 200bp, but in the NGS analysis this sample showed 0 reads (Table 2.11). This could also be explained by differences in the primer sets applied to the sample. Potentially the F342 and F18R primers could be amplifying something non-specific, which was not present in the mice gDNA (Thomas and Touchman, 2002) during the optimisation, though this is difficult to confirm as we did not have any human brain samples which were otherwise confirmed as completely clear of bacterial gDNA. There is also the possibility that the sample could have been contaminated before the second PCR amplification.

Of the samples that tested positive to gDNA by the primer set F342 and F18R, 5 of the samples also produced bacterial reads by NGS (AP16, AP26, AP28, AP37 and AP40)

(Table 2.11). 9 samples which had shown bacterial reads by NGS were not showing a clear 200 bp band with primer set F342 and F18R (AP8, AP9, AP10, AP15, AP17, AP18, AP25, AP32 and AP39) and though 2 samples appeared to be of poor gDNA quality (AP9 and AP15, did not show clear bands with the mammalian primer set), this would indicate that F342 and F18R were not sensitive enough to pick up gDNA in 7 AD cases and 2 controls or the primer sets used for the NGS were better at targeting the bacterial gDNA in the samples, the latter is most likely as the detection level by PCR at UCLan for bacteria was 0.08 ng. This is significantly more than, as an example 500 bacterial reads would represent, if one bacterium is approximately $0.5 - 20 \times 10^{-15}$ g. Two of the samples in this group were the samples AP8 and AP18 which had high read numbers by NGS which raises questions about the suitability of the primer set F342 and F18R for the analysis of our human samples. As the controls used in the optimisation and application of these primers suggest the primer set was working, this could potentially be explained by limitations of using just one primer set compared with the NGS (Fakruddin *et al.*, 2012). Sequencing is expected to have a high analytical sensitivity but relies on a high amount of amplicon for analysis (Shendrue and Hanlee, 2008; Schuster, 2008). The limitation of using NGS is the cost and the potential for false positives, as this method reads short sequences which may allocate reads in error (Fakruddin *et al.*, 2012).

Widening the search for a cause of discrepancy between the two methods in relation to the presence or absence of bacterial gDNA in the samples, there is also the potential that some of the samples could have been contaminated at some stage. The challenge of working with microbiome studies in post-mortem tissues is the possibility of the microorganisms and/or their DNA entering the tissues after death. This relates both to the conditions of the surroundings where the samples were collected and the delay from the person died until the sample was collected. It is possible that the DNA amplified in the study came from cross-contamination, which could have been introduced to the samples at any stage in the autopsy or lab process. The samples came from the same tissue bank and were all

harvested at different times which makes it difficult to exclude cross contamination, but the finding that the phylum ratio in the positive samples were similar, in both controls and AD patients, reduces the likelihood of cross contamination being the source of the bacterial reads. This finding corresponds with other similar studies (Emery *et al.*, 2017; Alonso *et al.*, 2018) who concluded that contamination during peri post-mortem storage was not the source of the bacterial reads, mainly because the same phyla were found in the control cases at lower levels, but they did acknowledge that some of the reads could come from the blood (discussed below).

We have the values of postmortem delay of our individuals (Table 2.1). In our study there was no clear relation between the number of bacteria reads by NGS and the time passing before autopsy (Figure 2.5), we did have a sample (AP7) without any bacterial reads and there were only low number of reads in our controls. These findings support the bacterial reads data being a true reflection of gDNA in the samples, but with any bacterial sequencing study like ours, it has to be acknowledged that there is a potential during the handling and storage of samples to introduce external contaminants and therefore produce bias (Emery *et al.* 2017).

Another challenge in using the high throughput sequencing technique in our study is using gDNA from tissues representing both sides of the BBB. This means that there is the potential that bacteria identified were residing in the vascular tissues and not in the brain parenchyma. There is a growing consensus that a microbiome of healthy human blood exists (Castillo *et al.*, 2019). Païssé *et al.* (2016) showed the presence of Proteobacteria, Firmicutes, Actinobacteria and Bacteroidetes in healthy blood, indicating that a person who is not clinically diseased will have presence of microorganisms in direct proximity to the BBB. Our sequencing data were very similar to this study in terms of phyla identified in both the AD and control cases (Table 2.10). This could mean that the gDNA found in our brain samples could potentially originate from the blood or from another microbiome feeding into the blood stream. This should be considered when drawing conclusions from the NGS data.

All the AD patients examined in our study were diagnosed as late onset AD patients and the findings of bacterial reads in both AD cases and controls could be a true representation, or potentially explained by the types of controls used in our study. Most of the controls selected for this study (AP26-40) passed away of causes which could have significantly weakened their immune system and BBB function (Montagne *et al.*, 2015) and this could have caused a higher systemic bacterial presence before death (Table 2.1). This highlights the limitations of this study design and the importance of selection of appropriate controls for a study of this nature. On average our data also shows more bacteria in the AD cases in terms of read numbers, but this is because of the high number of reads in two of the AD cases (AP8 and AP18). And though these two individuals represented some of the oldest members in the group (95 and 91 years of age at the time of death), looking at the data from the whole cohort tested, there was no clear correlation between a high number of bacterial reads and progressed age (Erdő and Krajcsi, 2019; Montagne *et al.*, 2015). The control group also contained two patients with a high age at time of death (AP26 at 97 years and AP28 at 99 years of age), who had very few reads detected (AP26- 18 and AP28-13 reads). It can therefore not be concluded that the high presence of bacterial reads in the two AD samples were due to their age, though it is recognized that there is increased BBB leakage occurring with progression of age (Erdő and Krajcsi, 2019; Montagne *et al.*, 2015).

Though there was a clear abundance of bacteria present in some of the AD patients in our study compared to the non-AD patients, it is important to be cautious linking the results to AD. Many of the AD patients had very low bacterial reads and some of the controls' cause of death could have had a significant effect on their BBB integrity.

As induced changes to the transport and barrier function in the BBB has been described in neurodegenerative disease and disruptive changes have been described in polymorphisms at risk to AD (Montagne *et al.*,2017), there are also potential for other so far unknown genetic variations which could leave individuals at risk of BBB disruption. This could be polymorphisms of pro-inflammatory cytokines IL-1 and TNF which have been associated

with both AD and PD (Watts *et al.*, 2008). Looking at the findings in the NGS data, gene polymorphisms at the BBB involved with inflammatory processes and/or transport could potentially explain why some individuals in the study had such an increased influx of microbes to the brain. If host polymorphisms are present at the BBB, then the microbiome could be involved with the onset of AD pathology, a hyperinflammatory phenotype could explain the high reads in two of our AD cases, although these individuals' increased susceptibility could also be a result of environmental factors or the virulence factors of the organisms' present. The chronic features of low-level infections producing endo/exotoxins and cytokines, could weaken a susceptible brains' defense ending up with a state where the cells (such as microglia) are no longer able to keep the barrier functions intact (Nara *et al.*, 2021). This makes it important to investigate further what happens when the systemic circulation meets the brains' main defense, the BBB.

2.5 Conclusion

Using high throughput sequencing genomic analysis, this study detected a wide range of bacterial gDNA in both AD and control post-mortem brain samples. The number of bacterial reads in the AD cases was 9-fold higher than in the control samples and two samples from AD patients had a significantly higher number of bacterial reads with a dominance of Proteobacteria, Bacteroidetes, Actinobacteria and Firmicutes.

The aim of the PCR amplification carried out at UCLan was to examine the full cohort with different primer sets to the ones used in the NGS study. Targets for primers were both the 16S rRNA gene conserved bacterial sequence and the fungal ITS region, but these techniques provided limited data. There was no fungal gDNA detected in the samples. The bacterial gDNA detection using the primer pair F342 and F18R provided amplicons of the

expected size visualised by electrophoresis, but the results from some of the samples were not corresponding with the NGS data. These findings limit the knowledge derived from this investigation and puts the strength of the data on the sequencing results.

Potentially the NGS results are simply the picture of a microbiome of the aged brain following the natural reduction in BBB defense but could also be the result of a chronic bacterial assault causing inflammation and weakening of the BBB. Or these individuals were so immunocompromised due to their advanced dementia that the influx of microorganisms to the brain parenchyma could no longer be controlled by the local immune cells. It has been acknowledged that this study has limitations, but the findings in terms of the number of bacterial reads in a few samples is likely to be a genuine find and could be a driver of further research. Going forward, if possible, it could be worth looking at these individuals in more detail and examine whether they had different aspects of their inflammatory profile upregulated or show other genetic variations. This could lead to further knowledge of how the microbiome interacts with certain individuals and why some are spared. It could potentially also divulge the role the microbiome plays in the initiation and progression of neurodegenerative diseases such as AD. This study has highlighted a need for further understanding of how bacteria could affect the integrity of the BBB and potentially cross the barrier. As there is an increasing body of proof emerging of a link between the microbiome of periodontal disease and neurodegeneration, the next part of the study will focus on getting further knowledge of how the key stone pathogen of PD *P. gingivalis* interacts with cells of an *in vitro* human BBB model.

Chapter 3

BBB-model techniques, characterisation and optimisation of *in vitro* model

3.1. Introduction, aim and objectives

The genomic examination of human brain tissues from AD patients and age matched controls revealed a marked inter individual variability in microbial load. These findings could be caused by multiple comorbidities in the individuals, cross contamination during the tissue storage or extraction process or PCR primer variability. Furthermore, the findings could be because of a weakness in these individuals physical defence against an influx to the brain parenchyma. The most important barrier protecting the human brain is the BBB and various models have been characterised to study microorganism interaction with these tissues both in animals and humans (Park *et al.*, 2018; Pflanzner *et al.*, 2010). Human studies of microorganism application to the BBB are important but for ethical reasons difficult to simulate. *In vitro* studies are therefore of great use as they give relevant species specific data particularly if primary cells are used rather than immortalised cell lines (Kumar *et al.*, 2014). Primary cell line *in vitro* models utilise a unique donor which enables a clear characterisation of the cells in terms of protein expression and growth pattern. Though this type of model has many merits for its use, it is also important to understand inter-assay variability that could arise when the donor source of cells is changed and control these.

Aim:

The *in vitro* BBB model utilised in this study has previously been validated in terms of protein expression and kinetics (Kumar *et al.*, 2014). The aim of this study was to characterise the BBB cells to ensure the cells utilised were suitable in terms of key markers such as growth kinetics, doubling times and morphology. In this characterisation phase it was also investigated whether the human serum added to the cell medium was more suitable from single sex or multiple pooled donors.

Objective 1:

To assess which serum (human serum blood type AB- off clot single male donor S-101D-EU or human serum pooled mixed gender S-105D-EU, Appendix 1, Table 2) would provide the best growth kinetics for the three primary cell lines human astrocytes (HA), human brain pericytes (HBPC) and human brain microvascular endothelial cells (HBMEC).

Objective 2:

To carry out morphological observations of the cell lines by visual examination using light microscopy.

3.2 Materials

Materials and equipment used are listed in Table 1 and 2, Appendix 1.

3.3 Methods for *in vitro* BBB model

All protocols for characterisation and optimisation in preparations for the BBB model were undertaken in a primary culture designated laminar class 2 hood. Hood, reagents and containers were cleaned with 70% methylated spirits and 1% Virkon before use.

3.3.1 Coating of tissue culture flasks and cell thawing

The cell lines; human brain microvascular endothelial cells (HBMEC), human astrocytes (HA) and human brain pericytes (HBPC) (Appendix 1, Table 2) were stored in liquid nitrogen prior to defrosting. A water bath (37 °C) was used to defrost cells and warm up HBSS and

media before use. All cells were initiated in pre-coated flasks (as outlined below) at predetermined seeding densities recommended by the suppliers (Appendix 1, Table 2).

In preparation for defrosting the HBMEC, 1 ml of AlphaBioCoat Solution was added to a T25 flask and the entire interior surface was coated. AlphaBioCoat Solution (Neuromics, USA) is a biocompatible complex of extracellular matrix binding solution that is supplemented with growth factors, which helps accelerate cell attachment and cell growth. The T25 flask was then left to incubate in the hood at room temperature. After 30 minutes the coating solution was removed by aspiration and the flask was gently rinsed with sterile phosphate buffer solution (PBS) (Appendix 1 Table 2). 4 ml of Endothelial basal medium (EBM) (Appendix 1, Table 2) were added to the flask before seeding of the HBMEC.

In preparation for defrosting of the HBPC and HA, T-75 tissue culture flasks were coated by adding 10 ml of sterile water with 15 μ l of poly-L-lysine stock solution. The vessels were left in a 37°C incubator for a minimum of one hour, where after they were rinsed twice with sterile water and 15 ml of medium were added respectively (astrocyte basal media (ABM) or pericyte media (PM) (Appendix 1, Table 2) prior to cell seeding.

The seeding densities at thawing were 5000 cells/cm² for HBPC and HA and 4000 cells/cm² for HBMEC.

Following thawing, the flasks were placed in the humidified incubator at 37 °C, 5 % CO₂ and left for 16 hours at which point all the culture medium was changed to remove residual DMSO (Appendix 1, Table 2) and unattached cells from the flask.

3.3.2 Sub culturing of cells

After initiation of the cell cultures, the media was changed in all culture vessels every 48 hours until 50% confluent and after this point every 24 hours. When the flask was 80 – 90 % confluent, the cells were used for the appropriate cell model, passaged or frozen (for time

scales please see Figure 3.1). First the media was removed by aspiration from the flask. The cells were washed with HBSS and trypsinised with 2 ml of Tryple Express in the 37 °C, 5 % CO₂ incubator (Appendix 1, Table 2). After 2 minutes incubation the cells were placed in a 15 ml centrifuge tube and placed in the benchtop centrifuge for 5 min at 93 x g. The supernatant was removed, and the pellet resuspended in the appropriate media, or the freezing protocol (3.3.3) was applied. The cell lines were not used past passage number 7, as after this time point the cells were considered quiescent (Kumar *et al.*, 2014). All observations of the cells were carried out under an inverted light microscope (Leica DMIL light microscope from Leica Microsystems GmbH, Germany) and light microscope images were taken with the MShot camera (MShot, China) and processed with MShot Digital Imaging System software (MShot, China).

3.3.3 Freezing of cells

The same protocol for freezing primary cells was applied to all three cell lines human astrocytes (HA), human brain microvascular endothelial cells (HBMEC) and human brain pericytes (HBPC) (Appendix 1, Table 2). The cells were first washed with HBSS and trypsinised using 2ml of TrypLe Express. After 2 min (5 min for HA), the cells were transferred to a 15 ml centrifuge tube and centrifuged for 5 minutes at 93 x g. The supernatant was removed and the cell pellet was resuspended in 1 ml human serum with 10% sterile DMSO (Sigma-Aldrich, UK). The cell suspension was placed in a cryotube which was placed in a Mr Frosty container with 250 ml 100% isopropanol. The container was placed in a -80°C freezer overnight and transferred to the liquid nitrogen dewar 24h later.

3.3.4 Cell counting

The viability of the cells was assessed by using 1:1 Trypan Blue 0.4% (Sigma-Aldrich, UK). For this cell count 50 µl of Trypan Blue was added to 50 µl of the cell sample, then 10 µl of this solution was placed under the coverslip on the haemocytometer (microscope magnification 10X, Leica DMIL light microscope from Leica Microsystems GmbH, Germany). For each cell count 4 squares were counted and averaged, corrected for dilution with Trypan Blue (x2) and then multiplied by the haemocytometer factor 10 000, which equated to the cell number x 10⁴ per ml.

3.3.5 Methods for characterization and optimisation of the *in vitro* BBB model cell lines

All equipment and materials are listed in Appendix 1, Table 2. Pipettes and flasks were cleaned prior to being placed inside the hood by autoclaving and/or spraying with 70% industrial methylated spirits (IMS). Unsterile reagents were filtered for sterilisation by using MillexGP 0.22 µm pore filters (Merck). The cells were placed in tissue culture flasks (T75/T25) (Table 2, Appendix 1) and cultivated as described in Sections 3.3.1, 3.3.2, 3.3.3. Counting of cells was conducted as described in Section 3.3.4.

Human brain microvascular endothelial cells (HBMECs) isolated from normal human brain tissue were obtained from Neuromics (USA) at passage 2, containing over 5 X10⁵ cells/ml. The HBMEC cells were not used past passage number 10, after this time point the cells were considered quiescent or to be at risk of losing the specific phenotype (Kumar *et al.*, 2014; Hughes *et al.*, 2007). The initial seeding density of HBMEC was recommended by

Neuromics as 4000 cells/cm² which were placed with EBM in an Alphabio pre-coated T25 tissue culture flask (Appendix 1, Table 2).

Human brain vascular pericytes (HBVP) were purchased from ScienCell (USA) at passage 2, each vial contained >5 x 10⁵ cells/mL. The HBPC cells were not used past passage number 10. A seeding density of 5,000 cells/cm² was adhered to when starting the culture in a Poly-L-lysine pre-coated T-75 flask.

Human astrocytes (HA) cells were purchased from ScienCell (USA) at passage 2, each vial containing >5 x 10⁶ cells/ mL. The HA cells were not used past passage number 10. A seeding density of 5,000 cells/cm² was recommended in a Poly-L-lysine precoated T75 flask.

After the initiation of the cell cultures, the cells were subcultured in 24 well tissue culture plates (Appendix 1, Table 2), to assess which serum (Human Serum AB- off clot single male donor (S-101D-EU) or Human Serum pooled mixed gender (S-105D-EU) would provide the best growth kinetics. The three primary cell lines (HA, HBPC and HBMEC) were grown to 70 % confluency in the 24 well plates in the appropriate media (EBM, ABM or PM) with either pooled human serum or single donor human serum added. The HA (pooled serum), HA (single donor serum), HBPC (pooled serum) and HBPC (single donor serum) were seeded in the 24 well plates at a density of 12500 cells/ml (all at passage 4) and the HBMEC (pooled serum) and HBMEC (single donor serum) were seeded at a density of 10000 cells/ml at passage 6. Each experimental condition was seeded in triplicate. The total volume in each well was 1000µl of cell suspension in media. The cells were counted every day for 10 days as per 3.3.4 and growth curves were plotted. The passages used in this study were all similar (4 HA,4 HBPC and 6 HBMEC) and considered low to midrange (Kumar *et al.*, 2014). The cells were imaged in a Leica DMIL light microscope (Germany) using the Mshot camera and software (China).

3.4 Results

3.4.1 Cell line growth kinetics

There was little difference in growth kinetics between the two serum types for the HBPCs, but a slightly higher cell count was seen for the pooled serum test group (Table 3.1).

The doubling time for these cells were 96 hours for the pooled serum wells and a little less than 96 hours for the single donor cells. This is significantly longer (52.3 h) than reported by Kumar *et al.* (2014) (Table 3.1) (Figure 3.1).

For the Human astrocytes (HA), the pooled serum gave a better result in terms of cell counts, which appeared to be higher compared to the single donor serum, but the overall doubling time for these cells were similar in the two sera: 60 hours in the single donor wells and 66 hours for the pooled serum test wells. This is significantly longer than reported by Kumar *et al.* (2014), who found the doubling time in these cells to be 24.6 hours (Table 3.1) (Figure 3.1).

In the endothelial cells (HBMEC) tested, there were unusual growth kinetics detected with a significant lag in growth early in the test period. However, there was no significant difference between the two exponential phases or the highest cell count. The doubling time for these cells were 36 hours for both the pooled serum wells and the single donor (Table 3.1), this is shorter than reported by Kumar *et al.* (2014), who noted 51.7 hours (Table 3.1) (Figure 3.1).

Table 3.1 comparison of growth kinetics of human brain microvascular endothelial cells (HBMEC), human brain pericytes (HBPC) and human astrocytes (HA) in media with addition of either single donor serum or multiple donor serum (appendix 1, Table 2). Data from Kumar *et al.*, (2014) compared to cell kinetics study data, data shown are mean values of each cell line (n=9).

Cell line	HBMEC	HBVP	HA
Exponential growth (days) (Kumar <i>et al.</i> ,2014)	3 -6	2 - 6	3 - 7
Late lag/plateau (days) (Kumar <i>et al.</i> ,2014)	9	9	10
Doubling times (hours)(Kumar <i>et al.</i> ,2014)	51.7 h	52.3 h	24.6
Seeding density (cells/ ml) (Kumar <i>et al.</i> ,2014)	2 x 10 ⁴ cells/ml	2 x 10 ⁴ cells/ml	2 x 10 ⁴ cells/ml
Exponential growth (days)	4 – 7	4 – 7	4 - 7
Late lag/plateau (days)	7	7	7
Doubling times (hours)	36 h	96 h	60/66 h
Seeding density (cells/ ml)	1 x 10 ⁴ cells/ml	1.2 x 10 ⁴ cells/ml	1.2 x 10 ⁴ cells/ml

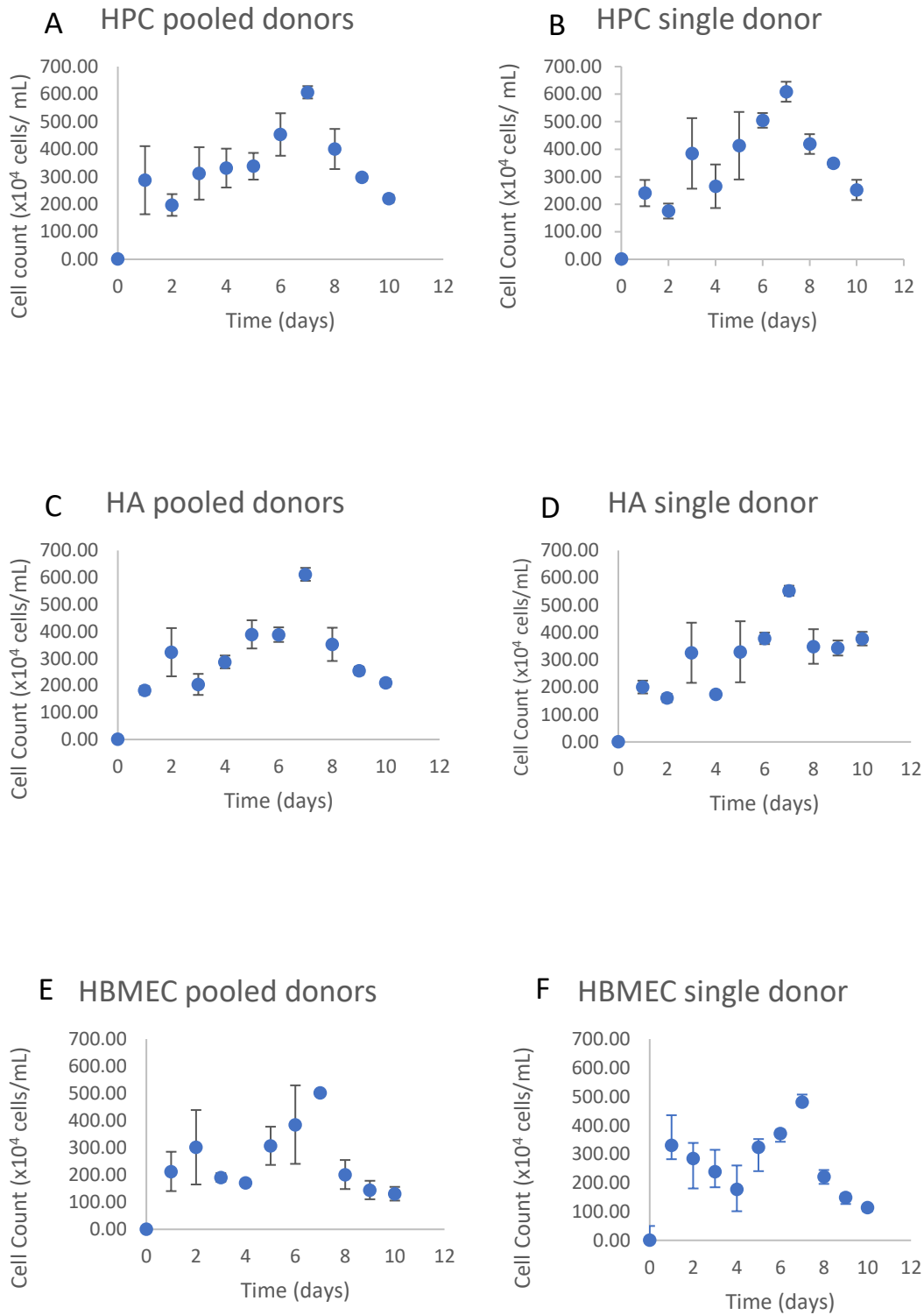


Figure 3.1 Cell count over time of primary cell lines, human brain pericytes (HBPC)(A and B), human astrocytes (HA)(C and D) and human brain microvascular endothelial cells (HBMEC)(E and F), growth kinetics with addition of either single donor human serum or pooled donor human serum (appendix 1, Table 2), data presented as average of triplicate wells +/- SD (n=9)

3.4.2 Cell morphology

The primary cell lines were observed in the light microscope on x10 magnification (Figure 3.2). The human brain pericytes (HBPC) showed initial faster growth and confluency than the human brain microvascular endothelial cells (HBMEC) and human astrocytes (HA), this correlates to the findings of Kumar *et al.* (2014). The morphology of the HBPCs was observed as elongated with thin processes (Figure 3.2). The HBMECs can be described as elongated cells with multiple processes initially, however these becomes less pronounced as the cells becomes more confluent appearing as cobblestones displaying a pronounced darker nucleus (Figure 3.2). The HA showed multiple processes attaching to neighbouring cells in a fibroblast like fashion (Figure 3.2). All the observed cell lines showed the expected morphological characteristics (Kumar *et al.*, 2014).

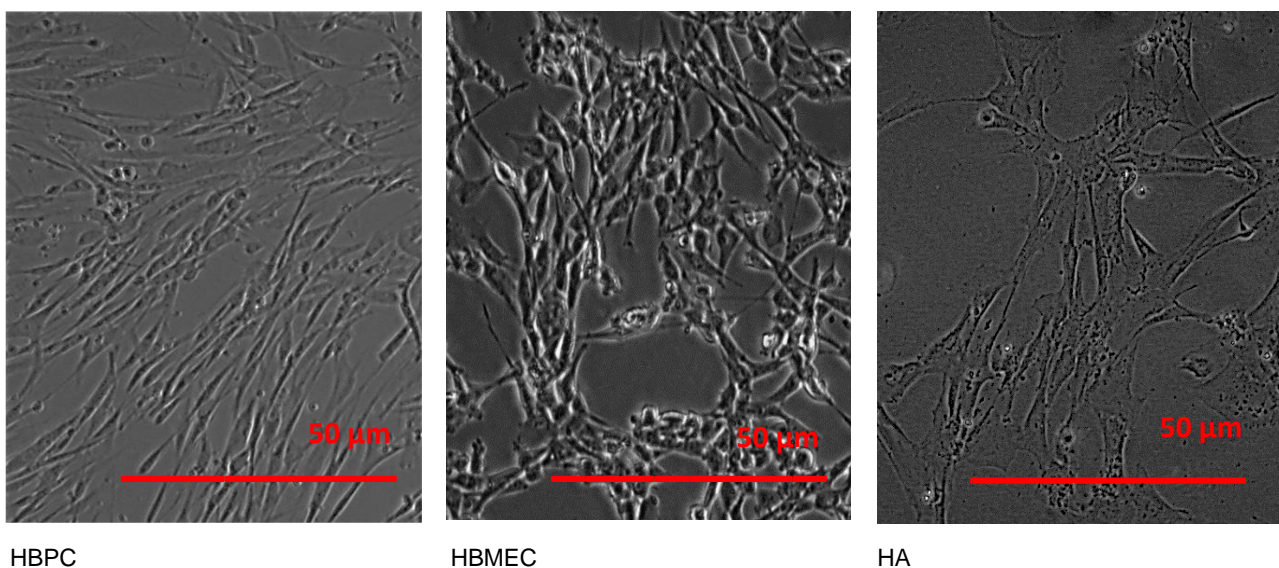


Figure 3.2 Three primary cell lines; human brain pericytes (HBPC), human brain microvascular endothelial cells (HBMEC) and human astrocytes (HA), imaged at X10 in inverted light microscope Leica

DMIL (Germany), Mshot camera and software (China). On day 2 after seeding. The scalebar represents 50 μm.

3.5 Discussion

The capillaries are the largest surface area of the BBB and remain an important target for therapeutics and this brain blood interface is a key area for investigation of bacteria brain interaction. In recent years much research of bacteria brain interaction has been conducted in animal and various *in vitro* cell models and the importance of human cell-based models have been recognised (Kim *et al.*, 2019, Fulop *et al.*, 2021). Both 2D and 3D models of the neurovascular unit with human primary or induced pluripotent stem cells have been used to investigate AD pathology, and disease models have been successful in inducing some of the hallmarks of the disease (Illievski *et al.*, 2018; Logan *et al.*, 2019). These have mainly been focused on investigated parenchymal pathogenesis and genetic mutated cell lines with an increased risk of AD development (Logan *et al.*, 2019). There appears to be a lack of studies examining the transport mechanisms in the human BBB in relation to bacterial exposure. Additionally, models must be validated in terms of protein expression such as ZO-1, occluding and Claudin-5 for this purpose (Kim *et al.*, 2019). The *in vitro* BBB model chosen for this project is exactly such a model which has been validated as physiologically relevant to imitate the BBB in humans (Kumar *et al.*, 2014), both in terms of protein expression and cellular integrity and structure. It was important to use a model which was already established as applications of the experimental protocols presented in this thesis were novel and required some optimisation.

When starting the work with the *in vitro* BBB model, the first objective was to characterise the cells in the tri-layered *in vitro* BBB model and to test whether supplementing the medium with single donor or pooled multiple donor serum would give the most favourable cell health and growth. The justification for testing multiple serum supplements was that theoretically multiple donor serum from both males and females would provide wider heterogeneity in serum components to the model and thereby strengthen the validity of the model data.

During the growth kinetics protocol, it was observed that cells grown with pooled serum in the media were harder to detach from the wells, this was seen as a positive feature and a sign of good health of the cells in these wells. The cells are expected to have an initial lag phase where they become established after seeding. This should be followed by a log phase which is an exponential growth phase followed by a point where a plateau is reached (second lag phase), because the cell population becomes confluent and slows down the growth, this represents the cells undergoing senescence (Kumar *et al.*, 2014).

The initial lag for all cells was in the first 4 days (Figure 3.1). All the tested cells showed an exponential growth phase between 4 and 7 days and all cell's growth peaked at day 7 to a plateau (Figure 3.1; Table 3.1). This was 2 to 3 days earlier than shown by Kumar *et al.* (2014) (Table 3.1) which is interesting as the initial lag phase was also found to be longer in our tested cells.

The doubling times varied for the three cell lines with the HBMEC doubling faster at 36 hours and the HA and HBPC taking much longer to double in numbers at 66 and 96 hours (Table 3.1).

There was no observed difference in growth kinetics between the two serum types in the HBPCs, but a slightly higher cell count was seen for the pooled serum test group. The doubling time for these cells were 96 hours for the pooled serum wells and a little less than 96 hours for the single donor cells, this is longer than reported by Kumar *et al.* (2014) who reported 52.3 hours for this cell line (Table 3.1). When making this comparison it must be noted that the seeding density used by Kumar *et al.* was higher (2×10^4 cells/ml) which could have influenced the behaviour of the cells and subsequently the data.

For HA, the pooled serum gave a better result in terms of the highest cell counts, though the doubling time for these cells were 60 hours in the single donor wells and 66 hours for the pooled serum test wells (Table 3.1). These mean doubling times are longer than reported by Kumar *et al.* (2014), who quoted doubling time as 24.6 hours (Table 3.1). This difference in

doubling times could be contributed to the difference in seeding density, cell batch or environmental differences such as variations in media content.

In the HBMECs there were some unusual growth kinetics detected with a significant lag in growth early in the test period. However, there was no observed difference between the two exponential phases or the highest cell count. The doubling time for these cells were 36 hours for both the pooled serum wells and the single donor (Figure 3.1), this is shorter than reported by Kumar *et al.* (2014) who measured a doubling time of 51.7 hours. Apart from differences in batches of cells and minor variations in growth conditions the initial lag in growth early on in our study could be down to the seeding density being half of the one used by Kumar *et al.* (2014), as the HBMEC thrive on being closer together in the initiation of the culture. This has been observed in this study and also noted by the suppliers of the cells (Neuromics, USA).

From observing the growth kinetics of the three cell lines with two types of serum, slightly better kinetics were observed in the cells which had pooled serum applied. The benefit of using pooled serum from multiple male and female donors would be, that this was more representable of a population study and this could also minimise batch to batch variability. Considering the benefits from using pooled serum and in the absence of any kinetic advantages from using single donor serum, the pooled serum was favoured for future experiments. The information on growth kinetics for the three primary cell lines used in this study is limited, but the variations in our findings to the data available from Kumar *et al.* (2014) could be explained by variations in cell donor, nutrient levels, attachment factors, mitogens present in the media, phenotypic drift, seeding density and passage level (Kumar *et al.*, 2014). The passage numbers used in this study were of similar level and considered low to midrange which should aid the accuracy of the results in terms of phenotype expression and homogeneity in the cell populations (Hughes *et al.*, 2007). Setting up *in vitro* BBB models with multiple (pooled) donors would add a wide genetic variability to the cells and minimise inter-assay variability every time a batch of cells is changed, but the cost

prohibited this study from using more than three primary cell vials, and therefore relied on the characterisation and optimisation completed here.

3.6 Conclusion

The exponential growth phase is seen as an optimal time point to apply the experimental protocol in the *in vitro* BBB model. As the exponential growth phases seen in the three cell lines tested in our study were similar to the ones found by Kumar *et al.* (2014) and the observed kinetics were comparable to the previous validation study of the model, the cells and the multi donor serum were acceptable for use in the application of the planned work with the *in vitro* BBB model. Therefore, it was concluded that the three characterised cell lines were to be used with the multiple donor serum for the *in vitro* BBB model (Kumar *et al.*, 2014). The next phase in this project was to set up the *in vitro* model and develop a protocol for application of *P. gingivalis* virulence factors to the BBB cells in order to assess if these could potentially have an effect on the integrity of the barrier.

Chapter 4

The *in vitro* Blood Brain Barrier model and *P. gingivalis* Lipopolysaccharide application

4.1 Introduction, aims and objectives of BBB model with *P. gingivalis* LPS study

The focus of this study is on PD pathogens interaction with the human BBB and in particular *P. gingivalis*. Though this keystone pathogen has been studied on multiple cell lines, there is no published data on the interaction of this microbe or its virulence factors with primary human cells of the BBB.

The three primary cell lines and media components were fully defined in Chapter 3 for use in the tri-layered *in vitro* BBB model (Kumar *et al.*, 2014). The next objective was to test the effect of *P. gingivalis* LPS on the integrity of the *in vitro* BBB model. The application of *P. gingivalis* virulence factors to an *in vitro* BBB model is novel as this method of evaluation has not previously been published and much of the pathogenesis of this microbe is still unknown, particularly regarding transport to the CNS. *P. gingivalis* has been investigated extensively in terms of effect and cell transport, but so far this research has been focused on tissues such as cardiac endothelial, lung endothelial, umbilical endothelium, gingival epithelial and gingival fibroblast cells (Dorn *et al.*, 2000; He *et al.*, 2020; Matsushita, 2021; Su *et al.*, 2021; Takeuchi *et al.*, 2019). Only one study was identified which investigated *P. gingivalis* effect on neuronal cells and this utilised human stem cells differentiated into neurons (Haditsch *et al.*, 2020) working on the theory that bacterial cells would enter the brain. With the increased focus recently on *P. gingivalis* involvement in neuroinflammation it is essential to learn more about how the cells of the BBB are affected by this periodontal pathogen. Even though other routes for microbials to reach the brain have been suggested, the capillaries of the BBB represent over 85% (650 km) of the total cerebral blood vessel length (Montagne *et al.*, 2017).

P. gingivalis LPS induces a different inflammatory response in mouse cells compared to humans' via TLR4 receptors. This is both *in vitro* and *in vivo* (Nativel *et al.*, 2017). The LPS has been found to only weakly induce proinflammatory cytokine secretion in mouse models

(Nativel *et al.*, 2017) and therefore conclusions from data from mouse models exposed to *P. gingivalis* LPS should only cautiously be applied to humans. The primary human cell lines utilised in the *in vitro* BBB model are a close representative to human physiological conditions mimicking BBB functionality and compound interaction (Nielsen *et al.*, 2011; Kumar *et al.*, 2014). Additional benefits to using this method is the relative low cost and no animals are used.

Aims

The overall aim of this study was to evaluate the effect of *P. gingivalis* lipopolysaccharide (LPS) on the integrity of the *in vitro* blood brain barrier (BBB) model and to examine whether the *P. gingivalis* LPS will cross the barrier in the model from the apical to the basolateral side.

Objective 1

To assess whether the repeated application of tracer compounds (evans blue dye (EBD) and FITC-dextran) would negatively affect the model's integrity. Tracer compounds were applied to the apical side of the BBB model and the integrity of the barrier and the appearance of tracer was measured at set time points using transendothelial resistance (TEER) and plate reader assays respectively.

Objective 2

To measure potential changes to the integrity of the BBB model after application of unconjugated *P. gingivalis* LPS. This was evaluated by co-application of *P. gingivalis* LPS and tracer compound (EBD/ FITC dextran) to the apical side of the BBB and then at variable

time points and concentrations. The integrity was evaluated by measurement of the transendothelial resistance (TEER) and by measurement of EBD and FITC-Dextran concentration in the basolateral compartment of the transwell system.

Objective 3

To investigate whether FITC conjugated *P. gingivalis* LPS cross the *in vitro* BBB model and how potential transport across the BBB model correlate with its integrity. This was evaluated by application of two types of FITC conjugated *P. gingivalis* LPS and measurements of the integrity of the BBB model by transendothelial resistance and the appearance of the conjugates in the basolateral compartment of the transwell system at set time points.

Objective 4

To measure, the biological activity of unconjugated *P. gingivalis* LPS and conjugated *P. gingivalis* LPS. This was assessed by application of the virulence factors to HBPC in monolayer and testing the cell assay for levels of human IL-6 by ELISA.

4.2 Materials

Materials and equipment used are listed in Table 1 and 2, Appendix 1.

4.3 *In vitro* BBB model methods

4.3.1 Coating of inserts for triculture BBB model

The transwell tissue culture inserts, (comprised of a 10 µm thick polycarbonate membrane with 8.0 µm size pores, Appendix 1, Table 2) separated each well into an upper (apical) and lower (basolateral) compartment. Each plate had 24 wells and 12 inserts. In the *in vitro* BBB model, the apical compartment represented the blood/vascular side of the BBB and the basolateral compartment represented the brain side of the BBB (Figure 4.1).

The 12 transwell membrane inserts were washed with 0.5 ml HBSS and then placed in a 37 °C humidified incubator under 5 % CO₂ for 30 minutes. The fibronectin was filtered before use with a 0.22µm sterilisation filter and syringe (Millex, Merck UK) and diluted to 5 µg/ml with HBSS. The HBSS was removed from the inserts and the inserts were placed upside down exposing the basolateral side of the membrane. This side of the membrane was incubated with 100µl of 5 µg/ml fibronectin in HBSS for 1 hour, at room temperature while in the hood covered up. After an hour the inserts were flipped back into the plates and 100µl of 5 µg/ml fibronectin in HBSS was placed in the apical side of the insert for 24 hours in 37 °C in the humidified incubator under 5 % CO₂.

4.3.2 Seeding primary cells triculture on the transwell inserts

After initiation, the three primary cell lines were grown on until a confluence of 85 – 90% was achieved (Kumar *et al.*, 2014). The precoated inserts (Section 4.3.1) were removed from the incubator and washed three times in 0.5 ml HBSS. The cells were removed from the culture vessels as described in Section 3.3.2 and counted as in Section 3.3.4. The HA and HBPC were seeded 48 hours prior to the HBMECs according to the protocol established by Kumar *et al.* (2014) and supported by the growth kinetics data obtained during the validation study of two serum types (Chapter 3). The orientation of the cells and arrangement of the plate is illustrated in Figure 4.1. The HA were seeded first on the basolateral side of the insert at a density of 200,000 cells/ml and left on the insert for 4 hours. Then the HBPCs were seeded at a density of 200,000 cells/ml and left in the hood for 4 hours. During this time the inserts were kept moist with a medium of equal volume pericyte basal media (PBM) and astrocyte basal media (ABM). Following this incubation period, the inserts were placed back in the plates with 600 μ l medium in the basolateral compartment and 200 μ l medium in the apical compartment. The plates were placed in the 37 °C humidified incubator under 5 % CO₂ for 48 hours, at which point the HBMEC were seeded at a seeding density of 250,000 cells/ml in the apical compartment. The plates were then incubated for 96 hours at 37 °C in a humidified incubator under 5 % CO₂ before the integrity of the triculture was tested.

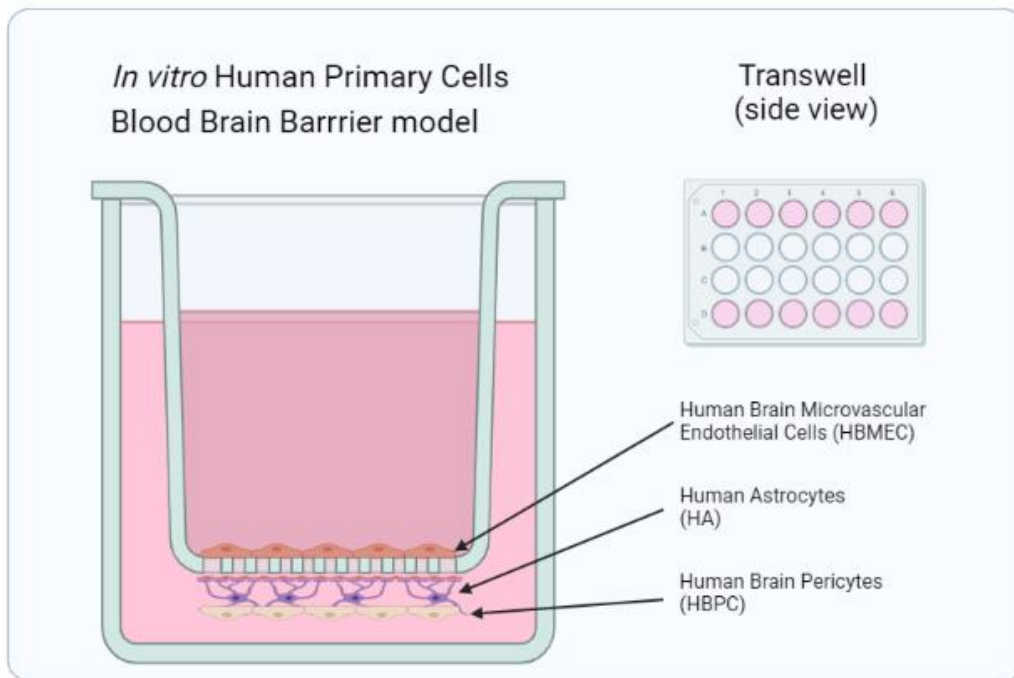


Figure 4.1 Transwell insert principle with the human brain microvascular endothelial cells (HBMEC) in the apical well and the human astrocytes (HA) and human brain pericytes (HBPC) in the basolateral compartment. Created in BioRender.com.

4.3.3 Testing the integrity of the *in vitro* BBB model and standard curves.

After 4 days, the integrity of the barrier model was tested by measuring the trans-endothelial electrical resistance (TEER) with an epithelial volt/ohm meter 2 (EVOM-2) instrument (WPI, UK).

As the barrier becomes established the TEER value rise expressed in Ohm/cm² (Srinivasan *et al.*, 2015). The triculture *in vitro* BBB model was considered ready for testing when the TEER values reached an average of 260 Ohm/cm² (Esposito *et al.*, 2016; Kumar *et al.*, 2014). The EVOM2 instrument was calibrated prior to each use, according to the manufacturer's directions using a calibration electrode. The TEER was measured by placing

two electrodes into the two compartments of the model (apical and basolateral). At each time point 5 TEER measurements were taken from each well (Kumar *et al.*, 2014).

The triculture barrier integrity were also assessed by application of a tracer compound (Evans blue dye (EBD) or Fluorescein isothiocyanate (FITC) dextran 3 -5 kD). The apparent permeability (Papp) of a compound can be measured to ascertain whether it is CNS positive (capable of penetrating the BBB) or CNS negative (poor permeability of the BBB) (Palumbo *et al.*, 2008). The EBD and FITC-dextran molecules can only penetrate the BBB when there are gaps between the cells and therefore gives an indication of the BBB models permeability or integrity.

A standard curve was prepared to spectrophotometrically quantify the appearance of EBD/ FITC dextran in the basolateral side of the BBB model, by plotting absorbance or fluorescence of known concentration standards of EBD/ FITC dextran respectively. The mean and standard deviation was calculated for each concentration and a linear line of best fit through the data to allow the samples from the BBB model to be quantified.

For the EBD standard curves, a 1 mg/ml stock solution of 10 mg of EBD (Sigma-Aldrich, UK) was dissolved in 10ml of sterile PBS and diluted with media (EMB, PM and ABM in a 1:1:1 ratio) at the following concentrations 1, 0.8, 0.6, 0.4, 0.1, 0.08, 0.06 and 0.04 µg/ml. For the FITC-dextran standard curves, a stock solution of 1 mg/ml was prepared in media (EMB, PM and ABM in a 1:1:1 ratio) and diluted to the following concentrations 100, 10, 1, 0.8, 0.6, 0.4, 0.1, 0.08, 0.06 and 0.04 µg/ml. All reagents containing FITC were prepared and stored at 5 °C shielded from light. Standard curves were also produced for all the FITC conjugated *P. gingivalis* LPS samples diluted with citrate buffer, HBSS or endothelial basal media (EBM), pericyte media (PM) and astrocyte basal media (ABM) 1:1:1.

FITC/ EBD was added to the apical compartment of the inserts and incubated in the 37 °C humidified incubator under 5 % CO₂. At the specified time points, 200 µl was removed from the basolateral compartment in triplicates and measured in a GENios Pro plate reader

(Tecan, Austria) at absorption 595 nm (gain 40, 22 °C) for the EBD and at 485 nm excitation and 535 nm emission (gain 40, 22°C) for FITC dextran and FITC-conjugate.

The apparent permeability was calculated to quantify the appearance of EBD, fluorescent labelled LPS or FITC-dextran. The appearance from the apical to the basolateral compartment measured and used to calculate the permeability (P_{app}) values in each experiment as shown in Equation 1.

$$P_{app} = \left(\frac{V}{A \times C_0} \right) \times \left(\frac{dQ}{dt} \right) \quad \text{Equation 1}$$

where:

V = Volume of basolateral compartment (V= 0.6 cm³)

A = surface area of the polycarbonate membrane (0.3 cm²)

C₀= Initial concentration of the *P. gingivalis* LPS-FITC conjugate, EBD or FITC-Dextran in the apical well

dQ = concentration of *P. gingivalis* LPS-FITC conjugate, EBD or FITC-Dextran collected from the basolateral part (µg/ ml) (passing across the cell layer to basolateral side).

dt = Change in time (sec)

4.3.4 Human IL-6 ELISA

As a quality assurance measure to check all virulence factors were capable of producing an inflammatory response, all test reagents were evaluated for inflammasome activity by incubation human brain pericyte (HBPC) cells with 100 or 200 µg/ml LPS, LPS-FITC conjugate or OMVs (see chapter 5) for 4 hours in triplicate in a 12 well tissue culture plate. The spent cell culture media was assayed for human IL-6 release using a commercially available enzyme-linked immunosorbent assay (ELISA) kit (Sigma-Aldrich, USA). The

sensitivity of detection in cell culture media was given as 3 pg/ml by the manufacturers (Sigma-Aldrich, USA).

A standard curve was prepared by dilution of human IL-6 with sample diluent buffer to concentrations of 1000, 333.3, 111.1, 37.04, 12.35, 4.12 and 1.37 pg/ml according to the manufacturer's instructions. After measurement in the GENios Pro plate reader (Tecan, Austria) at absorption 450 nm, a standard curve was produced, and calculations of concentrations made using line of best fit.

Test samples (spent media), controls (sample diluent buffer) and human IL-6 standards (100 μ L) were added to the precoated 96 well ELISA plate. This was incubated at 4 °C for 24 hours with gentle shaking on a benchmark Everlast rocker (SKS, USA). After removal of the samples the wells washed with 1x wash buffer four times. Biotinylated detection antibody was added and incubated for 1 hour at room temperature with gentle shaking. The wells were washed four times with 1x wash buffer and horseradish peroxidase (HRP) - streptavidin solution was incubated for 45 minutes at room temperature with gentle shaking. After washing four times with 1x wash buffer, ELISA colorimetric tetramethylbenzidine (TMB) reagent was added. This was incubated for 30 minutes at room temperature covered to exclude light while gently shaking. Then stop solution (supplied in kit) was added and the absorbance was measured in the 96-well plate immediately at 450 nm (Tecan, Austria). This test was repeated every time a new virulence factor reagent was used for the first time in triplicates.

4.3.5 *In vitro* BBB Methods testing barrier integrity after virulence factor application

Primary-derived HBMECs (Neuromics USA), HBVP (ScienCell, USA) and HA (ScienCell, USA) were initiated in cell culture vessels as described in 3.3.1 and 3.3.2. The BBB model was established as detailed in section 4.3.1 and 4.3.2. After 96 hours the *in vitro* BBB was tested to assess the barrier properties as described in 4.3.3 prior to application of a *P. gingivalis* virulence factors (LPS and LPS-FITC conjugate). The concentrations of virulence factors applied were deduced from previous studies (Blufstein *et al.*, 2018; Guo *et al.*, 2018) and when optimising the test protocols, both high and low doses were included.

The transendothelial electrical resistance (TEER) gives an indication of the tri-cultures paracellular permeability (Kumar *et al.*, 2014 and Esposito *et al.*, 2016). The aim was to reach a value of 260 Ohm/cm² before testing. The integrity of the BBB model was also tested by a permeability assay (4.3.3) and when these measurements confirmed the model was established sufficiently for testing, the test protocol outlined below in Section 4.3.5.1-3 were applied.

The unconjugated and conjugated *P. gingivalis* lipopolysaccharide (LPS) (commercially prepared, Appendix 1, Table 2) were diluted with media containing ABM, PM and EBM 1:1:1 at various concentrations as outlined in Sections 4.3.5.1 and 4.3.5.2 and stored at 5 °C during the test period. The virulence activity of the unconjugated and conjugated *P. gingivalis* LPS was evaluated using a commercial kit for Human IL-6 ELISA (Sigma-Aldrich, UK), as detailed in Section 4.3.4.

4.3.5.1 Application of *P. gingivalis* LPS to the *in vitro* BBB model at various concentrations, permeability tested with Evans Blue permeability assay

The passage numbers for the three primary cell lines seeded were HA passage 4, HBMEC passage 5 and HBPC passage 4. When media was replenished during the growth phase of the model, 600 µl of EBM, PM and ABM 1:1:1 (Table 2, Appendix 1) was placed in the basolateral compartments and 200 µl in the apical compartments.

Unconjugated *P. gingivalis* LPS 1000µg/ml stock was diluted with media (EBM,PM and ABM 1:1:1) to the concentrations (0.1, 0.3 and 1 µg/ mL). The *P. gingivalis* LPS was applied to the *in vitro* BBB model in triplicates at the time intervals 0.5, 1, 2, 4, 24, 48, 72, 96 120, 144 and 168 hours. For further details of distribution of test concentrations and controls are shown in Appendix 2 (Table 2).

Initially, 3 wells were tested to assess whether the sole placement of EBD would interrupt the barrier or if there were any potential binding of between EBD and the unconjugated *P. gingivalis* LPS and thereby preventing transport across the barrier (see test protocol Appendix 2, Table 1). The allocation of test protocol to which well was chosen at random. A standard curve for EBD was plotted as described in 4.3.3.

The experiment was stopped when the TEER readings indicated a drop in the integrity of the barrier (TEER \leq 200 Ohm/cm²) potentially due the cells becoming senescent, this was expected approximately 10 days after the model being established (Kumar *et al.*, 2014). TEER measurements of a blank well (just fibrinogen coating) and cells without LPS was carried out at all main time points in the test period as a control.

The preliminary data showed no signs of EBD-LPS binding or significant BBB model disruption by repeated application of EBD (Figure 4.3) and therefore the full test protocol was applied after 24 hours. The test protocol was repeated twice to ensure results were a true representation.

All TEER measurements during the test period were done as the first step before any other interventions, as while measuring the TEER values in the first 4 days after seeding the barrier model (before the test protocol was started), it was evident that the TEER values increased after changing the media in the wells. By measuring the TEER values before any other intervention to the BBB model this bias was minimised. The read values of TEER were displayed throughout the data set, as the study was assessing the relative changes in TEER after testing. However, the true TEER value is TEER (read) minus TEER (blank).

4.3.5.2 Application of *P. gingivalis* LPS to the *in vitro* BBB model at various concentrations, permeability tested with FITC-dextran permeability assay

The passage numbers for the three primary cell lines utilised were HA passage 5, HBMEC passage 6 and HBPC passage 6. Unconjugated *P. gingivalis* LPS 1000µg/ml stock was diluted with media (EBM,PM and ABM 1:1:1) to the concentrations 0.1, 0.3 and 1, 10 and 100 µg/mL. The aliquots were stored at 5 °C.

All the LPS reagents were tested on wells in triplicates and control wells were tested with either media or FITC-dextran only. In addition, TEER measurements were made on a blank well (no cells, with fibrinogen 5 µg/ml coated transwell) at all main time points in the test period.

After LPS application, the integrity of the *in vitro* BBB model was assessed by TEER measurements and FITC-dextran 3-5 kD 100 µg/mL mixed with media (EBM, ABM and PM) at the set time points prior to and after LPS application. The model wells had the test protocols allocated at random. The time points for sampling were: 0.5, 1, 2, 4, 24, 48 and 72 hours. Each well had 5 TEER measurements carried out each time.

At each set time point the permeability of the *in vitro* BBB model wells were tested by placing 200 µl of FITC-dextran 3-5 kD (100 µg/ml) in the apical compartment. After 30 min incubation 3 x 200 µl were removed from the basolateral compartment, placed in a 96 well tissue plate and measured in the plate reader as detailed in Section 4.3.3. The whole test protocol was repeated twice to ensure results were a true representation. For further details on well allocation please see Appendix 2 (Table 2).

4.3.5.3 *P. gingivalis* LPS-FITC conjugates application to the *in vitro* BBB model in various concentrations and checked with FITC- dextran permeability assay

To assess if the *P. gingivalis* LPS could pass the barrier model, two different LPS conjugates were obtained and tested by a similar protocol to previously described. The passage numbers for the three primary cell lines were HA passage 5, HBMEC passage 7 and HBPC passage 6. The Nanocs *P. gingivalis* LPS FITC conjugate was purchased from Nanocs, USA (2mg/ml) and the Dojindo *P. gingivalis* LPS FITC conjugate was made by using a labelling kit from Dojindo (Japan) combined with *P. gingivalis* LPS 1 mg/ml (Invivogen, France). The conjugation method using the kit from Dojindo is described in 4.3.5.3.1. The biological activity of the *P. gingivalis* LPS conjugates were tested by application to HBPC cells and tested for IL-6 activity by ELISA (see Section 4.3.4).

4.3.5.3.1 *P. gingivalis* LPS conjugate from Dojindo

P. gingivalis LPS (Invivogen, France) was labelled with FITC following a protocol described by Takeuchi *et al.* (2019). The protocol utilised a labelling kit by Dojindo (Japan) which conjugates the fluorescein with *P. gingivalis* LPS. The labelling is achieved by forming a

bond between a NH₂ reactive fluorescein ester group to an amino group on the LPS. This conjugation has been reported to have no noticeable effect on the virulence of the *P. gingivalis* LPS molecule (Takeuchi *et al.*, 2019). For the conjugation 100 µl of X1 wash buffer (Dojindo, Japan) and 100 µl of *P. gingivalis* LPS (1 mg/ml) (Invivogen, France) were placed in the kit filtration tube (capturing molecules >50 kDa). This was centrifuged for 10 minutes at 8000x g. The NH₂ reactive fluorescein tube content was mixed with 10 µl of DMSO and 8 µl of this was added to the filtration tube with 100 µl of kit reaction buffer (Dojindo, Japan). This was incubated for 10 minutes at 37 °C. Then 100 µl of wash buffer was added to the filtration tube which was centrifuged at 8000x g for 10 minutes. The filtrate was discarded and a further two washes with 200 µl wash buffer and centrifugation at 8000x g for 10 minutes were carried out to remove any un-conjugated fluorescent molecules. The conjugate was recovered with 200 µl of wash buffer and stored at 5 °C. The LPS molecules by this method forms aggregates of various sizes (Takeuchi *et al.*, 2019) and to prevent this, a buffer containing detergent was applied to the conjugate (X1 citrate buffer and 0.05% tween-20, pH 8) for 45 minutes at 37°C, resulting in a LPS conjugate stock of 100 µg/ml (private email correspondence with Dr Takeuchi, 2019).

Samples of the *P. gingivalis* LPS FITC conjugate for the *in vitro* BBB application were made up at various concentrations in both HBSS and Media (ABM,PM,EBM 1:1:1) to assess fluorescence and virulence in both reagents and to assess potential interactions with media components.

Standards for both dilutions of *P. gingivalis* LPS FITC conjugates were made (0.001, 0.01, 0.1, 1, 10 and 100 µg/ml) and curves were plotted after measuring these in the plate reader (Section 4.3.3). These conjugation samples were also tested for virulence by application to HBPC and cell media sampling was completed for an IL-6 ELISA as described in Section 4.3.4. This was to evaluate whether the virulence activity of the *P. gingivalis* LPS could have been noticeably affected by the conjugation process.

4.3.5.3.2 *P. gingivalis* LPS conjugate from Nanocs.

A custom made FITC- *P. gingivalis* LPS conjugate was purchased from Nanocs (USA). Nanocs produced this conjugate from the *P. gingivalis* LPS (1 mg/mL) which is used throughout this study (Invivogen, France) and the concentration of the custom-made stock product was 2 mg/ml of *P. gingivalis* LPS-FITC conjugate suspended in sterile H₂O. Test samples were made up of the LPS conjugate with citrate buffer (CB) (X1 CB and 0.05% tween-20, pH 8) with incubation for 45 minutes at 37°C or media only (AGM, PM and EBM 1:1:1 Table 2, Appendix 1) at concentrations of 0.001, 0.01, 0.1, 0.3, 1, 10 µg/ml, 50 and 100 µg/ml. This was to assess whether the FITC-LPS molecules by this method would potentially form aggregates or show differences in behaviour with or without the addition of citrate buffer. These samples were applied to the *in vitro* BBB model and also used to produce a standard curve (section 4.3.3). Test samples with and without citrate buffer were applied to evaluate if the addition of the buffer influenced the LPS samples' virulence activity and integrity of the *in vitro* BBB model.

4.3.5.3.3 Application of LPS-FITC conjugates (Dojindo and Nanocs) to the *in vitro* BBB model

The test protocol with *P. gingivalis* LPS-FITC conjugates were repeated three times. In the first experiment Dojindo conjugate in media (AGM, PM and EBM 1:1:1, and HBSS) were tested.

In the latter two experiments both LPS conjugates were tested and samples were suspended in CB and media or media only (AGM, PM and EBM 1:1:1).

A number of wells were only tested with 200 µl FITC-dextran 3-5 kD (100 µg/ml) as a control, to assess the integrity of the model and any potential effects of applying FITC-dextran to the cells (Objective 1). At the set time points, the FITC-dextran was left in the apical compartment for 30 minutes before samples were taken from the basolateral compartment and measured in the plate reader. For the FITC LPS conjugate protocols, control wells also included no treatment (cell and media alone) and a cell blank (fibronectin insert, no cells). At time point 0, 200 µl of *P. gingivalis* LPS- FITC conjugate test samples (Dojindo and Nanocs) were placed in the apical compartment. At each time points 0.5, 1, 2, 4, 24, 48 and 72 hours TEER measurements were made from each well five times. To measure permeability (Papp), three times 100 µl were removed from the basolateral compartments (also at each timepoint) and measured in the plate reader. Each plate had three wells of each concentration (intraassay variability check). A standard curve for was plotted for all the FITC conjugate test samples and FITC-dextran as described in 4.3.3. The well distribution of the test protocol was allocated at random. Further details of the sample distribution can be seen in Appendix 2 (Table 3, 4, 5). The TEER and permeability (Papp) data obtained from the *in vitro* BBB model was tested for homogeneity of variances and normality using the Shapiro - Wilk test. Differences between treatment groups were analysed using an ANOVA (two tailed) with Dunnett's post-hoc analysis or an independent t-test was used for comparison between independent experiments. The data collected were evaluated in SPSS v 26 and 27 (IBM, USA) and the Microsoft Excel software for Microsoft office360 (Microsoft Corporation, USA). The analysis of variance was statistically significant when (*) $P < 0.05$, and highly significant when (**) $P < 0.01$ and (***) $P < 0.001$.

4.3.5.4 Human IL-6 ELISA of HBPC assay after application of unconjugated and FITC- conjugated *P. gingivalis* LPS

HBPC passage 4 were defrosted and seeded at a density of 2×10^5 as described in 3.3.1 in 12 well plates with PM. The cells were placed in a humidified incubator at 37 °C, 5 % CO₂ for 24 hours. After 24 hours the cells were 90 % confluent. The media was removed and the cells were washed in 600 µl HBSS. 100 µl of test reagents in pericyte media (PM) were placed on the cells for 4 hours. The samples tested were: *P. gingivalis* LPS in PM (100 µg/ml), FITC *P. gingivalis* LPS conjugate from Dojindo diluted in citrate buffer and media (100 µg/ml), LPS conjugate from Nanocs in citrate buffer and PM (0.1, 1 and 10 µg/ml) and LPS conjugate from Nanocs in PM only (10 µg/ml). The controls were PM only. All samples were tested in triplicates. After incubation, the media was removed for ELISA testing as described in 4.3.4.

4.4 Results

4.4.1 Results from *P. gingivalis* LPS application to *in vitro* BBB model and Evans Blue Dye permeability assay.

Prior to the start of the experiment, TEER values were consistent from day 7, with a typical variation of $\pm 10 \Omega/\text{cm}^2$ over a 4-hour period (data not shown). The effects of the *P. gingivalis* LPS applied to the *in vitro* BBB model, was measured by evaluating changes of permeability to the reference compound (EBD) and Papp values were calculated at certain time points, to enable assessment of any change with time (Appendix 2, Table 6). Disruption of the BBB by the LPS could potentially lead to an increase in Papp when compared to the intact barrier not exposed to this virulence factor. The baseline of the experimental model and optimisation was carried out to establish whether the primary cells and the 3-layer

model were suitable for the planned experiments and not affected by the presence of the tracer compound. A standard curve for EBD was prepared to allow quantification of EBD in the basolateral compartment after co-application with *P. gingivalis* LPS to assess Papp (Figure 4.2).

The initial evaluation of the repeated use of EBD as a tracer compound found no evidence of reduced barrier integrity in the control wells (EBD only) (Figure 4.3) and therefore the protocol progressed to apply the various concentrations of *P. gingivalis* LPS over the remaining test period.

In the test period the % Appearance of EBD generally peaked at 24 h and then reduced to 0 % in most wells (Figure 4.3). This data set shows that the control wells without *P. gingivalis* LPS application (Figure 4.3B) display very similar results in terms of TEER and appearance of EBD compared to the wells treated with 1 µg/ml *P. gingivalis* LPS (Figure 4.3A) alone or *P. gingivalis* LPS in combination with EBD (Figure 4.3C), i.e. the LPS concentration applied in this first experiment was not inducing a measurable change in TEER compared to the controls. In the test periods most wells had continuous TEER value between 250 – 300 ohms/cm², which is what was expected (Kumar *et al.*, 2014; Srinivasan *et al.*, 2015). In some of the experiments some wells had overall higher TEER values. These wells were treated the same as all the others, but appeared to have more favourable readings, potentially due to variations in cell viability and expansion (Srinivasan *et al.*, 2015). Generally, the TEER recovery values gradually decreased as the model lost viability (Figure 4.3A-D), in these first protocols the measurements were continued for 7 days.

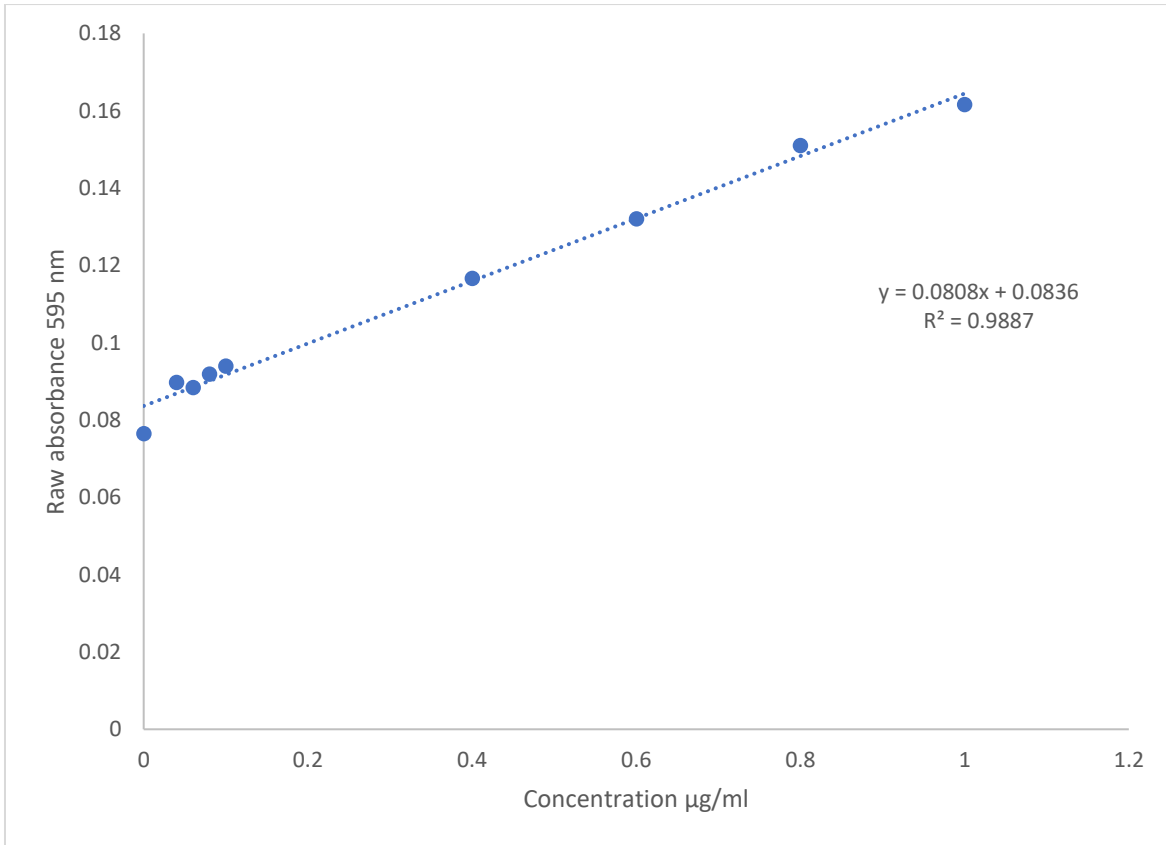


Figure 4.2 Standard curve for permeability assay with Evans Blue Dye, absorbance measured at 595 nm (gain 40, 22°C), minimal concentration 0.04 $\mu\text{g/ml}$, dotted line of best fit.

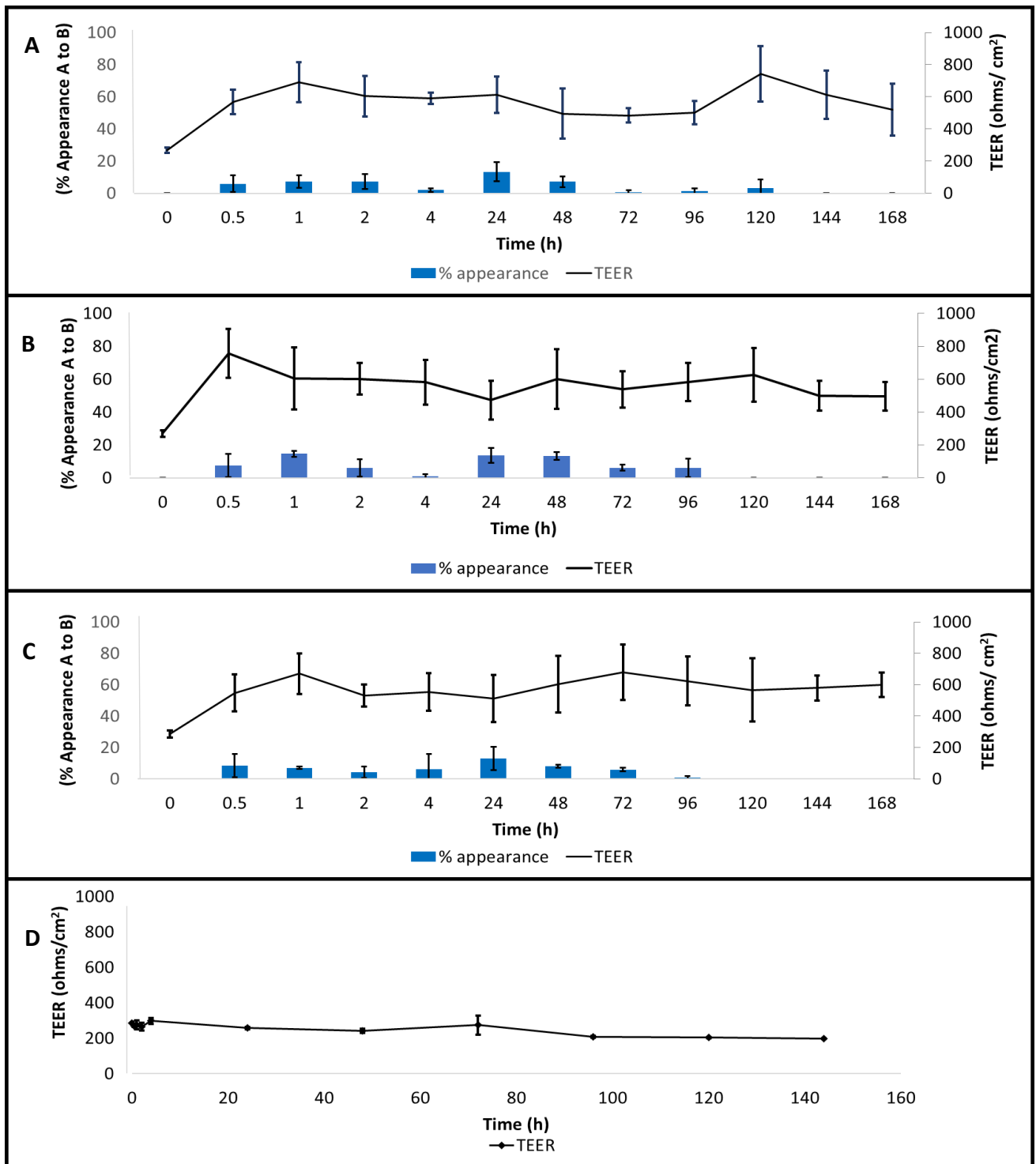


Figure 4.3 transendothelial electrical resistance (TEER) readings and permeability of Evans blue dye (EBD) in transwell tri-layer primary human cell BBB model after application of: **A** *P. gingivalis* LPS 1 µg/ml, **B** no LPS (Evans Blue 1 µg/ml), **C** *P. gingivalis* LPS + EB (1:1 µg/mL), **D** TEER only. Where % appearance A to B indicates the concentration of the tracer compound (EBD) applied to the apical compartment of the model (A) to the basolateral compartment (B) after passing through the membrane and cell barrier. Statistical significance of response was measured using an ANOVA with Dunnett's post-hoc relative to the control (EBD) where * $P < 0.05$. Data shown Mean \pm SD, N=9. No statistical significance was detected.

4.4.2 Results from *P. gingivalis* LPS application to *in vitro* BBB model and FITC-dextran permeability assay

The *in vitro* BBB model was established and continuous increase in TEER values were observed which signified that the three primary cell lines were continuously expanding and healthy. The exponential growth phase of the cells of the *in vitro* BBB model was deemed optimal at 4 days after the BBB model was seeded and this was chosen as time point 0 for the experimental protocol. This timeline matches the findings of both Kumar *et al.* (2014) and growth kinetics carried out in and described previously (Chapter 3).

Upon addition of unconjugated *P. gingivalis* LPS (test wells), media (blank wells) or FITC (control wells) to the apical side of the BBB, there was a small initial dip in TEER at the start of the experiment. This was attributable to a movement artefact and slight disturbance of the BBB in all wells, typically this was $\pm 25 \Omega/\text{cm}^2$ and recovery to baseline was observed in the control wells within 2 hours. The response of TEER in test wells upon addition of unconjugated LPS often showed a lower drop in TEER and that did not always recover to pre-baseline TEER. To determine whether the change in TEER was significantly different from baseline variation or movement artefacts, the pattern of response was modelled and the magnitude (ΔTEER), recovery time and rate of change were defined as shown in Figure 4.4 and were then used for statistical comparison between the control and test wells at different LPS concentrations. In these calculations the gradient of the change in TEER ($Y1-Y2/X2-X1$), recovery time ($X3-X2$) and gradient of recovery ($Y3-Y2/X3-X2$) could be analysed. Time of FITC-dextran appearance and time of maximum % appearance was also compared between the test groups and controls (Appendix 2, Table 7 and 8). Statistical analysis was applied to the data (SPSS v.26, IBM, USA). Significance of response was measured using an ANOVA with Dunnett's post-hoc relative to the control (administration of FITC alone) where * $P < 0.05$ and ** $P < 0.01$.

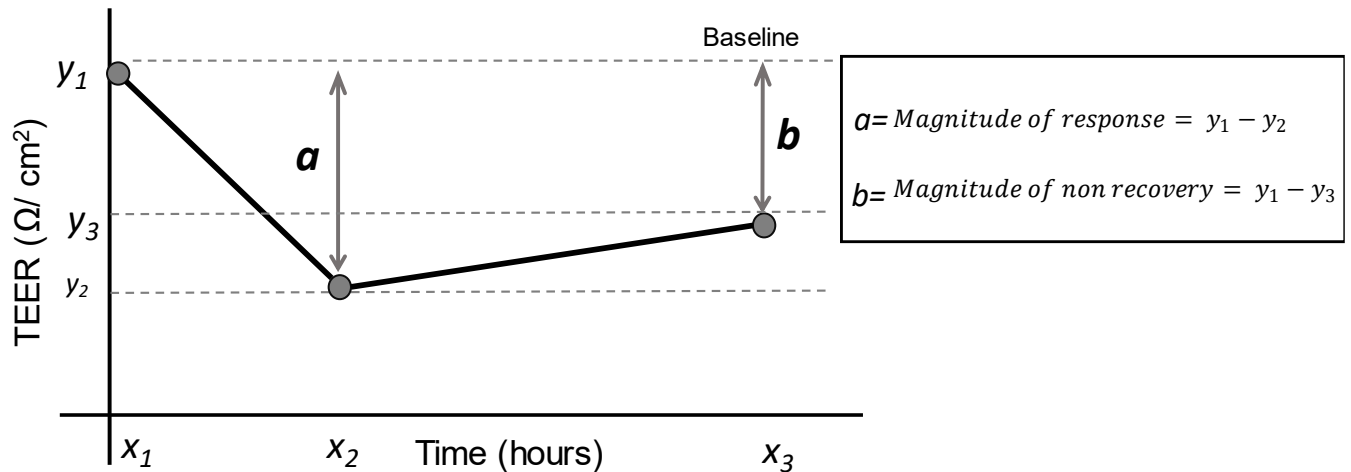


Figure 4.4 Modelling the magnitude and rate of change in TEER after application of test sample to the *in vitro* BBB model

The application of unconjugated *P. gingivalis* LPS to the BBB caused a significant decrease in TEER for 0.3 µg/ml ($P \leq 0.05$), 10 µg/ml ($P \leq 0.05$) and 100 µg/ml ($P \leq 0.05$) when compared the magnitude of change to the control well, where FITC alone or media alone were administered (Figure 4.5A). The magnitude of recovery of TEER values was determined as the maximum TEER measured during the recovery phase (x_2 to x_3). For all wells treated with unconjugated *P. gingivalis* LPS there was still a deficit in recovery of the BBB integrity compared to the pre-incubation phase, as indicated by the deficit in TEER 72 hours post incubation relative to the baseline at time zero.

The magnitude of deficit in TEER was significantly greater in the test wells where unconjugated *P. gingivalis* LPS was applied at 0.3 µg/ml ($P \leq 0.05$), 10 µg/ml ($P \leq 0.05$) and highly significant with 100 µg/ml ($P \leq 0.01$) compared to the control wells where FITC-alone was applied to the BBB (Figure 4.5B). It was evident that the control wells recovered much better to a level approximately 5 ohm/cm² below the levels seen at timepoint 0 (Figure 4.5B). Whereas the test wells struggled to recover after the LPS application, their TEER levels were significantly lower (* $P < 0.05$, ** $P < 0.01$) than before the exposure (Figure 4.5B).

The wells with the highest concentration applied (100 $\mu\text{g/ml}$) also took longer (25 - 40 hours) than the other wells to reach a recovery plateau (Figure 4.8f).

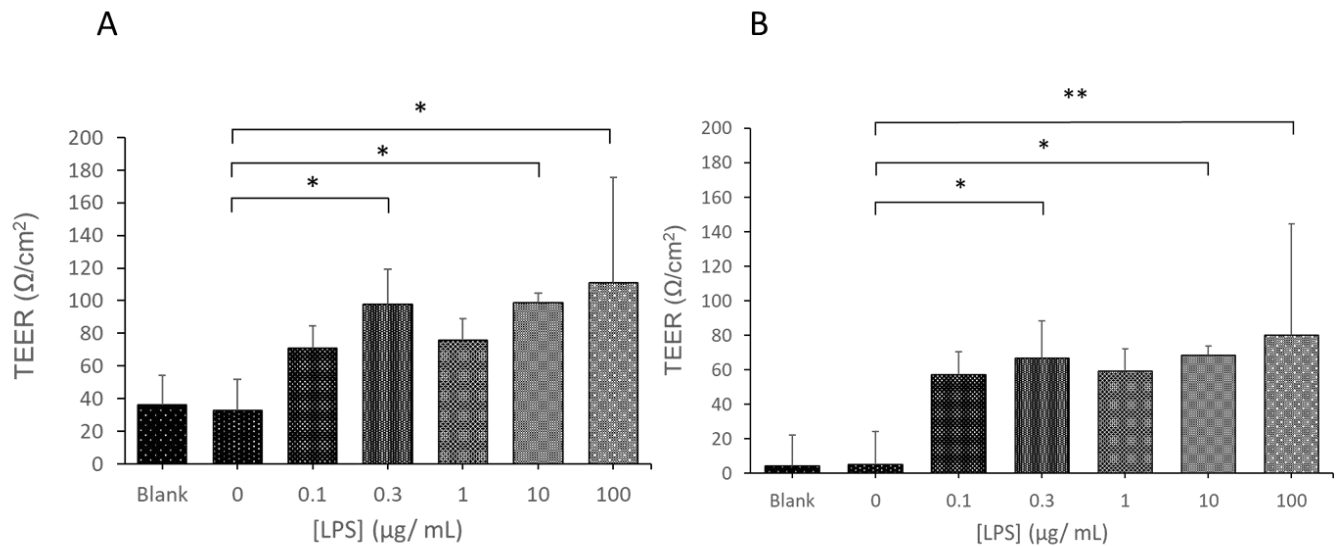


Figure 4.5 Changes in BBB integrity measured by calculating the magnitude of decrease in TEER in response to application of unconjugated *P. gingivalis* LPS (A) and the magnitude of deficit in recovery of TEER 72 hours post application of unconjugated *P. gingivalis* LPS relative to initial baseline TEER (B). Statistical significance of response was measured using an ANOVA with Dunnett's post-hoc relative to the control (administration of FITC alone) where $*P < 0.05$ and $**P < 0.01$. Data represents mean \pm SD from three wells and two experimental repeats ($n=6$).

The integrity of the *in vitro* BBB model was also assessed by testing the wells with FITC-Dextran 3-5 kD as a marker of tight junction permeability and a standard curve for FITC-dextran 3-5 kD known concentrations to line of best fit (Figure 4.6) was produced.

After incubation with unconjugated *P. gingivalis*. LPS or media (blank) for set time points, FITC-Dextran 3-5 kD was added to the wells and the fluorescent appearance of FITC-dextran on the basolateral side of the BBB was measured. The percentage appearance of

FITC-dextran appeared to increase following longer exposure (24-72 hours) to *P. gingivalis* LPS, as shown in Figure 4.7D and 4.7E.

It was observed that the FITC-Dextran appeared earlier in the wells with 10 and 100 µg/ml of unconjugated *P. gingivalis* LPS following pre-incubation (60 minutes) (Figure 4.8e and 4.8f) compared to the lower concentrations and controls (Figure 4.8a-d). However, this was not statistically significant relative to the blank wells and no significant concentration dependent effect in *P. gingivalis* LPS treatment related to FITC-dextran appearance was observed for the complete test period.

The apparent permeability (Papp) was calculated for three time points (60,120 and 240 minutes) as described in 4.3.3. This showed that the relative appearance of the FITC dextran molecules at these time points were low. The Papp of FITC-dextran (100 µg/ mL) after incubation for 30 minutes was calculated for three time points, at 60 min, 120 min and 240 min were found to be $1.04 \times 10^{-8} \pm 2.3 \times 10^{-8}$ cm/s, $8.7 \times 10^{-8} \pm 1.7 \times 10^{-7}$ cm/s and $4.8 \times 10^{-8} \pm 4.7 \times 10^{-8}$ cm/s. The whole protocol was repeated twice. The percentage appearance was plotted with the TEER values to assess correlation and this confirmed that the appearance happened earlier in the higher concentrations and also correlated with a drop in average TEER values (Figure 4.8). The wells with no LPS or FITC-dextran (TEER only) showed steady TEER values with an increase in values as the experiments progressed (Figure 4.8 and 4.9).

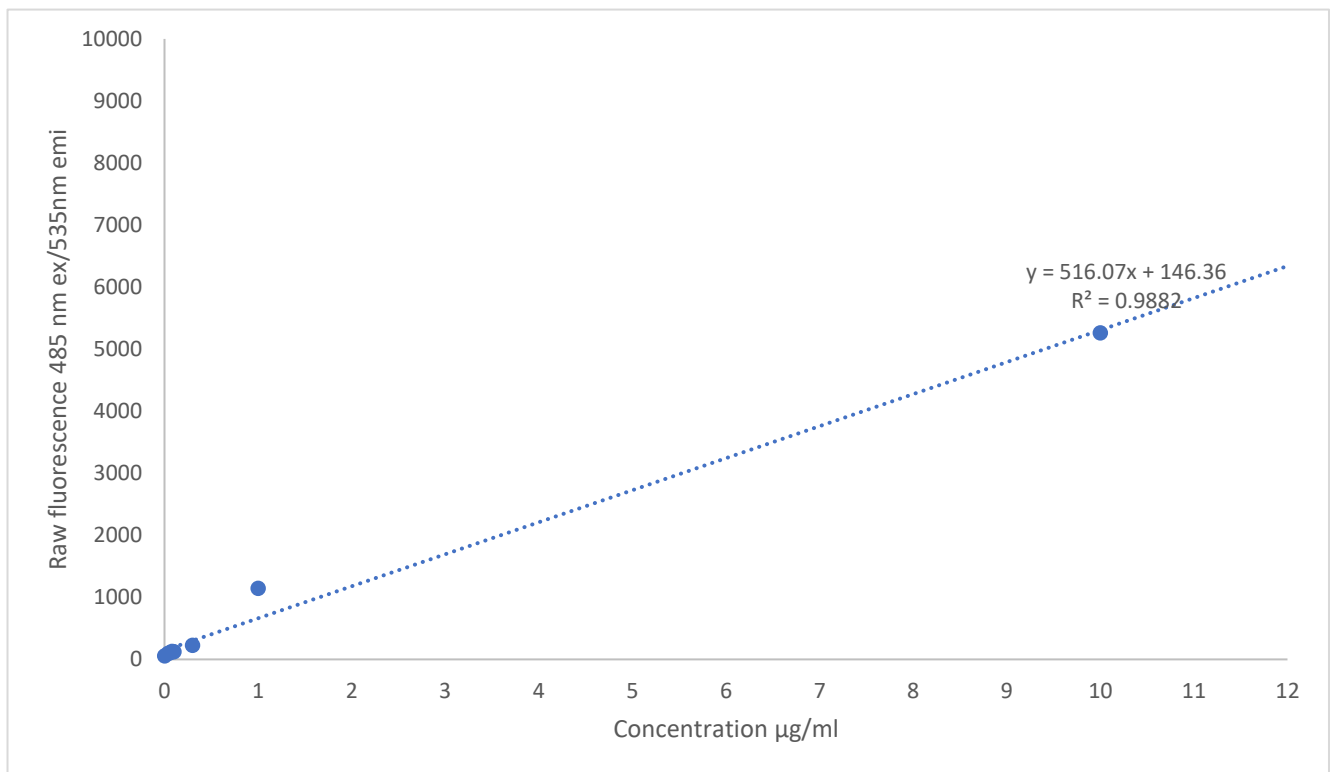


Figure 4.6 FITC-dextran 3-5 kD standard curve for permeability assay in in vitro BBB model. Fluorescence measured at 485nm excitation and 535 emission (gain 40, 22°C). Dotted line of best fit.

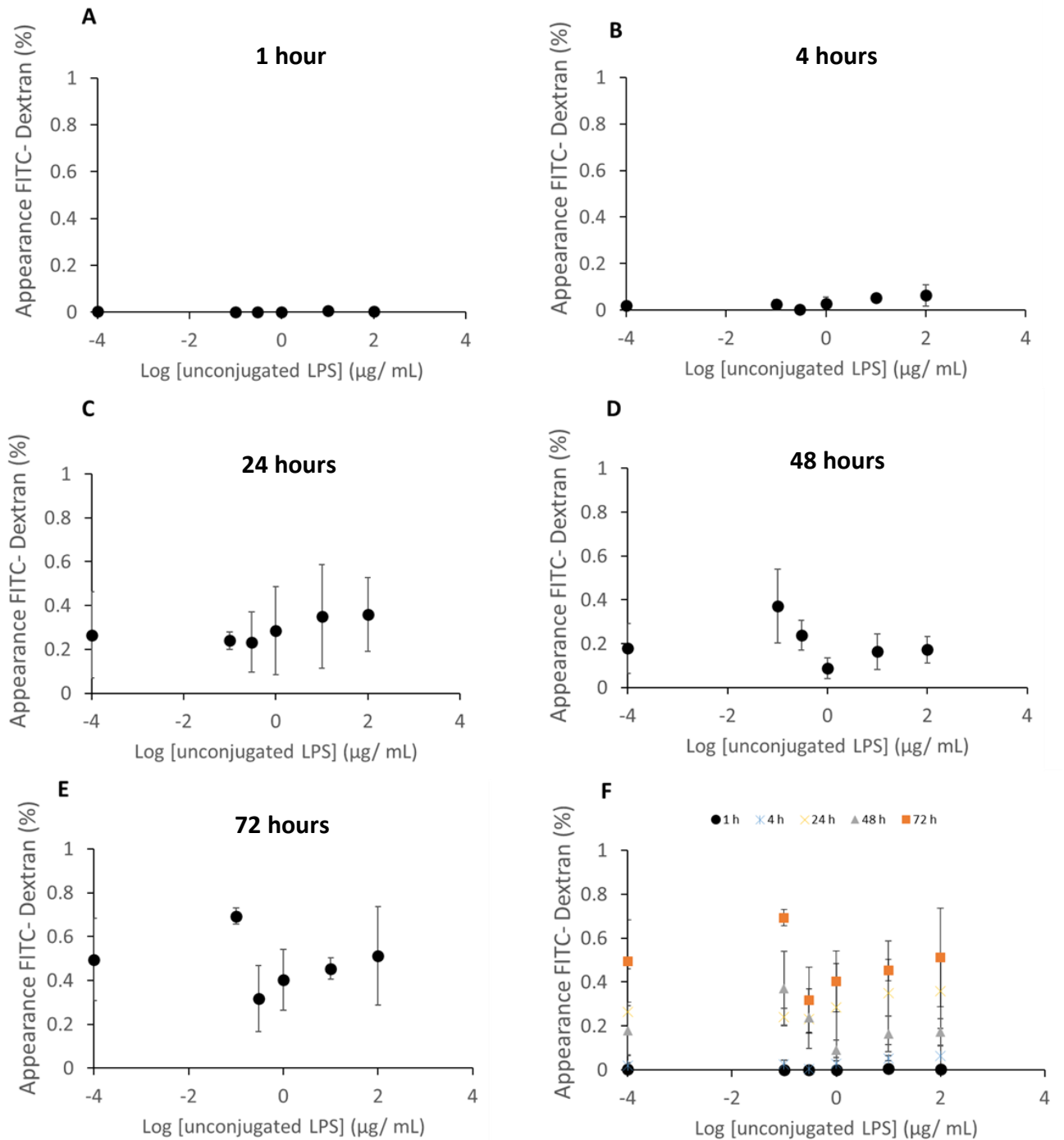
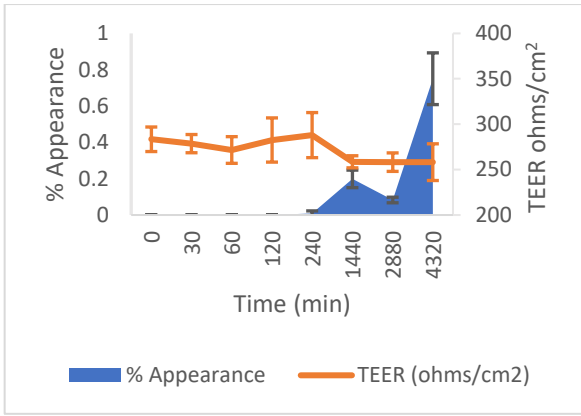
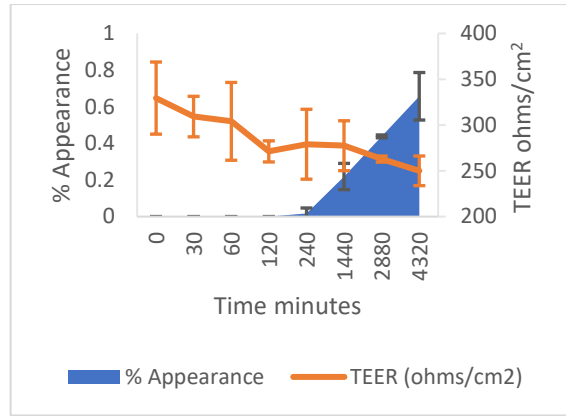


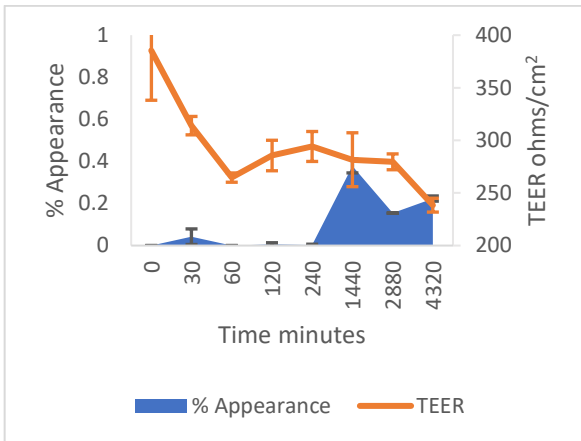
Figure 4.7 Shows the percentage of FITC-dextran (3-5 kDa) permeating through the in vitro BBB after incubation with increasing concentrations of unconjugated P.g. LPS (0-100 µg/mL) for 1 h (A); 4 h (B); 24 h (C); 48 h (D); 72 h (E) and all exposure times compared together (F). Each data point represents mean \pm SD from three wells and two experimental repeats (n=6).



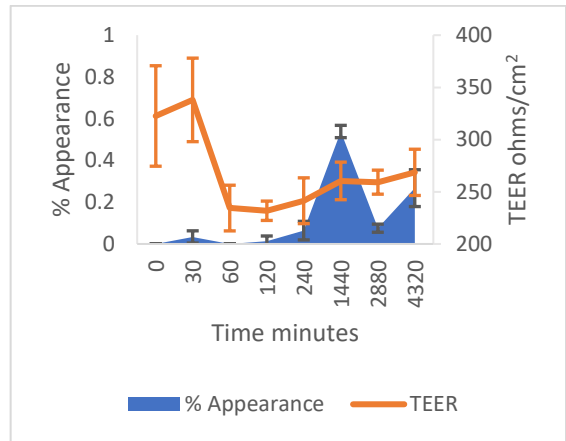
a



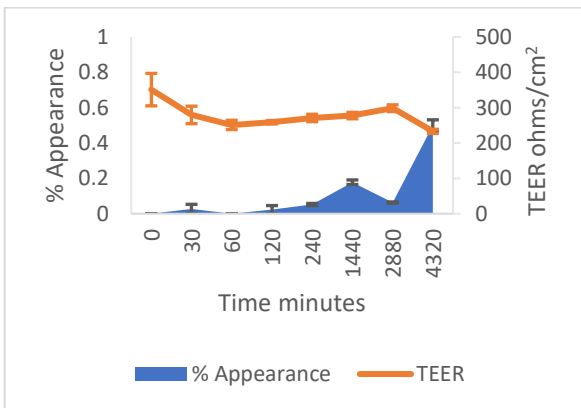
b



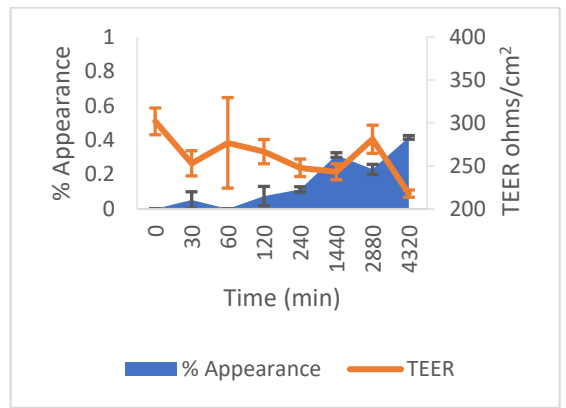
c



d



e



f

Figure 4.8 TEER (Ohms/cm²) compared to % Appearance at different test protocols: **a** - FITC only, **b**- 0.1 µg/ml P.g LPS, **c**- 0.3 µg/ml P.g LPS, **d** - 1 µg/ml P.g LPS, **e** - 10 µg/ml P.g LPS, **f** - 100 µg/ml P.g LPS. Data presented as Mean +/- SD.

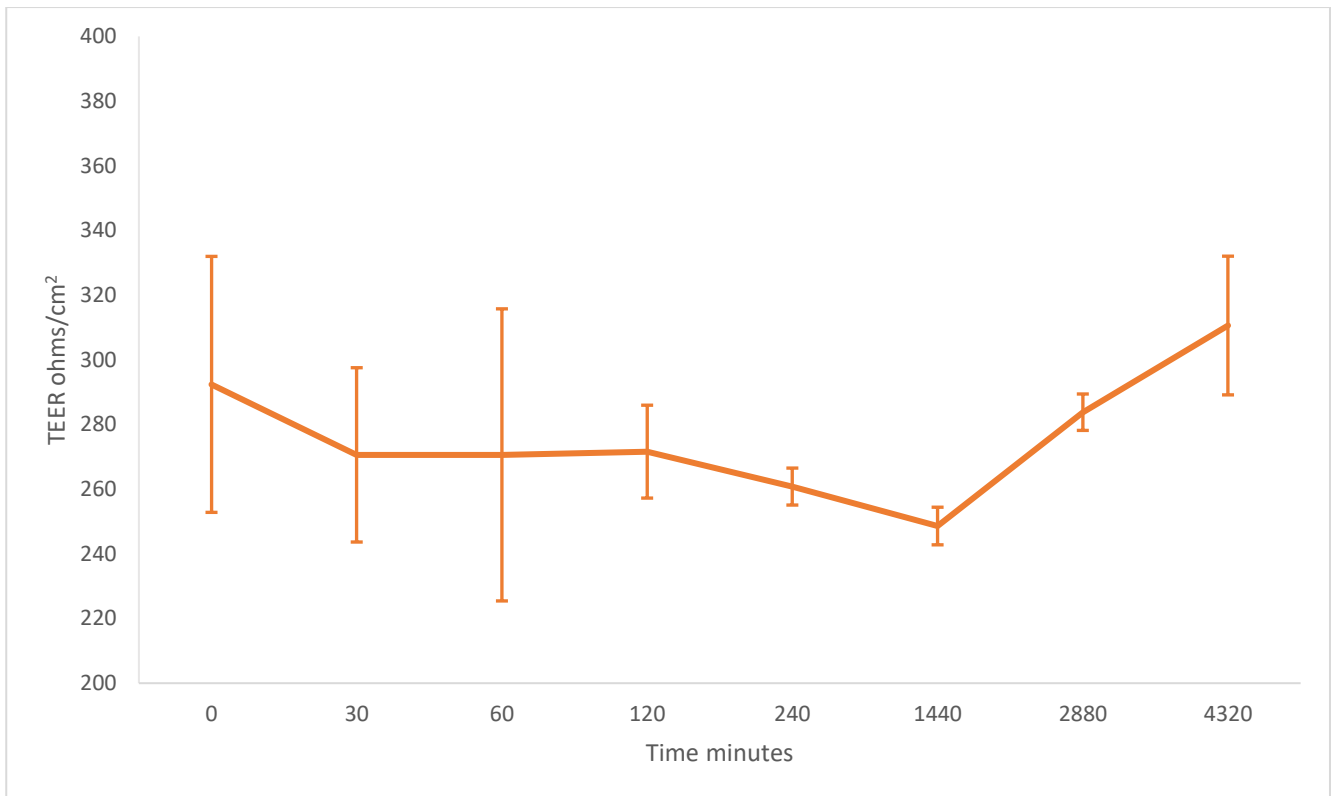


Figure 4.9 transendothelial electrical resistance (TEER) in control wells (media only) of human primary cell tri-layer BBB model, Data presented as Mean +/- SD N=15

4.4.3 Results from application of *P. gingivalis* LPS-FITC conjugates on the *in vitro* BBB model

4.4.3.1 Results Dojindo conjugate

The Dojindo conjugate was tested on the *in vitro* BBB model suspended in either HBSS or media (astrocyte basal media (ABM), pericyte media (PM) and endothelium basal media (EBM) 1:1:1) (Appendix 1, Table 2) and appearance in the basolateral compartment was observed for all the test concentrations early in the protocol (starting at 30 minutes) and at a low level (most wells $\leq 2\%$) (Appendix 2, Table 9). However, this FITC *P. gingivalis* LPS

conjugate data indicated that the values from the standard curve were too close to the values of the controls, i.e. close to the limit of detection. This indicated that the fluorescein in the labelling kit was too dilute when mixed in the media media (astrocyte basal media (ABM), pericyte media (PM) and endothelium basal media (EBM) 1:1:1) or HBSS (Figure 4.10 and 4.11). These findings were confirmed when the protocol was repeated, where no appearance could be detected based on the data from the standard curve.

The standard curve was repeated twice with gain 40 and gain 60, but this did not improve on the measured data from the well samples. Consequently, it was concluded not to use the Dojindo conjugate in the *in vitro* BBB model study.

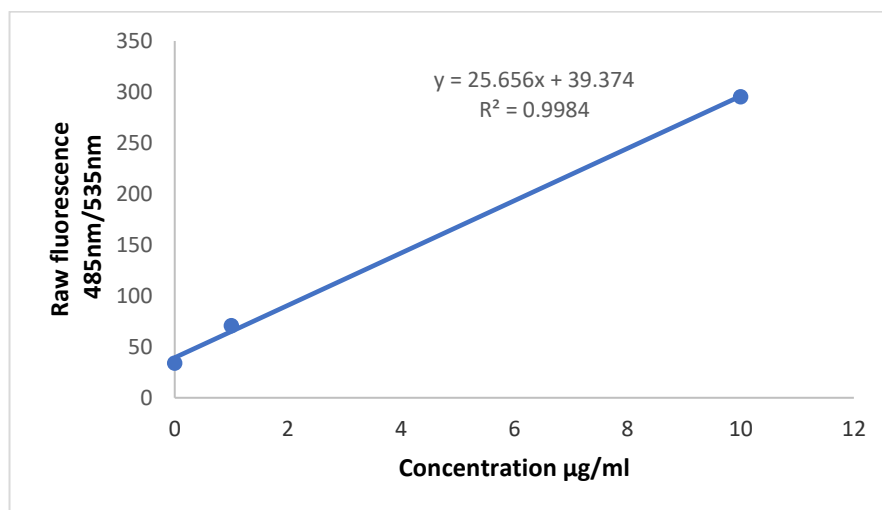


Figure 4.10 Standard curve produced from the Dojindo FITC- *P. gingivalis* LPS conjugate in media (astrocyte basal media (ABM), pericyte media (PM) and endothelium basal media (EBM) 1:1:1). Fluorescence measured at 485nm excitation and 535nm emission (gain 40, 22°C). Minimum concentration used were 0.01 µg/ml.

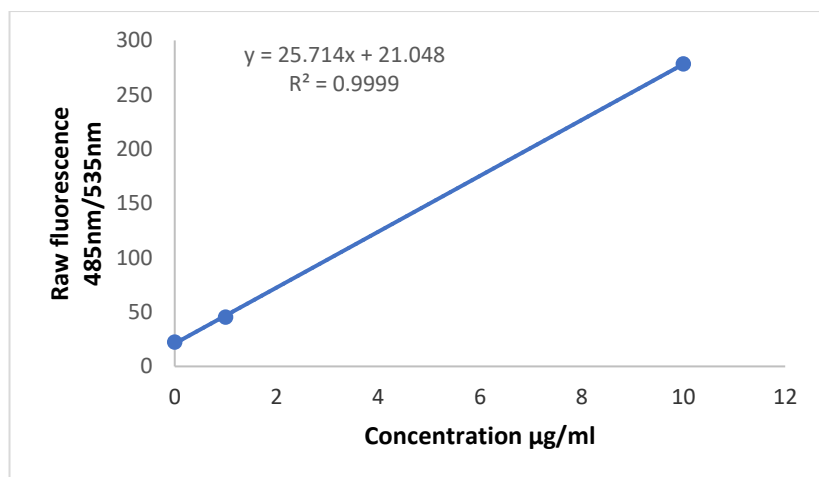


Figure 4.11 standard curve produced from the Dojindo FITC- *P. gingivalis* LPS conjugate in HBSS (Appendix 1, Table 2). Fluorescence measured at 485nm excitation and 535nm emission (gain 40, 22°C). Minimum concentration used were 0.01 µg/ml.

The TEER values from the study with application of the Dojindo conjugate showed that most of the wells tested with the conjugate had a small increase in the TEER values in the first 24 hours which was followed by a slow decrease in the following 48 hours. The TEER values in this study were similar to the controls which had FITC applied alone (Data not shown).

4.4.3.2 Results Nanocs *P. gingivalis* LPS conjugate

After experiencing problems with the FITC *P. gingivalis* LPS conjugate from Dojindo a custom made FITC LPS conjugate was purchased from Nanocs, USA to investigate potential transport across the *in vitro* BBB model. This conjugate was tested on the model both suspended in citrate buffer and media and media only, as previously described to assess whether there would be any difference in the compound's appearance in the basolateral compartment. The protocol with Nanocs conjugate was repeated twice for both suspensions (n=6). Standard curves were prepared for FITC dextran 3-5 kD, Nanocs conjugate in media only and Nanocs conjugate in media and citrate buffer (Figures 4.12).

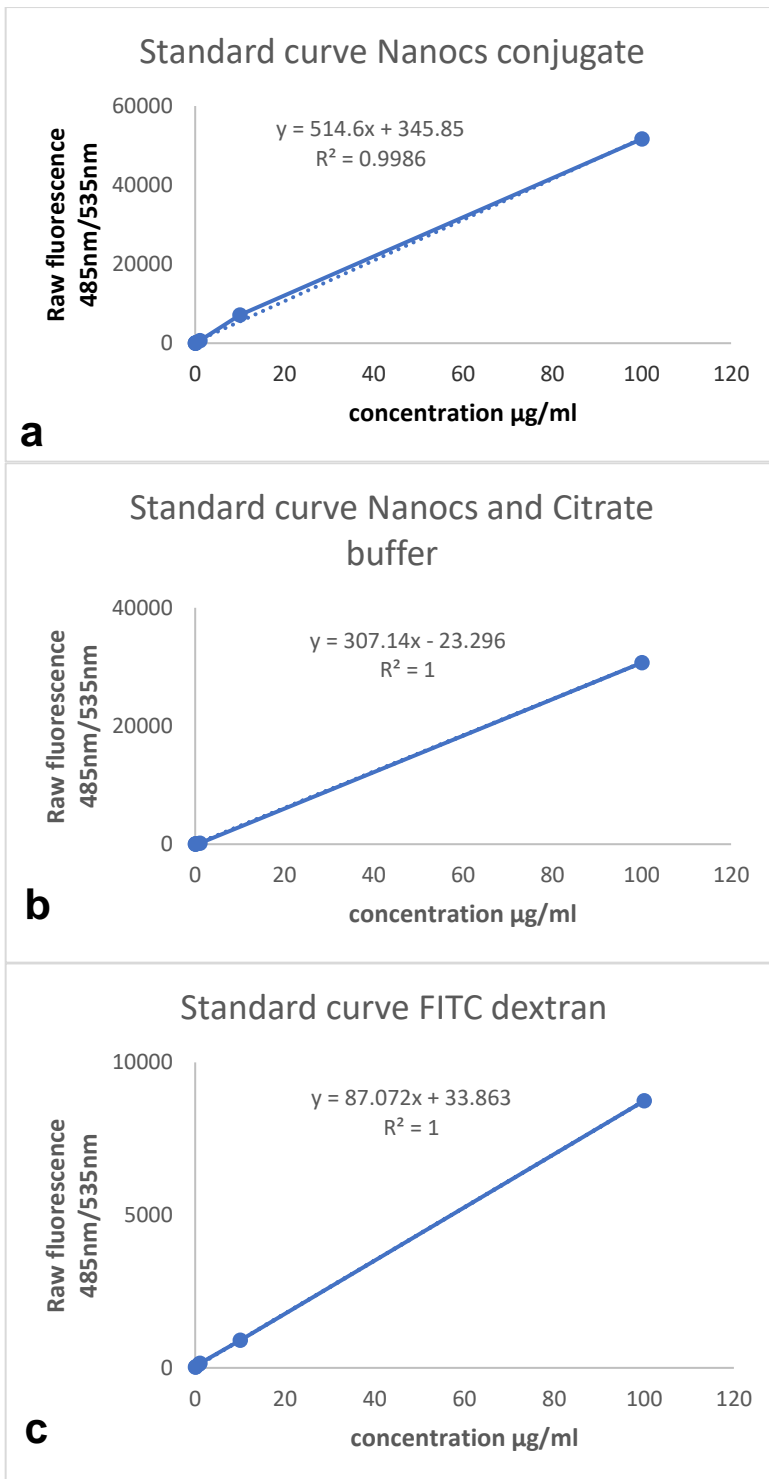


Figure 4.12 Standard curve **a** Nanocs conjugate with media only (astrocyte basal media (ABM), pericyte media (PM) and endothelium basal media (EBM) 1:1:1), **b** Nanocs conjugate with media and citrate buffer **c** FITC dextran 3-5 kD. Fluorescence measured at 485nm excitation and 535nm emission (gain 40, 22°C). Minimum concentration used were 0.01 $\mu\text{g/ml}$ for Nanocs conjugate and 0.06 $\mu\text{g/ml}$ for FITC dextran. Solid blue line is fluorescence values plotted, dotted blue line is line of best fit.

The application of Nanocs conjugate in media showed that there were no significant differences in the magnitude of TEER response between the wells with application of all concentrations of FITC-*P. gingivalis* LPS conjugate and the control (FITC alone), however a decrease in TEER was observed in all wells after application of 1,10,50 and 100 µg/ml of FITC-*P. gingivalis* LPS conjugate in media (astrocyte basal media (ABM), pericyte media (PM) and endothelium basal media (EBM) 1:1:1) (Figure 4.13A). These wells did not appear to recover as well compared to controls (Figure 4.13B).

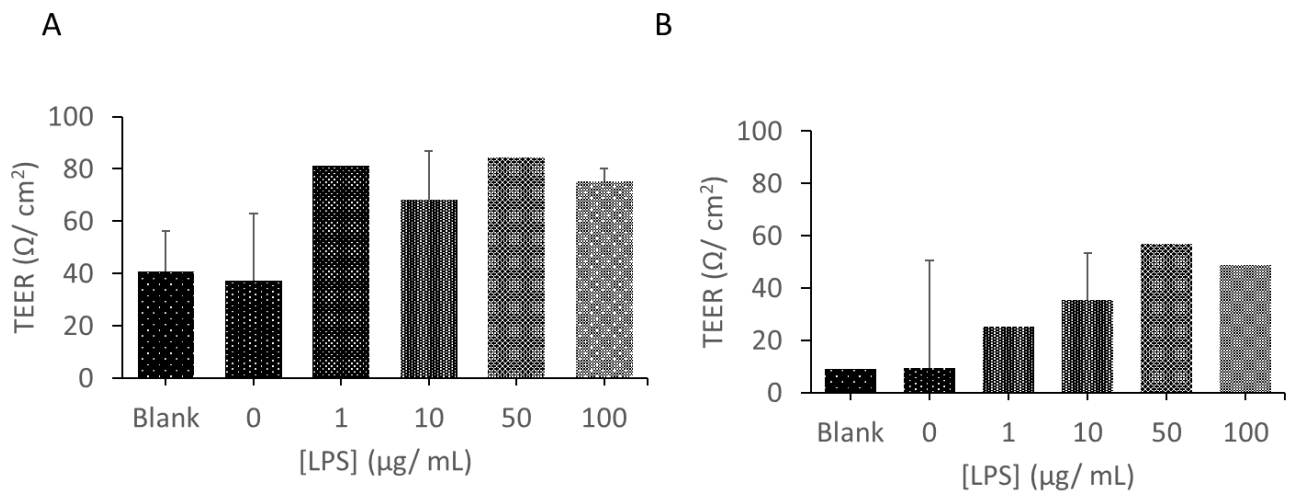


Figure 4.13 Changes in BBB integrity measured by calculating the magnitude of decrease in TEER in response to application of conjugated FITC-*P. gingivalis* LPS (Nanocs in media) (A) and the magnitude of deficit in recovery of TEER 72 hours post application of conjugated FITC-*P. gingivalis* LPS (Nanocs in media (astrocyte basal media (ABM), pericyte media (PM) and endothelium basal media (EBM) 1:1:1)) relative to initial baseline TEER (B). No statistical significance of response was measured using an ANOVA with Dunnett's post-hoc relative to the control (administration of FITC alone). Data represents mean \pm SD from three wells and two experimental repeats ($n=6$). No statistical significance was detected.

The Nanocs conjugate in media (astrocyte basal media (ABM), pericyte media (PM) and endothelium basal media (EBM) 1:1:1) appeared in the basolateral compartment of all the wells with the higher concentrations (10, 50 and 100 µg/ml LPS) at or after 240 minutes, but

the lower concentration wells did not appear in the 72 hour test period and the appearance of the FITC *P. gingivalis* LPS was greatest in the highest concentration (100µg/ml) at 1 and 4 hours (Figure 4.14A and 4.14B) and an increase of percentage appearance was observed with the concentrations 10 and 50 µg/ml as the experiment progressed at 24 and 48 hours (Figure 4.14C and 4.14D).

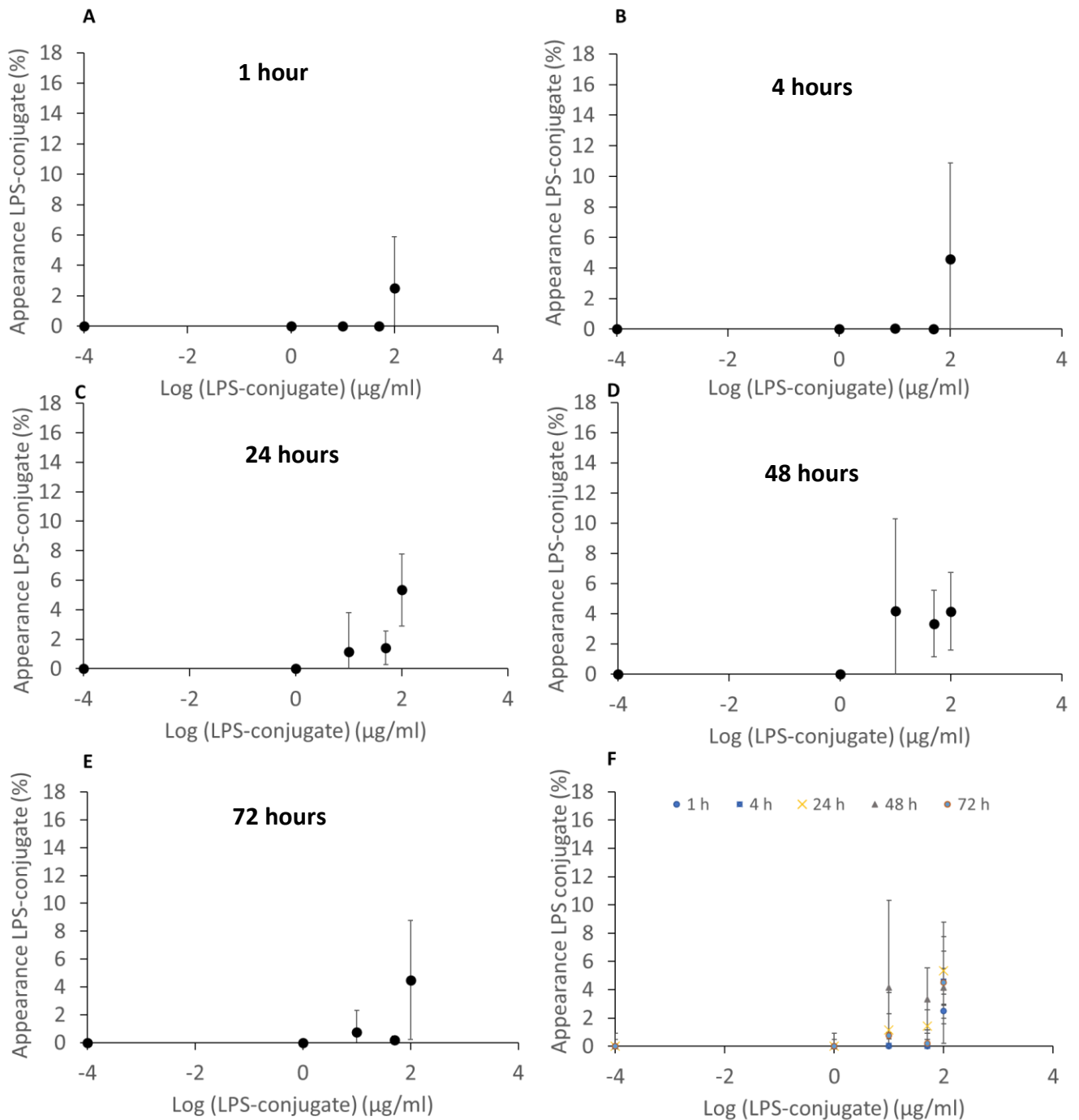


Figure 4.14 Percentage appearance of FITC *P. gingivalis* LPS conjugate on the apical side of the *in vitro* BBB model relative to the stock FITC *P. gingivalis* LPS administered to the basolateral side after 1 h (A); 4 h (B); 24 h (C); 48 h (D); 72 h (E) and a comparison of all time points (E). Statistical significance of response was measured using an ANOVA with Dunnett's post-hoc relative to the control (administration of FITC alone) where * $P < 0.05$ and ** $P < 0.01$. Data represents mean \pm SD from three wells and two experimental repeats ($n=6$). No statistical significance was detected.

The wells which had Nanocs conjugate 100 µg/ml in citrate buffer applied showed a sharp decrease in the TEER values (Figure 4.15a). The remaining test wells showed a very similar TEER response at similar levels to the controls, though the wells with 50 µg/ml LPS showed less of a recovery in TEER values at 72 hours (Figure 4.15b).

The wells with Nanocs conjugate with citrate buffer in the concentrations 1-100 µg/ml showed to appear in the basolateral compartment from the beginning of the experiment with a noticeable increase after 240 minutes (Figure 4.15a,4.15b and 4.15c). The wells with the lower concentrations of Nanocs in citrate buffer (0.1 and 0.01 µg/ml LPS) were not seen to appear in the basolateral compartment, but the TEER values dropped at 48 hours in all these wells (data not shown). A drop in the TEER values were seen to correlate with the appearance of the conjugate in the wells of the higher concentrations (50 µg/ml and 100 µg/ml LPS) (Figure 4.15a and 4.15b).

The Nanocs in citrate buffer and media suspension data set was tested for normality using SPSS v 27. The data from all test groups were compared to the controls with a one-way ANOVA (two tailed) with Dunnett's as posthoc (sign $p \leq 0.05$). The parameters tested were 1. Time point FITC appearance started, 2. Maximum volume % appearance, 3. Maximum % appearance time point and 4. The FITC-dextran appearance when the final integrity state of the barrier was measured.

The statistical analysis showed a highly significant difference in the magnitude of change (Y1-Y2) between the TEER response in the wells with application of 100µg/ml and citrate buffer and the controls ($p \leq 0.0001$) (Figure 4.16A) and a highly significant difference between the maximum TEER and the recovery values for this reagent ($p \leq 0.000002$) (Figure 4.16B).

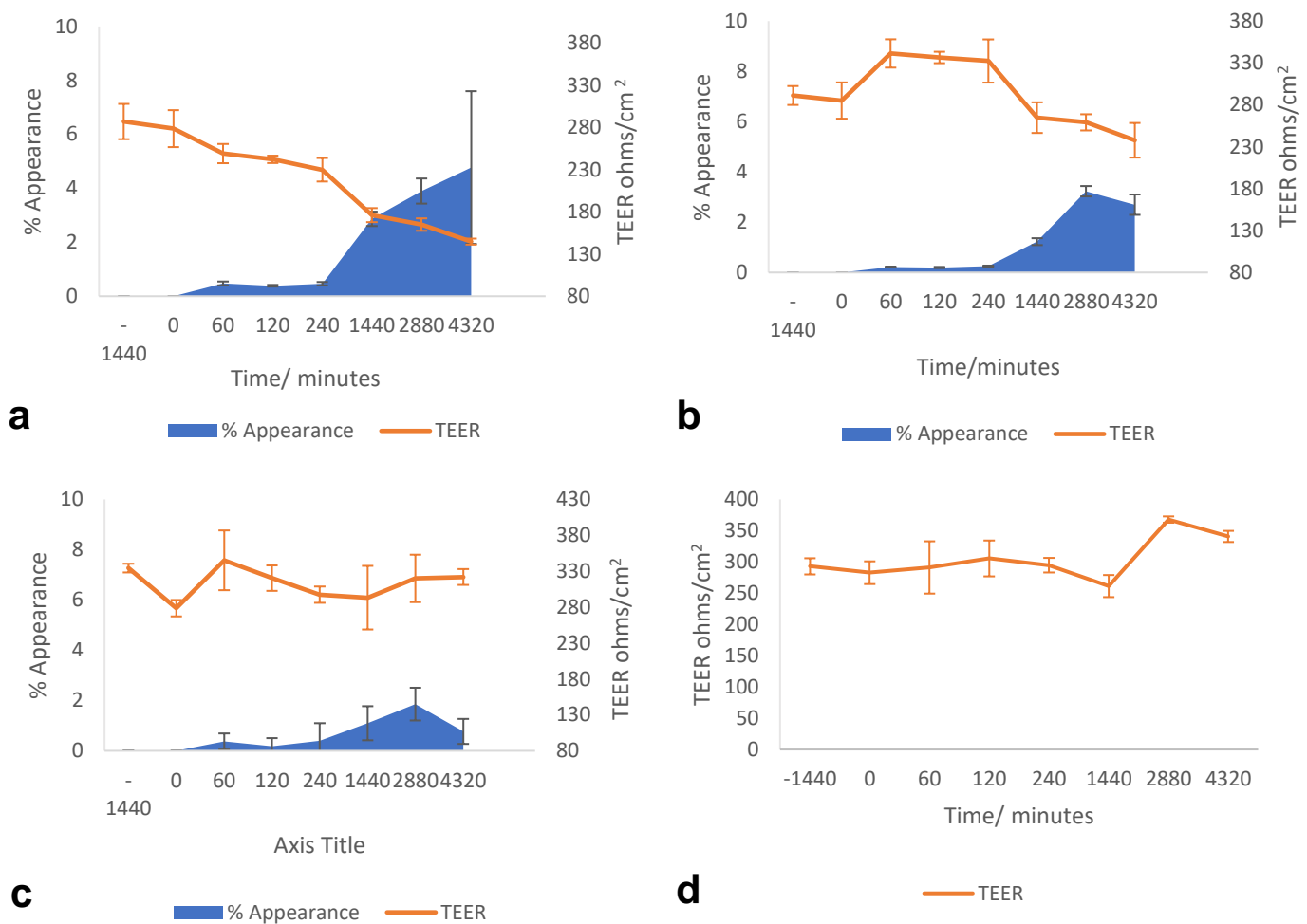


Figure 4.15 *in vitro* human primary cell BBB model with application of *P. gingivalis* LPS-FITC conjugate. Integrity of model barrier was assessed by transendothelial electrical resistance (TEER) and % appearance of Nanocs LPS conjugate diluted in citrate buffer and media (astrocyte basal media (ABM), pericyte media (PM) and endothelium basal media (EBM) 1:1:1). **a** 100 µg/ml Nanocs with CB and media, **b** 50 µg/ml Nanocs with CB and media. **c** 1 µg/ml Nanocs with CB and media (astrocyte basal media (ABM), pericyte media (PM) and endothelium basal media (EBM) 1:1:1), **d** TEER measurements only control with no LPS or FITC applied. Data represents mean ± SD from three wells and two experimental repeats (n=6).

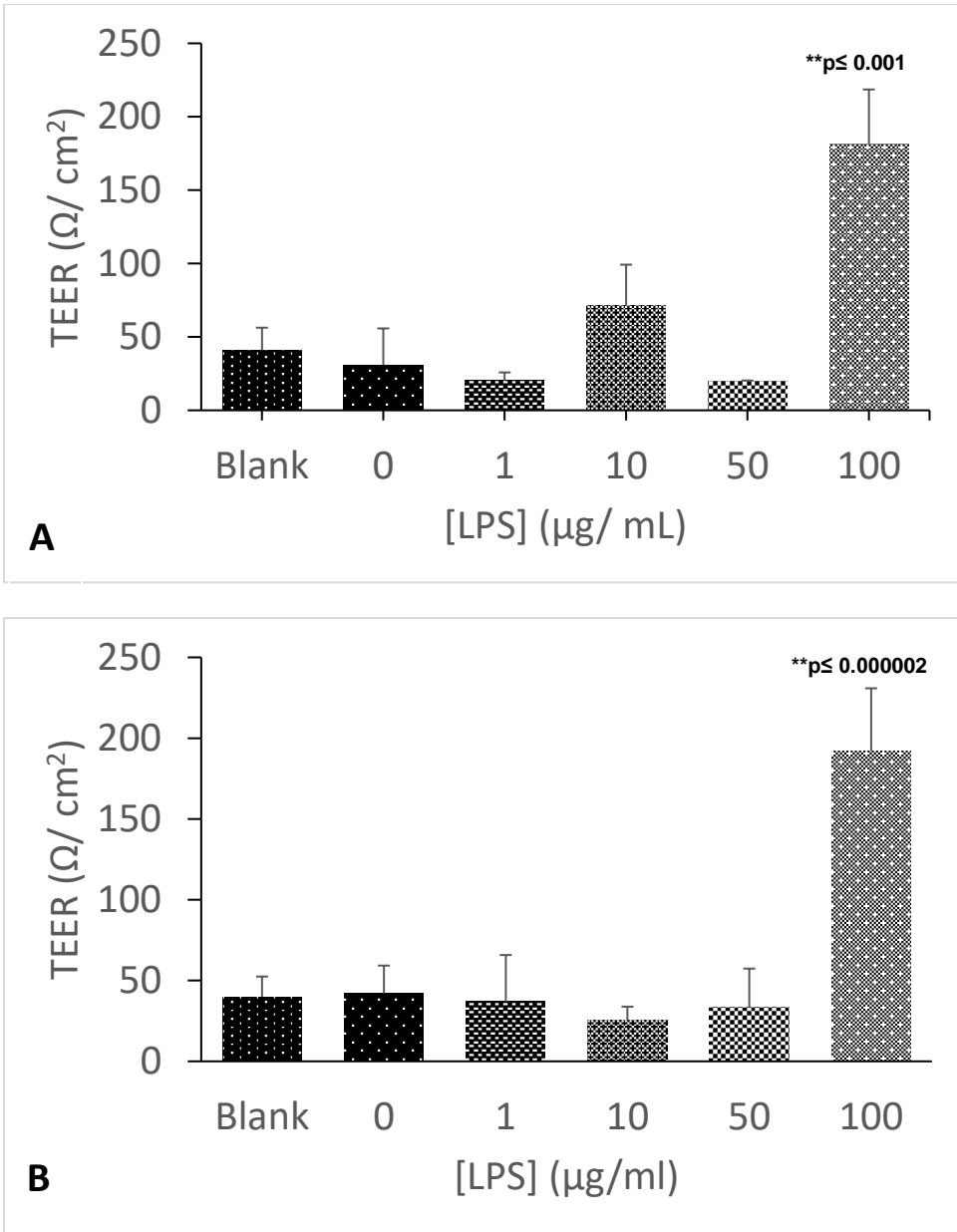


Figure 4.16 **A** Difference in the magnitude of change (Y1-Y2) between the TEER response in the wells with application of Nanocs conjugate in citrate buffer and media (astrocyte basal media (ABM), pericyte media (PM) and endothelium basal media (EBM) 1:1:1) compared to the controls (TEER or FITC-dextran only), **B** Difference between highest TEER and recovery value after application of Nanocs LPS conjugate suspended in citrate buffer with media (astrocyte basal media (ABM), pericyte media (PM) and endothelium basal media (EBM) 1:1:1). (**p≤ 0.0001) Data shown as Mean +/- SD

At the completion of the experiment all the wells were tested to assess the final level of integrity, this was done by a final TEER measurement and the application of FITC-dextran

3-5 kD to all the apical compartments followed by 30 minutes of incubation and triplicate basolateral sampling. This final test showed that all the wells which had the highest concentration (100 µg/ml conjugate with and without citrate buffer) applied had a uniform loss of integrity with an average appearance of 5%, but the remaining wells showed a much smaller level of penetration to the FITC-dextran (0 - 2%). There was no correlation observed between the appearance of the FITC-dextran and the level of TEER at this point.

4.4.4 Results IL-6 ELISA

All the reagents tested on the *in vitro* BBB model were tested for biological activity on HBPC cells in monolayer. For the ELISA a standard curve was prepared and used to assess the concentrations of IL-6 in the samples, an example standard curve is shown in Figure 4.17. The test samples were applied in triplicate wells and the ELISA was done in triplicate wells. The ELISAs all showed an elevated level of IL-6 in the test samples compared to controls (Figure 4.18). These results were seen as a positive control of the virulence activity in the samples tested.

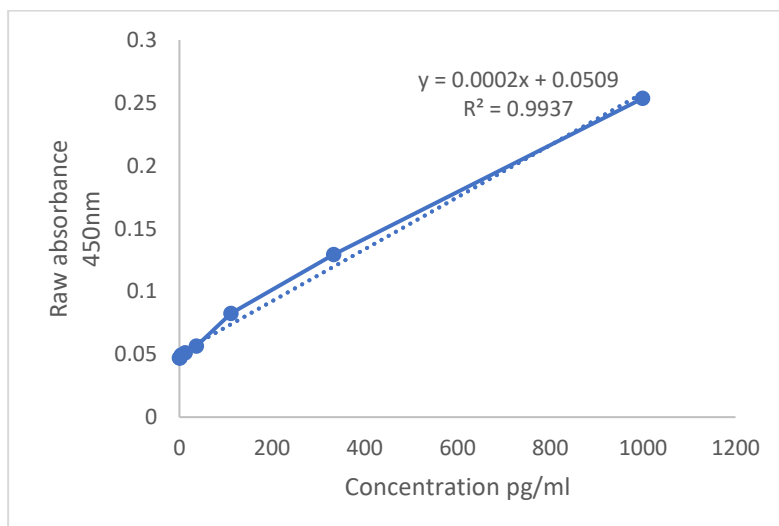


Figure 4.17 Example of standard curve of human IL-6 concentration (pg/ml) applied in ELISA test of biological activity of reagents applied to BBB model. The solid blue line are the absorbance values plotted against known concentrations and the dotted line is the line of best fit.

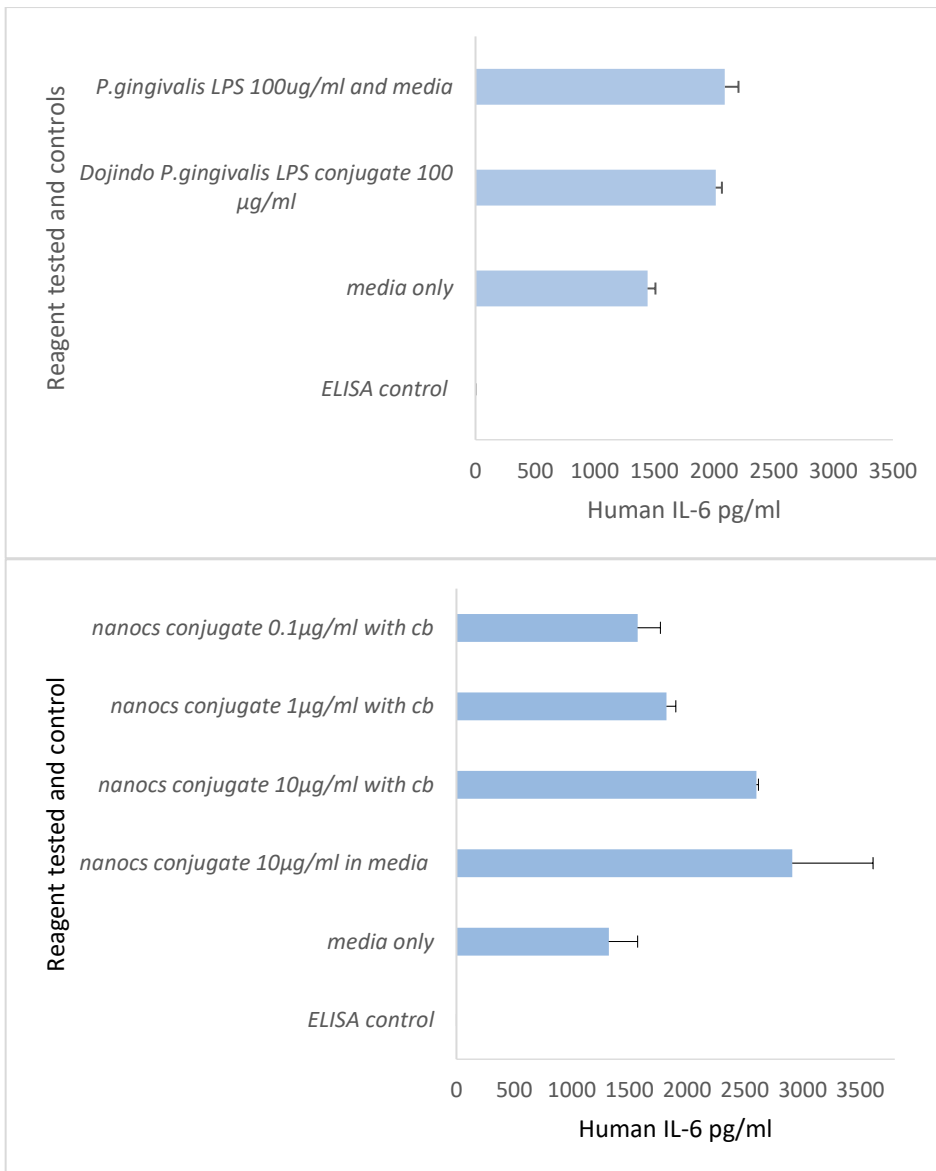


Figure 4.18 ELISA of Human IL-6 response to applications of reagents to human brain pericytes (HBPC) in monolayer and incubation for 4 hours. A *P. gingivalis* LPS and Dojindo *P. gingivalis* conjugate B Nanocs *P. gingivalis* conjugate Data shown as Mean \pm SD. (N= 9) in each experiment which was repeated three times..

4.5 Discussion

In this study we investigated the effect of *P. gingivalis* LPS on the cells in a human *in vitro* BBB model. The integrity of the barrier model following application of unconjugated LPS was evaluated firstly by using EBD as a tracer compound, then repeated using FITC dextran. Furthermore, the integrity of the barrier model was assessed after application of a FITC conjugated *P. gingivalis* LPS which appearance in the basolateral or CNS side of the model was measured.

Our observations regarding the effect on the barrier integrity and movement of *P. gingivitis* LPS across to the CNS side of the model (Figures 4.13, 4.14 and 4.15) supports findings from animal and other *in vitro* studies showing evidence of LPS travelling to the brain across the BBB (Dominy *et al.*, 2019; Poole *et al.*, 2013; Ilievski *et al.*, 2018). The methodology used in this study has not, to our knowledge been previously published.

Designing robust human studies of chronic bacterial interaction at the BBB is challenging and making a link to sporadic AD must be carried out cautiously for numerous reasons, such as the latent period before AD pathological changes are first identified in brain tissues, and time to clinical symptomatology development both in the arena of multiple other risk factors associated with AD development. *In vitro* BBB models have been widely used for decades to investigate drug transport and individual disease processes, including A β clearance mechanisms in relation to AD (Pflanzner *et al.*, 2010; Helms *et al.*, 2016). Most BBB model studies investigating bacterial related interactions have focused on acute events (Iarosh, 1992; Kanoh *et al.*, 2011).

The *in vitro* BBB model utilised in this study was developed by Kumar *et al.* (2014) and subsequently validated for investigation of drug transportation across the BBB. Although the main protocols for the model were established, some adjustments had to be made for it to be meaningful in our investigation. It was vital to establish continuous barrier integrity or

function and to ensure the model was suitable for the duration of testing and not affected by the application of EBD and FITC tracer compounds. As mentioned in the methods section (4.3.5), the concentrations of virulence factors applied were deduced from previous studies (Blufstein *et al.*, 2018; Guo *et al.*, 2018) and when optimising the test protocols, both high and low doses were included. Starting with low concentrations, the virulence factors assessment evidenced whether there was a concentration dependent relationship with the endotoxin which would indicate the resilience of the BBB model to this virulence factors. Then, as the experiments progressed higher concentrations of endotoxin were applied in pursuit of identifying a dose dependent relationship. As the experiments progressed it was clear that no clear concentration of LPS IC₅₀ was detectable, but there appeared to be an intolerance in the model to the highest concentration of 100 µg/ml FITC-LPS conjugate with citrate buffer as these cells responded with significant differences in magnitude of change and absence of recovery in the wells (Figures 4.13A and B, 4.15 and 4.16A and B) (further discussion below).

One of the observations in the first experiments using EBD was that the TEER values increased with time (Figure 4.3) and the tracer compound detected in the basolateral compartment would either decrease after 4 or 24 hours for all the tested sample concentrations including the EBD only control (Figure 4.3), suggesting an improvement in the barrier integrity after this point. This pattern could potentially reflect the exponential growth phase of the cells or a response to the applied reagents such as an upregulation in the cells, and no distinction was apparent between the concentrations of LPS (1 µg/ml) used in these initial studies and the control wells. This would suggest that any disruptions which could be measurable by TEER or EBD appearance would have to counteract this progression in cell density and tight junction maturation or would otherwise go undetected by this method. It is most likely that the recovery of the BBB seen throughout these experiments reflects the increased number of cells in the BBB, as there was no other significant increase in permeability seen for the rest of the test periods when repeated

endotoxin was applied to the cells. At this point it was considered that the concentrations of LPS applied were not high enough to cause a measurable response in this model.

After these first sets of experiments the LPS concentrations were raised and the tracer compound was changed to a fluorescent marker (FITC-dextran) instead of EBD.

Fluorophore and dye tracer compounds are not always sensitive enough to show subtle changes in barrier model permeability (Srinivasan *et al.*, 2015) which is a weakness of this type of study and bias can be introduced if the sensitivity in the measuring equipment is not high enough to pick up the compound at small levels. Further to this, when constructing the standard curves for EBD (example in Figure 4.2) in the initial protocols, it became apparent that the absorbance values could fluctuate depending on the temperature of the media so this had to be very carefully monitored. Though it was possible to distinguish the controls from the test samples containing EBD and measure the absorbance in the experiment samples, it was found that the media alone (control) could present with a very similar absorbance to EBD under certain conditions. Therefore, it was decided to select an alternative agent for testing the permeability of the barrier model in the future protocols. The FITC dextran molecule used here has been shown to cross the BBB model via intercellular diffusion (Hoffmann *et al.*, 2011) and any increase in intercellular channels, due to modulation of tight junctions, would allow greater amounts to pass into the basolateral compartment (BLC). Our study demonstrated that the appearance of FITC dextran into the BLC occurred early (between 1 and 4 hours) after the initial application of unconjugated *P. gingivalis* LPS. This was particularly evident with the testing of the higher concentrations of LPS, but subsequent applications failed to demonstrate any clear correlation between the concentration of applied endotoxin and the percentage appearance measured in the BLC. This implies that the higher concentrations of LPS were able to induce an increase in paracellular flow, possibly by increasing paracellular gaps, at initial application compared to controls (Figure 4.7). However, further increases were not demonstrated by additional applications implying a finite capacity for paracellular flow increase. These findings were

supported by the Papp calculations of the EBD and FITC dextran throughout the protocols and the percentage appearance values which also remained low after application of unconjugated LPS. The levels of FITC-dextran appearance seen throughout the unconjugated LPS experiments were persistently low with the maximum appearance at 0.7% (Figure 4.7) which is encouraging in terms of demonstrating the quality of the barrier model (Kumar *et al.*, 2014).

After expanding the protocols to include application of unconjugated *P. gingivalis* LPS at higher concentrations and more control wells, a clear pattern emerged (Figure 4.4), of an initial drop in TEER values including the controls, but it was observed that the drop in the wells which had endotoxin applied were both greater in values and failed to recover as well as those in the control wells indicating a lasting measurable effect in the BBB model barrier function. It was concluded that the initial small drop in TEER values in the control wells (average of 25 ohms/cm²) would need to be regarded as an artefact and test results within these ranges were reviewed taking this into consideration by ensuring appropriate blank (media only) and zero controls (FITC only) were included in every experiment where appropriate. This artifact was not observed by Kumar *et al.* (2014) because the protocols utilised here included continuously measuring of the TEER levels throughout the experiments, whereas Kumar *et al.*, (2014) used TEER as a quality control of the barrier function before and after the experimental drug transport protocols. This artifact can be explained as following the application of the Evom electrodes or the media change, a short-lived disturbance could have occurred in the conductance across the BBB model. This initial drop recovered in all the control wells and as the protocol continued for 72 hours, a clear distinction between the test and control wells was facilitated (Figure 4.5 and 4.13).

In the unconjugated LPS study tested by FITC dextran, a significant decrease in TEER values was seen in wells tested with the concentrations of *P. gingivalis* LPS (0.3, 10, 100µg/ml) (Figure 4.5A) and the magnitude of deficit in recovery of TEER in these wells were also significantly less compared to controls (in 100 µg/ml highly significant, $P < 0.01$)

(Figure 4.5B). The reductions in TEER values in the wells with lower concentrations (0.1 and 1 µg/ml) were temporary followed by partial or complete recovery (Figure 4.5B).

Again, the wells demonstrating less ability to recover their TEER values, could indicate that the cells in those wells were unable to survive or expand, or the LPS could have influenced the continuity of the cell layer either by causing pyroptosis (Brown, 2019), apoptosis or irreversible tight junction disruption (Takeuchi *et al.*, 2019; Hirasawa & Kurita-Ochiai, 2018) and the biphasic pattern observed in the wells showing recovery could indicate that such a response has been followed by a reparatory upregulation event. These observations are important as they indicate the cells of the BBB model have an ability to recover if the endotoxin is applied at a low level. Applied to a human clinical condition, this means that after a low level, low frequency endotoxin contact with the BBB, the NVU cells appear to retain the ability to preserve the barrier's integrity. Clinically this could correlate with the adoption of an improvement in oral hygiene or if systemic risk factors for PD, such as diabetes, were eliminated or reduced. In the experiments with application of FITC *P. gingivalis* LPS conjugate in media compared to controls, it was recorded that there were reductions in TEER readings in the wells receiving the virulence factor and that these TEER levels also did not recover as well, though none of these TEER value differences were statistically significant compared to the controls (Figure 4.13A and 4.13B).

The TEER measurements of an *in vitro* BBB model reflect the ionic conduction paracellularly in the cell layers, whereas the percentage appearance of a tracer compound in the BLC represents paracellular waterflow associated with increased pore size at the tight junctions (Srinivasan *et al.*, 2015). Transcellular ion transport function and paracellular permeability of solute transport are differentially regulated, where the factors affecting perfusion of a molecule across the BBB is size, shape and lipophilicity (Srinivasan *et al.*, 2015).

TEER is a valuable assessment of the *in vitro* BBB integrity as it is easy to quantify and if carried out with care, non-invasive. It is however important to be aware of the limitations of

TEER measurements, where variations can occur due to factors such as medium content, temperature and the passage numbers in the cell lines at the time of measurements (Srinivasan *et al.*, 2015). As the protocols in this study were performed under the same conditions using the same equipment and cell passage numbers, some of the potential variables could be excluded. As an example, the EVOM probe was calibrated in the same manner before each measurement and five readings were taken from the individual wells with each experiment, providing the investigator with confidence in the longitudinal magnitude of change and TEER endpoint results.

Previous validation studies of *in vitro* BBB models like ours have shown that a TEER (read) value in the range of 120 – 130 ohms/cm² is enough for transport studies (Wilhelm *et al.*, 2011). When setting up the BBB model for testing transport and permeability in this project the aim was to achieve values of TEER (read) minus TEER (blank) \geq 260 ohms/cm² (Wilhelm *et al.*, 2011), this was achieved in all the protocols.

The appearance of FITC dextran in the basolateral compartment gave an indication of disruption to the barrier integrity after unconjugated *P. gingivalis* LPS application at various concentrations. It was observed that FITC dextran appeared earlier after application of LPS at 10 and 100 μ g/ml and this increased after 24 hours (Figure 4.7). Average Papp values were then calculated at 60 min, 120 min and 240 min and were found to be 1.04×10^{-8} cm/s, 8.7×10^{-8} cm/s and 4.8×10^{-8} cm/s. In permeability assays for drug transportation poor permeability is indicated by Papp values of 0 - 1.4×10^{-6} cm/s and high permeability by values in the range of 5×10^{-5} - 9×10^{-5} cm/s, respectively. The low calculated Papp values in our study suggest that the Papp for the tracer compound FITC-dextran were low indicating the BBB model retained its overall barrier function for the first four hours, though allowing enough permeation to measure a difference between test wells.

To further investigate a potential transport of the endotoxin across the *in vitro* BBB model the application of *P. gingivalis* LPS-FITC conjugates were utilised. Two types of conjugates

were tested on the model and the one from Nanocs (USA) was deemed more suitable due to persistent suitable results from standard curves and barrier model protocols.

A previous study investigating the transport of *P. gingivalis* LPS (Takeuchi *et al.*, 2019) have indicated that the LPS can have a tendency to form conglomerates and that dilution with a buffer containing a detergent (Tween20) and media (EBM, ABM and PM) would be necessary in this type of cell study. Therefore, both conjugates were tested with and without the addition of citrate buffer with Tween20 in parallel protocols. The experiments were conducted in the same format as the previous LPS studies and were repeated twice. The observations made indicated very similar patterns as the previous LPS with FITC studies. The wells which had Nanocs conjugate of 100 µg/ml in CB applied showed a significant decrease in the TEER values ($p \leq 0.001$) compared to FITC only controls (Figure 4.15 and 4.16A) and there was also a highly significant magnitude of deficit in these wells ($p \leq 0.00002$) (Figure 4.16B). This could indicate that the higher concentrations of endotoxin in these protocols had a more significant effect on the viability of the cells, or the response could be induced by a potential negative effect from the citrate buffer applied in these higher concentration wells. The conjugates mixed with media only at the same concentrations also had an effect on the integrity of the BBB cells and appeared to travel across the barrier without the need for a detergent. Therefore, it was decided to proceed with the test protocols diluting the LPS conjugate in media only.

The FITC LPS conjugate from Nanocs in various concentrations did affect the integrity of the barrier model measured by TEER. Though no significant magnitudes of change were seen there were a decrease in TEER after application of the LPS conjugate (1, 10, 50 and 100 µg/ml) and less recovery was seen compared to controls (Figure 4.13).

The maximum percentage appearance of the FITC LPS conjugate in the basolateral compartment (BLC) was 5% during the experiments (Figure 4.14), where 100 µg/ml showed the highest appearance after 4 and 24 hours. It was apparent that the higher concentrations

(10, 50 and 100µg/ml) were observed in the BLC, though no concentration correlation to the percentage appearance was noted, which was encouraging in terms of the barrier function of the model. The drop in TEER in the wells with 50 and 100µg/ml did correlate with the appearance in the BLC indicating a weakening effect from these concentration on the integrity in these cells.

There were differences in percentage appearance between the FITC *P. gingivalis* LPS and the FITC dextran molecules. The percentage detected in the BLC of FITC *P. gingivalis* LPS was approximately 5 fold larger than FITC dextran appearance after unconjugated LPS and this could be explained as a potential difference in the virulence between the two compounds (conjugated and unconjugated LPS) inflicting different effects on the pore sizes within the barrier, or variances in the size, shape and/or lipophilicity between FITC dextran and FITC LPS molecules could attribute to this observation. The *P. gingivalis* LPS could also affect the cells of the BBB model differently at receptor level after being conjugated, even though the LPS product used for both reagents originated from the same source.

The immune response of the *P. gingivalis* LPS and *P. gingivalis* LPS FITC conjugates (Dojindo and Nanocs) utilised in the experiments was examined by an IL-6 ELISA after application for 4 hours to HBPC. IL-6 is a proinflammatory cytokine and the induction of this cytokine would give an indication of the biological activity of the virulence factors utilised in this study, as the presence of LPS would induce TNF- α pathways in the HBPC to release IL-6 (Fabry *et al.*, 1993). The response and induction of IL-6 from all reagents measured in the cell media, were of a similar quantity and levels were increased compared to controls (media only) (Figure 4.18).

The unconjugated *P. gingivalis* LPS used in this study was the standard preparation (defined by preparation by supplier) which has been noted to induce a stronger inflammatory response than the pure version (both supplied by Invivogen, France) possibly as a result of impurities of lipoproteins in the standard preparation, activating TLR2 as well as TLR4

(Behm *et al.*, 2020). Furthermore, the standard *P. gingivalis* LPS has also been found to show a stronger inflammatory response in human periodontal stem cells after 24 hours than the pure version (Behm *et al.*, 2020). In our BBB protocols we saw an increased response at 24 hours with both *P. gingivalis* LPS which indicates that the induced response could be more complex than a simple apoptosis of the cells and involve inflammatory pathways affecting the integrity of the barrier.

The barrier was tested with FITC-dextran at the end of each experiment and these measurements showed that all the wells which had the highest concentration (100 µg/ml conjugate with and without citrate buffer) appeared to have a uniform loss of paracellular integrity with an average appearance of 5% in the basolateral compartments. All the remaining wells showed a smaller level of penetration to the FITC-dextran (0 - 2%). Interestingly the levels of appearance of the FITC conjugate at the last measurement 20 minutes before the FITC dextran was applied did not all correlate, which could mean the appearance of the FITC conjugate does not happen in the same manner as the FITC dextran. There was no correlation observed between the appearance of the FITC-dextran and the level of TEER at this point, again indicating that ionic conduction is not always related to the paracellular flow.

The *in vitro* BBB model has limitations such as the delicate nature of working with primary-derived cell lines and the measurements derived from this study do not divulge much information about a cellular level activity.

There is evidence to suggest that *P. gingivalis* may not need to enter the brain to cause neuroinflammation (Brown, 2019). Even healthy humans have been shown to have low levels of LPS in their blood (Zhang *et al.*, 2009; Nádházi *et al.*, 2002), but this is found to be elevated in AD and PD patients (Zhao *et al.*, 2017; Vargas-Caraveo *et al.*, 2017; Jaeger *et al.*, 2009). AD patients have been found to have 2-3 times as much LPS in the brains as healthy individuals (Bryant *et al.*, 2010). LPS is released from the bacteria either when it is

degraded or when outer membrane vesicles are released (Muioio *et al.*, 2014) and the GI microbiome has been shown to be the main contributor to a systemic presence (Zhao *et al.*, 2017). LPS has been suggested as an intermediary between bacteria and the CNS at low levels (physiological) conditions (Morris *et al.*, 2015) in rodents, and a lipo-protein transport mechanism to the CNS has been suggested, but it is not yet known exactly how LPS enters the brain in humans. It is possible that transport mechanisms are responsible for the appearance of the LPS on the BLC (CNS) side of the model used in this study and this topic warrants further investigation.

Bacterial LPS has been found to change the permeability of the BBB at high doses (Wendeln *et al.*, 2018) as seen in sepsis causing significant CNS disability. *P. gingivalis* LPS has the potential to cause neuroinflammation via the blood directly acting at the BBB, by inducing pro-inflammatory cytokines, initiating pro inflammatory pathways in the tissues of the neuro vascular unit and activating microglial cells without entering the brain (Muioio *et al.*, 2014). In addition, our study has indicated that *P. gingivalis* LPS also has the potential to cross the BBB as seen in the FITC *P. gingivalis* LPS experiments, potentially explaining how systemic circulating LPS could induce neuroinflammation. The subsequent immunological response to LPS is well documented (for a review see Montagne *et al.*, 2020) and the toxicity of an endotoxin is determined by how the host reacts to it (Sandiego *et al.*, 2015). Both immunological activation and tolerance (Skelly *et al.*, 2013; Belardi *et al.*, 2020) can explain how chronic exposure to even medium and low levels of *P. gingivalis* LPS could lead to neurodegeneration by induction of pro-inflammatory pathways and activation of microglia and it is plausible that a low concentration of *P. gingivalis* virulence factors can induce damage to the NVU cells (Tornavaca *et al.*, 2015; Stamatovic *et al.*, 2016). Here we have shown, in a BBB model, that whole bacteria do not need to be present as *P. gingivalis* LPS have the armoury to induce alteration of the barrier integrity providing access to the CNS tissues.

This study however has demonstrated that the integrity of a BBB model is reduced by the presence of *P. gingivalis* LPS seen by a measurable reduction in TEER levels and making the barrier more permeable and the subsequent increased appearance of LPS in the BLC (CNS side of BBB).

Another virulence factor of *P. gingivalis* is the release of its outer membrane vesicles (OMVs) which are also known to have the ability to be internalised by human cells (Olsen *et al.*, 2020). OMVs interaction with the cells of the BBB is also worth exploring and to expand our study, the next step was to test *P. gingivalis* OMVs on the *in vitro* BBB model.

OMVs have been shown to contain both LPS and proteolytic enzymes and have recently been hypothesised to be an important particle linked to neuroinflammation and other remote organ pathologies (Nara *et al.*, 2021; Olsen *et al.*, 2020). Investigation of OMVs effect on the integrity of the *in vitro* BBB model could provide further evidence for how bacteria from PD can act at remote organ sites to promote inflammation and cause disease.

4.6 Conclusion

The conclusion drawn from these sets of experiments is that *P. gingivalis* LPS has an effect on the integrity of the *in vitro* BBB model which is measurable by TEER and % appearance at certain concentrations, where higher doses of LPS showed a larger drop in TEER after application and a slower and smaller recovery in the TEER values. It can also be concluded that the higher doses of unconjugated LPS (10 µg/ml and 100 µg/ml) applied to the BBB model made penetration of the tracer compound happen earlier indicating an effect on the cell connections or viability in the *in vitro* BBB model. These experiments confirmed that the endotoxin from *P. gingivalis* was seen to cross the barrier model, also at a physiologically relevant level (0.3 µg/ml) and that further investigations at cellular level are warranted in

order to contribute to the knowledge pool of how virulence factors from periodontal disease could have an influence on CNS inflammatory states.

Chapter 5

***In vitro* BBB model with *P. gingivalis* Outer membrane vesicles and lipopolysaccharide application**

5.1 Introduction, Aims and Objectives of *in vitro* BBB model with *P. gingivalis* OMV and LPS application study

In the previous chapter we established a protocol for testing the *in vitro* BBB model integrity with unconjugated and FITC conjugated *P. gingivalis* LPS and our findings were that the *P. gingivalis* LPS did pass through the *in vitro* BBB model and the model was suitable for testing this type of virulence molecule and a measurable effect in integrity was detected. Much focus of PD research recently has been on the OMVs from *P. gingivalis*. These are secreted from the bacteria and have the potential to explain the remote organ pathology which has been linked to *P. gingivalis* in recent years (Olsen *et al.*, 2020; Nara *et al.*, 2021, Zhang *et al.*, 2021). The OMVs from *P. gingivalis* have been shown to be packed with enzymes which could potentially cause a weakening of the CNS defence at the BBB interface (Singhrao and Olsen, 2018). Not only could OMVs cross the BBB (Han *et al.*, 2019), but they also have the potential to increase the influx of other inflammagens to potentiate neuroinflammation.

Aim:

The aim of this study was to investigate the potential effect of *P. gingivalis* OMVs on the *in vitro* BBB models integrity and to measure if the presence of OMVs will have an effect on the rate and extent of appearance of a FITC labelled *P. gingivalis* LPS in the basolateral compartment of the model.

Objective 1:

Measure changes to the integrity of the *in vitro* human primary cells BBB model after application of *P. gingivalis* OMVs by TEER and percentage appearance of a tracer compound (FITC-dextran 3-5 kD).

Objective 2:

Measure changes to the integrity of the *in vitro* human primary cells BBB model after application of the combination of FITC *P. gingivalis* LPS and OMV by TEER and percentage appearance of FITC *P. gingivalis* LPS conjugate.

Objective 3:

To assess if there is a difference in the transport of FITC *P. gingivalis* LPS conjugate across the *in vitro* BBB model in the presence of *P. gingivalis* OMV (10 µg/ml) by comparing the data from the *in vitro* model with application of conjugated *P. gingivalis* LPS (Nanocs, USA) from chapter 4 to the data from application of conjugated *P. gingivalis* LPS with the presence of OMVs in this chapter (5).

Objective 4:

Measure the IL-6 levels released from HBPC after application of *P. gingivalis* OMV in cell culture, measured by Human IL-6 ELISA.

5.2 Materials and methods

Materials and equipment used as listed in Tables 1 and 2 in Appendix 1.

The justification for using these methods was based on published studies which had shown the interaction of *P. gingivalis* OMVs with cells in other models, both *in vivo* (Farrugia *et al.*, 2021; Seyama *et al.*, 2020) and *in vitro* (Fleetwood *et al.*, 2017). Also concentrates of *P. gingivalis* OMVs have been shown to induce a higher level of pro-inflammatory cytokines in human macrophages *in vitro* compared to the bacterial cells themselves (Fleetwood *et al.*, 2017). The response in the BBB model could be more significant by applying the OMVs rather than the bacterial culture. The choice of cultivating *P. gingivalis* strain FDC 381 for the OMV extraction, was based on the literature which indicated that this strain would have a

high ability to affect the penetration into human cells, but otherwise have a relatively low gingipain activity (Olsen and Progulske-Fox, 2015).

5.2.1 Cultivation of *P. gingivalis*

P. gingivalis ATCC-BAA-1703 (strain FDC 381) was purchased from LGC limited (UK) in freeze dried vials. The bacteria were cultured according to the supplier's instructions (Table 5.1). Briefly the *P. gingivalis* FDC 381 were cultured in ATCC medium 2722, supplemented tryptic soy broth (TSB). The reagents were added to distilled water to make a liter of broth: TSB 3%, yeast extract 0.5%, L-cystein hydrochloride 0.05%, hemin (5 mcg/ml) with K_2HPO_4 (17.4 mcg/ml), vitamin K1 (1mcg/ml) (Sigma Aldrich, UK). The solution was autoclaved at 121 °C and stored in the dark. *P. gingivalis* FDC 381 were also cultured on commercially bought TSA with 5% sheep blood (Thermo Scientific, UK) and fastidious anaerobe agar (FAA) agar with 7% horse blood neomycin (75mg/l) (E and O, UK). All cultures were incubated for 3 days at 37°C in an anaerobic chamber (Bactron, USA) using an anaerobic gas mixture of 5% H₂, 5% CO₂ and 90% N₂. Exponential growth was observed by daily sampling and cell number monitoring by Gram staining (5.2.2). Furthermore, the optical density (OD) of the broth cultures were measured daily in a Biochrom S1200 Spectrawave (USA), as described by Seyama *et al.* (2020). Cultures were used only if the OD₆₅₅ were between 0.1 and 1 after 3 days of growth (Seyama *et al.*, 2020).

Table 5.1 Materials for cultivation of *P. gingivalis*.

Reagent	Supplier
Distilled water	UCLan
FAA agar with Neomycin 75 mg/l	E and O, UK PP0140
Hemin 5 mcg/ml	Sigma Aldrich, UK H9039-1G
K ₂ PO ₄ 17.4 mcg/ml	Sigma Aldrich, UK P2222
L-cystein hydrochloride 0.5%	Sigma Aldrich, UK C7880
Tryptic soy broth 3%	Sigma Aldrich, UK, 22092
TSA with 5% sheep blood	Thermo Scientific, UK # WZ-14206-72
Vitamin K1 1 mcg/ml	Sigma Aldrich, UK V3501
Yeast extract 0.5%	Sigma Aldrich, UK Y1625

5.2.2 Gram stain of *P. gingivalis*

The *P. gingivalis* cultures were Gram stained using a kit (Merck, UK) and imaged for quality control on a daily basis, following a protocol for anaerobe bacteria (Johnson *et al.*, 1995). Briefly, the bacteria were placed on glass slides in a droplet of distilled water inside the anaerobic chamber. The slides were heat fixed as soon as they left the chamber in a Bunsen flame for 30 seconds. The fixed specimen was flooded with Gram's crystal violet Solution (Merck, UK) and left for 60 seconds. The specimen was then washed with distilled water and subsequently flooded with Gram's iodine Solution, which was left on the sample for 60 seconds. After another wash with tap water, the sample was decolourized with Gram's Decolorizer Solution (Merck, UK) until the dye was no longer running off the slide. The sample was then washed with tap water and counterstained with Gram's safranin Solution (Merck, UK) for 60 seconds. The safranin solution was removed with tap water and

the sample was gently dabbed with absorbent paper to remove excess moisture. The slides were examined under an inverted light microscope using a X40 and X100 objectives (Nicon DS L4, Japan) using immersion oil (Fisher Scientific, UK) and imaged using Nikon DS L4 software (Japan).

5.2.3 Isolation of *P. gingivalis* outer membrane vesicles

The outer membrane vesicles of *P. gingivalis* FDC 381 were isolated following the protocol used by Seyama *et al.* (2020). The bacterial culture in tryptic soy broth (TSB) was centrifuged at 2800 $\times g$ for 15 min at 4 °C to separate the vesicles from the bacterial cells. The supernatant was passed through a 0.2 μm syringe filter (Millipore, UK) and then concentrated to under 1 mL by using an Ultra-15 Centrifugal Filter for the nominal molecular weight limit (NMWL) 100K (Sigma-Aldrich, UK). The concentrate was mixed with total exosome isolation reagent for culture (Life technologies, UK) and this was incubated at 4 °C overnight. The samples were centrifuged at 10,000 $\times g$ for 60 min at 4 °C. The vesicles were eluted in 100 μL 1xPBS. The TSB without bacteria was treated by the same method as a negative control. The concentrations of the samples were measured on the NanoDrop Spectrophotometer (280 nm) (Nanodrop 2000, Thermo Scientific, UK).

5.2.4 Measurement of size of outer membrane vesicles

The diameter of the outer membrane vesicles was measured and mono-dispersity ensured using a Zetasizer (Malvern Zetasizer Nano, Panalytical Instalment Ltd., UK) (Danaei *et al.*, 2018). Samples were diluted in PBS which was also used as a negative control, the polydispersity index (measured in a zetasizer, Appendix 1, Table 1) aimed for ≤ 0.323 (Danaei *et al.*, 2018).

5.2.5 Human IL-6 ELISA testing OMV on HBPC

The OMVs extracted from the cultures of FDC 381 were evaluated for inflammasome activity by incubation with HBPC Passage 6 at OMV concentrations of 100 µg/ml and 200 µg/ml in triplicates. Controls were 6 wells with PM only. The cell culture media was examined for human IL-6 by enzyme-linked immunosorbent assay (ELISA) as described in 4.3.4.

5.2.6 Application of *P. gingivalis* OMVs to the *in vitro* BBB model

The *in vitro* BBB model was set up and tested using the equipment listed in Table 1, Appendix 1 and the materials in Table 2. The methodology as described in Section 4.3.1 and 4.3.2. The passage numbers of all three primary cell lines utilised at seeding were P5. After 96 hours the *in vitro* BBB was tested to assess the barrier properties. The integrity of the BBB model was tested as described in 4.3.3. The integrity of the BBB model was also tested by a permeability assay and when these measurements confirmed the model was established sufficiently for testing the test protocol outlined below was applied.

5.2.6.1 *In vitro* BBB model test protocol with *P. gingivalis* OMVs application

The *in vitro* BBB model response to virulence factors of *P. gingivalis* OMVs was tested in triplicate samples at various concentrations (0.1, 0.3, 1, 10, 50 and 100 µg/ml). Prior to commencing the sample application, 5 TEER measurements were performed of each well. At time 0, 200 µl of the test samples were placed in the apical compartment selected at random. Control wells included no application (medium and TEER only), FITC dextran

100µg/ml only, fibronectin only (no cells) and a clean insert. At time points 1 hour, 4 hours the TEER was measured at 5 points in each well. The OMV samples were removed and 200 µl of FITC dextran (100µg/ml) was placed in the apical compartments, this was incubated for 20 minutes in a humidified incubator at 37 °C, 5 % CO₂. After the incubation triplicate samples were collected from the basolateral compartment and measured as described in Section 4.3.3. After sampling the content of the basolateral compartment, the volume was replaced with 600 µl media (EBM, PM, ABM 1:1:1). These measurements were repeated at further time points at 24 hours, 48 hours and 72 hours. The appearance in % from the apical to the basolateral compartment (BLC) was calculated from standard curves of known concentrations of both FITC- dextran (3-5 kDa) (Sigma-Aldrich, UK) and the data from the standard curves were used to calculate the percentage appearance giving a measure of the integrity of the barrier model at that time point. This protocol was repeated twice (n=6 for each concentration). Statistical analysis was applied to the data (SPSS v.27, IBM, USA). Significance of response was measured using an ANOVA with Dunnett's post-hoc relative to the control (administration of FITC alone) where *P<0.05 and **P <0.01.

5.2.6.2 Application of FITC conjugated *P. gingivalis* LPS with OMVs to the *in vitro* BBB model

The *in vitro* BBB model was established as described in 4.3.1 and 4.3.2. The passage numbers in these protocols were P5 for all three cell lines (HBMEC, HBPC and HA). The *in vitro* BBB model response to FITC *P. gingivalis* LPS combined with OMVs was tested in triplicate samples at various concentrations (*P. gingivalis* LPS conjugate 0.1, 0.3, 1, 10, 50 and 100 µg/ml, all in combination with 10 µg/ml OMVs). The OMV sample was from the same stock as used in 5.2.6.1. Prior to commencing the sample application 5 TEER measurements were performed of each well. At time 0, 200 µl of the test samples were

placed in the apical compartment selected at random. Control wells included no application (TEER only), FITC dextran 100µg/ml only, fibronectin only (no cells) and a clean insert.

At time points 1, 4, 24, 48 and 72 hours the TEER was measured at 5 points in each well, followed by triplicate samples collected from the basolateral compartment and measured in according to Section 4.3.3. After each sampling, the content of the basolateral compartment was replaced with 600 µl media (EBM, PM, ABM 1:1:1). The appearance in % from the apical to the basolateral compartment was calculated from standard curves of known concentrations of FITC *P. gingivalis* LPS conjugate (Nanocs, USA) and the data from the standard curves were used to calculate the percentage appearance giving a measure of the integrity of the barrier model at that time point and how much LPS crossed to the BLC. Control wells with fibronectin coating only, media only and 10 µg/ml OMV only were tested in the same manner. This protocol was repeated twice (n=6 for each concentration) and statistical analysis was applied to the data (SPSS v.27, IBM, USA). Significance of response was measured using an ANOVA with Dunnett's post-hoc relative to the control (administration of FITC alone) where *P<0.05 and **P <0.01.

5.3 Results

5.3.1 Results cultivation of *P. gingivalis* FDC 381

P. gingivalis was cultivated successfully under anaerobic conditions and the turbidity and OD values were checked on a daily basis. The cultures for OMV extraction were grown for 72 hours which correspond to data from Takeuchi *et al.*, (2019). The cultures were checked by Gram staining daily to ensure monoculture and exclude contamination (Figure 5.1A), demonstrating the characteristic coccobacillus morphology. The cultures were also

cultivated on various agar plates such as FAA Neomycin (E&O, UK) demonstrating *P. gingivalis* black stain colonies of the strain with haemolytic halos (Figure 5.1B).

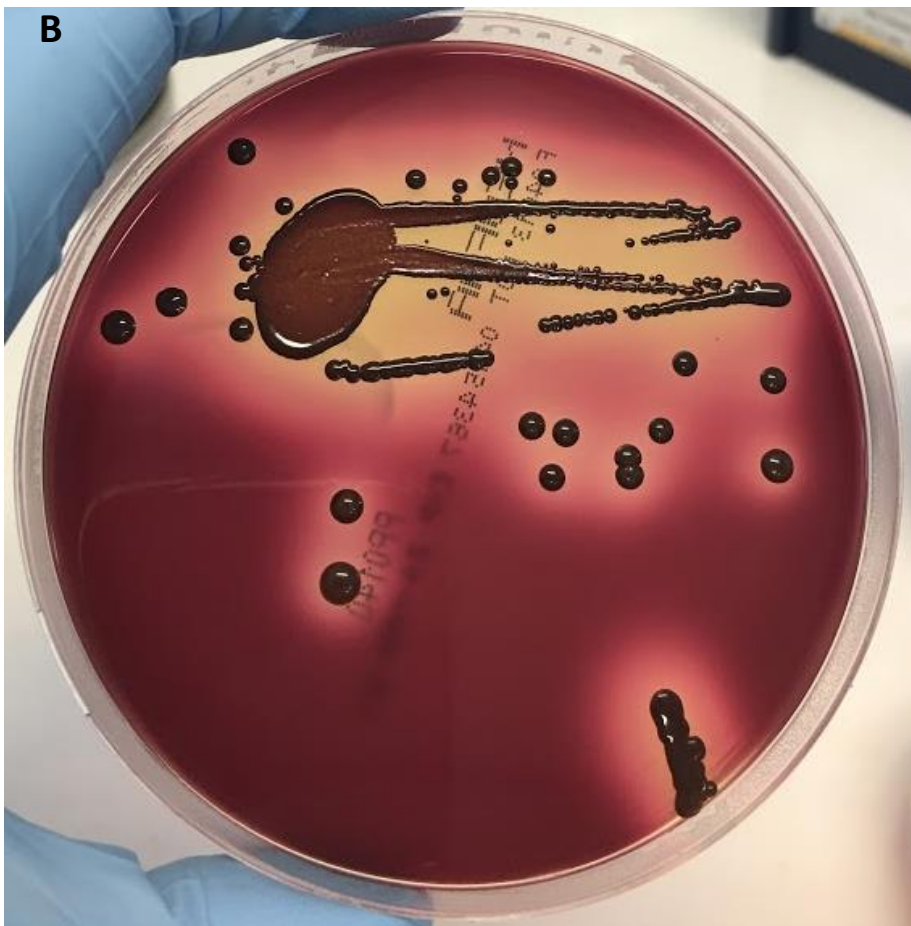
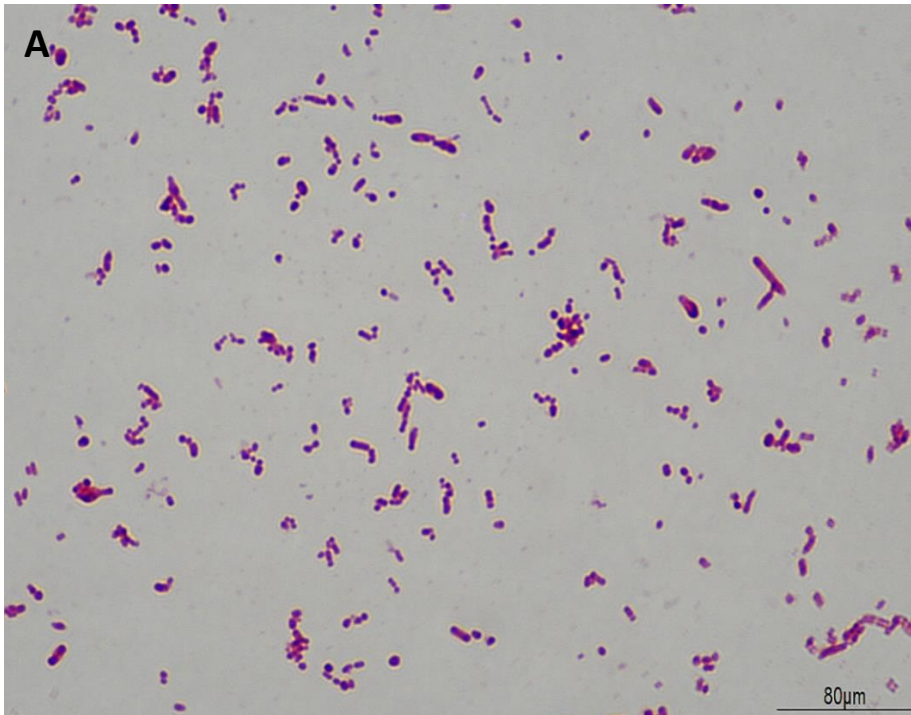


Figure 5.1 A, *P. gingivalis* FDC 381 Gram stain shows coccobacillus at x100, scale bar represents 80 μm and B, *P. gingivalis* FDC 381 on FAA Neomycin (E&O, UK), black stain colonies of the strain with haemolytic halos.

5.3.2 Extraction of OMVs from *P. gingivalis* FDC 381 and measurement in Zetasizer

The OMVs isolated from *P. gingivalis* grown in TSB were suspended in PBS and stored at 5°C for up to a week or – 20 ° C for long term storage. The concentration of the OMV samples were measured on the nanodrop 2000 (Protein A280) (Thermo Scientific, UK) and the samples ranged from 0.4 – 1.8 mg/ml. The OMV samples particle size was assessed by dynamic light scattering analysis (DLS) in a Zetasizer (Figure 5.2). The OMV samples showed variations in particle sizes (sample heterogeneity) within the expected range (20-500 nm) for FDC 381 (Vermilyea *et al.*, 2021; Nara *et al.*, 2021) and test samples for cell application were selected because of monodispersity with a polydispersity index (Pdl) ≤ 0.323 (Danaei *et al.*, 2018).

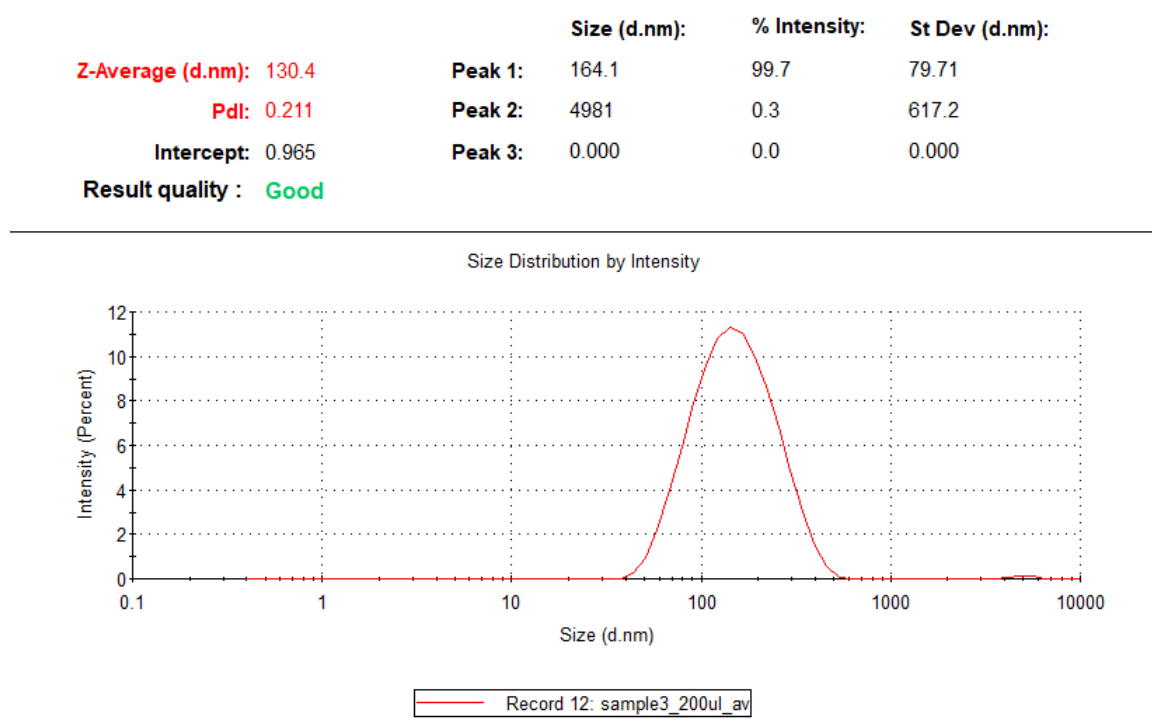


Figure 5.2 Zetasizer reading of particle size in *P. gingivalis* outer membrane vesicles (OMV) isolated from broth culture. The data shown is the average of 3 readings (n=3).

5.3.3 IL-6 ELISA after application of OMVs to HBPC

A standard curve was prepared and used to assess the concentrations of IL-6 in the samples (Figure 5.3). The HBPC cells IL-6 response to samples of *P. gingivalis* OMVs and PM only (Table 2, Appendix 1) after 4 hours of co-incubation showed an elevated level of IL-6 in the test samples compared to controls (Figure 5.4). These results were seen as a positive control of the biological activity in the samples tested.

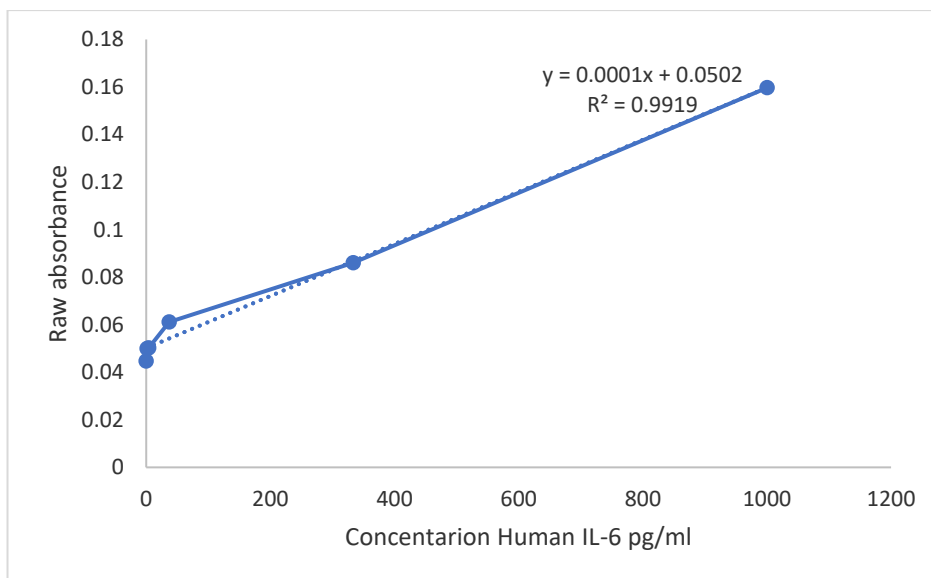


Figure 5.3 Standard curve for measurement of Human IL-6 levels by ELISA after application of *P. gingivalis* outer membrane vesicles (OMV) to human brain pericytes (HBPC) in monolayer. Solid blue line Raw absorbance plotted against known concentrations of human IL-6 pg/ml, dotted blue line is line of best fit.

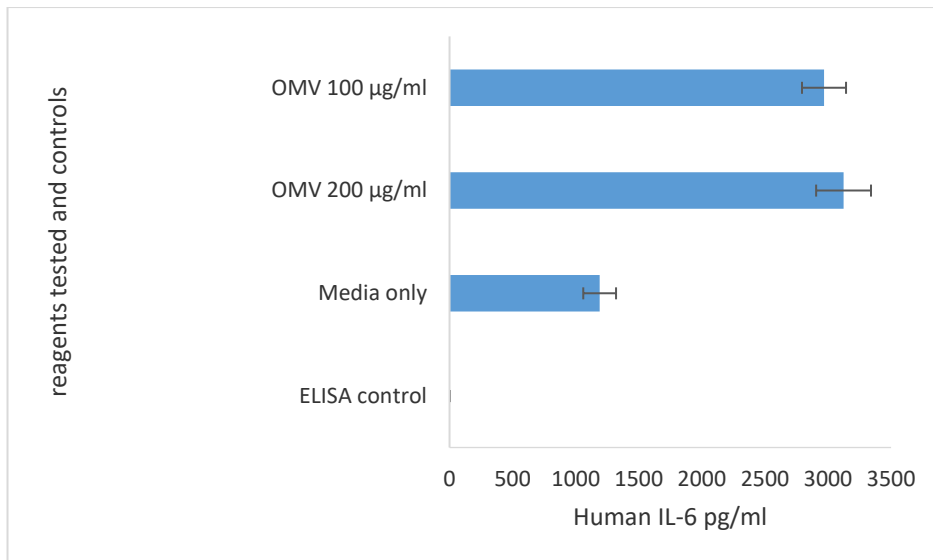


Figure 5.4 Levels of IL-6 secreted by HBPC after incubation with *P. gingivalis* OMV and PM only. The data shown is Mean \pm SD. ($n=9$).

5.3.4 Effect of *P. gingivalis* OMVs to the *in vitro* BBB model

The application of *P. gingivalis* OMVs showed similar patterns to the LPS study. The magnitude of decrease in TEER observed in response to treatment with OMVs was significantly different from the control group for the 0.1 µg/ mL ($P<0.01$); 0.3 µg/ mL ($P<0.05$); 50 µg/ mL ($P<0.05$) and 100 µg/ mL ($P<0.01$) (Figure 5.5A). This decrease in TEER did not recover to pre-treatment baseline for the wells treated with 50 and 100 µg/ mL *P. gingivalis* OMVs as the magnitude of deficit was highly significantly different to the control group ($P<0.001$), as shown in Figure 5.5B.

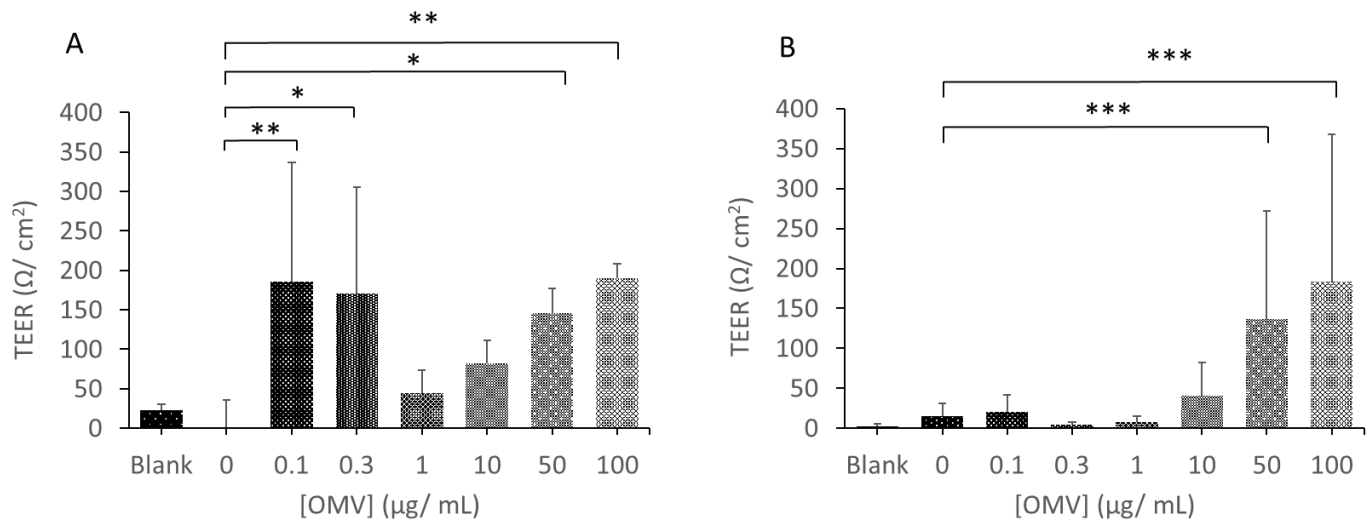


Figure 5.5 Changes in BBB integrity measured by calculating the magnitude of decrease in TEER in response to application of *P. gingivalis* OMVs (A) and the magnitude of deficit in recovery of TEER 72 h post application of *P. gingivalis* OMVs relative to initial baseline TEER (B). Statistical significance of response was measured using an ANOVA with Dunnett's post-hoc relative to the control (administration of FITC alone) where * $P < 0.05$, ** $P < 0.01$ and *** $P < 0.001$. Data represents mean \pm SD from three wells and two experimental repeats ($n=6$).

Figure 5.6 shows the appearance of FITC-dextran permeation following incubation of the *in vitro* BBB with increasing concentrations of *P. gingivalis* OMVs exposed for varying durations. Similar to the unconjugated LPS, the effect of OMV treatment on the extent of FITC-dextran permeation was fairly constant after the 24-hour exposure, but this time the permeation did appear to increase as the concentration of OMV increased (Figure 5.6C-E).

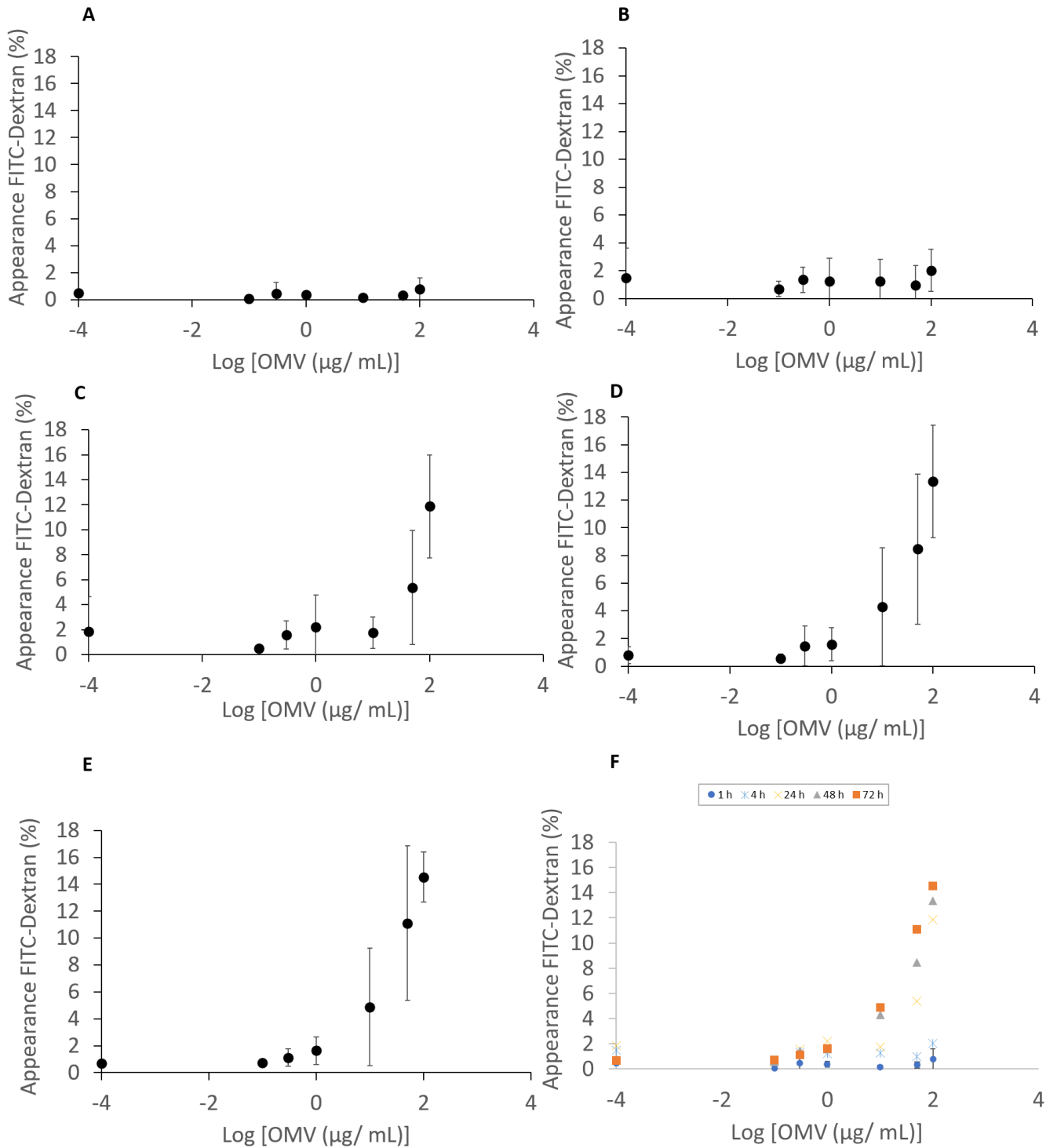


Figure 5.6 Percentage appearance of FITC-dextran (3-5 kDa) on the apical side of the *in vitro* BBB model after application of *P. gingivalis* OMVs, percentage appearance relative to the stock FITC-dextran administered to the basolateral side after 1 h (A); 4 h (B); 24 h (C); 48 h (D); 72 (E) and a comparison of all time points (F). Statistical significance of response was measured using an ANOVA with Dunnett's post-hoc relative to the control (administration of FITC alone) where * $P < 0.05$ and ** $P < 0.01$. Data represents mean \pm SD from three wells and two experimental repeats ($n=6$).

5.3.5 Application of conjugated FITC *P. gingivalis* LPS combined with 10 µg/ml

P. gingivalis OMV to the *in vitro* BBB model

The *in vitro* BBB model was tested with FITC conjugated *P. gingivalis* LPS in the presence of a constant concentration of OMVs to assess the effect the OMVs could potentially have on the appearance of the conjugated LPS in the basolateral compartment. The concentration of 10 µg/ml OMVs was selected, as this was the lowest concentration which showed an effect in the BBB models integrity in the OMV only experiment previously (Figure 5.6D).

The controls for the combined experiment were media only and OMVs (10 µg/ml) only. The data was compared to the previous experiments with FITC *P. gingivalis* LPS only by unpaired analysis (Figure 4.13). The application of *P. gingivalis* LPS-FITC conjugate in conjunction with 10 µg/ml *P. gingivalis* OMVs showed a similar pattern in terms of response in the BBB model as seen in the previous experiments. The TEER responses in these experiments showed a significant difference in the 100µg/mL FITC *P. gingivalis* LPS conjugate with larger magnitudes of change in TEER compared to the controls ($P < 0.05$) (Figure 5.7A). The higher the concentration of FITC *P. gingivalis* LPS with OMV, a reduced recovery was observed, although this was only significant in the highest concentration of 50 µg/mL and highly significant in the 100µg/mL FITC *P. gingivalis* LPS with 10 µg/ml OMVs ($P < 0.05$) and ($P < 0.001$) (Figure 5.7B). An increase in the permeability was seen especially after 24 hours where some of the increases were 5-fold compared to the experiment with *P. gingivalis* LPS-FITC conjugate application only, though this increase was not significant ($P < 0.05$) (Figures 4.13 and 5.8C).

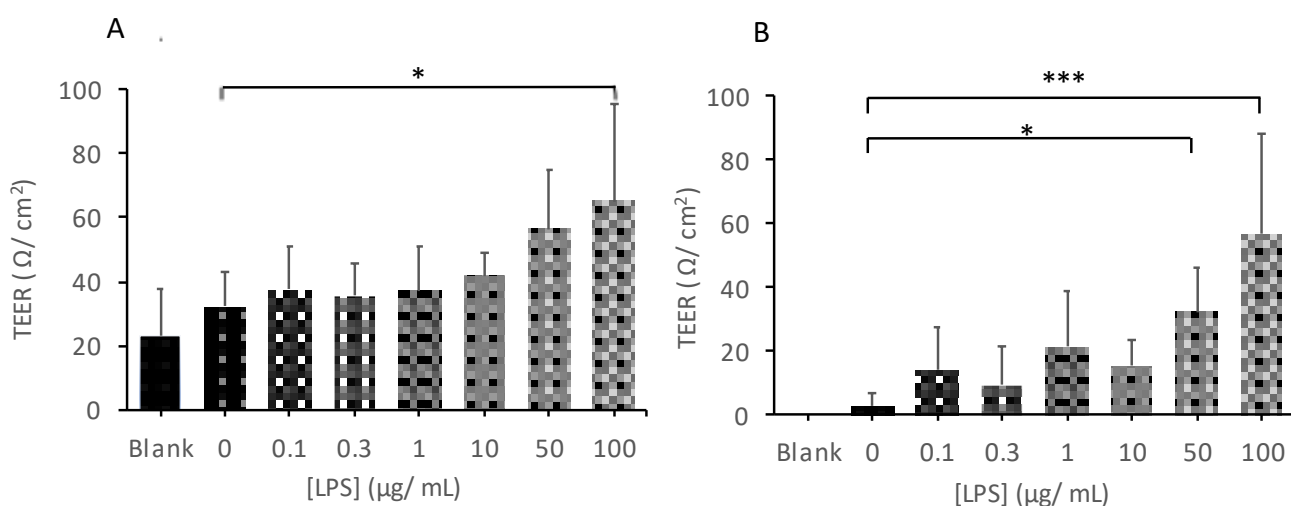


Figure 5.7 Changes in BBB integrity measured by calculating the magnitude of decrease in TEER in response to application of FITC *P. gingivalis* LPS conjugate and 10 μg/ml *P. gingivalis* OMVs, compared to FITC-dextran only (Blank) (A) and the magnitude of deficit in recovery of TEER 72 hours post application of FITC *P. gingivalis* LPS conjugate and 10 μg/ml *P. gingivalis* OMVs relative to initial baseline TEER (B) compared to FITC-dextran only (Blank). Statistical significance of response was measured using an ANOVA with Dunnett's post-hoc relative to the control (administration of FITC alone) where * $P < 0.05$ and *** $P < 0.001$. Data represents mean \pm SD from three wells and two experimental repeats ($n=6$).

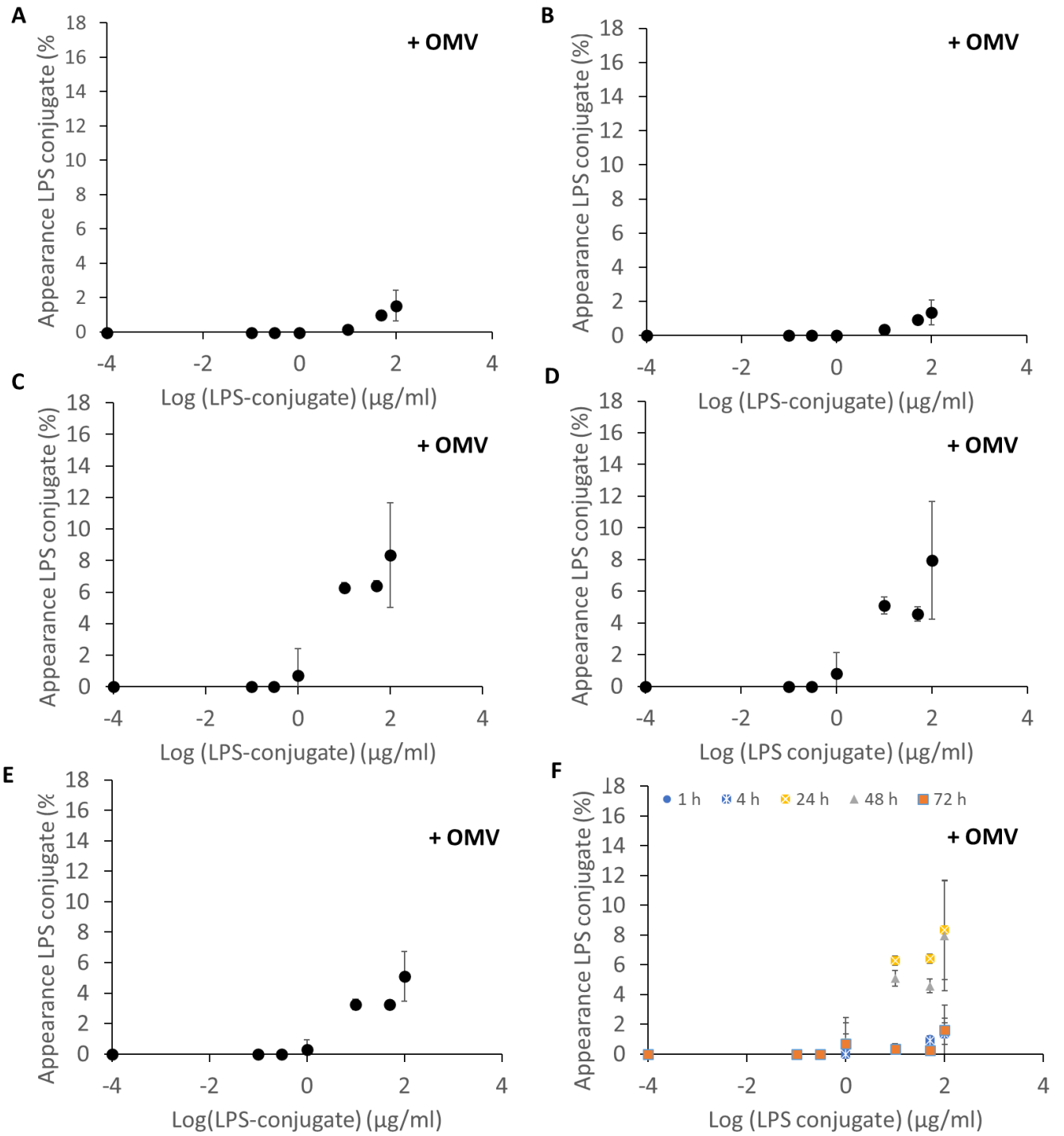


Figure 5.8 Percentage appearance of FITC *P. gingivalis* LPS conjugate on the basolateral side of the in vitro BBB model(+OMV) relative to the stock administered to the apical side after 1 h (A); 4 h (B); 24 h (C); 48 h (D); 72 (E) and a comparison of all time points (F). Statistical significance of response was measured using an ANOVA with Dunnett's post-hoc relative to the control (administration of FITC alone) where * $P < 0.05$ and ** $P < 0.01$. Data represents mean \pm SD from three wells and two experimental repeats ($n=6$).

5.4 Discussion

The extraction method of *P. gingivalis* OMVs was selected as utilised in published studies investigating this vesicle's interaction with other cell lines (Seyama *et al.*, 2020; Ono *et al.*, 2018). It was important throughout the study to test the biological activity of the virulence factors which were applied to the BBB model. Therefore, the test reagents were applied to a monolayer of pericytes and the assays were tested for levels of human IL-6 which in this context is a measure of the inflammatory induction capacity of the virulence factors applied.

In this study we measured the integrity of the *in vitro* BBB model after application of *P. gingivalis* OMVs alone and in combination with FITC conjugated *P. gingivalis* LPS.

A significant drop in TEER was observed after application of *P. gingivalis* OMVs (0.3 and 50 µg/ml) ($P < 0.05$) which were highly significant after application of 0.1 and 100µg/ml ($P < 0.01$) (Figure 5.5A). The non-recovery of TEER in the wells following treatment with 50 and 100µg/ml *P. gingivalis* OMVs was a highly significant ($P < 0.001$) deficit compared to the controls (Figure 5.5B), indicating that these virulence factors affected the *in vitro* BBB model in a prolonged and negative fashion. However, at lower concentrations (0.1, 0.3 and 1 µg/ml) the TEER value reductions were temporary followed by partial or complete recovery (Figure 5.5B).

Comparing the TEER response after the OMV applications to the BBB and the response after un and conjugated *P. gingivalis* LPS, it was found that the OMV appeared to have a more significant effect on the cells of the BBB model, than that of either utilised LPS reagents (Apart from the experiment with application of 0.3 µg/ml unconjugated *P. gingivalis* LPS (Figure 4.5), which did induce significant changes to the TEER measurements).

These findings (of a more significant effect after OMV application) are likely to be because of the nature of the OMVs, also described in some literature as “micro bullets” (Olsen, 2020) as they contain LPS and proteases. Or the comparable lesser response after LPS

application could be because the *P. gingivalis* LPS FITC conjugate could have lost some of its virulent effect in the conjugation process, if this was the case then this was not demonstrated during the IL-6 ELISA experiment.

The permeability of the barrier to FITC dextran after *P. gingivalis* OMV application appeared to have a dose dependant response (Figure 5.6 C-E) compared to the LPS only application studies (Chapter 4). This highlights the OMVs concentration dependant virulence potential, mentioned previously, which emphasises how a reduction in the bacterial load clinically could be important to maintaining a healthy BBB interface. These findings could also be a reflection of the differences between the LPS and OMV utilised in this study, as described above.

The changes in the BBB model cells after application of the FITC-*P. gingivalis* LPS in conjunction with 10 µg/ml of *P. gingivalis* OMVs showed a highly significant difference in the magnitude of change in the TEER values for the wells with 100 µg/ml conjugated *P. gingivalis* LPS in combination with the OMVs (Figure 5.7A) and a significant deficit in recovery of the TEER values in the wells with 50 µg/ml conjugated LPS and which was highly significant in 100 µg/ml FITC-*P. gingivalis* LPS (5.7B). These results share similarities with the previous LPS conjugate study (Chapter 4), which suggests that the presence of the OMVs in this study did not have a potentiated impact on the TEER values and did not prevent the BBB model recovering if the LPS conjugate concentrations were lower.

In the OMV only study, there was an OMV dose response relationship observed in the permeability of FITC dextran which was seen to increase after 24 hours (Figure 5.6).

In comparison the percentage appearance of FITC dextran seen in the OMV alone experiment were higher, with the maximum percentage appearance being 15-fold higher than the LPS alone (Figure 5.6). The increase in permeability after 24 hours was also observed in the combined LPS conjugate and OMV study, and there was an enhancement seen in the LPS conjugate permeation when OMVs were present compared to LPS

conjugate alone (Figure 5.8) which, highlighted the potency of the OMVs containing gingipains. A small increase to 8% maximum percentage appearance was observed when 10 µg/ml was added to the FITC-LPS conjugate (Figure 5.8). The increased percentage appearance in the OMV alone (Figure 5.6) could be explained by the presence of the proteolytic enzymes or gingipains within the OMVs which could also explain the increased permeability of the FITC *P. gingivalis* LPS in the presence of 10 µg/ml of OMV (Figure 5.8). The enzymes could create greater gaps between the barriers cell layers allowing greater perfusion of the molecules to the BLC. Interestingly, the combined study showed a reduction in permeability after 72 hours suggesting a defensive /reparative process in the barrier, though this did not correlate to the TEER deficit seen in the wells with 50 and 100 µg/ml FITC *P. gingivalis* LPS and 10 µg/ml OMV (Figure 5.7B and 5.8F). This finding shows that the ionic conduction across the barrier expressed by TEER was reduced though the junctions between the cells were intact at this point.

The OMVs applied in this study were extracted from a culture of the laboratory strain *P. gingivalis* FDC 381 which is classed as a less virulent *P. gingivalis* strain but has a high ability to be internalized in human cells (Olsen and Progulsk-Fox, 2015). This non-capsular strain has been shown to be a strong immune stimulant, (even activating TLR2) a property attributed to an intact fimB allele, but with less gingipain activity (Coats *et al.*, 2019).

It is possible that the difference in appearance of the *P. gingivalis* LPS FITC conjugate on the CNS side of the model with and without the presence of the OMVs would have been more significant if a less virulent *P. gingivalis* LPS product had been used, such as the purified product mentioned previously.

As previously mentioned, evidence suggests that *P. gingivalis* may not need to enter the brain to cause neuroinflammation (Brown, 2019) and its OMVs could be an important inflammagen, such as described above for unbound LPS. OMVs from *P. gingivalis* could potentially cause neuroinflammation via the blood directly at the BBB by inducing cytokines and initiate pro inflammatory pathways in the tissues of the NVU and activate microglial cells

without entering the brain (Brown, 2019). OMVs in the circulation would be able to internalise in cells of the NVU and therefore could also gain access to the brain. In the BBB protocols, an increased response was observed at 24 hours with both *P. gingivalis* LPS and OMVs which indicates that the induced response by both virulence factors are likely to be more complex than a simple apoptosis of the cells in the model.

Here it has been shown that the application of *P. gingivalis* OMVs alone and in combination with *P. gingivalis* LPS FITC conjugate can affect the cells of the BBB and potentially act as inducers of neuroinflammation. We have shown that the applied virulence factors could induce a response in the cells which was measurable by TEER and % appearance of a tracer compound. The finding that there was decreased or low % appearance with time after application of the lower concentrations of LPS and/or OMVs is encouraging as it suggests that the BBB cells were able to induce a reparative response potentially to recover from the insult. As previously posed in the LPS study above, the question is, for how long are the BBB cells able to recover, until enough damage tips the balance towards a chronic neuroinflammatory state?

Multiple studies have investigated the effect of *P. gingivalis* LPS and OMVs on cells, both human and animal, but not on cells of the human BBB. It was clear from our study that the *P. gingivalis* LPS and OMVs have an effect on the cells of the *in vitro* BBB model and that much more information at cellular level could be revealed using this method. There is potential to investigate more nuanced changes in the cells by using the protocol described here and applying further protocols which could also reveal changes at the lower concentration of LPS level which the TEER and % appearance methods did not have the sensitivity to reveal.

There is an increased consensus that to gain more accurate knowledge of AD, microbial pathology human models need to be developed, as pathological and inflammatory pathways in rodents significantly differ from humans (Nativel *et al.*, 2017; Fulop *et al.*, 2021) especially in relation to molecules such as LPS (Brown, 2019). The expression in our human BBB

model cells is closer to the *in vivo* state than a murine model and there is potential in our model to gain further cellular level information by applying further protocols to the tri-culture. The role of microglial cells in neurodegeneration is undisputed and expansion of this model to include human microglial cells could broaden the applications for this type of protocol.

The *in vitro* BBB model has limitations such as the delicate nature of working with primary cells and the measurements applied in this study do not divulge much information at a cellular level. It could also be considered developing other human cell-based models such as BBB organoids which could potentially be applied to this type of study, though a lengthy optimisation period would need to be applied to secure suitability (Bergman *et al.*, 2018).

To further investigate how *P. gingivalis* LPS and OMVs affect the vascular cells used in our *in vitro* BBB model, we applied these virulence factors to a monolayer of HBMECs and examined the cells by fluorescent microscopy with an aim to uncover more information at a cellular level and to potentially understand some of the findings that we had discovered in the previous experiments of the *in vitro* BBB model.

5.5 Conclusion

The two virulence factors of *P. gingivalis* (LPS conjugate and OMVs) were seen to induce changes in the human *in vitro* BBB model cells. FITC conjugated *P. gingivalis* LPS with 10 µg/ml of OMV and OMVs alone had a significant effect on the integrity of the *in vitro* BBB model which were measurable by TEER showing a significantly greater magnitude of change after application and a significant deficit in recovery of the models TEER values and an enhancement of *P. gingivalis* LPS conjugate in the BLC was seen in the presence of *P. gingivalis* OMVs.

Chapter 6

Assessment of *P. gingivalis* virulence factors interaction with HBMEC in monolayer, measured by immunofluorescence microscopy

6.1 Introduction, aims and objectives of *P. gingivalis* OMVs and LPS application to HBMEC in monolayer study

In the previous two chapters it has become apparent that the virulence factors of *P. gingivalis* (LPS and OMV) are able to induce a change in the integrity of the cells of an *in vitro* BBB model. Observations have been made which showed an increased permeability in the barrier model to FITC dextran after application of the bacterial products. To explore in more detail the interactions of LPS and OMVs with molecular components of the tight junctions (TJs) proteins in HBMECs, *P. gingivalis* LPS (conjugated and un-conjugated) and OMVs were applied to a monolayer of HBMECs. The cells were examined by fluorescent microscopy targeting the tight junction protein Zona occludens 1 (ZO-1), Claudin 5 (CL5) and junctional adhesion molecule 1 (Jam-1) to examine the hypothesis that *P. gingivalis* LPS/OMV interact with TJ proteins in the endothelial cells of the human BBB. The primary antibody targets were chosen after review of the literature (Takeuchi *et al.*, 2019; Mori *et al.*, 2015; Guo *et al.*, 2018; Greene *et al.*, 2019). FITC conjugated *P. gingivalis* LPS was also applied to the HBMEC monolayer using the same protocol to observe any potential co-localization of the FITC LPS conjugate in the cell layer.

Aim:

The aim of this study was to explore the molecular interactions between *P. gingivalis* OMV and LPS with molecular components of the TJs proteins in HBMECs.

Objective 1:

To observe HBMEC after application of unconjugated *P. gingivalis* LPS and OMV in a monolayer model, by application of immunofluorescent protocol targeting the ZO-1 tight junction protein.

Objective 2:

To observe HBMEC after application of FITC- conjugated *P. gingivalis* LPS in monolayer model, by application of immunofluorescent protocol of the ZO-1 tight junction protein, to assess whether there were signs of co-location of the FITC conjugated LPS to any particular areas in the cells.

6.2. Materials

The materials and equipment utilised in this study are listed in Table 1 and 2, Appendix 1.

6.3 Methods

6.3.1 Method HBMEC monolayer model

Human brain microvascular endothelial cells (HBMECs) P4 and P6 (Neuromics, USA) were seeded at a density of 250,000 cells/ml in black, tissue culture treated 24 well plates (IBIDI at Thistle scientific, UK) and grown in EBM (Lonza, Switzerland) in a 37 °C humidified incubator under 5 % CO₂ for 8 days. The cells were tested for viability with trypan blue (Sigma-Aldrich, UK) and by daily visual inspection (3.3.4). On day 7 the cells were treated with 0.1 µg/ml and 0.3 µg/ml of *P. gingivalis* LPS (Invivogen, France), *P. gingivalis* LPS-FITC conjugate (Nanocs, USA) or *P. gingivalis* outer membrane vesicles (OMV) (Chapters 4 and 5) diluted in EBM (Lonza, Switzerland) which were placed on the cells and incubated for 24 hours. After this incubation period the cells were fixed for the immunofluorescent protocol described in 6.3.2.

6.3.2 Immunofluorescent protocol for detection of tight junction proteins

An immunofluorescent protocol was applied to the HBMEC in the monolayer model after incubation of virulence factors (6.3.1). After incubation with the test samples the cells were washed in 1x PBS and fixed with 4% formaldehyde for 25 minutes, washed and permeabilised with 1x PBS and 0.1% Triton-X (Sigma- Aldrich, UK) and blocked with 20 % normal goat serum (Stratech, UK) in 1x PBS with 0.1% Triton-X for 60 minutes. In the optimisation phase the cells were incubated with the primary antibody ZO-1 rabbit monoclonal Ab (1:400) (Cell signalling, NL), claudin 5 mouse monoclonal antibody (1:100 or 1:200) (Invitrogen, UK) and junctional adhesion molecule 1/JAM-A rabbit monoclonal (1:50 or 1:100) (Abcam, UK) at 4°C overnight while shaking on a benchmark Everlast rocker (SKS, USA) and the secondary antibody CyTM5 AffiniPure Goat Anti-Rabbit IgG (1:800) or CyTM5 AffiniPure goat anti-mouse IgG (1:100/1:200/1:400/1:800) (Jacksonimmuno, USA) for an hour at 4°C, while shaking gently. The cells were counter stained with 4',6-diamidino-2-phenylindole (DAPI) (1:3500) (Stratech, UK) and imaged in a Zeiss Cell Observer system featuring the Zeiss definite focus, Colibri LED illumination and AxioVision 4 digital image processing software (Carl Zeiss Microscopy, Germany) detecting the signal for DAPI at ex:358 nm em:463 nm, Cy5 ex:646 nm em:664 nm and FITC ex:470 em:525 (for the samples which had the FITC LPS conjugate applied). Images were taken with 60x objective oil lens with the same exposure times and scale bar 20 µm. The images were viewed and processed using Zen 2.3 Lite software.

6.4 Results

The optimisation of the model was prolonged and involved multiple stages of alteration. First the HBMEC cells growth conditions had to be optimised in the Ibidi plates to ensure a maturity in the cell layer expressing TJs without developing over confluence and contact apoptosis. The optimal time for this was found to be after day 7 which corresponds with the growth kinetics for the HBMEC in chapter 3. The fixing, blocking and DAPI application was also optimised by testing various timings and it was found that the optimal times these steps were 25, 60 and 5 minutes respectively. During the optimisation of the primary and secondary antibodies various concentrations were tested in combination with various wash cycles to achieve optimal conditions for the experiment. The application of Claudin 5 mouse monoclonal antibody (Invitrogen, UK) and junctional adhesion molecule 1/JAM-A rabbit monoclonal (Abcam, UK) were unsuccessful as the samples with CL5 and Jam-1 persistently showed non-specific signal in the whole cytoplasm making the antibodies unsuitable for our investigation (Figure 6.1).

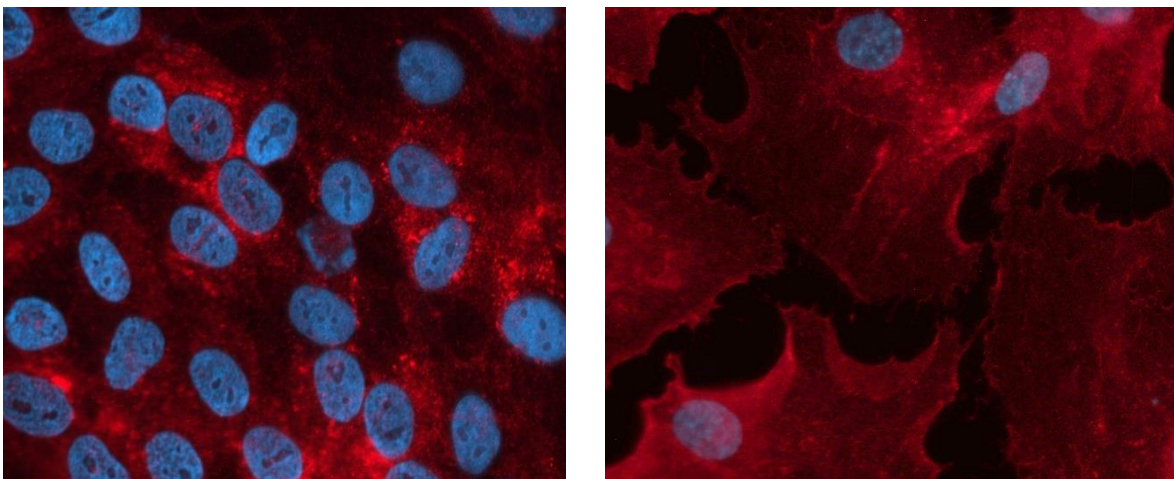


Figure 6.1 A. HBMEC fluorescent protocol Claudin5 Mab 1:100 + Cy5 anti rabbit IgG 1:800, with 5 washes. B. HBMEC fluorescent protocol Jam1 Mab 1:100 and Cy5 anti mouse IgG 1:400 10 washes.

The optimisation of the ZO-1(1:400) and the secondary CyTM5 goat anti-rabbit IgG (1:800) was successful and was applied throughout the experiment.

The experiments of application of virulence factors to the BBB model (Chapters 4 and 5) indicated a potential disruption of the barrier. These findings were considered when the protocol for the monolayer model of HBMEBs was designed and lead to the application of i) unconjugated *P. gingivalis* LPS (0.1 and 0.3 µg/ml), ii) FITC conjugated *P. gingivalis* LPS (0.1 and 0.3 µg/ml) and iii) *P. gingivalis* OMVs (0.1 and 0.3 µg/ml) to the model with an aim to determine how the observed BBB model disruption happened.

All the experiments were repeated 3 times independently. The HBMEC cells were chosen for this experiment as these are the first cells coming into contact with the virulence factors in the *in vitro* model and any in the systemic circulation. The negative control cells (endothelium basal media (EBM) only, Appendix 1, Table 2) showed the expected position of the ZO-1 protein at the cell-cell junctions and the signal of the ZO-1 protein appeared clear and well organised in these controls (Figure 6.2B and 6.2C). The concentrations for these experiments were based on observations after application of virulence factors of higher concentrations in the optimisation stages showed the HBMEC cells viability were consistently acceptable at these concentrations. All the test wells and controls were imaged using the same exposure times and all post exposure modifications were carried out to the same level with the Zen software.

The HBMEC monolayer with application of FITC conjugated and unconjugated *P. gingivalis* LPS showed no noticeable effect on the ZO-1 signal compared to the controls (Figure 6.2 D-F) (only unconjugated 0.3 µg/ml LPS shown) and similar observations were made in the wells with 0.1 µg/ml *P. gingivalis* OMV application (Figure 6.2 G-I) compared to the untreated controls (media only).

No co localisation was observed when the FITC conjugated *P. gingivalis* LPS was imaged (data not shown).

The wells with application of 0.3 µg/ml *P. gingivalis* OMVs showed a more diffused signal from the ZO-1 proteins compared to untreated controls, which could appear as a reduction in the signal (Figure 6.2 J-L). Though a change in the signal from the application of 0.3 µg/ml *P. gingivalis* OMVs were seen in all 3 repeat experiments, it was not clear if the change was a displacement of the ZO-1 protein or reduced numbers, as the experiment here did not quantify the protein. All experiments were conducted with controls both for treatments, antibodies and counterstains and all showed the correct results.

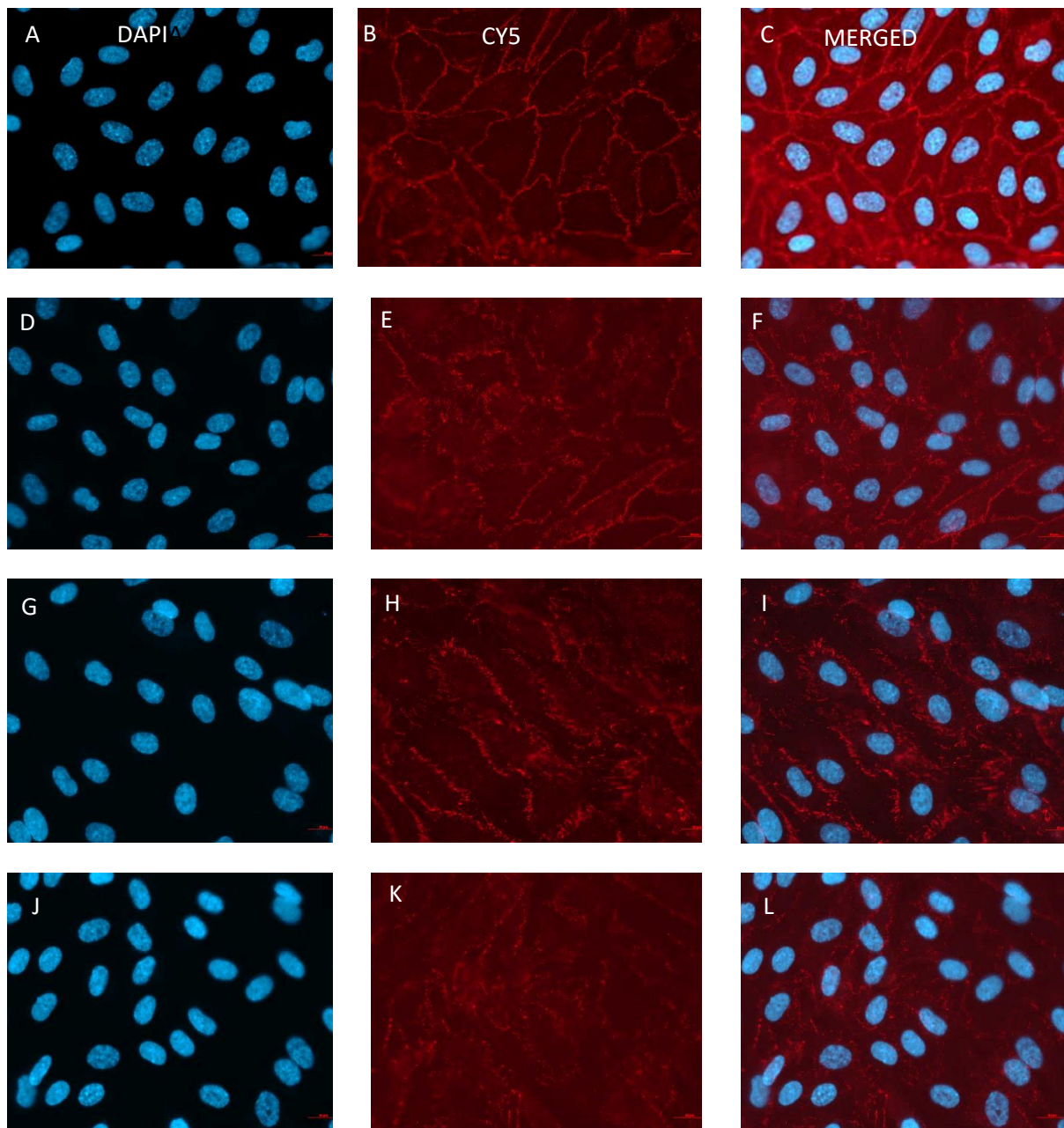


Figure 6.2 Immunofluorescent study of application of *P. gingivalis* virulence factors to human brain microvascular endothelial cells (HBMEC). HBMEC cells in monolayer were treated with EBM (A-C) (negative control), unconjugated 0.3 µg/ml *P. gingivalis* LPS (D-F), 0.1 µg/ml *P. gingivalis* OMVs (G-I) or 0.3 µg/ml *P. gingivalis* OMVs (J-L) for 24 hours. Panels A, D, G and J show the nuclei stained with DAPI and detected at 358 nm (blue). Panels B, E, H and K show Cy5 signal detected at 646 nm (red) detecting the primary ZO-1 (D6L1E) Rabbit mAb. Panels C, F, I and L represent the composite pictures. Images were taken with 60x objective oil lens with the same exposure times. Scale bar 20 µm. (For interpretation of the reference to colour in this figure legend, the reader is referred to the text).

6.5 Discussion

The effect of *P. gingivalis* OMVs and LPS has been examined in various monolayer cell studies previously, but not on human HBMECs. The aim of applying *P. gingivalis* LPS and OMVs to a HBMEC monolayer was to investigate whether the changes observed in the BBB model protocols could be seen at a cellular level and to determine how these changes occurred. As we were interested in how the PD pathogen could disrupt the integrity of the BBB, we wanted to examine any effect on the TJs in the HBMECs, the first cell layer which comes into contact with the systemic circulation. The choice of proteins examined in the HBMEC monolayer model was based on reviewing the literature to seek out targets that have been associated with degradation by *P. gingivalis* and we also looked for TJs that were likely to be expressed in our HBMEC monolayer model (Farrugia *et al.*, 2021; Guo *et al.*, 2018; Greene *et al.*, 2019). Claudin 5 (Cl5) was selected, which is highly enriched in the BBB HBMECs and belongs to the TJ family (Kumar *et al.*, 2014). Zona occludens 1 (ZO-1) is a protein which links Claudin to the actin skeleton at the BBB (Belardi *et al.*, 2020) and junctional adhesion molecule 1 (Jam-1) is a protein related to the TJs and plays an important role for the regulation of junctional permeability and integrity (Naik and Eckfeld, 2003). Jam-1 has also been shown to be degraded after contact with *P. gingivalis* (Takeuchi *et al.*, 2019), which made this a strong contender for the study. Other junction/adherens proteins, as outlined below, could have been chosen, but we had to limit our selection in this study.

Cl5 is highly enriched in the BBB endothelium and its dysfunction has been associated with AD (Greene *et al.*, 2019). When the *in vitro* BBB model was developed by Kumar *et al.* in 2014 it was evidenced that the HBMEC expressed Cl5 (Kumar *et al.*, 2014), therefore this was the first choice of TJs target for our investigation.

Farrugia *et al.*, (2021) have recently showed that *P. gingivalis* expressing gingipains on their surface degraded endothelial cells in Zebrafish larvae by reducing the numbers of vascular

endothelial cadherin (VE cadherin) and platelet endothelial cell adhesion molecule 1 (PECAM 1), causing the cells to lose the cell to cell contact thereby increasing vascular permeability (Farrugia *et al.*, 2021; Cerutti and Ridley, 2017). Hajishengallis (2021) suggested that the damage Farrugia discovered, increased permeability and inflammatory change and could form the link between PD and atherosclerotic plaques in cardiovascular disease (CD) (Figure 6.3). Though this research was aimed at showing the link between PD and CD, these findings are very relevant to our study because we are interested in how *P. gingivalis* could cause neuroinflammatory changes at the vessels in the BBB.

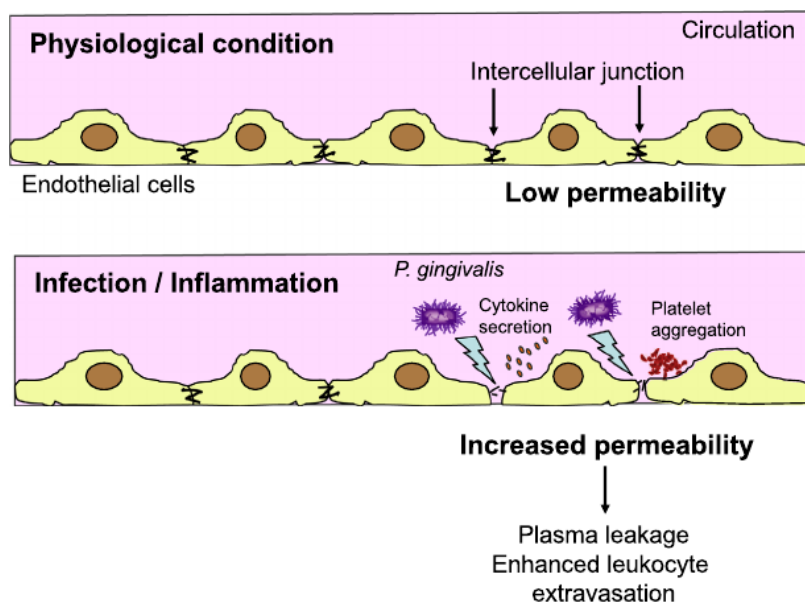


Figure 6.3 Systemic *P. gingivalis* disrupting endothelial tight junctions by degrading platelet endothelial cell adhesion molecule one (PECAM1) and vascular endothelial cadherin (VE-cadherin) by gingipain proteolysis increasing the endothelial permeability. This could potentially induce platelet aggregation, release proinflammatory cytokines and aid extravasation of leukocytes causing further inflammatory changes in the surrounding tissues (Hajishengallis, 2021)

The protective role of VE cadherin in BBB integrity is significant and BBB dysregulation caused by neuroinflammatory events can affect the function of this adherence junction protein negatively (Li *et al.*, 2018). Though the disruption of VE cadherin has been linked to

BBB disruptive neurological conditions such as ischaemic stroke (Li *et al.*, 2018), there is no research yet that has established a connection between VE cadherin disruption and AD, and therefore we did not select VE cadherin as our target but chose the closely related ZO-1 (Belardi *et al.*, 2020). The tight junction adaptor protein ZO-1 is closely associated with VE-cadherin at the BBB. Tornavaca *et al.* (2015) showed that in primary endothelial cells ZO-1 is a central regulator of tight junctions depending on the strictly endothelial specific adhesion molecule VE-cadherin. These endothelial junctions were found to influence the spatial actomyosin organization, cell–cell tension and migration across the endothelium, but also angiogenesis and barrier formation. ZO-1 connects the actin skeleton to tight junctions such as claudin and occludin and the binding of ZO-1 to actin is essential for regulation of permeability in epithelial cells and BBB endothelium (Belardi *et al.*, 2020; Li *et al.*, 2018) (Figure 6.4).

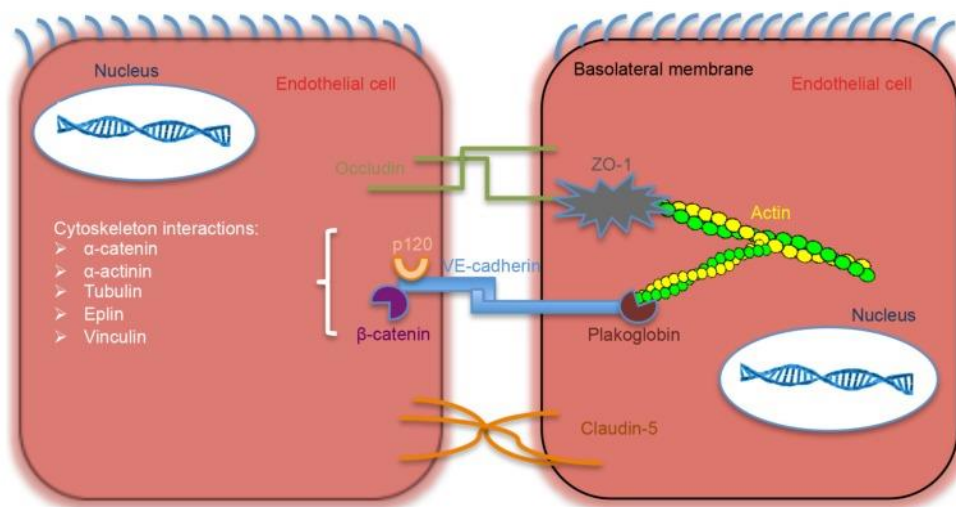


Figure 6.4 The cerebral endothelial cells junction structure. The main transmembrane tight junction proteins are Claudin 5 and Occludin. ZO-1 connects the actin skeleton to the tight junctions and VE cadherin forms the majority of adherens junctions interacting with the cytoplasmic anchor proteins: β-catenin, plakoglobin (γ-catenin), and p120 linking to the cytoskeleton (Li *et al.*, 2018)

Tornavaca *et al.* (2015) used human dermal microvascular endothelial cells (HDMEC-c) and not HBMECs, but this places ZO-1 central to the development, integrity and maintenance of the BBB. The plausibility that ZO-1 could be disrupted by *P. gingivalis* OMS containing gingipains in human HBMECs is likely, considering the results Farrugia *et al.*, (2021) discovered in Zebra fish larvae. Therefore ZO-1 was selected to be investigated in the HBMEC monolayer model.

The disruption of cell stability evidenced by Farrugia *et al.*, (2021) were also seen when Andrian *et al.*, (2004) examined the penetration of *P. gingivalis* in engineered human oral mucosa (epithelial and fibroblast cells). This group concluded that it was the gingipains contributing to the invasion of the bacteria into the cells. Andrian *et al.* (2004) showed the ability of *P. gingivalis* to penetrate the basement membrane in a gingival mucosal model and Katz *et al.*, (2002) showed that *P. gingivalis* gingipains can hydrolyse epithelial tight junction proteins, namely E-cadherin. Guo *et al.* (2018) found that *P. gingivalis* and its LPS were able to alter the expression of tight junction proteins in oral epithelial cells *in vitro*, they observed an upregulation in the expression of ZO-1 and downregulation of Jam-1 after 2-4 hours of incubation with 1 µg/ml of *P. gingivalis* LPS (Guo *et al.*, 2018), the results of this study also influenced the selection of Jam-1 and ZO-1 as a target in our study.

More recently Takeuchi *et al.*, (2019) found that *P. gingivalis* was able to penetrate immortalized human gingival epithelial cells by degradation of Jam-1 and He *et al.*, (2020) showed that OMVs from *P. gingivalis* reduced cell viability and caused disruption of the distribution of tight junctions proteins in human lung epithelial cells in a time dependant manner. We included Jam1 in our investigation because of the findings by Takeuchi *et al.* (2019) and Guo *et al.* (2018). Also, we expected this adhesion molecule to be expressed in our HBMEC cells (Greene *et al.*, 2019).

Endogenous autofluorescence is a common problem undertaking fluorescent protocols and this is particularly seen in brain tissue samples (Sun *et al.*, 2017; Pascu *et al.*, 2009).

We established (through negative controls) that the excessive signal in our images from the CL5 and Jam-1 (Figure 6.1) were related to the primary antibodies binding to something in the cell's cytoplasm, rather than caused by autofluorescence, i.e. there was a problem with the specificity of the primary antibodies (Burry, 2011). Various concentrations of both primary and secondary antibodies were tested and the wash cycles were increased.

We would expect to find Jam-1 and Claudin 5 (Cl5) at the cell-cell junctions (Kummer and Ebnet, 2018; Greene *et al.*, 2019). Cl 5 is only expressed in the cytoplasm to any significance during foetal development and Jam-1 is specifically enriched in cell to cell contact areas (Greene *et al.*, 2019; Ebnet *et al.*, 2004) and the widespread signal we found was too extensive to come from ribosomal protein labelling. Therefore, the position of the signal in the optimisation of the Cl5 and Jam-1 antibodies had to be seen as an artefact. There could have been other factors influencing the non-specific labelling by these antibodies, the heterogenous environment in the sample and also other effects from the fixation and reagent treatment of the cells could have contributed to the widespread signal in the samples (Burry, 2011).

The protocol was successful with the ZO-1 primary antibody and negative control cells (no virulence factors applied) showed the expected position of the ZO-1 protein at the cell-cell junctions (Eigenmann *et al.*, 2013; Tornavaca *et al.*, 2015). The signal of the ZO-1 protein appeared well organised and it was therefore decided to progress with the experiment using the ZO-1 protocol only (Figure 6.1B and 6.1C).

The HBMEC monolayer with application of *P. gingivalis* LPS showed no noticeable effect on the ZO-1 signal (Figure 6.1 D-F) (only 0.3 µg/ml shown) and similar observations were made in the wells with 0.1 µg/ml *P. gingivalis* OMV application (Figure 6.1 G-I) compared to the untreated controls (media only). This would suggest that the virulence factors were not able to cause a change in the organisation and integrity of the tight junction proteins at this concentration, or the application period (24 hours) was not long enough to bring a visual

change in these HBMEC cells. The wells with application of 0.3 µg/ml *P. gingivalis* OMVs showed a more diffused signal from the ZO-1 proteins compared to untreated controls, which could appear as a reduction in the signal and disorganisation (Figure 6.1 J-L). If *P. gingivalis* OMVs are able to disrupt the functionality of ZO-1 at the BBB, this could have devastating consequences to the integrity of the blood brain interface. ZO-1 is a large phosphoprotein and post-translational alterations such as phosphorylation would lead to ZO-1 dissociation from the tight junction complex (Stamatovic *et al.*, 2016). This could potentially be how *P. gingivalis* OMVs affected this protein in the HBMECs in our study, both in the monolayer diffusion of the ZO-1 signal and potentially the changes we observed in the TEER in the *in vitro* BBB model, where notably the application of *P. gingivalis* OMVs had the greatest effect on both measurements (TEER and ZO-1 signal).

Though a change in the Cy5 signal after the application of 0.3 µg/ml *P. gingivalis* OMVs were seen in all 3 repeat experiments compared to untreated controls, it was not clear if the change was a displacement of the ZO-1 protein or reduced numbers as the experiment here did not quantify the protein.

FITC conjugated *P. gingivalis* LPS was applied to the monolayer model in an attempt to see any potential co-localisation and after incubation and fluorescent protocol the cells were observed in the same way as the other test wells. There was no detectable cell disruption seen in the wells which had the FITC conjugate applied and no co-localisation was observed, in fact no traceable FITC signal was detected in any of the wells. This could be because the LPS conjugate did not bind with any of the cells in the monolayer, or any fluorophore and LPS were not successfully fixed and subsequently washed off in the protocol that followed.

If the observations made in the monolayer model study are applied to the human BBB, then infection with *P. gingivalis* and their inflammagens LPS and OMVs could cause damage to an otherwise healthy and non-predisposed individual.

6.6 Conclusion

The ZO-1 proteins in a HBMEC monolayer model showed disruption after contact with *P. gingivalis* OMVs compared to controls. The cells which had *P. gingivalis* LPS only did not persistently show the disruption pattern when the experiment was repeated 3 times independently. No co localisation or binding of the FITC *P. gingivalis* LPS conjugate was detected.

Further investigations at cellular level are warranted to contribute to the knowledge pool of how *P. gingivalis* OMV containing LPS and gingipains from periodontal disease could have an influence on neuroinflammatory states by affecting the cells of the BBB and potentially contribute to or exacerbate neurodegeneration, such further work is discussed below.

Chapter 7

Thesis conclusion and future work

Thesis conclusion

Research activity investigating a link between PD pathogens, neuroinflammation and neurodegeneration has grown exponentially since the beginning of this project in 2016. In 2016 very few studies had looked at the potential involvement of oral pathogens with neuroinflammation, though after our experiments had commenced in 2017, a study was published (Emery *et al.*, 2017), which examined post-mortem AD brain samples for genetic remnants of bacteria. The study by Emery *et al.* (2017) identified a range of bacteria to phylum level in the AD brains and found more bacterial reads in the AD cohort compared to the controls. Further to this, two other high throughput studies were published in 2017 and 2018 identifying fungal and bacterial gDNA in AD brains (Alonso *et al.*, 2017; Alonso *et al.*, 2018), but none of these studies made a specific link to oral bacteria. As our study had a greater cohort and was focussing on the oral microbiome, the project still had novelty and could contribute to the knowledge pool. Then in 2018 an animal study (Illievski *et al.*, 2018) described to have induced amyloid plaques and NFT's similar to the ones found in AD pathology by application of *P. gingivalis* in a population of wild type C57BL/6 mice. The Illievski study was encouraging as it confirmed the subject of our project to be novel in particularly as we were working with human tissues rather than rodents. The findings in the first part (chapter 3) of our project, by next generation sequencing (NGS) and PCR and the publication of the above-mentioned studies influenced the direction of the investigations described in the remaining part of the thesis. In summary there have been multiple publications linking periodontal disease to AD in the past few years, but many questions remain on this subject.

Though there is now more evidence of how pathogens such as *P. gingivalis* could contribute to disease in the brain, a bacterial cell associated with PD has still not been found in the brain, neither in animal studies or in human post mortem specimens. The initial aims were to investigate whether the brain tissues of 25 AD patients and 15 age matched control

patients contained remnants of bacterial gDNA and if so, which bacteria had been present in the brain at the time of death. This was to provide support to the inflammatory or infectious theory of AD causation. NGS analysis was successful in 15 of the samples (9 AD and 6 controls) and this detected a wide range of bacterial gDNA in both the AD samples and controls, but there was a 9-fold increase in bacterial reads in the AD cases. It was also discovered that 2 of the AD samples had a very high bacterial read number compared to the other AD cases and controls. The phyla identified by NGS were dominated by Proteobacteria, Bacteroidetes, Actinobacteria and Firmicutes. The NGS analysis was followed up by PCR amplification at UCLan of all 40 samples, using primers for fungal and bacterial gDNA. This was to investigate if the samples which had not produced a result in the NGS showed signs of microbial gDNA. The aim was to potentially draw further conclusions regarding a link between microbial gDNA in the brain and AD diagnosis, also to conclude if there were any differences between the two cohorts in this respect. The PCR amplification using the fungal primer pair ITS1 and ITS2r proved to divulge limited data as there was no conclusive evidence of fungal gDNA detected in the samples. The bacterial primer pair F342 and F18R, though providing amplicons of the expected size visualised by electrophoresis, were in some cases not corresponding with the NGS data, so the conclusions drawn from this work were also limited. Key findings from the genomics work were that the bacterial reads in the two cohorts were of similar phylum ratio and that the AD group had higher average bacterial reads. The finding of a very high numbers in two of the AD cases suggests a vulnerability in some individuals to influx of bacteria to the CNS, compared to others.

This discovery guided the project towards investigating further how the BBB could be affected by pathogens and the main focus was on the keystone bacteria involved in PD; *P. gingivalis* and one of its virulence factors LPS. The aim was to examine how this endotoxin would affect the integrity of the cells in an *in vitro* human primary cell blood brain barrier model. The *in vitro* model had previously been validated for drug transportation

studies and as our aim was to investigate a potential disease state, a protocol had to be established for this purpose. Part of this entailed examining the three BBB model cell lines growth kinetics and test two separate serum supplements (single male donor or mixed gender donors). This also provided the opportunity to examine whether the observed kinetics were similar to the description in the validation study previously carried out by Kumar *et al.* in 2014. The results of this study were found to be similar to Kumar *et al.*, (2014) and though no great difference was seen in the behaviour between the two serum supplements, it was decided to carry on with the mixed donor serum supplement as this would provide the most genetic variability to the model. Once the suitability of the BBB model to the proposed aim of investigating *P. gingivalis* LPS effect on the integrity of the cells of the model had been established, another aim was to investigate whether the LPS could cross the barrier in the model. This was investigated by applying a FITC *P. gingivalis* LPS conjugate to the barrier model. These experiments showed that *P. gingivalis* LPS has an effect on the integrity of the *in vitro* BBB model which was measurable by TEER and % appearance at certain concentrations. It was evident that higher doses of LPS showed a larger magnitude of change and any recovery of TEER values were both less and slower compared to controls, indicating an effect on the cell layers integrity or viability in the *in vitro* BBB model. The LPS conjugate experiments showed that the endotoxin from *P. gingivalis* crossed the barrier model, also at a physiologically relevant level (0.3 µg/ml). Following on from the *P. gingivalis* LPS study the aim was to investigate if another *P. gingivalis* virulence factor, its OMVs could also have an effect on the *in vitro* BBB models integrity. We also aimed to measure if the presence of OMVs (containing proteolytic enzymes) on the vessel side of the model could influence the appearance of a FITC labelled *P. gingivalis* LPS in the CNS side. *P. gingivalis* OMVs were seen to induce changes in the *in vitro* BBB model cells and both FITC conjugated *P. gingivalis* LPS with 10 µg/ml of OMV and OMVs alone had a significant effect on the integrity of the *in vitro* BBB model which were measurable by TEER. Also, an enhancement of *P. gingivalis* LPS conjugate in the BLC was seen in the presence

of *P. gingivalis* OMVs, suggesting that the OMVs could potentiate influx of other virulence molecules contributing to an inflammatory response.

To seek more detail of molecular interactions between *P. gingivalis* OMVs or LPS with molecular components of the TJs of the first cell layer of contact in the BBB, these two virulence factors were applied to a monolayer model of HBMEC in various concentrations. The cells were then examined by fluorescent microscopy targeting a selection of TJ proteins. By application of the FITC *P. gingivalis* LPS conjugate to HBMEC in monolayer another aim of this investigation was to see if any co-localisation could be visualised by this method. The application of *P. gingivalis* OMVs to the HBMEC monolayer showed disruption of the ZO-1 protein compared to controls. The application of *P. gingivalis* LPS only, did not persistently show the disruption pattern when the experiment was repeated 3 times independently and no co-localisation or binding of the FITC *P. gingivalis* LPS conjugate was detected.

In conclusion to answer the hypothesis set out at the beginning of this thesis, could microorganisms associated with periodontal disease be identified in human Alzheimer's Disease brain tissues and could virulence factors from the keystone pathogen *P. gingivalis* affect the integrity of cells of the brain's main defence, the Blood brain barrier?

Our study did find a 9-fold higher bacterial read number in post-mortem AD brain samples compared to age matched controls and this was mainly contributed to high numbers in two individual AD samples. We also identified the bacterial gDNA to genus level and found that the origin and ratio of the bacteria was similar between the two groups. There was no conclusive evidence of PD bacteria in the brain samples as it was not possible to identify the gDNA to species level, but we did identify phyla that could originate from the oral microbiome. The keystone pathogen *P. gingivalis* produces virulence factors and two of those, OMV and free LPS molecules, could induce changes to the cells of the BBB contributing to inflammation and weakness to this barrier. This supports the idea that if *P. gingivalis* is able to cause neuroinflammation, the bacterial cell may not need to be in the

vicinity of the BBB but can act from afar by secreting virulence factors into the systemic circulation. From the evidence we present here we cannot claim that PD leads to AD, but we have provided evidence in support of that theory by showing that microbial products can influence human cells of the blood brain interface. Further investigations at cellular level are warranted to contribute to the knowledge pool of how virulence factors from periodontal disease could have an influence on neuroinflammatory states and potentially contribute to or exacerbate neurodegeneration. If our observations are applied to the human BBB, then infection with *P. gingivalis* and their inflammagens LPS and OMVs could cause damage to an otherwise healthy and non-predisposed individual.

Reflecting on this thesis, it is important to evaluate what went well and what could have been done differently.

The development of the method investigating *P. gingivalis* virulence factors on an *in vitro* human primary cell BBB model was novel and found to be a suitable tool for this type of investigation. The cultivation of *P. gingivalis* followed by extraction of the outer membrane vesicles (OMV) were challenging and the latter a less frequently used method at UCLan, which limited the available support. These methods were successful and proved to be very valuable for the project, as recent focus in this type of research is aimed at the *P. gingivalis* virulence factors' effect on human tissues.

Some of the methods applied in this project did have limitations which should be addressed prior to future work. Though the NGS methods revealed a 9-fold increase in bacterial reads compared to controls, which is in line with other studies in this field, these were not identified to species level. This meant that no conclusions could be drawn on a link to the oral microbiome. The outsourcing of the NGS also meant that there was no information available regarding why only 15 of the human tissue samples produced data. Further consideration and evaluation of the methods in the earlier stages of the NGS work could have led to a change in the protocol and potentially have increased the number of viable samples. If undertaking future genomics work of this nature and if using post-mortem samples, selection

of the controls could be improved to find individuals without medical conditions resulting in a weakened immune defence. It would also strengthen any such investigation if further details of the donors were available, such as periodontal disease status in later life. The problems encountered in this project in relation to the PCR work are most likely due to the design of the primers that were used. This could have been addressed by re-designing the primers to be more specific and this could potentially have improved the quality and volume of the data, to enable more firm conclusions in the genomic study. Limitations of working with human post-mortem tissues have been addressed previously and it was important in this study to apply a variety of methods addressing the hypothesis of *P. gingivalis* potential involvement in induction of neuroinflammation and dementia, which is why the *in vitro* BBB model was used. It proved to be the human primary cell culture methods that provided the most valuable data addressing the hypothesis of a potential contribution from periodontal disease microorganisms potentially being associated with the loss of BBB integrity and neuroinflammation observed in Alzheimer's disease.

It is tempting to attribute the link between sporadic Alzheimer's Disease and periodontal disease to the effect of the multi-faceted pathogen (*P. gingivalis*), when the chronicity of the inflammatory state seen in established periodontal disease could be the main culprit. This highlights not only the need for good oral hygiene, but also the importance of diagnosis and optimal management of dental patients presenting with unstable periodontal disease. Until there is a therapeutic remedy which can protect the BBB from chronic inflammation, prevention remains key.

Future work

One of the key findings of this project was that some individuals had a very high bacterial gDNA content in their brain tissues at the time of death compared to others. If inflammation is the cause of AD, future work should aim to understand if susceptibility to influx of microorganisms to the CNS is genetic or induced by risk factors or both. It would be interesting to establish if there is a difference in genetic polymorphisms in the BBB endothelial cells of individuals with AD compared to controls and in particular in the cells of the individuals who showed a high read number in this thesis. This could be investigated by mass spectrometry (Cui *et al.*, 2020) if we are able to extract BBB endothelial/pericytes/astrocytes for examination. Gene expression could also be investigated by microarrays of the cells in the primary *in vitro* BBB model before and after application of virulence factors (Wang *et al.*, 2011). As the primary cells originate from individual donors, it would be valuable to test multiple donors this way as would reduce individual variation, however this would require a large budget as the primary cells in the BBB model are expensive and hard to acquire. There is also potential to develop the *in vitro* model further and add other cell types or grow the model differently. Another cell type which is of great interest in neurodegeneration is the microglial cell and adding this to our model could introduce further knowledge of their role in keeping the BBB healthy or what could make them fail to do so (Liebner *et al.*, 2018; Kim *et al.*, 2019). Growing the model on a rigid membrane such as the transwell introduces problems with certain investigations such as microscopy, where holding the tissues together during cryo- sectioning can be difficult. Growing the model in a gel scaffold (Bastiaens *et al.*, 2019) or leaving cells to self-assemble in organoids (Wray, 2021) could overcome some of these problems. Though it could prove difficult to get the sensitive primary cell lines to thrive under more challenging growth conditions and if induced pluripotent stem cells (iPSCs) or immortalised cells were used the question is how well they represent the full complement of proteins expressed (genomic/

proteomic/ activity) *in vivo*, they are certainly considered inferior in that respect to primary cell lines (Wray, 2021; Park *et al.*, 2018).

It has been clear from our work and reviewing the literature of recent PD studies that OMVs are a significant virulence factor of *P. gingivalis* (Olsen, 2021) and it is evident that different strains of this bacteria have different levels of virulence (Igboin *et al.*, 2009; Kulkarni *et al.*, 2018). Therefore, it would be interesting to expand the microbiology work to different strains of *P. gingivalis* as any new knowledge of strain variations in the interaction with the cells of the BBB could add to our understanding of how PD can affect remote organs including the brain. This knowledge could also be useful in developing clinical screening methods to identify microorganisms with a higher risk potential. In our study we only studied the virulence factors of *P. gingivalis* and this is a limitation of our study. It is recognised that other pathogens, also some considered commensal organisms, could contribute to the development of PD, as this is the dysbiotic nature of the disease. Further work could be to investigate other bacteria involved with PD and their interaction with the cells of the human BBB in a similar model to the one described in this thesis.

Designing clinical studies to investigate the potential link between PD and AD is problematic. If we were to do this type of research in the future, we would need to follow the individuals over a long time period (middle age to 70s) and confounding factors such as co-existing comorbidities and multiple other factors which could introduce bias would need to be excluded. Otherwise, this could make it difficult to make clear conclusions on any connections between clinical evidence of PD and AD. It would be important to follow the participants closely in terms of their periodontal status and the clinical process of examination and measurements would have to be standardised so that inter clinician variability was minimised. Any oral hygiene interventions over the test period and fluctuation in effectiveness of such measures could introduce bias and lack of intervention would be ethically problematic. If the test subjects had been diagnosed with PD, allowing the disease to progress over the years to make a link to AD, could have serious consequences for the

individual's health and wellbeing and subsequently be unethical. As AD has emerged as a multifactorial condition with a number of risk factors, it could also be difficult to find suitable participants for any such study.

In the immediate future it is certain that we need to develop human models to study this field of research to come closer to learning how PD pathogens can affect remote organs and potentially cause tissue modifications that could lead to dementia in old age.

References

Abbott, N.J., Patabendige, A.A., Dolman, D.E., Yusof, S.R., Begley, D.J. (2010) Structure and function of the blood-brain barrier. *Neurobiol Dis.* 37(1):13-25.

doi:10.1016/j.nbd.2009.07.030. PMID: 19664713.

Abe, N., Kadowaki, T., Okamoto, K., Nakayama, K., Ohishi, M., Yamamoto, K. (1998)

Biochemical and functional properties of lysine-specific cysteine proteinase

(Lys- gingipain) as a virulence factor of *Porphyromonas gingivalis* in periodontal disease. *J Biochem.* 123(2):305-12. doi:0.1093/oxfordjournals.jbchem.a021937.

PMID: 9538207.

Agrawal, S., Anderson, P., Durbeej, M., van Rooijen, N., Ivars, F., Opdenakker, G., Sorokin,

L.M. (2006) Dystroglycan is selectively cleaved at the parenchymal basement membrane at sites of leukocyte extravasation in experimental autoimmune encephalomyelitis. *J Exp Med.* 203(4):1007-19. doi: 10.1084/jem.20051342.

PMID: 16585265.

Akanuma, S.I., Uchida, Y., Ohtsuki, S., Tachikawa, M., Terasaki, M., Hosoya, K.I. (2011)

Attenuation of prostaglandin E2 elimination across the mouse blood-brain barrier in lipopolysaccharide-induced inflammation and additive inhibitory effect of cefmetazole. *Fluids Barriers CNS*, 8:24. doi: 10.1186/2045-8118-8-24.

PMID: 22014165

Allen, H.B. (2017) Alzheimer's disease: Assessing the role of spirochetes, biofilms, the

immune system, and amyloid- β with regard to potential treatment and prevention In: Handbook of Infection and Alzheimer's Disease. ed. J. Miklossy (IOS Press, Amsterdam, The Netherlands), 83-88. doi:10.3233/JAD-160388

Allt, G., Lawrenson, J.G. (2001) Pericytes: cell biology and pathology. *Cells Tissues Organs* 169(1):1-11. doi: 10.1159/000047855. PMID: 11340256.

Alonso, R., Pisa D., Aguado, B., Carrasco, L. (2017). Identification of fungal species in brain tissue from Alzheimer's disease by next-generation sequencing. *J. Alzheimers Dis.* 58(1):55-67. doi: 10.3233/JAD-170058. PMID: 28387676

Alonso, R., Pisa, D., Fernández-Fernández, A.M., Carrasco, L. (2018) Infection of fungi and bacteria in brain tissue from elderly persons and patients with Alzheimer's disease. *Front. Aging Neurosci.* 10:159. doi: 10.3389/fnagi.2018.00159. PMID: 29881346

Andrian, E., Grenier, D., Rouabhia, M. (2004) In vitro models of tissue penetration and destruction by *Porphyromonas gingivalis*. *Infect Immun.* 72(8):4689-98. doi: 10.1128/IAI.72.8.4689-4698.2004. PMID: 15271930.

Area-Gomez, E., de Groof, A., Bonilla, E., Montesinos, J., Tanji, K., Boldogh, I., Pon, L., Schon, E. A. (2018). A key role for MAM in mediating mitochondrial dysfunction in Alzheimer disease. *Cell Death Dis.* 9(3), 335. doi.org/10.1038/s41419-017-0215-0. PMID: 29491396.

Arimatsu, K., Yamada, H., Miyazawa, H., Minagawa, T., Nakajima, M., Ryder, M.I., Gotoh, K., Motooka, D., Nakamura, S., Iida, T., Yamazaki, K. (2014) Oral pathobiont

induces systemic inflammation and metabolic changes associated with alteration of gut microbiota. *Sci Rep.* 4:4828. doi: 10.1038/srep04828.

PMID: 24797416.

Armulik, A., Genové, G., Mäe, M., Nisancioglu, M.H., Wallgard, E., Niaudet, C., He, L., Norlin, J., Lindblom, P., Strittmatter, K., Johansson, B.R., Betsholtz, C. (2010) Pericytes regulate the blood-brain barrier. *Nature.* 468(7323):557-61. doi: 10.1038/nature09522. PMID: 20944627.

Attems, J., Jellinger, K.A. (2014) The overlap between vascular disease and Alzheimer's disease lessons from pathology. *BMC Med.* 12:206. doi: 10.1186/s12916-014-0206-2. PMID: 25385447.

Atri, A. (2019) The Alzheimer's Disease Clinical Spectrum: Diagnosis and Management. *Med Clin North Am.* 103(2):263-293. doi: 10.1016/j.mcna.2018.10.009. PMID: 30704681.

Bakhsheshian, J., Wei, B.R., Hall, M.D., Simpson, R.M., Gottesman, M.M. (2016) In vivo bioluminescent imaging of ATP-binding cassette transporter-mediated efflux at the blood-brain barrier. *Methods Mol Biol.* 1461:227-39. doi: 10.1007/978-1-4939-3813-1_19. PMID: 27424909.

Banks, W.A., Gray, A.M., Erickson, M.A., Salameh, T.S., Damodarasamy, M., Sheibani, N., Meabon, J.S., Wing, E.E., Morofuji, Y., Cook, D.G., Reed, M.J. (2015) Lipopolysaccharide-induced blood-brain barrier disruption: roles of cyclooxygenase, oxidative stress, neuroinflammation and elements of the

neurovascular unit. *J Neuroinflammation*. 12:223. doi: 10.1186/s12974-015-0434-1. PMID: 26608623.

Barar, J., Rafi, M.A., Pourseif, M.M., Omid, Y. (2016) Blood-brain barrier transport machineries and targeted therapy of brain diseases. *Bioimpacts*. 6(4):225-248. doi: 10.15171/bi.2016.30. PMID: 28265539.

Bastiaens, A., Xie, S., & Luttge, R. (2019). Nanogroove-enhanced hydrogel scaffolds for 3D neuronal cell culture: an easy access brain-on-chip model. *Micromachines*. 10(10):638. doi: 10.3390/mi10100638. PMID: 31548503.

Barkalow, F.J., Goodman, M.J., Gerritsen, M.E., Mayadas, T.N. (1996) Brain endothelium lack one of two pathways of P-selectin-mediated neutrophil adhesion. *Blood*. 88(12):4585-93. PMID: 8977250.

Behm, C., Blufstein, A., Abhari, S. Y., Koch, C., Gahn, J., Schäffer, C., Moritz, A., Rausch-Fan, X., & Andrukhov, O. (2020). Response of human mesenchymal stromal cells from periodontal tissue to LPS depends on the purity but not on the LPS source. *Mediators of inflammation*, 2020:8704896. doi: 10.1155/2020/8704896. PMID: 32714091.

Bekris, L. M., Yu, C. E., Bird, T. D., & Tsuang, D. W. (2010). Genetics of Alzheimer disease. *J Geriatr Psychiatry Neurol*. 23(4), 213–27. doi.org/10.1177/0891988710383571. PMID: 21045163.

Belardi, B., Hamkins-Indik, T., Harris, A.R., Kim, J., Xu, K., Fletcher, D.A. (2020) A weak

link with actin organizes tight junctions to control epithelial permeability. *Dev Cell.* 54(6):792-804.e7. doi: 10.1016/j.devcel.2020.07.022.

PMID: 32841596.

Belstrøm, D., Holmstrup, P., Damgaard, C., Borch, T.S., Skjødt, M.O., Bendtzen, K., Nielsen, C.H. (2011) The atherogenic bacterium *Porphyromonas gingivalis* evades circulating phagocytes by adhering to erythrocytes. *Infect Immun.* 79(4):1559-65. doi: 10.1128/IAI.01036-10. PMID: 21245264.

Bergmann, S., Lawler, S. E., Qu, Y., Fadzen, C. M., Wolfe, J. M., Regan, M. S., Pentelute, B. L., Agar, N.Y.R., Cho, C. F. (2018). Blood-brain-barrier organoids for investigating the permeability of CNS therapeutics. *Nat Protoc.* 13(12):2827-43. doi: 10.1038/s41596-018-0066-x. PMID: 30382243.

Berridge, M.J. (2010) Calcium hypothesis of Alzheimer's disease. *Pflugers Arch.* 459(3):441-9. doi: 10.1007/s00424-009-0736-1. PMID: 19795132.

Biagi, E., Nylund, L., Candela, M., Ostan, R., Bucci, L., Pini, E., Nikkila, J., Monti, D., Satokari, R., Franceschi, C., Brigidi, P., De Vos, W. (2010). Through ageing, and beyond: gut microbiota and inflammatory status in seniors and centenarians. *PLoS One.* 17;5(5):e10667. doi: 10.1371/journal.pone.0010667. Erratum in: *PLoS One.* 2010;5(6). doi: 10.1371/annotation/df45912f-d15c-44ab-8312-e7ec0607604d. PMID: 20498852.

Bielecka, E., Scavenius, C., Kantyka, T., Jusko, M., Mizgalska, D., Szmigielski, B., Potempa, B., Enghild, J.J., Prossnitz, E.R., Blom, A.M., Potempa, J. (2014) Peptidyl

arginine deiminase from *Porphyromonas gingivalis* abolishes anaphylatoxin C5a activity. *J Biol Chem.* 289(47):32481-7. doi: 10.1074/jbc.C114.617142.

PMID: 25324545.

Blanchette, M., Daneman, R. (2015) Formation and maintenance of the BBB. *Mech Dev.*

138 (1):8-16. doi: 10.1016/j.mod.2015.07.007. PMID: 26215350.

Blom, C., Deller, B.L., Fraser, D.D., Patterson, E.K., Martin, C.M., Young, B., Liaw, P.C.,

Yazdan-Ashoori, P., Ortiz, A., Webb, B., Kilmer, G., Carter, D.E., Cepinskas, G.

(2015) Human severe sepsis cytokine mixture increases β 2-integrin-dependent polymorphonuclear leukocyte adhesion to cerebral microvascular endothelial cells in vitro. *Crit Care.* 19(1):149. doi: 10.1186/s13054-015-0883-z.

PMID: 25882865.

Blufstein, A., Behm, C., Nguyen, P.Q., Rausch-Fan, X., Andrukhov, O. (2018) Human

periodontal ligament cells exhibit no endotoxin tolerance upon stimulation with

Porphyromonas gingivalis lipopolysaccharide. *J Periodont Res.* 53(4): 589– 97.

doi: 10.1111/jre.12549. PMID: 29582430.

Bohnstedt, S., Cullinan, M.P., Ford, P.J., Palmer, J.E., Leishman, S.J., Westerman, B.,

Marshall, R.I., West, M.J., Seymour, G.J. (2010). High antibody levels to *P.*

gingivalis in cardiovascular disease. *J Dent Res.* 89(9):938-42.

doi: 10.1177/0022034510370817. PMID: 20519492.

Braak, H., Braak, E. (1991) Neuropathological staging of Alzheimer-related changes. *Acta*

Neuropathol. 82(4):239-59. doi: 10.1007/BF00308809. PMID: 1759558.

Braak,H., Braak, E. (1995). Staging of Alzheimer's disease-related neurofibrillary changes.

Neurobiol. Aging 16, 271-78. doi.org/10.1016/0197-4580(95)00021-6.

PMID: 7566337

Brandscheid, C., Schuck, F., Reinhardt, S., Schafer, K-H., Pietrzik, C.U., Grimm, M.,

Hartmann, T., Schwiertz, A., Endres, K. (2017) Altered Gut Microbiome

Composition and Tryptic Activity of the 5xFAD Alzheimer's Mouse Model.

J Alzheimers Dis. 56(2):775-88. doi: 10.3233/JAD-160926. PMID: 28035935.

Branton, W. G., Ellestad, K. K., Maingat, F., Wheatley, B. M., Rud, E., Warren, R. L., Holt,

R.A., Surette, M.G., Power, C. ((2013) Brain microbial populations in HIV/AIDS:

α -proteobacteria predominate independent of host immune status. PLoS One.

8(1):e54673. doi: 10.1371/journal.pone.0054673. PMID: 23355888.

Bregaint, S., Boyer, E., Fong, S.B., Meuric, V., Bonnaure-Mallet, M., Jolivet-Gougeon, A.

(2022) Porphyromonas gingivalis outside the oral cavity.

Odontology. 110(1):1-19. doi: 10.1007/s10266-021-00647-8. PMID: 34410562.

Bronzuoli, M.R., Iacomino, A., Steardo, L., Scuderi, C. (2016) Targeting neuroinflammation

in Alzheimer's disease. J Inflamm Res. 9:199–208. doi: 10.2147/JIR.S86958.

PMID: 27843334.

Brooks, J.P. (2016) Challenges for case-control studies with microbiome data. Ann

Epidemiol. 26(5):336–41.e1. doi: 10.1016/j.annepidem.2016.03.009.

PMID: 27255739.

Brown, G.C. (2019) The endotoxin hypothesis of neurodegeneration. J Neuroinflammation.

16(1):180. doi: 10.1186/s12974-019-1564-7. PMID: 31519175.

Bryant, C.E., Spring, D.R., Gangloff, M., Gay, N.J. (2010). The molecular basis of the host response to lipopolysaccharide. *Nat Rev Microbiol.* 8(1):8-14.

doi: 10.1038/nrmicro2266. PMID: 19946286.

Burry, R. W. (2011). Controls for immunocytochemistry: an update. *J Histochem Cytochem.*

59(1):6-12. doi: 10.1369/jhc.2010.956920. PMID: 20852036.

Carrasco, L., Alonso, R., Pisa, D., Rábano, A. (2017) Alzheimer's disease and fungal

infection. In: Miklossy J, editor. *Handbook of infection and Alzheimer's Disease.*

Amsterdam: IOS Press; p. 281–94. doi: 10.3233/978-1-61499-706-1-281.

Carter, C.J., France, J., Crean, S., Singhrao, S.K. (2017) The *Porphyromonas*

gingivalis/host interactome shows enrichment in GWASdb genes related to

Alzheimer's disease, diabetes and cardiovascular diseases. *Front Aging*

Neurosci. 9:408. doi: 10.3389/fnagi.2017.00408. PMID: 29311898.

Carvalho-Tavares, J., Hickey, M.J., Hutchison, J., Michaud, J., Sutcliffe, I.T., Kubes, P.

(2000) A role for platelets and endothelial selectins in tumor necrosis factor α

-induced leukocyte recruitment in the brain microvasculature. *Circ Res.*

87(12):1141-8. doi: 10.1161/01.res.87.12.1141. PMID: 11110771.

Castillo, D.J., Rifkin, R.F., Cowan, D.A., Potgieter, M. (2019) The Healthy Human Blood

Microbiome: fact or fiction? *Front Cell Infect Microbiol.* 9:148.

doi:10.3389/fcimb.2019.00148. PMID: 31139578.

Cerutti, C., Ridley, A.J. (2017) Endothelial cell-cell adhesion and signalling. *Exp Cell Res.*

358(1):31-8. doi: 10.1016/j.yexcr.2017.06.003.

PMID:28602626.

Chen, C., Chen, Y.H., Lin, W.W. (1999). Involvement of p38 mitogen-activated protein kinase in lipopolysaccharide-induced iNOS and COX-2 expression in J774 macrophages. *Immunology* 97(1), 124-9. doi:10.1046/j.1365-2567.1999.00747.x
PMID: 10447723.

Chen, C.K., Wu, Y.T., Chang, Y.C. (2017a). Association between chronic periodontitis and the risk of Alzheimer's disease: a retrospective, population-based, matched-cohort study. *Alzheimers Res Ther.* 9(1):56. doi:10.1186/s13195-017-0282-6.
PMID: 28784164.

Chen, T., Siddiqui, H., Olsen, I. (2017b). In silico comparison of 19 *Porphyromonas gingivalis* strains in genomics, phylogenetics, phylogenomics and functional genomics. *Front Cell Infect Microbiol.* 7:28. doi: 10.3389/fcimb.2017.00028.
PMID: 28261563.

Chen, T., Yu, W.H., Izard, J., Baranova, O.V., Lakshmanan, A., Dewhirst, F.E. (2010). The human oral microbiome database: a web accessible resource for investigating oral microbe taxonomic and genomic information. *Database (Oxford).* 2010:baq013. doi: 10.1093/database/baq013. PMID: 20624719.

Chui, R., Dorovini-Zis, K. (2010) Regulation of CCL2 and CCL3 expression in human brain endothelial cells by cytokines and lipopolysaccharide. *J Neuroinflammation.* 7:1. doi: 10.1186/1742-2094-7-1. PMID: 20047691.

Cipolla, M.J. (2009) *The Cerebral Circulation*. San Rafael (CA): Morgan & Claypool Life Sciences. PMID: 21452434.

Coats, S.R., Kantrong, N., To, T.T., Jain, S., Genco, C.A., McLean, J.S., Darveau, R.P. (2019). The distinct immune-stimulatory capacities of *Porphyromonas gingivalis* strains 381 and ATCC 33277 are determined by the *fimB* allele and gingipain activity. *Infect Immun.* 87(12):e00319-19. doi: 10.1128/IAI.00319-19. PMID: 31570556.

Coleman, A.W. (2013) Analysis of mammalian rDNA internal transcribed spacers. *PLOS ONE* 8(11): e79122. doi: 10.1371/journal.pone.0079122. PMID: 24260162.

Costa, A. S., Agostini, S., Guerini, F. R., Mancuso, R., Zanzottera, M., Ripamonti, E., Racca, V., Nemni, R., Clerici, M. (2017). Modulation of immune responses to herpes simplex virus type 1 by IFNL3 and IRF7 polymorphisms: a study in Alzheimer's disease. *J. Alzheimers.* 60(3), 1055–63. doi: 10.3233/JAD-170520. PMID: 28984602.

Coureuil, M., Lécuyer, H., Bourdoulous, S., Nassif, X. (2017) A journey into the brain: insight into how bacterial pathogens cross blood-brain barriers. *Nat Rev Microbiol.* 15(3):149-59. doi: 10.1038/nrmicro.2016.178. PMID: 28090076.

Cui, J.J., Wang, L.Y., Tan, Z.R., Zhou, H.H., Zhan, X., Yin, J.Y. (2020) MASS Spectrometry-based personalized drug therapy. *Mass Spectrom Rev.* ;39(5-6):523-52. doi: 10.1002/mas.21620. PMID: 31904155.

- Danaei, M., Dehghankhold, M., Ataei, S., Hasanzadeh Davarani, F., Javanmard, R.,
Dokhani, A., Khorasani, S., Mozafari, M.R. (2018). Impact of particle size and
polydispersity index on the clinical applications of lipidic nanocarrier systems.
Pharmaceutics. 10(2):57. doi: 10.3390/pharmaceutics10020057.
PMID: 29783687.
- Dando, S.J., Mackay-Sim, A., Norton, R., Currie, B.J., St John, J.A., Ekberg, J.A.,
Batzloff, M., Ulett, G.C., Beacham, I.R. (2014) Pathogens penetrating the
central nervous system: infection pathways and the cellular and molecular
mechanisms of invasion. Clin Microbiol Rev. 27(4):691–726.
doi:10.1128/CMR.00118-13. PMID: 25278572.
- Daneman, R., Prat, A. (2015) The blood-brain barrier. Cold Spring Harb Perspect Biol.
5;7(1):a020412. doi: 10.1101/cshperspect.a020412.
PMID: 25561720.
- de Molon, R.S., Rossa C. Jr., Thurlings, R.M., Cirelli, J.A., Koenders, M.I. (2019). Linkage of
Periodontitis and Rheumatoid Arthritis: Current Evidence and Potential
Biological Interactions. Int J Mol Sci. 20(18):4541. doi: 10.3390/ijms20184541.
PMID: 31540277.
- Deatherage, B.L., Cookson, B.T. (2012) Membrane vesicle release in bacteria, eukaryotes,
and archaea: a conserved yet underappreciated aspect of microbial life. Infect
Immun. 80(6):1948-57. doi: 10.1128/IAI.06014-11. PMID: 22409932.
- Deo, P. N., Deshmukh, R. (2019). Oral microbiome: Unveiling the fundamentals.

J Oral Maxillofac Pathol. 23(1):122-8. doi: 10.4103/jomfp.JOMFP_304_18.

PMID: 31110428.

Devanga, N. K., Muthuirulandi, D. P., Inbanathan, F. Y., Veeraraghavan, B. (2017).

Accurate differentiation of Escherichia coli and Shigella serogroups: challenges and strategies. New Microbes New Infect. 21:58-62.

doi: 10.1016/j.nmni.2017.09.003. PMID: 29204286.

Di Benedetto, A., Gigante, I., Colucci, S., Grano, M. (2013). Periodontal disease:

Linking the primary inflammation to bone loss. Clin Dev Immunol. 2013:503754.

doi: 10.1155/2013/503754. PMID: 23762091.

Dicarlo, G., Wilcock, D., Henderson, D., Gordon, M., Morgan, D. (2001). Intrahippocampal

LPS injections reduce A β load in APP+PS1 transgenic mice. Neurobiol Aging

22(6):1007-12. doi: 10.1016/s0197-4580(01)00292-5. PMID: 11755009.

Di Marco, L.Y., Venneri, A., Farkas, E., Evans, P.C., Marzo, A., Frangi, A.F. (2015) Vascular

dysfunction in the pathogenesis of Alzheimer's disease—a review of

endothelium-mediated mechanisms and ensuing vicious circles. Neurobiol Dis

82:593–606. doi: 10.1016/j.nbd.2015.08.014. PMID: 26311408.

Ding, D., Wang, X., Li, Q., Li, L., Wu, J. (2021). Research on the glial-lymphatic system

and its relationship with Alzheimer's disease. Front Neurosci. 15:605586.

doi: 10.3389/fnins.2021.605586. PMID: 34220413.

Do Carmo, S., Spillantini, M.G., Cuello, A.C. (2021) Tau pathology in neurological

disorders. Front Neurol. 12:754669. doi: 10.3389/fneur.2021.754669.

PMID:34630315.

Dominy, S.S., Lynch, C., Ermini, F., Benedyk, M., Marczyk, A., Konradi, A., Nguyen, M.,
Haditsch, U., Raha, D., Griffin, C., Holsinger, L.J., Arastu-Kapur, S., Kaba, S.,
Lee, A., Ryder, M.I., Potempa, B., Mydel, P., Hellvard, A., Adamowicz, K.,
Hasturk, H., Walker, G.D., Reynolds, E.C., Faull, R.L.M., Curtis, M.A.,
Dragunow, M., Potempa, J. (2019) *Porphyromonas gingivalis* in Alzheimer's
disease brains: evidence for disease causation and treatment with small-
molecule inhibitors. *Sci Adv.* 5(1):eaau3333. doi: 10.1126/sciadv.aau3333.

PMID: 30746447.

Dorn, B.R., Burks, J.N., Seifert, K.N., Progulske-Fox, A. (2000) Invasion of endothelial and
epithelial cells by strains of *Porphyromonas gingivalis*. *FEMS Microbiol*
Lett. 187(2):139-44. doi: 10.1111/j.1574-6968.2000.tb09150.x. PMID:
10856647.

Dou, K.X., Tan, M.S., Tan, C.C., Cao, X.P., Hou, X.H., Guo, Q.H., Tan, L., Mok, V., Yu, J.T.
(2018) Comparative safety and effectiveness of cholinesterase inhibitors and
memantine for Alzheimer's disease: a network meta-analysis of 41 randomized
controlled trials. *Alzheimers Res Ther.* 10(1):126. doi: 10.1186/s13195-018-
0457-9. PMID: 30591071.

Drachman, D.A., Leavitt, J. (1974) Human memory and the cholinergic system. A
relationship to aging? *Arch Neurol.* 30(2):113-21. doi:
10.1001/archneur.1974.00490320001001. PMID: 4359364.

- Ebnet, K., Suzuki, A., Ohno, S., Vestweber, D. (2004) Junctional adhesion molecules (JAMs): more molecules with dual functions? *J Cell Sci.* 117(Pt 1):19-29. doi: 10.1242/jcs.00930. PMID: 14657270.
- Eigenmann, D.E., Xue, G., Kim, K.S., Moses, A.V., Hamburger, M., Oufir, M. (2013) Comparative study of four immortalized human brain capillary endothelial cell lines, hCMEC/D3, hBMEC, TY10, and BB19, and optimization of culture conditions, for an in vitro blood-brain barrier model for drug permeability studies. *Fluids Barriers CNS.* 10(1):33. doi: 10.1186/2045-8118-10-33. PMID: 24262108.
- Emery, D.C., Shoemark, D.K., Batstone, T.E., Waterfall, C. M., Coghill, J.A., Cerajewska, T.L., Davies, M., West, N.X., Allen, S.J. (2017) 16S rRNA next generation sequencing analysis shows bacteria in Alzheimer's post-mortem brain. *Front Aging Neurosci.* 20;9:195. doi: 10.3389/fnagi.2017.00195. PMID: 28676754.
- Erdő, F., Denes, L., de Lange, E. (2017) Age-associated physiological and pathological changes at the blood-brain barrier: A review. *J Cereb Blood Flow Metab.* 37(1):4-24. doi: 10.1177/0271678X16679420. PMID: 27837191.
- Erdő, F., Krajcsi, P. (2019) Age-related functional and expressional changes in efflux pathways at the blood-brain barrier. *Front Aging Neurosci.* 11:196. doi:10.3389/fnagi.2019.00196. PMID: 31417399.
- Eribe, E.R.K., Olsen, I. (2017) *Leptotrichia* species in human infections II. *J Oral Microbiol.* 9(1):1368848. doi: 10.1080/20002297.2017.1368848. PMID: 29081911.

Esposito, C. L., Nuzzo, S., Kumar, S. A., Rienzo, A., Lawrence, C. L., Pallini, R., Shaw, L.,

Alder, J. E., Ricci-Vitiani, L., Catuogno, S., de Franciscis, V. (2016) A

combined microRNA-based targeted therapeutic approach to eradicate

glioblastoma stem-like cells. *J Control Release*. 238:43-57.

doi: 10.1016/j.jconrel.2016.07.032. PMID: 27448441.

Fabry, Z., Fitzsimmons, K.M., Herlein, J.A., Moninger, T.O., Dobbs, M.B., Hart, M.N. (1993)

Production of the cytokines interleukin 1 and 6 by murine brain microvessel

endothelium and smooth muscle pericytes. *J Neuroimmunol*. 47(1):23-34. doi:

10.1016/0165-5728(93)90281-3. PMID: 8376546.

Fakruddin, M., Chowdhury, A. (2012). Pyrosequencing-an alternative to traditional sanger

sequencing. *Am J Biochem Biotechnol* 8(1):14-20.

doi: 10.3844/ajbb.2012.14.20.

Fan, Y.Y., Cai, Q.L., Gao, Z.Y., Lin, X., Huang, Q., Tang, W., Liu, J.H. (2017) APOE ϵ 4

allele elevates the expressions of inflammatory factors and promotes

Alzheimer's disease progression: A comparative study based on Han and She

populations in the Wenzhou area. *Brain Res Bull*. 132:39-43.

doi: 10.1016/j.brainresbull.2017.04.017. PMID: 28461186.

Farkas, I., Takahashi, M., Fukuda, A., Yamamoto, N., Akatsu, H., Baranyi, L., Tateyama, H.,

Yamamoto, T., Okada, N., Okada, H. (2003). Complement C5a receptor-

mediated signalling may be involved in neurodegeneration in Alzheimer's

disease. *J. Immunol*. 170(11), 5764-71. doi:10.4049/jimmunol.170.11.5764.

PMID: 12759460.

Farley, M.M. (1995) Group B streptococcal infection in older patients. Spectrum of disease and management strategies. *Drugs Aging*;6(4):293-300. doi: 10.2165/00002512-199506040-00004. PMID: 7613018.

Farrugia, C., Stafford, G.P., Potempa, J., Wilkinson, R.N., Chen, Y., Murdoch, C., Widziolek, M. (2021) Mechanisms of vascular damage by systemic dissemination of the oral pathogen *Porphyromonas gingivalis*. *FEBS J.* 288(5):1479-95. doi: 10.1111/febs.15486. PMID: 32681704.

Fleetwood, A.J., Lee, M.K.S., Singleton, W., Achuthan, A., Lee, M.C., O'Brien-Simpson, N.M., Cook, A.D., Murphy, A.J., Dashper, S.G., Reynolds, E.C., Hamilton, J.A. (2017) Metabolic Remodeling, Inflammasome activation, and pyroptosis in macrophages stimulated by *Porphyromonas gingivalis* and its outer membrane vesicles. *Front Cell Infect Microbiol.* 7:351. doi: 10.3389/fcimb.2017.00351. PMID: 28824884.

Fornier, L., Larsen, T., Kilian, M., Holmstrup, P. (2006) Incidence of bacteremia after chewing, tooth brushing and scaling in individuals with periodontal inflammation. *J Clin Periodontol.* 33(6):401-7. doi: 10.1111/j.1600-051X.2006.00924.x. PMID: 16677328.

Frost, B., Jacks, R.L., (2009) Diamond MI. Propagation of tau misfolding from the outside to the inside of a cell. *J Biol Chem.* 284(19):12845-52. doi: 10.1074/jbc.M808759200. PMID: 19282288.

Fu, B.M. (2018) Transport across the blood-brain barrier. *Adv Exp Med Biol*.

1097:235-59. doi: 10.1007/978-3-319-96445-4_13. PMID:

30315549.

Fulop, T., Tripathi, S., Rodrigues, S., Desroches, M., Bunt, T., Eiser, A., Bernier, F.,

Beauregard, P.B., Barron, A.E., Khalil, A., Plotka, A., Hirokawa, K., Larbi, A.,

Bocti, C., Laurent, B., Frost, E.H., Witkowski, J.M. (2021) Targeting impaired

antimicrobial immunity in the brain for the treatment of Alzheimer's disease.

Neuropsychiatr Dis Treat. 17:1311-39. doi: 10.2147/NDT.S264910. PMID:

33976546.

Fung, T., Olson, C., Hsiao, E. (2017) Interactions between the microbiota, immune and

nervous systems in health and disease. *Nat Neurosci* 20(2): 145–55.

doi: 10.1038/nn.4476. Epub 2017 Jan 16. PMID: 28092661.

Furuta, N., Tsuda, K., Omori, H., Yoshimori, T., Yoshimura, F., Amano, A. (2009)

Porphyromonas gingivalis outer membrane vesicles enter human epithelial cells

via an endocytic pathway and are sorted to lysosomal compartments. *Infect*

Immun 77(10):4187-96. doi: 10.1128/IAI.00009-09. PMID: 19651865.

Gaugler, J., James, B., Johnson, T., Scholz, K., and Weuve, J. (2016). Alzheimer's

association report; Alzheimer's disease facts and figures. *Alzheimers Dement*.

12(4): 459-509. doi:10.1016/j.jalz.2016.03.001. PMID: 27570871.

Genco, R.J., Van Dyke, T.E. (2010) Prevention: Reducing the risk of CVD in patients with

periodontitis. *Nat Rev Cardiol*. 7(9):479-80. doi: 10.1038/nrcardio.2010.120.

PMID: 20725103.

Ghannoum, M.A., Jurevic, R.J., Mukherjee, P.K., Cui, F., Sikaroodi, M., Naqvi, A., Gillevet, P.M. (2010) Characterization of the oral fungal microbiome (mycobiome) in healthy individuals. *PLoS Pathog.* 6(1):e1000713. doi: 10.1371/journal.ppat.1000713. PMID: 20072605.

Gloor, G.B., Wu, J.R., Pawlowsky-Glahn, V., Egozcue, J.J. (2016) It's all relative: analyzing microbiome data as compositions. *Ann Epidemiol.* 26(5):322–9. doi: 10.1016/j.annepidem.2016.03.003. PMID: 27143475.

Greene, C., Hanley, N., Campbell, M. (2019) Claudin-5: gatekeeper of neurological function. *Fluids Barriers CNS* 16(1):3. doi: 10.1186/s12987-019-0123-z. PMID: 30691500.

Guo, W., Wang, P., Liu, Z.H., Ye, P. (2018) Analysis of differential expression of tight junction proteins in cultured oral epithelial cells altered by *Porphyromonas gingivalis*, *Porphyromonas gingivalis* lipopolysaccharide, and extracellular adenosine triphosphate. *Int J Oral Sci* 10(1):e8. doi: 10.1038/ijos.2017.51. PMID: 29319048.

Guo, T., Zhang, D., Zeng, Y., Huang, T.Y., Xu, H., Zhao, Y. (2020) Molecular and cellular mechanisms underlying the pathogenesis of Alzheimer's disease. *Mol Neurodegener.* 15(1):40. doi: 10.1186/s13024-020-00391-7. PMID: 32677986.

Gyarmati, P., Kjellander, C., Aust, C., Kalin, M., Öhrmalm, L., Giske, C.G. (2015) Bacterial landscape of bloodstream infections in neutropenic patients via high

throughput sequencing. PLoS One. 2015;10(8):e0135756.

doi:10.1371/journal.pone.0135756. PMID: 26270467

Ha, J.Y., Choi, S.Y., Lee, J.H., Hong, S.H., Lee, H.J. (2020) Delivery of

periodontopathogenic extracellular vesicles to brain monocytes and microglial

IL-6 promotion by RNA cargo. Front Mol Biosci 7:596366.

doi: 10.3389/fmolb.2020.596366. PMID: 33330627

Haditsch, U., Roth, T., Rodriguez, L., Hancock, S., Cecere, T., Nguyen, M., Arastu-Kapur,

S., Broce, S., Raha, D., Lynch, C.C., Holsinger, L.J., Dominy, S.S., Ermini, F.

(2020) Alzheimer's disease-like neurodegeneration in Porphyromonas

gingivalis infected neurons with persistent expression of active gingipains. J

Alzheimers Dis 75 (4):1361-76. doi: 10.3233/JAD-200393. PMID: 32390638.

Hajishengallis, G. (2011). Immune evasion strategies of Porphyromonas gingivalis. J Oral

Biosci. 2011;53(3):233-40. doi: 10.2330/joralbiosci.53.233. PMID: 22162663.

Hajishengallis, G. (2015) Periodontitis: from microbial immune subversion to systemic

inflammation. Nat Rev Immunol. 15(1):30-44. doi: 10.1038/nri3785.

PMID: 25534621.

Hajishengallis, G. (2021), Oral bacteria and leaky endothelial junctions in remote extraoral

sites. FEBS J. 288(5):1475-78. doi: 10.1111/febs.15510. PMID: 32844552.

Hajishengallis, G., Darveau, R.P., Curtis, M.A. (2012) The keystone-pathogen hypothesis.

Nat Rev Microbiol. 10(10):717-25. doi: 10.1038/nrmicro2873. PMID: 22941505.

Hajishengallis, G., Lamont, R.J. (2012) Beyond the red complex and into more complexity:

the polymicrobial synergy and dysbiosis (PSD) model of periodontal disease etiology. *Mol Oral Microbiol.* 27(6):409-19.

doi: 10.1111/j.2041-1014.2012.00663.x. PMID: 23134607.

Hajishengallis, G., Lamont, R.J. (2014). Breaking bad: manipulation of the host response by *Porphyromonas gingivalis*. *Eur J Immunol.* 44(2): 328-38.

doi:10.1002/eji.201344202. PMID: 24338806.

Hajishengallis, G., Lamont, R.J. (2016). Dancing with the stars: How choreographed bacterial interactions dictate nosymbiocity and give rise to keystone pathogens, accessory pathogens, and pathobionts. *Trends Microbiol.*

24(6): 477-89. doi:10.1016/j.tim.2016.02.010. PMID: 26968354.

Hajishengallis, G., Lamont, R.J. (2021) Polymicrobial communities in periodontal disease: their quasi-organismal nature and dialogue with the host. *Periodontol 2000.*

86(1): 210–30. doi: 10.1111/prd.12371.PMID: 33690950.

Halliday, M.R., Rege, S.V., Ma, Q., Zhao, Z., Miller, C.A., Winkler, E.A., Zlokovic, B.V.

(2016). Accelerated pericyte degeneration and blood-brain barrier breakdown in apolipoprotein E4 carriers with Alzheimer's disease. *J. Cereb. Blood Flow*

Metab. 36(1): 216-27. doi:10.1038/jcbfm.2015.44. PMID: 25757756.

Han, E.C., Choi, S.Y., Lee, Y., Park, J.W., Hong, S.H., Lee, H.J. (2019) Extracellular RNAs in periodontopathogenic outer membrane vesicles promote TNF- α production

in human macrophages and cross the blood-brain barrier in mice. *FASEB J.*

33(12):13412-22. doi: 10.1096/fj.201901575R. PMID: 31545910.

Harris, S.A., and Harris, E.A. (2017). Herpes simplex virus type I and other pathogens are key causative factors in sporadic Alzheimer's disease. In: Handbook of Infection and Alzheimer's Disease, ed. J. Miklossy (IOS Press, Amsterdam, The Netherlands), 241-78. doi:10.3233/JAD-142853.

He, Y., Shiotsu, N., Uchida-Fukuhara, Y., Guo, J., Weng, Y., Ikegame, M., Wang, Z., Ono, K., Kamioka, H., Torii, Y., Sasaki, A., Yoshida, K., Okamura, H. (2020) Outer membrane vesicles derived from Porphyromonas gingivalis induced cell death with disruption of tight junctions in human lung epithelial cells. Arch Oral Biol. 118:104841. doi: 10.1016/j.archoralbio. PMID: 32717445.

Helms, H.C., Abbott, N.J., Burek, M., Cecchelli, R., Couraud, P.O., Deli, M.A., Förster, C., Galla, H.J., Romero, I.A., Shusta, E.V., Stebbins, M.J., Vandenhoute, E., Weksler, B., Brodin, B. (2016) In vitro models of the blood-brain barrier: An overview of commonly used brain endothelial cell culture models and guidelines for their use. J Cereb Blood Flow Metab. 36(5):862-90. doi: 10.1177/0271678X16630991. PMID: 26868179.

Helms, H.C.C., Nielsen, C.U., Waagepetersen, H.S., Brodin, B. (2017) Glutamate transporters in the blood-brain barrier. Adv Neurobiol. 16:297-314. doi:10.1007/978-3-319-55769-4_15. PMID: 28828617.

Heneka, M. T., Golenbock, D. T., Latz, E. (2015). Innate immunity in Alzheimer's disease. Nat. Immunol. 16(3): 229–36. doi: 10.1038/ ni.3102. PMID: 25689443.

Herber-Jonat, S., Mittal, R., Gsinn, S., Bohnenkamp, H., Guenzi, E., Schulze, A. (2011).

Comparison of lung accumulation of cationic liposomes in normal rats and LPS-treated rats. *Inflam. Res.* 60(3): 245-53. doi:10.1007/s00011-010-0260-y. PMID: 20938712.

Herzberg, M.C., Meyer, M.W. (1996) Effects of oral flora on platelets: possible consequences in cardiovascular disease. *J Periodontol.* 67(10):1138-42. doi: 10.1902/jop.1996.67.10s.1138. PMID: 8910832.

Hill, J.M., Clement, C., Pogue, A.I., Bhattacharjee, S., Zhao, Y., Lukiw, W.J. (2014). Pathogenic microbes, the microbiome, and Alzheimer's disease (AD). *Front Aging Neurosci.* 6:127. doi: 10.3389/fnagi.2014.00127. PMID: 24982633.

Hintermann, E., Haake, S.K., Christen, U., Sharabi, A., Quaranta, V. (2002). Discrete proteolysis of focal contact and adherens junction components in *Porphyromonas gingivalis*-infected oral keratinocytes: a strategy for cell adhesion and migration disabling. *Infect. Immun.* 70(10): 5846-56. doi:10.1128/IAI.70.10.5846-5856.2002. PMID: 12228316.

Hirasawa, M., Kurita-Ochiai, T. (2018). *Porphyromonas gingivalis* induces apoptosis and autophagy via ER stress in human umbilical vein endothelial cells. *Mediators Inflamm.* 2018:1967506. doi: 10.1155/2018/1967506. PMID: 30150893.

Hoffmann, A., Bredno, J., Wendland, M., Derugin, N., Ohara, P., Wintermark, M. (2011). High and low molecular weight fluorescein isothiocyanate (FITC)-dextrans to assess blood-brain barrier disruption: technical considerations.

Transl Stroke Res. 2(1):106-11. doi: 10.1007/s12975-010-0049-x.

PMID: 21423333.

Holmes, C., Cunningham, C., Zotova, E., Woolford, J., Dean, C., Kerr, S., Culliford, D.,

Perry, V.H. (2009). Systemic inflammation and disease progression in

Alzheimer disease. *Neurology* 73(10):768-74.

doi: 10.1212/WNL.0b013e3181b6bb95.

PMID: 1973817.

Holmstrup, P., Damgaard, C., Olsen, I., Klinge, B., Flyvbjerg, A., Nielsen, C.H., Hansen,

P.R. (2017) Comorbidity of periodontal disease: two sides of the same coin?

An introduction for the clinician. *J Oral Microbiol.* 9(1):1332710.

doi: 10.1080/20002297.2017.1332710. PMID: 28748036.

Huang, H., Rose, J.L., and Hoyt, D.G. (2004). p38 mitogen-activated protein kinase

mediates synergistic induction of inducible nitric-oxide synthase by

lipopolysaccharide and interferon-gamma through signal transducer and

activator of transcription 1 Ser727 phosphorylation in murine aortic

endothelial cells. *Mol Pharmacol.* 66(2):302-11. doi: 10.1124/mol.66.2.302.

PMID: 15266021.

Hughes, P., Marshall, D., Reid, Y., Parkes, H., Gelber, C. (2007) The costs of using

unauthenticated, over-passaged cell lines: how much more data do we

need? *Biotechniques.* 43(5):575, 577-8, 581-2 passim. doi:

10.2144/000112598. Erratum in: *Biotechniques.*;44(1):47. PMID: 18072586.

Iarosh, O.A. (1992). Matematicheskiĭ analiz pronitsaemosti gematoéntsefalicheskogo ber'era pri bakterial'nom meningoéntsefalite [Mathematical analysis of permeability of the blood-brain barrier in bacterial meningoencephalitis]. Zh Nevropatol Psikiatr Im S S Korsakova. 92(2):33-6. PMID: 1326169.

Igboin, C. O., Griffen, A. L., Leys, E. J. (2009). Porphyromonas gingivalis strain diversity. J Clin Microbiol. 47(10):3073-81. doi: 10.1128/JCM.00569-09. PMID: 19675220.

Ilievski, V., Zuchowska, P.K., Green, S.J., Toth, P.T., Ragozzino, M.E., Le, K., Aljewari, H.W., O'Brien-Simpson, N.M., Reynolds, E.C., Watanabe, K. (2018) Chronic oral application of a periodontal pathogen results in brain inflammation, neurodegeneration and amyloid beta production in wild type mice. PLoS One. 13(10):e0204941. doi: 10.1371/journal.pone.0204941. PMID: 30281647.

Itzhaki, R.F., Lathe, R., Balin, B.J., Ball, M.J., Bearer, E.L., Braak, H., Bullido, M.J., Carter, C., Clerici, M., Cosby, S.L., Del Tredici, K., Field, H., Fulop, T., Grassi, C., Griffin, W.S., Haas, J., Hudson, A.P., Kamer, A.R., Kell, D.B., Licastro, F., Letenneur, L., Lövheim, H., Mancuso, R., Miklossy, J., Otth, C., Palamara, A.T., Perry, G., Preston, C., Pretorius, E., Strandberg, T., Tabet, N., Taylor-Robinson, S.D., Whittum-Hudson, J.A. (2016). Microbes and Alzheimer's Disease. J Alzheimers Dis. 51(4):979-84. doi: 10.3233/JAD-160152. PMID: 26967229.

Itzhaki, R.F. (2016). Herpes and Alzheimer's disease: subversion in the central nervous

system and how it might be halted. *J Alzheimers Dis.* 54(4):1273-81.

doi: 10.3233/JAD-160607. PMID: 27497484.

Jaeger, L. B., Dohgu, S., Sultana, R., Lynch, J. L., Owen, J. B., Erickson, M. A., Shah, G.N.,

Price, T.O., Fleegal-Demotta, M.A., Butterfield, D.A., Banks, W.A. (2009).

Lipopolysaccharide alters the blood-brain barrier transport of amyloid beta

protein: a mechanism for inflammation in the progression of Alzheimer's

disease. *Brain Behav Immun.* (4):507-17. doi: 10.1016/j.bbi.2009.01.017.

PMID: 19486646.

Jayadev, S., Case, A., Alajajian, B., Eastman, A.J., Moller, T., Garden, G.A. (2013).

Presenilin 2 influences miR146 level and activity in microglia. *J. Neurochem.*

127 (5):592-9. doi: 10.1111/jnc.12400. PMID: 23952003.

Jia, J., Wei, C., Jia, L., Tang, Y., Liang, J., Zhou, A., Li, F., Shi, L., Doody, R.S. (2017)

Efficacy and safety of Donepezil in Chinese patients with severe

Alzheimer's disease: A Randomized Controlled Trial. *J Alzheimers Dis.*

56(4):1495-04. doi: 10.3233/JAD-161117. PMID: 28157100.

Jiang, C., Li, G., Huang, P., Liu, Z., Zhao, B. (2017). The gut microbiota and Alzheimer's

disease. *J. Alzheimers Dis.* 58(1), 1-15. doi:10.3233/JAD-161141.

PMID: 28372330.

Jin, M., O'Nuallain, B., Hong, W., Boyd, J., Lagomarsino, V. N., O'Malley, T. T., Liu, W.,

Vanderburg, C. R., Frosch, M. P., Young-Pearse, T., Selkoe, D. J., Walsh,

D. M. (2018). An in vitro paradigm to assess potential anti-A β antibodies for

Alzheimer's disease. *Nat Commun.* 9(1), 2676.

doi:10.1038/s41467-018-05068-w. PMID: 29992960.

Johnson, J.S., Spakowicz, D.J., Hong, B.Y, Petersen, L.M., Demkowicz, P., Chen, L., Leopold, S.R., Hanson, B.M., Agresta, H.O., Gerstein, M., Sodergren, E., Weinstock, G.M. (2019). Evaluation of 16S rRNA gene sequencing for species and strain-level microbiome analysis. *Nat Commun.* 10(1):5029.

doi: 10.1038/s41467-019-13036-1. PMID: 31695033.

Johnson, M. J., Thatcher, E., Cox, M. E. (1995). Techniques for controlling variability in gram staining of obligate anaerobes. *J Clin Microbiol.* 33(3):755-8.

doi: 10.1128/jcm.33.3.755-758.1995. PMID: 7538512.

Kamer, A.R., Craig, R.G., Pirraglia, E., Dasanayake, A.P., Norman. R. G., Boylan, R.J., Nehorayoff, A., Glodzik, L., Brys, M., de Leon, M.J. (2009). TNF-alpha and antibodies to periodontal bacteria discriminate between Alzheimer's disease patients and normal subjects. *J Neuroimmunol.* 216(1-2):92-7.

doi: 10.1016/j.jneuroim.2009.08.013. PMID: 19767111.

Kanoh, Y., Ohara, T., Akahoshi, T. (2011). Acute inflammatory biomarkers in cerebrospinal fluid as indicators of blood cerebrospinal fluid barrier damage in Japanese subjects with infectious meningitis. *Clin Lab.* 57(1-2):37-46. PMID:

21391463.

Katz, J., Sambandam, V., Wu, J.H., Michalek, S.M., Balkovetz, D.F. (2000).

Characterization of *Porphyromonas gingivalis*-induced degradation of

epithelial cell junctional complexes. *Infect. Immun.* 68(3), 1441-49.

doi:10.1128/IAI.68.3.1441-1449.2000. PMID: 10678958.

Katz, J., Yang, Q. B., Zhang, P., Potempa, J., Travis, J., Michalek, S. M., Balkovetz, D. F.

(2002). Hydrolysis of epithelial junctional proteins by *Porphyromonas*

gingivalis gingipains. *Infection and immunity*, 70(5): 2512–18.

doi: 10.1128/IAI.70.5.2512-2518.2002. PMID: 11953390.

Kaur, D., Behl, T., Sehgal, A., Singh, S., Sharma, N., Bungau, S. (2021). Multifaceted

Alzheimer's disease: building a roadmap for advancement of novel

therapies. *Neurochem Res.* 46(11):2832-51. doi: 10.1007/s11064-021-

03415-w. PMID: 34357520.

Khan, S.S., Bloom, G.S. (2016) Tau: the center of a signalling nexus in Alzheimer's disease.

Front Neurosci 10:31. doi: 10.3389/fnins.2016.00031.

PMID: 26903798.

Khanna, S., Tosh, P. K. (2014). A clinician's primer on the role of the microbiome in human

health and disease. *Mayo Clin Proc.* 89(1):107-14.

doi: 10.1016/j.mayocp.2013.10.011. PMID: 24388028.

Khot, P. D., Fisher, M. A. (2013). Novel approach for differentiating *Shigella* species and

Escherichia coli by matrix-assisted laser desorption ionization-time of flight

mass spectrometry. *J Clin Microbiol.* 51(11):3711-6.

doi: 10.1128/JCM.01526-13. PMID: 23985919.

Kim, B.J., Shusta, E.V., Doran, K.S. (2019). Past and current perspectives in modelling

bacteria and blood–brain barrier interactions. *Front Microbiol.* 10:1336.

doi: 10.3389/fmicb.2019.01336. PMID: 31263460.

Kishi, T., Matsunaga, S., Oya, K., Nomura, I., Ikuta, T., Iwata, N. (2017). Memantine for Alzheimer's disease: an updated systematic review and meta-analysis. *J Alzheimers Dis.*60(2):401–25. doi: 10.3233/JAD-170424. PMID: 28922160.

Ko, Y., Lee, E.M., Park, J.C., Gu, M.B., Bak, S., Ji, S. (2020). Salivary microbiota in periodontal health and disease and their changes following nonsurgical periodontal treatment. *J Periodontal Implant Sci.* 50(3):171-82.

doi:10.5051/jpis.2020.50.3.171. PMID: 32617182.

Kouki, M.A., Pritchard, A.B., Alder, J.E., Crean, S. (2022). Do periodontal pathogens or associated virulence factors have a deleterious effect on the blood-brain barrier, contributing to Alzheimer's disease? *J Alzheimers Dis.*

85(3):957-73. doi: 10.3233/JAD-215103. PMID: 34897087.

Kozak, M., Dabrowska-Zamojcin, E., Mazurek-Mochol, M., Pawlik, A. (2020). Cytokines and Their Genetic Polymorphisms Related to Periodontal Disease.

J Clin Med. 9(12):4045. doi: 10.3390/jcm9124045. PMID: 33327639.

Kramer, M.F., Coen, D.M. (2001) Enzymatic amplification of DNA by PCR: standard procedures and optimization. *Curr Protoc Immunol.* Chapter 10:Unit 10.20.

doi: 10.1002/0471142735.im1020s24. PMID: 18432685.

Kulkarni, M.R., Bhat, K.G., Thomas, B.S., Bhat, G.S., Kulkarni, R.D. (2018). Identification of multiple strains of *Porphyromonas gingivalis* using heteroduplex

polymerase chain reaction in varying severity of chronic periodontitis.

Indian J Med Microbiol. 36(1):81-6. doi: 10.4103/ijmm.IJMM_17_434.

PMID: 29735832.

Kumar, D.K.V., Choi, S.H., Washicosky, K.J., Eimer, W.A., Tucker, S., Ghofrani, J.,

Lefkowitz, A., McColl, G., Goldstein, L.E., Tanzi, R.E., Moir, R.D. (2016).

Amyloid- β peptide protects against microbial infection in mouse and worm

models of Alzheimer's disease. Sci Transl Med. 8(340):340ra72.

doi: 10.1126/scitranslmed.aaf1059. PMID: 27225182.

Kumar, P.S., Leys, E.J., Bryk, J.M., Martinez, F.J., Moeschberger, M.L., Griffen, A.L. (2006)

Changes in periodontal health status are associated with bacterial

community shifts as assessed by quantitative 16S cloning and

sequencing. J Clin Microbiol 44(10), 3665–73. doi: 10.1128/JCM.00317-06.

PMID: 17021095.

Kumar, S., Shaw, L., Lawrence, C., Lea, R., Alder, J. (2014). 'P50 * Developing a

Physiologically Relevant Blood Brain Barrier Model for the Study of Drug

Disposition in Glioma'. Neuro-Oncology, 16(suppl 6):8.

doi:10.1093/neuonc/nou249.38.

Kummer, D., Ebnet, K. (2018). Junctional Adhesion Molecules (JAMs): The JAM-Integrin

connection. Cells. 7(4):25. doi: 10.3390/cells7040025. PMID: 29587442.

Kuczynski, J., Lauber, C.L., Walters, W.A., Parfrey, L.W., Clemente, J.C., Gevers, D.,

Knight, R. (2011). Experimental and analytical tools for studying the human

microbiome. *Nat Rev Genet.* 13(1):47-58.

doi: 10.1038/nrg3129. PMID: 22179717.

Larsen, N., Vogensen, F.K., van den Berg, F.W., Nielsen, D.S., Andreasen, A.S., Pedersen,

B.K., Al-Soud, W.A., Sørensen, S.J., Hansen, L.H., Jakobsen, M. (2010)

Gut microbiota in human adults with type 2 diabetes differs from non-

diabetic adults. *PLoS One.* 5(2):e9085. doi: 10.1371/journal.pone.0009085.

PMID: 20140211.

Laugisch, O., Johnen, A., Maldonado, A., Ehmke, B., Bürgin, W., Olsen, I., Potempa, J.,

Sculean, A., Duning, T., Eick, S. (2018). Periodontal Pathogens and

Associated Intrathecal Antibodies in Early Stages of Alzheimer's Disease.

J Alzheimers Dis. 66(1):105-14. doi: 10.3233/JAD-180620. PMID: 30223397.

Lee, D.C., Rizer, J., Selenica, M.B., Reid, P., Kraft, C., Johnson, A., Blair, L., Gordon, M.N.,

Dickey, C.A., Morgan, D. (2010). LPS- induced inflammation exacerbates

phospho-tau pathology in rTg4510 mice. *J Neuroinflammation.* 7:56.

doi: 10.1186/1742-2094-7-56. PMID: 20846376.

Leira, Y., Dominguez, C., Seoane, J., Seoane-Romero, J., Pias-Peleiteiro, J.M., Takkouche,

B., Blanco, J., Aldrey, J.M. (2017). Is periodontal disease associated with

Alzheimer's disease? A systematic review with meta-analysis.

Neuroepidemiology. 48 (1-2):21-31. doi: 10.1159/000458411. PMID: 28219071.

Levi, S., Finazzi, D. (2014). Neurodegeneration with brain iron accumulation: update on

pathogenic mechanisms. *Front Pharmacol.* 5:99.

doi: 10.3389/fphar.2014.00099. PMID: 24847269.

Li, W., Chen, Z., Chin, I., Chen, Z., Dai, H. (2018). The role of VE-cadherin in blood-brain barrier integrity under central nervous system pathological conditions.

Current Neuropharmacology. 16(9):1375-84.

doi:10.2174/1570159x16666180222164809. PMID: 29473514.

Li, X., Kolltveit, K.M., Tronstad, L., and Olsen, I. (2000). Systemic diseases caused by oral infection. Clin. Microbiol. Rev. (4):547-58. doi: 10.1128/CMR.13.4.547.

PMID: 11023956.

Liebner, S., Dijkhuizen, R. M., Reiss, Y., Plate, K. H., Agalliu, D., Constantin, G. (2018).

Functional morphology of the blood-brain barrier in health and disease.

Acta Neuropathol. 135(3), 311–36. doi: 10.1007/s00401-018-1815-1.

PMID: 29411111.

Liu, P., Wu, L., Peng, G., Han, Y., Tang, R., Ge, J., Zhang, L., Jia, L., Yue, S., Zhou, K., Li,

L., Luo, B., Wang, B. (2019) Altered microbiomes distinguish Alzheimer's

disease from amnesic mild cognitive impairment and health in a Chinese

cohort. Brain Behav Immun. 80:633-43. doi: 10.1016/j.bbi.2019.05.008.

PMID: 31063846.

Lloyd-Price, J., Mahurkar, A., Rahnavard, G., Crabtree, J., Orvis, J., Hall, A.B., Brady, A.,

Creasy, H.H., McCracken, C., Giglio, M.G., McDonald, D., Franzosa, E.A.,

Knight, R., White, O., Huttenhower, C. (2017). Strains, functions and dynamics

in the expanded human microbiome project. Nature. 550(7674):61-66.

doi: 10.1038/nature23889. PMID: 28953883.

Lochhead, J. J., Yang, J., Ronaldson, P.T., Davis, T. P. (2020). Structure, function, and regulation of the blood-brain barrier tight junction in central nervous system disorders. *Front Physiol.* 11:914. doi: 10.3389/fphys.2020.00914. PMID: 32848858.

Loesche, W.J., Lopatin, D.E. (1998). Interactions between periodontal disease, medical diseases and immunity in the older individual. *Periodontol.* 2000, 16:80–105. doi: 10.1111/j.1600-0757.1998.tb00117.x. PMID:10337306.

Logan, S., Arzua, T., Canfield, S.G., Seminary, E.R., Sison, S.L., Ebert, A.D., Bai, X. (2019). Studying human neurological disorders using induced pluripotent stem cells: from 2D monolayer to 3D organoid and blood brain barrier models. *Compr Physiol.* 9(2):565-611. doi: 10.1002/cphy.c180025. PMID: 30873582.

Lorenz, T. C. (2012). Polymerase chain reaction: basic protocol plus troubleshooting and optimization strategies. *J Vis Exp.* (63):e3998. doi: 10.3791/3998. PMID: 22664923.

Lukiw, W.J. (2016). *Bacteroides fragilis* lipopolysaccharide and inflammatory signaling in Alzheimer's disease. *Front. Microbiol.* 7:1544. doi:10.3389/fmicb.2016.01544. PMID: 27725817.

Ma, Y., Ji, J., Li, G., Yang, S., Pan, S. (2018). Effects of donepezil on cognitive functions and the expression level of β -amyloid in peripheral blood of patients with Alzheimer's disease. *Exp Ther Med.*15(2):1875-78.

doi:10.3892/etm.2017.5613.

Maheshwari, P., Eslick, G.D. (2017). Bacterial infection increases the risk of Alzheimer's disease: An evidence-based assessment. In Handbook of Infection and Alzheimer's Disease, Miklossy J, ed. IOS Press, Amsterdam.

doi:10.3233/978-1-61499-706-151.

Margaryan, H., Dorosh, A., Capkova, J., Manaskova-Postlerova, P., Philimonenko, A.,

Hozak, P., Peknicova, J. (2015). Characterization and possible function of

glyceraldehyde-3-phosphate dehydrogenase-spermatogenic protein GAPDHS

in mammalian sperm. *Reprod Biol Endocrinol.* 13:15.

doi: 10.1186/s12958-015-0008-1. PMID: 25888749.

Mariat, D., Firmesse, O., Levenez, F., Guimarães, V., Sokol, H., Doré, J., Corthier, G.,

Furet, J.P. (2009). The Firmicutes/Bacteroidetes ratio of the human

microbiota changes with age. *BMC Microbiol.* 9:123. doi: 10.1186/1471-

2180-9-123. PMID: 19508720.

Markoulatos, P., Siafakas, N., & Moncany, M. (2002). Multiplex polymerase chain reaction: a

practical approach. *J Clin Lab Anal.* 16(1):47–51.

doi: 10.1002/jcla.2058. PMID: 11835531.

Marsh, S. E., Abud, E. M., Lakatos, A., Karimzadeh, A., Yeung, S. T., Davtyan, H., Fote,

G.M., Lau, L., Weinger, J.G., Lane, T.E., Inlay, M.A., Poon, W.W.,

Blurton-Jones, M. (2016). The adaptive immune system restrains Alzheimer's

disease pathogenesis by modulating microglial function.

Proc Natl Acad Sci U S A. 13(9):E1316-25. doi: 10.1073/pnas.1525466113.

PMID: 26884167.

Matthews, F., Stephan, B., Robinson, L., Jagger, C., Barnes, L.E, Arthur, A., Brayne, C.

(2016). A two decade dementia incidence comparison from the cognitive function and ageing studies I and II. *Nat Commun*; 7:11398.

doi: 10.1038/ncomms11398. PMID: 27092707.

Matsushita, K. (2021) Analysis of Interaction Between *Porphyromonas gingivalis* and

endothelial cells in vitro. *Methods Mol Biol.* 2210:225-33. doi:

10.1007/978-1-0716-0939-2_22. PMID: 32815143.

McClelland, R.S., Fowler, V.G., Sanders, L.L., Gottlieb, G., Kong, L.K., Sexton, D.J.,

Schmader, K., Lanclos, K.D., Corey, R. (1999). *Staphylococcus aureus*

bacteremia among elderly vs younger adult patients: comparison of clinical features and mortality. *Arch Intern Med.* 159(11):1244-7.

doi: 10.1001/archinte.159.11.1244. PMID: 10371233.

McGeer, P.L., Rogers, J., McGeer, E.G. (2017). "Inflammation, anti-inflammatory

agents, and Alzheimer's disease: The last 22 years". In: *Handbook of*

Infection and Alzheimer's Disease, ed. J. Miklossy (IOS Press, Amsterdam,

The Netherlands), 11-15. doi:10.3233/JAD-160488.

McKhann, G.M., Knopman, D.S., Chertkow, H., Hyman, B.T., Jack, C.R.Jr., Kawas, C.H.,

Klunk, W.E., Koroshetz, W.J., Manly, J.J., Mayeux, R., Mohs, R.C., Morris,

J.C., Rossor, M.N., Scheltens, P., Carrillo, M.C., Thies, B., Weintraub, S.,

Phelps, C.H. (2011). The diagnosis of dementia due to Alzheimer's disease: recommendations from the National Institute on Aging-Alzheimer's Association workgroups on diagnostic guidelines for Alzheimer's disease. *Alzheimers Dement.* 7(3):263-9. doi: 10.1016/j.jalz.2011.03.005. PMID: 21514250.

Meghil, M. M., Tawfik, O. K., Elashiry, M., Rajendran, M., Arce, R. M., Fulton, D. J., Schoenlein, P. V., Cutler, C. W. (2019). Disruption of immune homeostasis in human dendritic cells via regulation of autophagy and apoptosis by *Porphyromonas gingivalis*. *Front Immunol.* 10:2286. doi: 10.3389/fimmu.2019.02286. PMID: 31608069.

Methia, N., André, P., Hafezi-Moghadam, A., Economopoulos, M., Thomas, K.L., Wagner, D.D. (2001). ApoE deficiency compromises the blood brain barrier especially after injury. *Mol Med.* 7(12):810-5. PMID: 11844869.

Michaud, D.S. (2013). Role of bacterial infections in pancreatic cancer. *Carcinogenesis.* 34(10):2193-7. doi: 10.1093/carcin/bgt249. PMID: 23843038.

Miklossy, J. (2016). Bacterial amyloid and DNA are important constituents of senile plaques: further evidence of the spirochetal and biofilm nature of senile plaques. *J. Alzheimers Dis.* 53:1459–73. doi: 10.3233/JAD160451.

Miles, B., Zakhary, I., El-Awady, A., Scisci, E., Carrion, J., O'Neill, J.C., Rawlings, A., Stern, J.K., Susin, C., Cutler, C.W. (2014). Secondary lymphoid organ homing phenotype of human myeloid dendritic cells disrupted by an intracellular oral

pathogen. *Infect Immun.* 82(1):101-11. doi: 10.1128/IAI.01157-13.

PMID: 24126519.

Moen, K., Brun, J.G., Valen, M., Skartveit, L., Eribe, E.K., Olsen, I., Jonsson, R. (2006).

Synovial inflammation in active rheumatoid arthritis and psoriatic arthritis

facilitates trapping of a variety of oral bacterial DNAs. *Clin Exp Rheumatol.*

24(6):656-63. PMID: 17207381.

Molinuevo, J. L., Ayton, S., Batrla, R., Bednar, M. M., Bittner, T., Cummings, J., Fagan, A.

M., Hampel, H., Mielke, M. M., Mikulskis, A., O'Bryant, S., Scheltens, P.,

Sevigny, J., Shaw, L. M., Soares, H. D., Tong, G., Trojanowski, J. Q.,

Zetterberg, H., Blennow, K. (2018). Current state of Alzheimer's fluid

biomarkers. *Acta neuropathologica*, 136(6):821-53.

doi: 10.1007/s00401-018-1932-x. PMID: 30488277.

Montagne, A., Barnes, S.R., Sweeney, M.D., Halliday, M.R., Sagare, A.P., Zhao, Z., Toga,

A.W., Jacobs, R.E., Liu, C.Y., Amezcua, L., Harrington, M.G., Chui, H.C.,

Law, M., Zlokovic, B.V. (2015). Blood-brain barrier breakdown in the aging

human hippocampus. *Neuron.* 85(2):296-302.

doi: 10.1016/j.neuron.2014.12.032. PMID: 25611508.

Montagne, A., Nation, D.A., Sagare, A.P., Barisano, G., Sweeney, M.D., Chakhoyan, A.,

Pachicano, M., Joe, E., Nelson, A.R., D'Orazio, L.M., Buennagel, D.P.,

Harrington, M.G., Benzinger, T.L.S., Fagan, A.M., Ringman, J.M., Schneider,

L.S., Morris, J.C., Reiman, E.M., Caselli, R.J., Chui, H.C., Tcw, J., Chen, Y.,

Pa, J., Conti, P.S., Law, M., Toga, A.W., Zlokovic, B.V. (2020). APOE4 leads to blood-brain barrier dysfunction predicting cognitive decline. *Nature*.

581(7806):71-76. doi: 10.1038/s41586-020-2247-3. PMID: 32376954.

Montagne, A., Zhao, Z., Zlokovic, B.V. (2017). Alzheimer's disease: A matter of blood-brain barrier dysfunction? *J Exp Med*. 214(11):3151-69.

doi:10.1084/jem.20171406.

Mori, H., Maruyama, F., Kato, H., Toyoda, A., Dozono, A., Ohtsubo, Y., Nagata, Y.,

Fujiyama, A., Tsuda, M., Kurokawa, K. (2014). Design and experimental application of a novel non-degenerate universal primer set that amplifies

prokaryotic 16S rRNA genes with a low possibility to amplify eukaryotic rRNA genes. *DNA Res*. 21(2):217-27. doi: 10.1093/dnares/dst052.

PMID: 24277737.

Mori, K., Yanagita, M., Hasegawa, S., Kubota, M., Yamashita, M., Yamada, S., Kitamura, M., Murakami, S. (2015). Necrosis-induced TLR3 activation promotes TLR2

expression in gingival cells. *J Dent Res*.94(8):1149-57.

doi: 10.1177/0022034515589289. PMID: 26045329.

Morris, M.C., Gilliam, E.A., Li, L. (2015) Innate immune programming by endotoxin and its pathological consequences. *Front Immunol*. 5:680.

doi:10.3389/fimmu.2014.00680.

Mukherjee, P.K., Chandra, J., Retuerto, M., Tatsuoka, C., Ghannoum, M.A., McComsey,

G.A. (2018). Dysbiosis in the oral bacterial and fungal microbiome of HIV-

infected subjects is associated with clinical and immunologic variables of HIV infection. *PLoS ONE*. 13(7): e0200285.

doi: 10.1371/journal.pone.0200285. PMID: 29995962.

Mulhall, H., Huck, O., Amar, S. (2020). *Porphyromonas gingivalis*, a long-range pathogen: systemic impact and therapeutic implications. *Microorganisms*. 8(6):869.

doi: 10.3390/microorganisms8060869. PMID: 32526864.

Muoio, V., Persson, P.B., Sendeski, M.M. (2014) The neurovascular unit - concept review.

Acta Physiol (Oxf). 210(4):790-8. doi: 10.1111/apha.12250. PMID: 24629161.

Nádházi, Z., Takáts, A., Offenmüller, K., Bertók, L. (2002). Plasma endotoxin level of healthy donors. *Acta Microbiol Immunol Hung*. 49:151–7.

doi: 10.1556/AMicr.49.2002.1.15.

Nagaoka, K., Yanagihara, K., Harada, Y., Yamada, K., Migiyama, Y., Morinaga, Y., Izumikawa, K., Kohno, S. (2017). Quantitative detection of periodontopathic bacteria in lower respiratory tract specimens by real-time PCR. *J Infect Chemother*. 23:69-73. doi: 10.1016/j.jiac.2016.09.013. PMID: 27894820.

Naik, U.P., Eckfeld, K. (2003) Junctional adhesion molecule 1 (JAM-1). *J Biol Regul Homeost Agents*. 17(4):341-7. PMID: 15065765.

Nara, P.L., Sindelar, D., Penn, M.S., Potempa, J., Griffin, W.S.T. (2021). *Porphyromonas gingivalis* outer membrane vesicles as the major driver of and explanation for neuropathogenesis, the cholinergic hypothesis, iron dyshomeostasis,

and salivary lactoferrin in Alzheimer's disease. *J Alzheimers Dis.*

82(4): 1417-50. doi:10.3233/JAD-210448. PMID: 34275903.

Nativel, B., Couret, D., Giraud, P., Meilhac, O., d'Hellencourt, C.L., Viranaïcken, W.,

Da Silva, C.R. (2017). Porphyromonas gingivalis lipopolysaccharides act exclusively through TLR4 with a resilience between mouse and human.

Sci Rep. 7(1):15789. doi: 10.1038/s41598-017-16190-y. PMID: 29150625.

Nauta, A.J., de Haij, S., Bottazzi, B., Mantovani, A., Borrias, M.C., Aten, J., Rastaldi, M.P.,

Daha, M.R., van Kooten, C., Roos, A. (2005). Human renal epithelial cells produce the long pentraxin PTX3. *Kidney Int.* 67(2):543-53.

doi: 10.1111/j.1523-1755.2005.67111.x. PMID: 15673302.

Nielsen, P. A., Andersson, O., Hansen, S. H., Simonsen, K. B. and Andersson, G. (2011)

Models for predicting blood-brain barrier permeation. *Drug Discov*

Today. 16(11-12):472-5. doi: 10.1016/j.drudis.2011.04.004.PMID: 21513815.

O'Brien, R. J., Wong, P. C. (2011). Amyloid precursor protein processing and Alzheimer's

disease. *Annu Rev Neurosci.* 34:185-204.

doi: 10.1146/annurev-neuro-061010-113613. PMID: 21456963.

Offenbacher, S., Beck, J.D., Moss, K., Mendoza, L., Paquette, D.W., Barrow, D.A., Couper,

D.J., Stewart, D.D., Falkner, K.L., Graham, S.P., Grossi, S., Gunsolley,

J.C., Madden, T., Maupome, G., Trevisan, M., Van Dyke, T.E., Genco, R.J.

(2009). Results from the Periodontitis and Vascular Events (PAVE) Study: a

pilot multicentered, randomized, controlled trial to study effects of

periodontal therapy in a secondary prevention model of cardiovascular disease. *J Periodontol.* 80(2):190-201. doi: 10.1902/jop.2009.080007.

PMID: 19186958.

Olsen, I. (2021) Can *Porphyromonas gingivalis* contribute to Alzheimer's disease already at the stage of gingivitis? *J Alzheimers Dis Rep.* 5(1):237-41.

doi: 10.3233/ADR-210006. PMID: 34113781.

Olsen, I., Amano, A. (2015). Outer membrane vesicles - offensive weapons or good samaritans? *J Oral Microbiol.* 7:27468. doi: 10.3402/jom.v7.27468.

PMID: 25840612.

Olsen, I., Chen, T., Tribble, G.D. (2018). Genetic exchange and reassignment in *Porphyromonas gingivalis*. *J Oral Microbiol.* 10(1):1457373.

doi: 10.1080/20002297.2018.1457373. PMID: 29686783.

Olsen, I., Kell, D.B., Pretorius, E. (2020). Is *Porphyromonas gingivalis* involved in Parkinson's disease? *Eur J Clin Microbiol Infect Dis.* 39(11):2013-18.

doi: 10.1007/s10096-020-03944-2. PMID: 32564247.

Olsen, I., Progulsk-Fox, A. (2015). Invasion of *Porphyromonas gingivalis* strains into vascular cells and tissue. *J Oral Microbiol.* 7:28788.

doi: 10.3402/jom.v7.28788. PMID: 26329158.

Olsen, I., Singhrao, S.K. (2015). Can oral infection be a risk factor for Alzheimer's disease?

J. Oral Microbiol. 7:29143. doi: 10.3402/jom.v7.29143. PMID: 26385886.

Olsen, I., Singhrao, S.K. (2016). Inflammasome involvement in Alzheimer's disease. *J.*

Alzheimers Dis. 54(1):45-53. doi: 10.3233/JAD-160197. PMID: 27314526.

Olsen, I., Taubman, M.A., Singhrao, S.K. (2016). Porphyromonas gingivalis suppresses adaptive immunity in periodontitis, atherosclerosis and Alzheimer's disease. J. Oral Microbiol. 8:33029. doi: 10.3402/jom.v8.33029.

Ono, K., Eguchi, T., Sogawa, C., Calderwood, S.K., Futagawa, J., Kasai, T., Seno, M., Okamoto, K., Sasaki, A., Kozaki, K.I. (2018). HSP-enriched properties of extracellular vesicles involve survival of metastatic oral cancer cells. J Cell Biochem. 119(9):7350-7362. doi: 10.1002/jcb.27039. PMID: 29768689.

Paganini-Hill, A., White, S.C., and Atchison, K.A. (2012). Dentition, dental health habits and dementia: The Leisure World Cohort Study. J. Am. Geriatr. Soc. 60(8):1556-63. doi:10.1111/j.1532-5415. PMID: 22860988.

Païssé, S., Valle, C., Servant, F., Courtney, M., Burcelin, R., Amar, J., Lelouvier, B. (2016). Comprehensive description of blood microbiome from healthy donors assessed by 16S targeted metagenomic sequencing. Transfusion. 56(5):1138-47. doi: 10.1111/trf.13477. PMID: 26865079.

Palumbo, P., Picchini, U., Beck, B., van Gelder, J., Delbar, N., DeGaetano, A. (2008). A general approach to the apparent permeability index. J Pharmacokinet Pharmacodyn. 35(2):235-48. doi: 10.1007/s10928-008-9086-4. PMID: 18351296.

Parada, A.E., Needham, D.M., Fuhrman, J.A. (2016). Every base matters: assessing small subunit rRNA primers for marine microbiomes with mock communities, time

series and global field samples. *Environ Microbiol.* 18(5):1403-14.

doi:10.1111/1462-2920.13023. PMID: 26271760.

Park, J., Wetzel, I., Marriott, I., Dréau, D., D'Avanzo, C., Kim, D. Y., Tanzi, R. E., Cho, H.

(2018). A 3D human triculture system modeling neurodegeneration and

neuroinflammation in Alzheimer's disease. *Nat Neurosci.* 21(7):941-51.

doi: 10.1038/s41593-018-0175-4. PMID: 29950669.

Park, O.J., Yi, H., Jeon, J.H., Kang, S.S., Koo, K.T., Kum, K.Y., Chun, J., Yun, C.H., Han,

S.H. (2015). Pyrosequencing Analysis of Subgingival Microbiota in Distinct

Periodontal Conditions. *J Dent Res.* 94(7):921-7. doi:

10.1177/0022034515583531. PMID: 25904141.

Pascu, A., Romanitan, M.O., Delgado, J.-M., Danaila, L., Pascu, M. (2009). Laser-

induced autofluorescence measurements on brain tissues. *Anat Rec.*

292: (12):2013-22. doi: 10.1002/ar.21034. PMID: 19943354.

Patterson, C. (2018), World Alzheimer Report 2018, The state of the art of dementia

research: New frontiers, Alzheimer's Disease International, London.

Pflanzner, T., Kuhlmann, C.R., Pietrzik, C.U. (2010). Blood-brain-barrier models for the

investigation of transporter- and receptor-mediated amyloid- β clearance in

Alzheimer's disease. *Curr Alzheimer Res.* 7(7):578-90. doi:

10.2174/156720510793499066. PMID: 20704558.

Pieper, C., Pieloch, P., Galla, H.J. (2013). Pericytes support neutrophil transmigration via

interleukin-8 across a porcine co-culture model of the blood-brain barrier.

Brain Res. 1524:11. doi: 10.1016/j.brainres.2013.05.047. PMID:
23769734.

Pisa, D., Alonso, R., Fernandez-Fernandez, A. M., Rabano, A., Carrasco, L. (2017).

Polymicrobial infections in brain tissue from Alzheimer's disease
patients. *Sci.Rep.*7:5559. doi:10.1038/s41598-017-05903-y.

Pistollato, F., Sumalla Cano, S., Elio, I., Masias Vergara, M., Giampieri, F., and Battino, M.

(2016). Role of gut microbiota and nutrients in amyloid formation and
pathogenesis of Alzheimer disease. *Nutr. Rev.* 74(10): 624-34.

doi:10.1093/nutrit/nuw023. PMID: 27634977.

Poole, S., Singhrao, S.K., Kesavalu, L., Curtis, M.A., and Crean, S. (2013). Determining the

presence of periodontopathic virulence factors in short-term post-mortem
Alzheimer's disease brain tissue. *J. Alzheimers Dis.* 36: 665-77.

doi:10.3233/JAD-121918.

Prince, M., Ali, G.C., Guerchet, M., Prina, A.M., Albanese, E., Wu, Y.T. (2016) Recent global

trends in the prevalence and incidence of dementia, and survival with
dementia. *Alzheimers Res Ther*, 8(1):23. doi: 10.1186/s13195-016-0188-8.

PMID: 27473681.

Prince, M., Knapp, M., Guerchet, M., McCrane, P., Prina, M., Comas-Herrera, A.,

Wittenberg, R. (2014). *Dementia UK: Update*. 2nd Edn. London:

Alzheimer's Society.

Pritchard, A.B., Crean, S., Olsen, I., Singhrao, S.K. (2017) Periodontitis, microbiomes and

their role in Alzheimer's disease. *Front Aging Neurosci.* 24;9:336. doi:
10.3389/fnagi.2017.00336. PMID: 29114218.

Raja, H.A., Miller, A.N., Pearce, C.J., Oberlies, N.H. (2017). Fungal identification using
molecular tools: a primer for the natural products research community. *J*
Nat Prod. 80(3):756-70. doi: 10.1021/acs.jnatprod.6b01085.PMID:
28199101.

Reyes, L., Phillips, P., Wolfe, B., Golos, T.G., Walkenhorst, M., Progulsk-Fox, A., Brown,
M. (2017). *Porphyromonas gingivalis* and adverse pregnancy outcome.
J Oral Microbiol. 10(1):1374153. doi: 10.1080/20002297.2017.1374153.
PMID: 29291034

Riviere, G.R., Riviere, K., and Smith, K. (2002). Molecular and immunological evidence of
oral *Treponema* in the human brain and their association with Alzheimer's
disease. *Oral Microbiol. Immunol.* 17(2):113-8.
doi: 10.1046/j.0902-0055.2001.00100.x. PMID: 11929559.

Rokad, F., Moseley, R., Hardy, R.S., Chukkapalli, S., Crean, S., Kesavalu, L., Singhrao,
S.K. (2017). Cerebral oxidative stress and microvasculature defects in TNF-
 α expressing transgenic and *Porphyromonas gingivalis*-infected ApoE^{-/-}
mice. *J Alzheimers Dis.* 60(2):359-369. doi: 10.3233/JAD-170304.
PMID: 28800332.

Rosenberg, A., Ngandu, T., Rusanen, M., Antikainen, R., Bäckman, L., Havulinna, S.,
Hänninen, T., Laatikainen, T., Lehtisalo, J., Levälähti, E., Lindström, J.,

- Paajanen, T., Peltonen, M., Soininen, H., Stigsdotter-Neely, A., Strandberg, T., Tuomilehto, J., Solomon, A., Kivipelto, M. (2018). Multidomain lifestyle intervention benefits a large elderly population at risk for cognitive decline and dementia regardless of baseline characteristics: The FINGER trial. *Alzheimers Dement.* 14(3):263-70. doi: 10.1016/j.jalz.2017.09.006. PMID: 29055814.
- Rucker, H.K., Wynder, H.J., Thomas, W.E. (2000). Cellular mechanisms of CNS pericytes. *Brain Res Bull.* 51(5):363-9. doi: 10.1016/s0361-9230(99)00260-9. PMID: 10715555.
- Rudge, J.S. (1993). Astrocyte-derived neurotrophic factors. In Murphy S, *Astrocytes: Pharmacology and Function* (pp 267-94). San Diego: Academic Press, Inc.
- Sabbagh, M., Han, S., Kim, S., Na, H. R., Lee, J. H., Kandiah, N., Phanthumchinda, K., Suthisisang, C., Senanarong, V., Pai, M. C., Narilastri, D., Sowani, A. M., Ampil, E., Dash, A. (2016). Clinical recommendations for the use of Donepezil 23 mg in moderate-to-severe Alzheimer's disease in the Asia-pacific region. *Dement Geriatr Cogn Dis Extra.*6(3):382-395. doi: 10.1159/000448214. PMID: 27703471.
- Saleem, H.G., Seers, C.A., Sabri, A.N., Reynolds, E.C. (2016) Dental plaque bacteria with reduced susceptibility to chlorhexidine are multidrug resistant. *BMC Microbiol.* 16:214. doi:10.1186/s12866-016-0833-1.
- Salingcarnboriboon, R., Tsuji, K., Komori, T., Nakashima, K., Ezura, Y., Noda, M. (2006).

Runx2 is a target of mechanical unloading to alter osteoblastic activity and bone formation in vivo. *Endocrinology*. 147(5):2296–05.

doi: 10.1210/en.2005-1020. PMID: 16455780.

Salminen, A., Kauppinen, A., Kaarniranta, K. (2017). Hypoxia/ischemia activate processing of amyloid precursor protein: impact of vascular dysfunction in the pathogenesis of Alzheimer's disease. *J Neurochem*. 140:536–49.

doi: 10.1111/jnc.13932. PMID: 27987381.

Sandiego, C.M., Gallezot, J.D., Pittman, B., Nabulsi, N., Lim, K., Lin, S.F., Matuskey, D., Lee, J.Y., O'Connor, K.C., Huang, Y., Carson, R.E., Hannestad, J., Cosgrove, K.P. (2015). Imaging robust microglial activation after lipopolysaccharide administration in humans with PET. *Proc Natl Acad Sci U S A*. 112:12468–73. doi: 10.1073/pnas.1511003112.

Sbordone, L., Bortolaia, C. (2003). Oral microbial biofilms and plaque-related diseases: Microbial communities and their role in the shift from oral health to disease. *Clin Oral Investig*. 7(4):181-8. doi: 10.1007/s00784-003-0236-1.

PMID: 14598129.

Schenk, G.J., de Vries, H.E. (2016). Altered blood-brain barrier transport in neuro-inflammatory disorders. *Drug Discov Today Technol*. 20:5-11. doi:

10.1016/j.ddtec.2016.07.002. PMID: 27986224.

Schoch, C. L., Seifert, K. A., Huhndorf, S., Robert, V., Spouge, J. L., Levesque, C. A., Chen, W. (2012). Nuclear ribosomal internal transcribed spacer (ITS) region as a

- universal DNA barcode marker for Fungi. *Proc Natl Acad Sci U S A*.
109(16):6241-6. doi: 10.1073/pnas.1117018109. PMID: 22454494.
- Schloss, P.D., Westcott, S.L., Ryabin, T., Hall, J.R., Hartmann, M., Hollister, E.B.,
Lesniewski, R.A., Oakley, B.B., Parks, D.H., Robinson, C.J., Sahl, J.W.,
Stres, B., Thallinger, G.G., Van Horn, D.J., Weber, C.F. (2009).
Introducing mothur: open-source, platform-independent, community-supported
software for describing and comparing microbial communities.
Appl Environ Microbiol. 75(23):7537-41. doi: 10.1128/AEM.01541-09.
PMID: 19801464.
- Schuster, S.C. (2008). Next-generation sequencing transforms today's biology.
Nat Methods. 5(1):16-8. doi: 10.1038/nmeth1156. PMID: 18165802.
- Selkoe, D.J., Hardy, J. (2016). The amyloid hypothesis of Alzheimer's disease at 25 years.
EMBO Mol Med. 8(6):595-608. doi: 10.15252/emmm.201606210.
PMID: 27025652.
- Sengupta, U., Nilson, A.N., Kaye, R. (2016). The role of amyloid- β oligomers in toxicity,
propagation, and immunotherapy. *EBioMedicine*. 6:42-9.
doi: 10.1016/j.ebiom.2016.03.035. PMID: 27211547.
- Serlin, Y., Shelef, I., Knyazer, B., Friedman, A. (2015) Anatomy and physiology of the blood-
brain barrier. *Semin Cell Dev Biol*. 38:2-6.
doi:10.1016/j.semcdb.2015.01.002. PMID: 25681530.
- Sevenich, L. (2018). Brain-resident microglia and blood-borne macrophages orchestrate

central nervous system inflammation in neurodegenerative disorders and brain cancer. *Front Immunol.* 9:697. doi: 10.3389/fimmu.2018.00697.

PMID: 29681904.

Seyama, M., Yoshida, K., Yoshida, K., Fujiwara, N., Ono, K., Eguchi, T., Kawai, H., Guo, J.,

Weng, Y., Haoze, Y., Uchibe, K., Ikegame, M., Sasaki, A., Nagatsuka, H.,

Okamoto, K., Okamura, H., Ozaki, K. (2020) Outer membrane vesicles of

Porphyromonas gingivalis attenuate insulin sensitivity by delivering

gingipains to the liver. *Biochim Biophys Acta Mol Basis*

Dis. 1866(6):165731. doi: 10.1016/j.bbadis.2020.165731. PMID: 32088316.

Shahi, S., Freedman, S., Mangalam, A. (2017). Gut microbiome in multiple sclerosis:

the players involved and the roles they play. *Gut Microbes.* 8(6):607-15.

doi: 10.1080/19490976.2017.1349041.PMID: 28696139.

Shao, Y., McCarhy, K.D. (1994). Plasticity of astrocytes. *Glia.* 11 (2):147-55.

doi: 10.1002/glia.440110209. PMID: 7927644.

Sheets, S.M., Potempa, J., Travis, J., Casiano, C.A., Fletcher, H.M. (2005). Gingipains

from *Porphyromonas gingivalis* W83 induce cell adhesion molecule

cleavage and apoptosis in endothelial cells. *Infect. Immun.* 73(3):1543-52.

doi:10.1128/IAI.73.3.1543-1552.2005. PMID: 15731052.

Shendure, J., Ji, H. (2008). Next-generation DNA sequencing. *Nat Biotechnol.*

26(10):1135-45. doi: 10.1038/nbt1486. PMID: 18846087.

Sheng, J.G., Bora, S.H., Xu, G., Borchelt, D.R., Price, D.L., Koliatsos, V.E. (2003).

Lipopolysaccharide-induced-neuroinflammation increases intracellular accumulation of amyloid precursor protein and amyloid beta peptide in APP^{swe} transgenic mice. *Neurobiol. Dis.* 14(1):133-45. doi:10.1016/S0969-9961(03)00069-X. PMID: 13678674.

Shergalis, A., Bankhead, A., Luesakul, U., Neamati, N. (2018). Current challenges and opportunities in treating glioblastoma. *Pharmacol Rev.* 70(3):412-45. doi: 10.1124/pr.117.014944. PMID: 29669750.

Shin, N., Whon, T., Bae, J., (2015). Proteobacteria: microbial signature of dysbiosis in gut Microbiota. *Trends Biotechnol.* 33(9):496-03. doi: 10.1016/j.tibtech.2015.06.011. PMID: 26210164.

Sims, D.E. (2000). Diversity within pericytes. *Clin Exp Pharmacol Physiol.* 27(10):842-6. doi: 10.1046/j.1440-1681.2000.03343.x. PMID: 11022980.

Singhrao, S.K., Chukkapalli, S., Poole, S., Velsko, I., Crean, S., and Kesavalu, L. (2017). Chronic *Porphyromonas gingivalis* infection accelerates the occurrence of age-related granules in ApoE^{-/-} mice. *J. Oral Microbiol.* 9(1):1270602. doi:10.1080/20002297.2016.1270602.

Singhrao, S. K., Harding, A., Poole, S., Kesavalu, L., Crean, S. (2015). *Porphyromonas gingivalis*: periodontal infection and its putative links with Alzheimer's disease. *Mediators Inflamm.* 2015:137357. doi: 10.1155/2015/137357.

Singhrao, S.K., Olsen, I. (2018). Are Porphyromonas gingivalis outer membrane vesicles microbullets for sporadic Alzheimer's disease manifestation? J Alzheimers Dis Rep. 2(1):219-28. doi: 10.3233/ADR-180080. PMID: 30599043.

Skelly, D.T., Hennessy, E., Dansereau, M., Cunningham, C. (2013). A systematic analysis of the peripheral and CNS effects of systemic LPS, IL-1B, TNF- α and IL-6 challenges in C57BL/6 mice. PLoS ONE, 8 (7):e69123. doi: 10.1371/journal.pone.0069123. PMID: 23840908.

Solbiati, J., Duran-Pinedo, A., Godoy Rocha, F., Gibson, F. C., Frias-Lopez, J. (2020). Virulence of the pathogen Porphyromonas gingivalis is controlled by the CRISPR-Cas protein Cas3. mSystems, 5(5), e00852-20. doi: 10.1128/mSystems.00852-20. PMID: 32994292.

Solleiro-Villavicencio, H., Rivas-Arancibia, S. (2018). Effect of chronic oxidative stress on neuroinflammatory response mediated by CD4+T Cells in neurodegenerative diseases. Front Cell Neurosci. 12:114. doi: 10.3389/fncel.2018.00114. PMID: 29755324.

Soscia, S.J., Kirby, J.E., Washicosky, K.J., Tucker, S.M., Ingelsson, M., Hyman, B., Burton, M.A., Goldstein, L.E., Duong, S., Tanzi, R.E., Moir, R.D. ((2010). The Alzheimer's disease-associated amyloid beta-protein is an antimicrobial peptide. PLoS One. 5(3):e9505. doi: 10.1371/journal.pone.0009505. PMID: 20209079.

Souto, R., Silva-Boghossian, C.M., Colombo. A.P. (2014). Prevalence of *Pseudomonas aeruginosa* and *Acinetobacter* spp. in subgingival biofilm and saliva of subjects with chronic periodontal infection. *Braz J Microbiol.* 45(2):495-501. doi:10.1590/s1517-83822014000200017.

Spangenberg, E. E., Green, K. N. (2017). Inflammation in Alzheimer's disease: Lessons learned from microglia-depletion models. *Brain Behav Immun.* 61:1-11. doi: 10.1016/j.bbi.2016.07.003. PMID: 27395435.

Srinivasan, B., Kolli, A.R., Esch, M.B., Abaci, H.E., Shuler, M.L., Hickman, J.J. (2015). TEER measurement techniques for in vitro barrier model systems. *J Lab Autom.* 20(2):107–126. doi:10.1177/2211068214561025.

Stamatovic, S. M., Johnson, A. M., Keep, R. F., Andjelkovic, A. V. (2016). Junctional proteins of the blood-brain barrier: New insights into function and dysfunction. *Tissue barriers.* 4(1), e1154641. doi: 10.1080/21688370.2016.1154641. PMID: 27141427.

Stephan, B.C.M., Birdi, R., Tang, E.Y.H., Cosco, T.D., Donini, L.M., Licher, S., Ikram, M.A., Siervo, M., Robinson, L. (2018). Secular trends in dementia prevalence and incidence worldwide: a systematic review. *J Alzheimers Dis.* 66(2):653-80. doi: 10.3233/JAD-180375. PMID: 30347617.

Stevens, D.A., Kim, K.K., Johnson, N., Lee, J.S., Hamilton, J.R. (2013). *Halomonas johnsoniae*: review of a medically underappreciated genus of growing

human importance. *Am J Med Sci.* 345(5):335-8. doi:

10.1097/MAJ.0b013e31825600de. PMID: 22814360.

Su, W., Shi, J., Zhao, Y., Li, H., Lei, L. (2021). Gingival fibroblasts dynamically reprogram cellular metabolism during infection of *Porphyromonas gingivalis*. *Arch Oral Biol.* 121:104963. doi: 10.1016/j.archoralbio.2020.104963. PMID: 33157496.

Sun, Y., Ip, P., Chakrabarty, A. (2017). Simple elimination of background fluorescence in formalin-fixed human brain tissue for immunofluorescence microscopy. *JoVE*, (127): 56188. doi: 10.3791/56188. PMID: 28892031.

Sundquist, A., Bigdeli, S., Jalili, R., Druzin, M.L., Waller, S., Pullen, K.M., El-Sayed, Y.Y., Taslimi, M.M., Batzoglou, S., Ronaghi, M. (2007). Bacterial flora-typing with targeted, chip-based pyrosequencing. *BMC Microbiol.*7:108. doi: 10.1186/1471-2180-7-108. PMID: 18047683.

Sutherland, K., Li, T., Cao, C. (2015) Alzheimer's disease and the immune system. *SOJ Neurol.* 2(1): 1-11. doi:10.15226/2374-6858/2/1/00112.

Sweeney, M.D., Sagare, A.P., Zlokovic, B.V. (2018) Blood-brain barrier breakdown in Alzheimer disease and other neurodegenerative disorders. *Nat Rev Neurol.*14(3):133-50. doi: 10.1038/nrneurol.2017.188.

Swerdlow, R. H. (2018). Mitochondria and Mitochondrial Cascades in Alzheimer's Disease. *Journal of Alzheimer's disease: JAD.* 62(3):1403–16. doi:10.3233/JAD-170585.

Szeto, J. Y., Lewis, S. J. (2016). Current treatment options for Alzheimer's disease and Parkinson's disease dementia. *Curr Neuropharmacol.* 14(4):326-38.

doi: 10.2174/1570159x14666151208112754. PMID: 26644155.

Takahashi, T., Muro, S., Tanabe, N., Terada, K., Kiyokawa, H., Sato, S., Hoshino, Y., Ogawa, E., Uno, K., Naruishi, K., Takashiba, S., Mishima, M. (2012).

Relationship between periodontitis-related antibody and frequent exacerbations in chronic obstructive pulmonary disease. *PLoS One.*

7:e40570. doi:10.1371/journal.pone.0040570.

Takeuchi, H., Furuta, N., Morisaki, I., Amano, A. (2011). Exit of intracellular *Porphyromonas gingivalis* from gingival epithelial cells is mediated by endocytic recycling

pathway. *Cell Microbiol* 13(5):677-91. doi: 10.1111/j.1462-5822.2010.01564.x.

PMID: 21155963.

Takeuchi, H., Sasaki, N., Yamaga, S., Kuboniwa, M., Matsusaki, M., Amano, A. (2019).

Porphyromonas gingivalis induces penetration of lipopolysaccharide and peptidoglycan through the gingival epithelium via degradation of junctional adhesion molecule 1. *PLoS pathogens.* 15(11):e1008124.

doi:10.1371/journal.ppat.1008124.

Tamagno, E., Guglielmotto, M., Aragno, M., Borghi, R., Autelli, R., Giliberto, L., Muraca, G.,

Danni, O., Zhu, X., Smith, M.A., Perry, G., Jo, D.G., Mattson, M.P., Tabaton,

M. (2008). Oxidative stress activates a positive feedback between the

gamma- and beta-secretase cleavages of the beta-amyloid precursor protein.

J Neurochem. 104(3):683-95. doi: 10.1111/j.1471-4159.2007.05072.x.

PMID: 18005001.

Tapia-Rojas, C., Cabezas-Opazo, F., Deaton, C. A., Vergara, E. H., Johnson, G.,

Quintanilla, R. A. (2019). It's all about tau. *Prog Neurobiol.* 175:54-76.

doi: 10.1016/j.pneurobio.2018.12.005. PMID: 30605723.

Tarkowski, E., Blennow, K., Wallin, A., Tarkowski, A. (1999). Intracerebral production of tumor necrosis factor-alpha, a local neuroprotective agent, in Alzheimer disease and vascular dementia. *J. Clin. Immunol.* 19, 223-30.

doi:10.1023/A:1020568013953.

Taylor-Robinson, D., Aduse-Opoku, J., Sayed, P., Slaney, J. M., Thomas, B. J., Curtis, M.A.

(2002). Oro-dental bacteria in various atherosclerotic arteries. *Eur J Clin*

Microbiol Infect Dis. 21(10):755-7. doi: 10.1007/s10096-002-0810-5.

PMID: 12415477.

Teunissen, C.E., Verberk, I.M.W., Thijssen, E.H., Vermunt, L., Hansson, O., Zetterberg, H.,

van der Flier, W.M., Mielke, M.M., Del Campo, M. (2022).

Blood-based biomarkers for Alzheimer's disease: towards clinical implementation. *Lancet Neurol.* 21(1):66-77.

doi: 10.1016/S1474-4422(21)00361-6. PMID: 34838239.

Therriault, J., Pascoal, T.A., Lussier, F.Z. et al. Biomarker modeling of Alzheimer's disease using PET-based Braak staging. *Nat Aging.* 2:526–35.

Doi:10.1038/s43587-022-00204-0.

Tipu, H.N., Shabbir, A. (2015). Evolution of DNA sequencing. *J Coll Physicians Surg Pak.* 25(3):210-5. PMID: 25772964.

Tonetti, M.S. (2009) Periodontitis and risk for atherosclerosis: an update on intervention trials. *J Clin Periodontol.* 10:15-9. doi: 10.1111/j.1600-051X.2009.01417.x. PMID: 19432627.

Tornavaca, O., Chia, M., Dufton, N., Almagro, L. O., Conway, D. E., Randi, A. M., Schwartz, M. A., Matter, K., Balda, M. S. (2015). ZO-1 controls endothelial adherens junctions, cell-cell tension, angiogenesis, and barrier formation. *J Cell Biol.* 208(6):821-38. doi: 10.1083/jcb.201404140. PMID: 25753039.

Thomas, J.W., Touchman, J.W. (2002). Vertebrate genome sequencing: building a backbone for comparative genomics. *Trends Genet.* 18(2):104-8. doi: 10.1016/s0168-9525(02)02599-4. PMID: 11818143.

Tribble, G.D., Lamont, G.J., Progulske-Fox, A., Lamont, R.J. (2007). Conjugal transfer of chromosomal DNA contributes to genetic variation in the oral pathogen *Porphyromonas gingivalis*. *J Bacteriol.* 189(17):6382-8. doi: 10.1128/JB.00460-07. PMID: 17573478.

Tsui, C.K., Woodhall, J., Chen, W., Lévesque, C.A., Lau, A., Schoen, C.D., Baschien, C., Najafzadeh, M.J., de Hoog, G.S. (2011). Molecular techniques for pathogen identification and fungus detection in the environment. *IMA Fungus.* 2(2):177-89. doi: 10.5598/ima fungus.2011.02.02.09. PMID: 22679603.

Underwood, D.C., Osborn, R.R., Bochnowicz, S., Webb, E.F., Rieman, D.J., Lee, J.C.,

Romanic, A.M., Adams, J.L., Hay, D.W., Griswold, D.E. (2000). SB 239063, a p38 MAPK inhibitor, reduces neutrophilia, inflammatory cytokines, MMP-9, and fibrosis in lung. *Am J Physiol Lung Cell Mol Physiol.* 279(5):L895-902.
doi: 10.1152/ajplung.2000.279.5.L895. PMID: 11053025.

Valdes, A. M, Walter, J., Segal, E., Spector, T. D. (2018). Role of the gut microbiota in nutrition and health *BMJ.* 361:k2179. doi: 10.1136/bmj.k2179.
PMID: 29899036.

VanItallie, T. B. (2017). Alzheimer's disease: innate immunity gone awry? *Metabolism.* 69S:S41–S49. doi:10.1016/j.metabol.2017.01.014. PMID: 28129888.

Varatharaj, A., Galea, I. (2017). The blood-brain barrier in systemic inflammation. *Brain Behav Immun.* 60:1-12. doi: 10.1016/j.bbi.2016.03.010.
PMID:26995317.

Vargas-Caraveo, A., Sayd, A., Maus, S.R., Caso, J.R., Madrigal, J.L.M., García-Bueno, B., Leza, J.C. (2017). Lipopolysaccharide enters the rat brain by a lipoprotein-mediated transport mechanism in physiological conditions. *Sci Rep.* 7(1):13113. doi: 10.1038/s41598-017-13302-6. PMID: 29030613.

Vasilache A.M., Qian, H., Blomqvist, A. (2015) Immune challenge by intraperitoneal administration of lipopolysaccharide directs gene expression in distinct blood-brain barrier cells toward enhanced prostaglandin E2 signalling. *Brain Behav Immun.* 48:31-41. doi: 10.1016/j.bbi.2015.02.003. PMID: 25678162.

Veith, P.D., Chen, Y.Y., Gorasia, D.G., Chen, D., Glew, M.D., O'Brien-Simpson, N.M., Cecil,

- J.D., Holden, J.A., Reynolds, E.C. (2014). Porphyromonas gingivalis outer membrane vesicles exclusively contain outer membrane and periplasmic proteins and carry a cargo enriched with virulence factors. *J Proteome Res.* 13:2420–32. doi: 10.1021/pr401227e. PMID: 24620993.
- Verheggen, I.C.M., de Jong, J.J.A., van Boxtel, M.P.J., Gronenschild, E.H.B.M., Palm, W.M., Postma, A.A., Jansen, J.F.A., Verhey, F.R.J., Backes, W.H. (2020). Increase in blood-brain barrier leakage in healthy, older adults. *Geroscience.* 42(4):1183-93. doi: 10.1007/s11357-020-00211-2. PMID: 32601792.
- Verkhatsky, A., Parpura, V., Rodriguez-Arellano, J. J., & Zorec, R. (2019a). Astroglia in Alzheimer's disease. *Adv Exp Med Biol.* 1175:273-324. doi: 10.1007/978-981-13-9913-8_11. PMID: 31583592.
- Verkhatsky, A., Rodrigues, J.J., Pivoriunas, A., Zorec, R., Semyanov, A. (2019b). Astroglial atrophy in Alzheimer's disease. *Pflugers Arch.* 471(10):1247-1261. doi: 10.1007/s00424-019-02310-2. PMID: 31520182.
- Vermilyea, D., Moradali, M., Kim, H., Davey, M., Comstock, L. (2021). PPAD activity promotes outer membrane vesicle biogenesis and surface translocation by *Porphyromonas gingivalis*. *J Bacteriol.* 203(4):e00343-20. doi: 10.1128/JB.00343-20. PMID: 33257525.
- Vogt, N.M., Kerby, R.L., Dill-McFarland, K.A., Harding, S.J., Merluzzi, A.P., Johnson, S.C., Carlsson, C.M., Asthana, S., Zetterberg, H., Blennow, K., Bendlin, B.B., Rey, F.E. (2017). Gut microbiome alterations in Alzheimer's disease.

Sci Rep.7(1):13537. doi: 10.1038/s41598-017-13601-y. PMID: 29051531.

Wahaidi, V.Y., Kowolik, M.J., Eckert, G.J., Galli, D.M. (2011) Endotoxemia and the host systemic response during experimental gingivitis. *J Clin Periodontol.* 38:412–17. doi: 10.1111/j.1600-051X.2011.01710.x.

Walsh, S., Merrick, R., Milne, R., Brayne, C. (2021). Aducanumab for Alzheimer's disease? *BMJ.* 374:n1682. doi: 10.1136/bmj.n1682. PMID: 34226181.

Wang, C., Chou, C. H., Tseng, C., Ge, X., Pinchuk, L. M. (2011). Early gene response of human brain microvascular endothelial cells to *Listeria monocytogenes* infection. *Canadian journal of microbiology*, 57(5) :441-6. doi: 10.1139/w11-018. PMID: 21542783.

Wang, H., Sun, J., Goldstein, H., (2008). Human immunodeficiency virus type 1 infection increases the in vivo capacity of peripheral monocytes to cross the blood-brain barrier into the brain and the in vivo sensitivity of the blood-brain barrier to disruption by lipopolysaccharide. *J Virol.* 82(15):7591-600. doi: 10.1128/JVI.00768-08. PMID: 18508884.

Wang, L., Yin, Y.L., Liu, X.Z., Shen, P., Zheng, Y.G., Lan, X.R., Lu, C.B., Wang, J.Z. (2020). Current understanding of metal ions in the pathogenesis of Alzheimer's disease. *Transl Neurodegener.* 9:10. doi: 10.1186/s40035-020-00189-z. PMID: 32266063.

Wang, X., Xue, G.X., Liu, W.C., Shu, H., Wang, M., Sun, Y., Liu, X., Sun, Y.E., Liu, C.F., Liu, J., Liu, W. Jin, X. (2017), Melatonin alleviates lipopolysaccharide-

compromised integrity of blood–brain barrier through activating AMP-activated protein kinase in old mice. *Aging Cell*. 16:414-21.

doi:10.1111/accel.12572.

Watts, A., Crimmins, E.M., Gatz, M. (2008). Inflammation as a potential mediator for the association between periodontal disease and Alzheimer's disease.

Neuropsychiatr Dis Treat. 4(5):865-76. doi: 10.2147/ndt.s3610.

PMID: 19183779.

Wendeln, A.C., Degenhardt, K., Kaurani, L., Gertig, M., Ulas, T., Jain, G., Wagner, J.,

Häsler, L.M., Wild, K., Skodras, A., Blank, T., Staszewski, O., Datta, M.,

Centeno, T.P., Capece, V., Islam, M.R., Kerimoglu, C., Staufienbiel, M.,

Schultze, J.L., Beyer, M., Prinz, M., Jucker, M., Fischer, A., Neher, J.J.

(2018). Innate immune memory in the brain shapes neurological disease

hallmarks. *Nature*.556:332–8. doi: 10.1038/s41586-018-0023-4.

Whon, T., Chung, W.H., Lim, M.Y., Song, E.J., Kim, P.S., Hyun, D.W., Shin, N.R., Bae,

J.W., Nam, Y.D. (2018). The effects of sequencing platforms on phylogenetic

resolution in 16 S rRNA gene profiling of human feces. *Sci Data*.5:180068.

doi: 10.1038/sdata.2018.68. PMID: 29688220.

Wilhelm, I., Fazakas, C. Krizbai, I. A. (2011). In vitro models of the blood-brain barrier, *Acta*

Neurobiol Exp, 71(1):113–28. PMID: 21499332.

Wittenberg, R., Hu, B., Jagger, C., Kingston, A., Knapp, M., Comas-Herrera, A., King, D.,

Rehill, A., Banerjee, S. (2020). Projections of care for older people with

dementia in England: 2015 to 2040. *Age Ageing*. 49(2):264-9.

doi: 10.1093/ageing/afz154. PMID: 31808792.

Wolff, A., Antfolk, M., Brodin, B, Tenje, M. (2015). In vitro blood–brain barrier models—an overview of established models and new microfluidic approaches.

J Pharm Sci. 104(9):2727-46. doi: 10.1002/jps.24329.PMID: 25630899.

Wray, S. (2021). Modelling neurodegenerative disease using brain organoids.

Semin Cell Dev Biol. 111:60-6. doi: 10.1016/j.semcdb.2020.05.012.

PMID: 32513498.

Wu, Z., Ni, J., Liu, Y., Teeling, J.L., Takayama, F., Collicutt, A., Ibbett, P., Nakanishi, H.

(2017). Cathepsin B plays a critical role in inducing Alzheimer's disease-like

phenotypes following chronic systemic exposure to lipopolysaccharide from

Porphyromonas gingivalis in mice. *Brain Behav Immun*. 65:350-61.

doi: 10.1016/j.bbi.2017.06.002. PMID: 28610747.

Xie, L., Kang, H., Xu, Q., Chen, M. J., Liao, Y., Thiyagarajan M., O'Donnell, J.,

Christensen, D.J., Nicholson, C., Iliff, J.J., Takano, T., Deane, R., Nedergaard,

M. (2013). Sleep drives metabolite clearance from the adult brain. *Science*.

342(6156):373-7. doi: 10.1126/science.1241224. PMID: 24136970.

Xu, W., Zhou, W., Wang, H., Liang, S. (2020). Roles of *Porphyromonas gingivalis* and its

virulence factors in periodontitis. *Adv Protein Chem Struct Biol*.120:45-84.

doi: 10.1016/bs.apcsb.2019.12.001. PMID: 32085888.

Yamamoto, Y. (2002). PCR in diagnosis of infection: detection of bacteria in cerebrospinal

fluids. Clin Diagn Lab Immunol. 9(3):508-14.

doi: 10.1128/cdli.9.3.508-514.2002. PMID: 11986253.

Yoneda, M., Naka, S., Nakano, K., Wada, K., Endo, H., Mawatari, H., Imajo, K., Nomura, R.,

Hokamura, K., Ono, M., Murata, S., Tohnai, I., Sumida, Y., Shima, T.,

Kuboniwa, M., Umemura, K., Kamisaki, Y., Amano, A., Okanou, T.,

Ooshima, T., Nakajima, A. (2012). Involvement of a periodontal pathogen,

Porphyromonas gingivalis on the pathogenesis of non-alcoholic fatty liver

disease. BMC Gastroenterol. 12:16. doi: 10.1186/1471-230X-12-16.

PMID: 22340817.

Yoon, S. S., Jo, S. A. (2012). Mechanisms of Amyloid- β peptide clearance: potential

therapeutic targets for Alzheimer's disease. Biomol Ther (Seoul).

20(3):245-55. doi: 10.4062/biomolther.2012.20.3.245. PMID: 24130920.

Yoshino, T., Laine, M.L., Van Winkelhoff, A.J., Dahlén, G. (2007). Genotype variation and

capsular serotypes of *Porphyromonas gingivalis* from chronic periodontitis

and periodontal abscesses. FEMS Microbiol Lett. 270(1):75-81.

doi: 10.1111/j.1574-6968.2007.00651.x. PMID: 17439635.

Zawadzki, P. J., Perkowski, K., Padzik, M., Mierzwińska-Nastalska, E., Szaflik, J. P., Conn,

D. B., Chomicz, L. (2017). Examination of oral microbiota diversity in

adults and older adults as an approach to prevent spread of risk factors

for human infections. Biomed Res Int. 2017:8106491.

doi: 10.1155/2017/8106491.PMID: 29082256.

Zenobia, C., Hajishengallis, G. (2015). Porphyromonas gingivalis virulence factors involved in subversion of leukocytes and microbial dysbiosis. *Virulence*. 6(3):236-43.

doi: 10.1080/21505594.2014.999567. PMID: 25654623.

Zhan, X., Stamova, B., Jin, L.W., DeCarli, C., Phinney, B., Sharp, F.R. (2016). Gram-negative bacterial molecules associate with Alzheimer disease pathology.

Neurology. 87(22):2324-32. doi:10.1212/WNL.0000000000003391.

Zhang, R., Miller, R.G., Gascon, R., Champion, S., Katz, J., Lancero, M., Narvaez, A., Honrada, R., Ruvalcaba, D., McGrath, M.S. (2009). Circulating endotoxin and systemic immune activation in sporadic amyotrophic lateral sclerosis (sALS).

J Neuroimmunol. 206(1-2):121-4. doi: 10.1016/j.jneuroim.2008.09.017.

PMID: 19013651.

Zhang, Z., Liu, D., Liu, S., Zhang, S., Pan, Y. (2021). The role of Porphyromonas gingivalis outer membrane vesicles in periodontal disease and related systemic

diseases. *Front Cell Infect Microbiol*. 10:585917.

doi: 10.3389/fcimb.2020.585917. PMID: 33585266.

Zhao, Y., Jaber, V., Lukiw, W.J. (2017). Secretory products of the human GI tract microbiome and their potential impact on Alzheimer's disease (AD):

detection of lipopolysaccharide (LPS) in AD hippocampus. *Front. Cell*

Infect. Microbiol. 7, 318. doi:10.3389/fcimb.2017.00318.

Zhou, H., Andonegui, G., Wong, C.H., Kubes, P. (2009). Role of endothelial TLR4 for neutrophil recruitment into central nervous system microvessels in

systemic inflammation. *J Immunol.* 183(8):5244-50.

doi:10.4049/jimmunol.0901309. PMID: 19786543.

Appendix 1: Additional information

Table 1 Equipment used in *in vitro* BBB model.

Equipment	Supplier
AxioCam MRm Zeiss camera	Carl Zeiss Microscopy GmbH, Germany
Bench centrifuge	ALC, Buckinghamshire, UK
Carl Zeiss fluorescence microscope	Carl Zeiss Microscopy GmbH, Germany
centrifuge tubes (15 and 50 ml), serological pipettes and Mr Frosty™ freezing containers	Fisher Scientific, UK. Product codes: Tubes: 11397201, 11347201 Pipettes: 16400901, 16410901, 16420901, 16430901, 16440901, 16450901
Class II microbiological safety cabinets	Labcaire Systems Limited, UK
Corning® Transwell® polycarbonate membrane cell culture inserts, 6.5 mm Transwell with 8.0 µm pore polycarbonate membrane insert, TC-treated, w/lid, sterile	Merck, UK Product code: CLS3421
EVOM	VPI, UK Product code: STX2
Genios Pro microtiter plate reader	Tecan, Austria
Haemocytometer slide	Marienfeld, Germany
Leica DMIL light microscope	Leica Microsystems GmbH, Germany
MShot camera and processed with MShot Digital Imaging System software	MShot, China
Sanyo CO2 incubator	Sanyo, Japan
SPSS statistical software package v.26 + 27	IBM, USA
Syringes and Millex® sterile syringe filters (0.22 µm pore size)	Merck, Fisher Scientific, UK. Product Code.11790453
T25 and T75 , sterile plates (6-well, 12-well, and 96-well)	Corning, Sigma-aldrich, UK Product code: CLS430372 and CLS430720

μ-plates 24 well, tissue culture treated black	IBIDI at Thistle scientific, UK Product code: IB-82426
Zetasizer	Malvern Panalytical, UK

Table 2 Reagents used in in vitro BBB model

Reagent	Supplier
AlphaBioCoat solution	Neuromics, USA Product code: AC001
Astrocyte basal medium (ABM) bullet kit comprise of 500ml basal media, 12ml insulin, 0.5 ml ascorbic acid, 0.5 ml epidermal growth factor human recombinant (rhEGF), 5 ml L-glutamine and 0.5 ml gentamycin sulphate amphotericin B. Human serum was added at 3 %. Recommended seeding density of 5,000 cells/cm ² by supplier.	Lonza, Switzerland Product code: cc-3187
Citrate buffer 10X pH 6	Sigma-Aldrich, UK Product code: C9999-100ML
Custom made CONJUGATION OF FITC TO LPS FROM <i>P. gingivalis</i> , (Invivogen, France)	Nanocs, USA
DMSO	Sigma-Aldrich, UK Product code: D2438
Endothelial cell basal medium (EBM) bullet kit comprise of 500 ml basal medium, 0.5 ml rhEGF, 20 ml human fibroblast growth factor B (rhFGF-B), 0.5 ml recombinated long R insulin like growth factor (R3-IGF-1), 0.5 ml Heparin, 0.5 ml gentamycin sulphate amphotericin B, 0.5 ml ascorbic acid, 0.2 ml hydrocortisone and 0.5 ml endothelial growth factor vascular human recombinant (VEGF). Human serum was added at 2 %. Recommended seeding density of 6600 cells/cm ² by supplier.	Lonza, Switzerland Product code: cc-3156
Evans blue dye (EBD)	Sigma Aldrich, UK Product code: E2129-50G
Fibronectin 1 mg	Sigma, UK.

	Product code: F2006
Fluorescein isothiocyanate–dextran average mol wt 3,000-5,000	Sigma-Aldrich, UK Product code: FD4-100MG
Fluorescein Labeling kit- NH ₂	Dojindo, Japan Product code: LK01-10
Hank's Balanced Salt Solution 500 ml (HBSS)	Gibco, ThermoFisher, USA Product code: 1758534
Human astrocytes HA)	ScienCell, USA Product code #1800
Human Brain Microvascular Endothelial Cells (HBMEC)	Neuromics, USA Product code: HEC02
Human Brain Pericytes (HBPC)	ScienCell, USA Product code: #1200
Human IL-6 ELISA kit	Sigma -Aldrich, UK Product code: RAB0306
Human Serum, French Off Clot serum, mixed gender French Off Clot serum Male AB.	Life Science Group, UK Product code: S-106A-EU
PBS	Thermo-Fisher, UK Product code: 10010023
Pericyte media (PM) bullet kit comprise of 500 ml basal media, 5 ml Penicillin 10000 U/ml Streptomycin 10000µg/ml and 5 ml pericyte growth supplement (PGS). Human serum was added at 2 %. Recommended seeding density of 5,000 cells/cm ² by supplier.	ScienCell, USA. Product code: #1201
<i>P. gingivalis</i> lipopolysaccharide 1mg/ml	Invivogen, France Product code: tlr1-pglps
Poly-L-Lysine 10 mg/ml	ScienCell, USA Product code: #0413
Trypan Blue 0.4%	Sigma-Aldrich, UK

	Product code: 93595
Trypsin (phenol red) TrypLeexpress 500 ml	Gibco, ThermoFisher, USA Product code: 12605-028
Tween-20	Sigma-Aldrich, UK Product code: 11332465001
70% IMS	Sigma-Aldrich, UK Product code: 02891

Appendix 2 Additional information from BBB model study

Table 1 Test protocol summary BBB model LPS application/EBD

WELL	protocol
well 1	200µl P.g LPS 1 µg/ml placed in apical compartment at time 0. At set time points this was removed and replaced with 200µl EBD 1 µg/ml which was incubated for 15 min before the 3x 200µl samples were taken from the basolateral compartment, replaced with media. After the sampling the EBD was removed and replaced with 200µl P.g LPS 1 µg/ml.
well 2	no LPS, (200µl EBD 1 µg/mL placed at time 0) samples collected from basolateral compartment (3x200µl) at set time points, absorbance measured, replaced with media.
well 3	LPS (1 µg/ml) + EBD (1 µg/ml) 1:1 placed at time 0, samples collected from basolateral compartment (3x200µl) at set time points, absorbance measured, replaced with media.
well 4	200µl P.g LPS 1 µg/ml placed in apical compartment at time 0. At set time points this was removed and replaced with 200µl EBD (1 µg/ml) which was incubated for 15 min before the 3x 200µl samples were taken from the basolateral compartment, replaced with media. After the sampling the EBD was removed and replaced with 200µl P.g LPS 1 µg/ml.

well 5	200µl P.g LPS 1 µg/ml placed in apical compartment at time 0. At set time points this was removed and replaced with 200µl EBD 1 µg/ml which was incubated for 15 min before the 3x 200µl samples were taken from the basolateral compartment, replaced with media. After the sampling the EBD was removed and replaced with 200µl P.g LPS 1 µg/ml.
well 6	200µl P.g LPS 0.3 µg/ml placed in apical compartment at time 0. At set time points this was removed and replaced with 200µl EBD 1 µg/ml which was incubated for 15 min before the 3x 200µl samples were taken from the basolateral compartment, replaced with media. After the sampling the EBD was removed and replaced with 200µl P.g LPS 0.3 µg/ml.
well 7	Control, TEER measured at time points.
well 8	no LPS, (200µl EBD 1 µg/mL placed at time 0) samples collected from basolateral compartment (3x200µl) at set time points, absorbance measured, replaced with media.
well 9	Control, TEER measured at time points.
well 10	200µl P.g LPS 0.1 µg/ml placed in apical compartment at time 0. At set time points this was removed and replaced with 200µl EBD 1 µg/ml which was incubated for 15 min before the 3x 200µl samples were taken from the basolateral compartment, replaced with media. After the sampling the EBD was removed and replaced with 200µl P.g LPS 0.1 µg/ml.
well 11	200µl P.g LPS 0.1 µg/ml placed in apical compartment at time 0. At set time points this was removed and replaced with 200µl EBD 1 µg/ml which was incubated for 15 min before the 3x 200µl samples were taken from the basolateral compartment, replaced with media. After the sampling the EBD was removed and replaced with 200µl P.g LPS 0.1 µg/ml.
well 12	200µl P.g LPS 0.3 µg/ml placed in apical compartment at time 0. At set time points this was removed and replaced with 200µl EBD 1 µg/ml which was incubated for 15 min before the 3x 200µl samples were taken from the basolateral compartment, replaced with media. After the sampling the EBD was removed and replaced with 200µl P.g LPS 0.3 µg/ml.
blank	5µg/ml fibronectin coating, no cells, TEER measured at time points

Table 2 Test protocol summary *P. gingivalis* LPS with FITC dextran permeability assay.

Well	protocol
well 1	At set time points 200µl FITC 100 µg/ml was placed in the apical compartment and incubated for 15 min before the 3x 200µl samples were taken from the basolateral compartment, After the sampling the FITC was removed and replaced with media.
well 2	At set time points 200µl FITC 100 µg/ml was placed in the apical compartment and incubated for 15 min before the 3x 200µl samples were taken from the basolateral compartment, After the sampling the FITC was removed and replaced with media..
well 3	At set time points 200µl FITC 100 µg/ml was placed in the apical compartment and incubated for 15 min before the 3x 200µl samples were taken from the basolateral compartment, After the sampling the FITC was removed and replaced with media..
well 4	200µl P.g LPS 0.1 µg/ml placed in apical compartment at time 0. At set time points this was removed and replaced with 200µl FITC 100 µg/ml which was incubated for 15 min before the 3x 200µl samples were taken from the basolateral compartment, replaced with media. After the sampling the FITC was removed and replaced with 200µl P.g LPS 0.1 µg/ml.
well 5	200µl P.g LPS 0.1 µg/ml placed in apical compartment at time 0. At set time points this was removed and replaced with 200µl FITC 100 µg/ml which was incubated for 15 min before the 3x 200µl samples were taken from the basolateral compartment, replaced with media. After the sampling the FITC was removed and replaced with 200µl P.g LPS 0.1 µg/ml.
well 6	Control, TEER measured at time points.
well 7	Control, TEER measured at time points.
well 8	Control, TEER measured at time points.
well 9	200µl P.g LPS 0.1 µg/ml placed in apical compartment at time 0. At set time points this was removed and replaced with 200µl FITC 100 µg/ml which was incubated for 15 min before the 3x 200µl samples were taken from the basolateral compartment, replaced with media. After the sampling the FITC was removed and replaced with 200µl P.g LPS 0.1 µg/ml.
well 10	Control, TEER measured at time points.

well 11	At set time points 200µl FITC 100 µg/ml was placed in the apical compartment and incubated for 15 min before the 3x 200µl samples were taken from the basolateral compartment, After the sampling the FITC was removed and replaced with media.
well 12	At set time points 200µl FITC 100 µg/ml was placed in the apical compartment and incubated for 15 min before the 3x 200µl samples were taken from the basolateral compartment, After the sampling the FITC was removed and replaced with media.
well 13	200µl P.g LPS 1 µg/ml placed in apical compartment at time 0. At set time points this was removed and replaced with 200µl FITC 100 µg/ml which was incubated for 15 min before the 3x 200µl samples were taken from the basolateral compartment, replaced with media. After the sampling the FITC was removed and replaced with 200µl P.g LPS 1 µg/ml.
well 14	200µl P.g LPS 1 µg/ml placed in apical compartment at time 0. At set time points this was removed and replaced with 200µl FITC 100 µg/ml which was incubated for 15 min before the 3x 200µl samples were taken from the basolateral compartment, replaced with media. After the sampling the FITC was removed and replaced with 200µl P.g LPS 1 µg/ml.
well 15	200µl P.g LPS 1 µg/ml placed in apical compartment at time 0. At set time points this was removed and replaced with 200µl FITC 100 µg/ml which was incubated for 15 min before the 3x 200µl samples were taken from the basolateral compartment, replaced with media. After the sampling the FITC was removed and replaced with 200µl P.g LPS 1 µg/ml.
well 16	200µl P.g LPS 10 µg/ml placed in apical compartment at time 0. At set time points this was removed and replaced with 200µl FITC 100 µg/ml which was incubated for 15 min before the 3x 200µl samples were taken from the basolateral compartment, replaced with media. After the sampling the FITC was removed and replaced with 200µl P.g LPS 10 µg/ml.
well 17	200µl P.g LPS 10 µg/ml placed in apical compartment at time 0. At set time points this was removed and replaced with 200µl FITC 100 µg/ml which was incubated for 15 min before the 3x 200µl samples were taken from the basolateral compartment, replaced with media. After the sampling the FITC was removed and replaced with 200µl P.g LPS 10 µg/ml.
well18	200µl P.g LPS 10 µg/ml placed in apical compartment at time 0. At set time points this was removed and replaced with 200µl FITC 100 µg/ml which was incubated for 15 min before the 3x 200µl samples were taken from the basolateral compartment, replaced with

	media. After the sampling the FITC was removed and replaced with 200µl P.g LPS 10 µg/ml.
well 19	200µl P.g LPS 100 µg/ml placed in apical compartment at time 0. At set time points this was removed and replaced with 200µl FITC 100 µg/ml which was incubated for 15 min before the 3x 200µl samples were taken from the basolateral compartment, replaced with media. After the sampling the FITC was removed and replaced with 200µl P.g LPS 100 µg/ml.
well 20	200µl P.g LPS 100 µg/ml placed in apical compartment at time 0. At set time points this was removed and replaced with 200µl FITC 100 µg/ml which was incubated for 15 min before the 3x 200µl samples were taken from the basolateral compartment, replaced with media. After the sampling the FITC was removed and replaced with 200µl P.g LPS 100 µg/ml.
well 21	200µl P.g LPS 100 µg/ml placed in apical compartment at time 0. At set time points this was removed and replaced with 200µl FITC 100 µg/ml which was incubated for 15 min before the 3x 200µl samples were taken from the basolateral compartment, replaced with media. After the sampling the FITC was removed and replaced with 200µl P.g LPS 100 µg/ml.
well22	200µl P.g LPS 0.3 µg/ml placed in apical compartment at time 0. At set time points this was removed and replaced with 200µl FITC 100 µg/ml which was incubated for 15 min before the 3x 200µl samples were taken from the basolateral compartment, replaced with media. After the sampling the FITC was removed and replaced with 200µl P.g LPS 0.3 µg/ml.
well 23	200µl P.g LPS 0.3 µg/ml placed in apical compartment at time 0. At set time points this was removed and replaced with 200µl FITC 100 µg/ml which was incubated for 15 min before the 3x 200µl samples were taken from the basolateral compartment, replaced with media. After the sampling the FITC was removed and replaced with 200µl P.g LPS 0.3 µg/ml.
well 24	200µl P.g LPS 0.3 µg/ml placed in apical compartment at time 0. At set time points this was removed and replaced with 200µl FITC 100 µg/ml which was incubated for 15 min before the 3x 200µl samples were taken from the basolateral compartment, replaced with media. After the sampling the FITC was removed and replaced with 200µl P.g LPS 0.3 µg/ml.

control	5µg/ml fibronectin coating, no cells, TEER measured at time points
---------	--

Table 3 First allocation of samples to wells FITC *P. gingivalis* LPS conjugate from Dojindo

Well number	Application
1	Dojindo 10 µg/ml + HBSS
2	Dojindo 10 µg/ml + HBSS
3	Dojindo 1 µg/ml + HBSS
4	Dojindo 1 µg/ml + HBSS
5	Dojindo 0.1 µg/ml + HBSS
6	Dojindo 0.1 µg/ml + HBSS
7	Dojindo 0.01 µg/ml + HBSS
8	Media only
9	Dojindo 0.01 µg/ml + HBSS
10	Media only
11	Dojindo 0.01 µg/ml + HBSS
12	Dojindo 0.01 µg/ml + HBSS
13	FITC-dextran 100 µg/ml only
14	FITC-dextran 100 µg/ml only
15	Dojindo 10 µg/ml + media
16	Dojindo 10 µg/ml + media
17	Dojindo 1 µg/ml + media
18	Dojindo 1 µg/ml + media
19	Dojindo 0.1 µg/ml + media

20	Dojindo 0.1 µg/ml + media
21	Dojindo 0.01 µg/ml + media
22	Dojindo 0.01 µg/ml + media
23	Dojindo 0.001 µg/ml + media
24	Dojindo 0.001 µg/ml + media
Control	Fibronectin 5 µg/ml
Control	blank

Table 4 second allocation of samples to wells FITC *P. gingivalis* LPS conjugates from Nanocs and Dojindo

Well number	Application
1	FITC-dextran 100 µg/ml
2	Media only
3	FITC-dextran 100 µg/ml
4	Nanocs conjugate in media only 10 µg/ml (no citrate buffer)
5	Nanocs conjugate in media only 10 µg/ml (no citrate buffer)
6	Nanocs in media 10 µg/ml
7	Nanocs in media 10 µg/ml
8	Nanocs in media 1 µg/ml
9	Nanocs in media 1 µg/ml
10	Nanocs in media 0.1 µg/ml
11	Nanocs in media 0.1 µg/ml
12	Nanocs in media 0.01 µg/ml

13	Nanocs in media 0.01 µg/ml
14	Nanocs in citrate buffer 100 µg/ml
15	Nanocs in citrate buffer 100 µg/ml
16	Dojindo in media 10 µg/ml
17	Dojindo in media 10 µg/ml
18	Dojindo in media 1 µg/ml
19	Dojindo in media 1 µg/ml
20	Dojindo in media 0.1 µg/ml
21	Dojindo in media 0.1 µg/ml
22	Dojindo in media 0.01 µg/ml
23	Dojindo in media 0.01 µg/ml
Control	Fibronectin 5 µg/ml
Control	Blank

Table 5 third allocation of test wells, FITC *P. gingivalis* conjugate from Nanocs with Citrate buffer and media or media only

Well number	Nanocs <i>P. gingivalis</i> LPS FITC conjugate
1	100 ug/ml Citrate Buffer
2	100 ug/ml Citrate Buffer
3	100 ug/ml Citrate Buffer
4	50 ug/ml Citrate Buffer
5	50 ug/ml Citrate Buffer
6	10 ug/ml Citrate Buffer
7	10 ug/ml Citrate Buffer

8	1 ug/ml Citrate Buffer
9	1 ug/ml Citrate Buffer
10	FITC-dextran 3-5 kD
11	FITC-dextran 3-5 kD
12	TEER only
13	100 ug/ml media
14	100 ug/ml media
15	100 ug/ml media
16	50 ug/ml media
17	50 ug/ml media
18	10 ug/ml media
19	10 ug/ml media
20	1 ug/ml media
21	1 ug/ml media
22	media sampling
23	Fibronectin only on membrane
24	Blank membrane

Table 6 Apparent permeability (Papp) well 1 – 12 at 1,2 and 4 hours, April 2019. EBD values designated poor permeability: 0 - 1.4x10-6 cm/s and high permeability: 5 x 10-5 - 9 x 10-5 cm/s

	Time (h)	Papp at 60 min (cm/min)	(cm/ s)	Papp at 120min cm/s	Papp at 240 m cm/s
well 1	LPS 1 µg/ml (EB removed)	0.001789466	2.98E-05	0.000875963 1.46E-05	0.000253403 4.22E-06
well 2	no LPS (Evans Blue)	0.004429868	7.38E-05	0.000932274 1.55E-05	0.00582828 9.71E-05
well 3	LPS + EB (1:1 µg/mL)	0.002152365	3.59E-05	0.000638201 1.06E-05	0.037059475 6.18E-04
well 4	LPS 1 µg/ mL (EB removed)	0.002227448	3.71E-05	0.001107467 1.85E-05	0.011884935 1.98E-04
well 5	LPS 1 µg/ mL (EB removed)	0.000275303	4.59E-06	0.001714384 2.86E-05	0.014034172 2.34E-04
well 6	LPS 0.3 µg/ mL	0.00050055	8.34E-06	0.000475523 7.93E-06	0.008615718 1.44E-04
well 7	Control	0	0.00E+00	0 0.00E+00	0 0.00E+00
well 8	no LPS (Evans Blue)	0.000963559	1.61E-05	0.00090099 1.50E-05	0.084736867 1.41E-03
well 9	Control	0	0.00E+00	0 0.00E+00	0 0.00E+00
well 10	0.1 µg/ mL LPS	0.001451595	2.42E-05	0.000857192 1.43E-05	0.046013064 7.67E-04
well 11	0.1 µg/ mL LPS	0.002089796	3.48E-05	0.000744568 1.24E-05	0.044345606 7.39E-04
well 12	0.3 µg/ mL LPS	0.003866749	6.44E-05	0.000669486 1.12E-05	0.097313188 1.62E-03

Table 7 Magnitude of changes March 2020

Well	TEER time 0	A: Y ₁ .Y ₂ TEER ohm/cm ²	B: X ₂ .X ₁ min	A/B	TEER minimum after protocol started Y ₂ at X ₂	Time to recover TEER value C: X ₃ -X ₂	Value recovered D: Y ₃ -Y ₂	Gradient of recovery D/C	Recovery point /min X ₃	Recovery value TEER Y ₃	Difference between highest TEER and recovery value	FITC penetration Started/min	% appearance max	% appearance max at Time/min
Nanocs 100 ug/ml in CB	335.2	184.2	30	6.14	151	2850 Did not recover	-22.2	-0.0078	2880	128.8	-206.4	30	10.76	240
Nanocs 100 ug/ml in CB	332.8	186.8	60	3.11	146	2220 Did not recover	-7.8	-0.003	2280	138.2	-194.6	30	12.15	240
Nanocs 10 ug/ml in CB	318.4	47.6	2880	0.02	270.8	1440 Did not recover	26.8	0.02	4320	297.6	-20.8	240	16.20	2880
Nanocs 10 ug/ml in CB	388.2	121.2	30	4.04	267	1410	156.6	0.11	1440	423.6	35.4	2880	0.78	2880
Nanocs 1 ug/ml in CB	328.4	21.6	1440	0.02	306.8	1440	25.4	0.02	2880	332.2	3.8	none	none	none
Nanocs 1	384.8	29.4	2880	0.01	355.4	1440 Did not recover	-43.8	-0.03	4320	311.6	-73.2	None	None	none

Well	TEER time 0	A: Y ₁ .Y ₂ TEER ohm/cm ²	B: X ₂ . X ₁ min	A/B	TEER minimum after protocol started Y ₂ at X ₂	Time to recover TEER value C: X ₃ -X ₂	Value recovered D: Y ₃ -Y ₂	Gradient of recovery D/C	Recovery point /min X ₃	Recovery value TEER Y ₃	Difference between highest TEER and recovery value	FITC penetration Started/min	% appearance max	% appearance max at Time/min
FIT C	379.4	34.8	2880	0.01	344.6	1440 Did not recover	-2.4	-0.002	4320	342.2	-37.2	240	7.74	2880
FIT C	362	72.4	2880	0.03	289.6	1440 Did not recover	6.6	0.005	4320	296.2	-65.8	30	14.93	2880
Nanos 10 ug/ml in media	320.2	59.2	2880	0.02	261	1440	17.2	0.01	4320	278.2	-42	60	1.27	2880
Nanos 10 ug/ml in media	304.6	42.2	2880	0.01	262.4	1440	36.8	0.03	4320	299.2	-5.4	1440	3.84	2880

TEER	279.4	37.6	2880	0.01	241.8	1440	14	0.01	4320	255.8	-23.6	n/a	n/a	n/a
------	-------	------	------	------	-------	------	----	------	------	-------	-------	-----	-----	-----

Table 8 Magnetude of changes July:

Well	TEER time 0	A: Y ₁ -Y ₂ TEER ohm/cm ²	B: X ₂ -X ₁ min	A/B	TEER minimum after protocol started Y ₂ at X ₂	Time to recover TEER value C: X ₃ -X ₂	Value recovered D: Y ₃ -Y ₂	Gradient of recovery D/C	Recovery point /min X ₃	Recovery value TEER Y ₃	Difference between highest TEER and recovery value	FITC penetration Started/min	% appearance max	% appearance max at Time/min	Final FITC
Nanocs 100 ug/ml in CB	287.2	122.2	2880	0.04	165	1440 Not recovered	-20.2	-0.01	4320	144.8	-142.4	60	4.7	4320	2.78
Nanocs 100 ug/ml in CB	376	232.8	2880	0.08	143.2	1440 Not recovered	-13.2	-0.01	4320	130	-246	60	9.35	2880	9.05
Nanocs 100 ug/ml in CB	303.6	156.2	2880	0.05	147.4	1440 Not recovered	-14.2	-0.01	4320	133.2	-170.4	60	6.55	2880	6.92
Nanocs 50 ug/ml in CB	280.2	18.8	1440	0.01	261.4	2880 Not recovered	12.4	0.004	4320	273.8	-6.4	60	2.42	2880	0.61
Nanocs 50 ug/ml in CB	285.2	20.4	1440	0.01	264.8	2880 Not recovered	-27	-0.01	4320	237.8	-47.4	60	3.23	2880	0.41

Well	TEER time 0	A: Y ₁ -Y ₂ TEER ohm/cm ²	B: X ₂ -X ₁ min	A/B	TEER minimum after protocol started Y ₂ at X ₂	Time to recover TEER value C: X ₃ -X ₂	Value recovered D: Y ₃ -Y ₂	Gradient of recovery D/C	Recovery point /min X ₃	Recovery value TEER Y ₃	Difference between highest TEER and recovery value	FITC penetration Started/min	% appearance max	% appearance max at Time/min	Final FITC
Nanocs 10 ug/ml in CB	330.2	65.6	240	0.27	264.6	2640	82.2	0.03	2880	346.8	16.6	60	3.33	240	1.41
Nanocs 10 ug/ml in CB	301.8	51	1440	0.04	250.8	2880	80	0.03	4320	330.8	29	60	5.29	4320	0.71
Nanocs 1 ug/ml in CB	282	15	1440	0.01	267	1440	44.6	0.03	2880	311.6	29.6	60	5.55	2880	1.79
Nanocs 1 ug/ml in CB	278.6	14.6	1440	0.01	293.2	1440	26.8	0.02	2880	320	41.4	60	1.86	2880	0.91
FITC	273.4	4.8	240	0.02	268.6	1200	45.2	0.04	1440	313.8	40.4	60	2.11	60	1.99
FITC	261.4	11.4	1440	0.01	272.8	1440	13.4	0.01	2880	286.2	24.8	60	3.36	4320	4.25
TEER	282.8	21.4	1440	0.01	261.4	1440	106.4	0.07	2880	367.8	85	n/a	n/a	n/a	0.13
Nanocs 100 ug/ml media	309	70.6	1440	0.05	238.4	1440 Not recovered	8.4	0.006	2880	246.8	-62.2	1440	7.71	2880	2.35
Nanocs 100 ug/ml media	303.6	72.4	1440	0.05	231.2	1440 Not recovered	21.2	0.01	2880	252.4	-51.2	1440	9.58	4320	8.13
Nanocs 100	306.8	82.8	1440	0.06	224	1440	34	0.02	2880	258	-48.8	1440	7.13	4320	1.28

ug/ml media						Not recovered									
Nanocs 50 ug/ml media	313.6	65.8	1440	0.05	247.8	1440 Not recovered	18.8	0.01	2880	266.6	-47	1440	1.80	2880	0.2
Nanocs 50 ug/ml media	358.6	103	1440	0.07	255.6	2880 Not recovered	36.2	0.01	4320	291.8	-66.8	1440	4.9	2880	0.37
Nanocs 10 ug/ml media	306.8	76.8	1440	0.05	230	1440 Not recovered	64.4	0.04	2880	294.4	-12.4	2880	3.70	2880	5.18
Nanocs 10 ug/ml media	314.4	95	1440	0.07	219.4	2880 Not recovered	31.8	0.01	1440	251.2	-63.2	None	None	None	0.08
Nanocs 1 ug/ml media	329.6	93.8	240	0.39	235.8	2640	100.2	0.04	2880	336	6.4	None	None	None	0.16
Nanocs 1 ug/ml media	298.8	68.6	1440	0.05	230.2	2880 Not recovered	12	0.004	4320	242.2	-56.6	None	None	None	0.12
TEER	297	66.8	240	0.28	230.2	4080	97.8	0.02	4320	328	31	n/a	n/a	n/a	1.21
Fibronectin															
Blank															

